La Actividad Ribonucleasa Modula el Reconocimiento Inmune del exRNA Desnudo y Determina la Composición del exRNA no Vesicular

Tesis de Doctorado PEDECIBA Biología

Mag. Mauricio Castellano

Orientadores
Dr. Juan Pablo Tosar
Dra. Mercedes Segovia

Laboratorio de Genómica Funcional y
Laboratorio de Inmunoregulación e Inflamación,
Insitut Pasteur de Montevideo

Unidad de Bioquímica Analítica, CIN,
Facultad de Ciencias, UdelaR

Tribunal
Dr. Ricardo Ehrlich
Dra. Graciela L. Boccaccio
Dra. María Moreno

Resumen

En los últimos años se ha consolidado la idea de que el RNA extracelular (exRNA) podría desempeñar un papel clave en la comunicación intercelular, esto está revolucionando múltiples áreas de la biología. El exRNA puede encontrarse dentro de vesículas extracelulares o en la fracción no vesicular, ya sea asociado a ribonucleoproteínas o como exRNA desnudo. Se ha considerado que el exRNA no vesicular carece de relevancia funcional, debido a su susceptibilidad a la degradación por ribonucleasas extracelulares (RNasas). Sin embargo, estudios previos de nuestro grupo, resultados de esta tesis de doctorado y de otros investigadores demuestran que la mayoría de los exRNAs son de hecho no vesiculares. En esta tesis de doctorado aportamos evidencia que sugiere que las células liberan gran parte de su transcriptoma al espacio extracelular no vesicular. Esta observación plantea una interrogante fundamental: ¿pueden las células detectar y responder al exRNA no vesicular y en particular al exRNA desnudo? La membrana plasmática es considerada una barrera física para la captación de exRNAs desnudos. Aunque ciertos tipos celulares podrían internalizar espontáneamente exRNA desnudo, el *delivery* funcional al citosol celular ha sido raramente observado. En esta tesis demostramos que las RNasas extracelulares, derivadas principalmente del suero fetal bovino utilizado como suplemento en cultivo celular, han oscurecido el estudio de la funcionalidad del exRNA desnudo. En presencia de un inhibidor activo de ribonucleasa (RI) observamos que el RNA bacteriano desnudo desencadena una potente respuesta proinflamatoria cuando se lo añade al medio de cultivo de células dendríticas y macrófagos. Mediante aproximaciones farmacológicas y genéticas, demostramos que la respuesta depende principalmente de la acción de los receptores endosomales de la familia *Toll-like receptors*. Además, también demostramos que el exRNA desnudo puede escapar de los endosomas y ser reconocido por sensores citoplasmáticos de RNA como RIG-I o MDA5 y llamativamente también por ribosomas. En este sentido, mRNAs extracelulares desnudos que codifican proteínas reporteras pueden ser internalizados espontáneamente y traducidos por diversos tipos celulares, de manera dependiente de RI. *In vivo*, el exRNA desnudo administrado de forma sistémica por vía intravenosa, compartimento rico en RNasas, estimula la activación de células inmunes innatas y adaptativas del bazo, y estos efectos se ven potenciados por la co-inyección de RI. Por otro lado, observamos que en compartimentos pobres en RNasas, como la cavidad peritoneal, el exRNA

desnudo posee un efecto proinflamatorio intrínseco, independiente de la presencia de inhibidores de RNasas.

En conjunto, y en contraste con lo que se consideraba previamente, los resultados de esta tesis de doctorado demuestran que el exRNA desnudo es bioactivo por sí mismo y no requiere encapsulación en vesículas lipídicas, sintéticas o biológicas, para su captación y funcionalidad celular. Estos hallazgos respaldan fuertemente la hipótesis de una forma de comunicación intercelular mediada por exRNAs desnudos que está supeditada a la presencia/ausencia de RNasas. Además, nuestros estudios aportan evidencia de que las múltiples RNasas presentes en el espacio extracelular podrían haber evolucionado como un mecanismo para controlar y regular los niveles de exRNAs desnudos circulantes, ya sea de origen endógeno o patógeno, y así evitar respuestas inflamatorias sistémicas que podrían contribuir a desencadenar o exacerbar patologías autoinflamatorias o autoinmunes.

Agradecimientos

En primer lugar, quiero agradecer muy especialmente a mis tutores de doctorado, Juan Pablo y Mercedes. Por la formación recibida a lo largo de estos años, por el apoyo incondicional con el que me acompañaron en las distintas aventuras en las que nos embarcamos, por las constantes oportunidades que me brindaron, por los valores científicos que me transmitieron y por haber creado un ambiente fértil que estimula la creatividad y convierte a la ciencia en una actividad casi lúdica. Haber trabajado junto a ellos durante este tiempo ha sido un verdadero placer.

A Alfonso y Marcelo por abrirme las puertas del Laboratorio de Genómica Funcional y del Laboratorio de Inmunoregulación e Inflamación, respectivamente. Sin el apoyo y generosidad de ellos, este trabajo no habría podido ocurrir.

A mis compañeros del Laboratorio de Genómica Funcional, del Laboratorio de Inmunorregulación e Inflamación y de la Unidad de Bioquímica Analítica del CIN, compartir mis jornadas con ellos hace que el trabajo diario sea, en la mayoría de los días, extremadamente gratificante y placentero. En definitiva, sin esto es imposible hacer Ciencia.

A la comisión de admisión y seguimiento del posgrado integrada por: la Dra. Ana Ferreira, el Dr. Ricardo Ehrlich y el Dr. Pablo Smircich por haber seguido este trabajo en los últimos años.

A las agencias financiadoras involucradas en esta tesis: ANII, CAP, CSIC, PEDECIBA, FOCEM y NIH.

A las plataformas tecnológicas del IPMon: UBA, UBC y UBAL.

Al Dr. Ricardo Ehrlich, a la Dra. Graciela L. Boccaccio y a la Dra. María Moreno por aceptar ser parte del tribunal de esta tesis de doctorado.

A Alexandra Elbakyan por facilitar el acceso a la literatura científica.

A mi familia y amigos por el amor y cariño incondicional de siempre.

Tabla de contenidos

Lista de abreviaturas

exRNA	RNA extracelular
exDNA	DNA extracelular
nV-exRNA	RNA extracelular no vesicular
EV-exRNA	RNA extracelular vesicular
EV	Vesículas extracelulares
MVB	Cuerpos multivesiculares
RNAase	Ribonucleasa de la familia A
PRR	Receptor de reconocimiento de patrones
TLR(#)	Receptor perteneciente a la familia Toll
RLR	Receptor tipo RIG-I
PAMPs	Patrones moleculares asociados a patógenos
DAMPs	Patrones moleculares asociados a daño
mRNA	RNA mensajero
tRNA	RNA de transferencia
rRNA	RNA ribosomal
miRNA	micro RNA
snRNA	RNA pequeño nuclear
snoRNA	RNA pequeño nucleolar
lncRNA	RNA largo no codificante
siRNA	RNA pequeños interferentes
piRNA	RNA que interactúa con Piwi
RNAi	Interferencia mediada por RNA
ASO	Oligonucleótido anti-sentido
ssRNA	RNA simple cadena
dsRNA	RNA doble cadena
RE	Retículo endoplasmático rugoso
RI	Inhibidor de RNasas
ANG	Angiogenina

Ago2	Argonauta 2
RNP	Ribonucleoproteínas
LLR	Repetidos de leucina
ISGs	Genes de respuesta a interferón
m6A	N6-metiladenosina
m5C	5-metilcitidina
Ψ	Pseudouridina
I	Inosina
KO	*Knockout*
WT	*Wild type*
LNP	Nanopartícula lipídica
LES	Lupus Eritematoso Sistémico
SI	Sistema inmune
SII	Sistema inmune innato
SIA	Sistema inmune adaptativo

Artículos científicos relacionados a la tesis de doctorado

Artículos científicos que conforman la tesis por compendio de artículos

- Tosar JP, Segovia M, **Castellano M,** Gámbaro F, Akiyama Y, Fagúndez P, Olivera Á, Costa B, Possi T, Hill M, Ivanov P, Cayota A (2020) Fragmentation of extracellular ribosomes and tRNAs shapes the extracellular RNAome. *Nucleic Acids Research* https://doi.org/10.1093/nar/gkaa674 **(Artículo 1)**

- **Castellano M**, Blanco V, Calzi ML, Costa B, Witwer K, Hill M, Cayota A, Segovia M, Tosar JP (2025) Ribonuclease activity undermines immune sensing of naked extracellular RNA. *Cell Genomics* https://doi.org/10.1016/j.xgen.2025.100874 **(Artículo 2)**

- **Castellano M**, Calzi ML, Garcia MR, Cayota A, Tosar JP (2025) Discrimination between vesicular and nonvesicular extracellular tRNAs and their fragments. *Methods in Enzymology*. https://doi.org/10.1016/bs.mie.2024.11.042 **(Artículo 3)**

Otros artículos científicos relacionados a la temática de la tesis de doctorado (ver anexo 1)

- Tosar JP, **Castellano M**, Costa B, Cayota A (2024) Small RNA structural biochemistry in a post-sequencing era. *Nature Protocols* https://doi.org/10.1038/s41596-023-00936-2 **(Artículo 4)**

- Costa B, Calzi ML, **Castellano M**, Blanco V, Cuevasanta E, Litvan I, Ivanov P, Witwer K, Cayota A, Tosar JP (2023) Nicked tRNAs are stable reservoirs of tRNA halves in cells and biofluids. *PNAS* https://doi.org/10.1073/pnas.2216330120 **(Artículo 5)**

Otros artículos científicos relevantes publicados durante el doctorado (ver anexo 2)

- Jimenez NA, **Castellano M**, Santillan EM, Boulias K, Boan A, Padilla LFA, Fernandino JI, Greer EL, Tosar JP, Cochella L, Strobl-Mazzulla PH (2022) Paternal methotrexate exposure affects sperm small RNA content and causes craniofacial defects in the offspring. *Nature Communications* https://doi.org/10.1038/s41467-023-37427-7 **(Artículo 6)**

Introducción

1. Breve resumen de algunas funciones del RNA

La biología molecular estuvo inicialmente marcada por un fuerte énfasis en comprender las funciones del DNA por sobre las del RNA. El DNA despertó un interés científico superior debido a su papel central como molécula de la herencia.[1] El hallazgo de su estructura en doble hélice por Watson y Crick[2] evidenció su papel fundamental en el almacenamiento, conservación y transmisión de la información genética en los seres vivos. Por el contrario, el RNA fue considerado en un principio solo un intermediario de vida corta o componente estructural para la síntesis de proteínas.

Maravilloso fue descubrir, a lo largo de las últimas 7 décadas, que el RNA es una verdadera navaja suiza molecular: una macromolécula extraordinariamente versátil en términos de secuencia nucleotídica (existen más de 200 modificaciones químicas introducidas post transcripcionalmente al RNA[3,4]), tamaños (desde unos pocos nucleótidos, hasta cientos de miles de pares de bases), diversidad estructural y funcional. Además de almacenar temporalmente la información genética, los RNAs pueden actuar como enzimas, desempeñar funciones estructurales, regular la expresión génica, actuar como sensores metabólicos, solo por nombrar algunos ejemplos.[5] Dentro de las células, los mRNAs, tRNAs y rRNAs (estos últimos formando parte del ribosoma) decodifican el código genético y orquestan la síntesis de proteínas.[6] Otros tipos de RNA no codificantes, como miRNAs, siRNAs, lncRNAs, piRNAs (solo por nombrar algunos), participan activamente en la regulación de la expresión génica a múltiples niveles[5]; los snRNAs guían el proceso de splicing alternativo[7] ; los snoRNAs modifican nucleótidos de algunos RNAs[8] ; la RNasaP[9] y el rRNA actúan como ribozimas; y ciertos lncRNAs introducen cambios epigenéticos.[10] Por si todo esto no fuera suficiente, los tRNAs, además de su función canónica pueden sufrir cortes selectivos en su estructura generando mitades y fragmentos de tRNAs[11] con nuevas funciones emergentes, como la regulación de la traducción entre otras.[12,13]

Toda esta diversidad funcional es producto de la capacidad del RNA de establecer apareamiento de bases con secuencias blanco, pero, sobre todo, a su capacidad notable de adquirir estructuras secundarias y terciarias, comparables a las proteínas.[14] Por todo esto, con las debidas disculpas a los "desoxi-fanáticos", creo no equivocarme en sostener que el RNA tiene una vida más diversa, interesante y divertida que su primo hermano, el DNA, que mayormente está encerrado en la biblioteca guardando información.

Como si fuera poco, en las últimas décadas, se ha constatado que las células liberan al exterior varios de los biotipos de RNAs mencionados previamente[15]. Este fascinante descubrimiento sugiere que los RNAs, más allá de las funciones intracelulares mencionadas anteriormente, también podrían participar en la comunicación intercelular de organismos multicelulares tanto en condiciones normales como patológicas[16] e incluso constituir un mecanismo de comunicación entre diferentes especies.[17] Además, la existencia de estas moléculas promete importantes aportes a la biomedicina al ser potencialmente útiles como biomarcadores de diferentes patologías.[18–20]

2. *Primeras evidencias de la existencia y posibles funciones del RNA extracelular*

a) Algunas generalidades sobre los RNAs extracelulares

El descubrimiento de que las células pueden liberar RNA al exterior (exRNA) está revolucionando múltiples aspectos de la biología molecular, celular y de la biomedicina. El término exRNA es una denominación amplia que comprende a todos aquellos RNAs presentes en el componente acelular de biofluidos (como sangre, líquido cefalorraquídeo, linfa, fluido amniótico, fluido pericárdico, peritoneal e intratumoral, entre otros) y secreciones corporales (tales como orina, lágrimas, sudor, leche materna o fluido seminal). A su vez, este término, también incluye a los RNAs detectados en el medio de cultivo de líneas celulares, cultivo de células primarias, tejidos y organoides.[21] Pero también podemos incluir dentro de esta definición a aquellos RNAs artificialmente introducidos a estos biofluidos, secreciones o medios de cultivo.

Un ejemplo de esto son las vacunas de mRNA y los ASOs terapéuticos. Además, como veremos en detalle en las próximas secciones, los exRNAs pueden estar asociados a distintos tipos de transportadores, como vesículas extracelulares, lipoproteínas, complejos ribonucleoproteicos o incluso encontrarse desnudos en el medio extracelular.[22]

b) Descubrimiento de los RNAs extracelulares en mamíferos

Los primeros indicios sobre la existencia de exRNAs en mamíferos se remontan a la década de 1940. Estudios pioneros de Mandel y Métais en 1948 detectaron por primera vez ácidos nucleicos en el plasma de personas sanas, así como de pacientes con patologías metabólicas.[23] Utilizando técnicas bioquímicas clásicas pudieron cuantificar los niveles de RNA y DNA extracelular. Notablemente el RNA constituyó la mayor parte de los ácidos nucleicos circulantes, sentando la idea de que esta macromolécula podría existir fuera de las células y circular en los biofluidos.[23] ¿De dónde provenía el exRNA? siguió siendo un misterio por un par de décadas más. En 1971 y 1972 Kolodny demostró que la línea de fibroblastos 3T3 liberaban exRNA al medio de cultivo. El patrón de sedimentación y estado de metilación sugería que estos exRNA podrían derivar del RNA ribosomal 5S o ser fragmentos ultraestables de rRNA de mayor tamaño previamente liberados.[24] Unos años después, otros investigadores observaron liberación de RNA en complejo con DNA y glicoproteínas en sistemas tan diversos como cultivos de linfocitos humanos purificados de sangre periférica y cultivos de aurículas de rana.[25]

Por otra parte, en una serie de ingeniosos experimentos, Kolodny observó que fibroblastos en co-cultivo eran capaces de transferir RNA marcado radiactivamente desde una célula donadora a una célula aceptora cuya transcripción había sido previamente inhibida. Aunque esta transferencia de RNA entre células podría, en principio, ocurrir por contacto directo célula-célula, o ser un artefacto generado por contaminación con nucleótidos radiactivos del cultivo, elegantes controles experimentales apoyaron que verdaderamente estaba ocurriendo la liberación de RNAs marcado al medio extracelular y su posterior captura por células aceptoras.[26,27] Estos experimentos constituyen, posiblemente, la primera evidencia de la intercomunicación celular mediada por exRNA. Sin embargo, ya desde la década del 60 existían indicios de que células murinas en cultivo podían incorporar y traducir mRNAs exógenos de origen hepático generando aún más fuerza a la idea de la comunicación intercelular mediada por exRNAs.[28]

3. El RNA extracelular en mamíferos:

a) Redescubrimiento de los RNAs extracelulares

En la aventura científica, es común que nuevos temas de investigación emerjan, caigan en el olvido y luego antiguos hallazgos sean redescubiertos y resignificados. Algo de este estilo ha ocurrido en el campo del exRNA. El renovado interés por estas moléculas probablemente se deba al trabajo de Valadi del 2007.[16] Valadi observó que mastocitos humanos y de ratón liberan exosomas conteniendo mRNAs y miRNAs funcionales. Además, al transferir exosomas de ratón a mastocitos humanos, detectó nuevas proteínas de origen murino, sugiriendo que los exRNAs pueden ser transferidos entre células y ser funcionales en las células receptoras.[16] En otro artículo de gran impacto, se observó que los astrocitos pueden liberar miRNAs empaquetados en exososmas que son luego internalizados por células tumorales del cerebro, inhibiendo la expresión de ciertos supresores tumorales y permitiendo así el establecimiento y crecimiento de metástasis en este órgano.[29]

b) Algunas Interrogantes sobre la biología de los RNAs extracelulares

Estos y otros descubrimientos, junto con el advenimiento de potentes técnicas de secuenciación masiva necesarias para la caracterización de estas moléculas, renovaron el interés por los exRNAs. En el año 2013 el NIH lanzó el "*Extracellular RNA communication consortium*", del cual nuestro laboratorio formó parte (durante el período 2019-2023), para aunar esfuerzos, lograr comprender mejor la biología de los exRNA en mamíferos y generar nuevas tecnologías analíticas para el estudio de los exRNAs.[30,31]

A pesar de este "*task force*" internacional, aún persisten numerosas interrogantes en el campo del exRNA, tales como: ¿Qué tipos de exRNAs existen en el espacio extracelular? ¿Mediante qué mecanismos son liberados? ¿son secretados de forma selectiva o pasiva? ¿cómo logran mantenerse estables el tiempo suficiente para cumplir sus funciones? ¿son verdaderamente funcionales o un simple producto de deshecho?, dado que el ambiente extracelular es rico en nucleasas como veremos en siguientes capítulos ¿por qué no todos se degradan fácilmente? ¿son dirigidos específicamente a células aceptoras? ¿cómo ingresan a estas células? ¿Una vez dentro, es su concentración suficientemente alta para tener alguna relevancia funcional? ¿cómo encuentran una pareja molecular que les permita ejercer su función? ¿Cuáles son estas parejas moleculares principales? ¿Qué efectos tienen sobre el sistema inmune, dado que dichas células cuentan con sensores de RNA? ¿Pueden estar implicados en el desarrollo y/o progresión de patologías? Aunque alguna de estas preguntas han sido abordadas en los últimos años, aún persisten muchas interrogantes, lo que vuelve a este un tema fascinante de estudio.

En este trabajo de doctorado abordaremos solamente algunas de estas preguntas.

c) RNAs extracelulares en biofluidos y su potencial como biomarcadores

Hoy sabemos que la composición de exRNAs varía notablemente entre diferentes biofluidos. Aunque se han detectado prácticamente todos los biotipos de RNA mencionados anteriormente, mayormente predomina miRNAs, yRNAs, tRNAs, fragmentos de tRNA, y fragmentos de rRNA.[22,32–34] ¿Qué poblaciones de RNAs se detectan en el espacio extracelular? Esto depende de múltiples factores como: el uso o no de estrategias para separar los diferentes tipos de cargo, los kits de purificación, estrategias de colección de las muestras[35] (ej: hay grandes diferencias entre suero y plasma), los protocolos de generación de librerías para secuenciación de RNA[36], entre otras. Por otra parte, se ha observado que los niveles de exRNAs circulantes en biofluidos están alterados en diversas patologías como cáncer[18,19,37,38], insuficiencia renal[39], falla cardíaca[40], infecciones[41] y enfermedades autoinmunes como el Lupus Eritematoso Sistémico (LES)[42], resultando auspiciosa la posibilidad de que estas moléculas puedan ser utilizadas para el diagnóstico temprano y/o seguimiento de alguna de estas enfermedades.[43,44]

d) Clasificación de los RNAs extracelulares.

Podemos clasificar a los exRNAs en 2 grandes categorías en función de si en el espacio extracelular se encuentra recubiertos por membranas o fuera de ellas.[15,22,45,46] Por un lado, tenemos a los RNAs extracelulares vesiculares (Ev-exRNAs), esta denominación comprende aquellos exRNAs empaquetados dentro de vesículas extracelulares (EV). Por otro lado, están los RNAs extracelular no vesiculares (nV-exRNAs). Dentro de esta categoría encontramos exRNAs asociados a lipoproteínas[47], formando complejos ribonculeoprotéicos[48], e incluso desprovistos de asociación a complejos macromoleculares, es decir exRNAs desnudos.[49] Los nV-exRNAs formando complejos con ribonucleoproteínas y en particular los exRNAs desnudos son el foco principal de esta tesis de doctorado.

e) RNAs extracelulares vesiculares

Existe una gran diversidad de EVs de diferente origen y tamaño. Las EVs incluyen microvesículas, ectosomas y oncosomas, que se originan por gemación de la membrana plasmáticas, así como exosomas, que se generan dentro de cuerpos multivesiculares (MVB) y son liberados al exterior cuando los MVB se fusionan con la membrana plasmática de la célula.[50,51] Se ha reportado que las EVs contienen RNA, proteínas, DNA y pequeños metabolitos, además de estar decoradas con distintas proteínas de superficie en sus membranas.[52] Por lo tanto, está claro que la biología de las EVs no está restringida únicamente a los exRNAs que puedan albergar en su interior, sino que el panorama es más complejo. De todas maneras, aquí describiremos brevemente (ya que no es el foco principal de la tesis) a los EV-exRNAs. Cómo ya fue mencionado, los EV-exRNAs existen en biofluidos, secreciones corporales y en el medio de células en cultivo. La aplicación de técnicas de secuenciación masiva ha permitido detectar prácticamente todos los biotipos de RNA, en algunos casos en forma entera o en fragmentos. Esfuerzos de catalogación, como la base de datos Vesiclepedia, enumeran más de 27,000 mRNA y 10,000 RNA no codificantes.[45] Sin embargo, debe considerarse que estas bases de datos pueden alimentarse de trabajos que no hayan logrado una eficiente separación entre los exRNAs vesiculares y no vesiculares.

La mayor atención ha sido puesta en pequeños RNAs no codificantes, sobre todos miRNAs ya que a priori estos serían de los de los biotipos más abundantes y tendrían la capacidad de regular finamente la expresión génica a distancia al ser internalizados por células aceptoras.[53] Aunque se ha postulado que las EV podrían descargar su cargo de exRNA al fusionarse con la membrana plasmática o al ser internalizadas por vía endosomal y luego escapar de las endosomas.[52] Hoy se acepta que esta última opción es la que generalmente predomina.[54]

Existe una amplia literatura (parte de la cual ya ha sido mencionada) que respalda la comunicación intercelular en mamíferos mediada por exRNAs transportados dentro de Evs.[52] Sin embargo, este campo enfrenta varios desafíos que cuestionan la relevancia fisiológica de este mecanismo de comunicación célula-célula[55]: 1) Muchos estudios se basan en la sobreexpresión artificial de RNAs, lo que da lugar a EVs con un contenido de RNA que probablemente no refleja su concentración fisiológica real.[56] 2) Los métodos empleados para purificar, concentrar y posteriormente agregar EVs a células en cultivo o animales no necesariamente reproducen con precisión las condiciones naturales en las cuales ocurriría este proceso de comunicación intercelular mediada por EVs.[57] 3) Es difícil determinar con certeza que los efectos atribuidos a los exRNAs no sean en realidad causados por otras moléculas presentes en las vesículas extracelulares (EVs), o por otros componentes del medio extracelular que co-purifican con las EVs.[58] Por ejemplo, la detección de una proteína en una célula receptora plantea la siguiente interrogante: ¿se debe a la transferencia de un mRNA que, tras la captación de la EV, fue traducido localmente, o a una proteína ya sintetizada en la célula de origen y transportada dentro de la vesícula?[55] 4) Pero, tal vez lo más importante es que en promedio, mediante estrategias finas de cuantificación se ha observado que las EVs contienen muy pocas copias de un RNA específico, frecuentemente menos de una molécula por vesícula. Esto sugiere que, por ejemplo, una célula debería internalizar cientos de miles o incluso millones de EVs portadoras de un miRNA para que estos tengan un impacto fisiológico significativo en la célula aceptora.[59,60]

4. El RNA extracelular no vesicular:

a) Los RNAs extracelulares no vesiculares son abundantes

Como ya fue mencionado, los nV-exRNAs comprenden una diversa gama de RNAs en el espacio extracelular, y estos pueden encontrarse asociados a lipoproteínas, proteínas o estar desnudos. Los EV-exRNAs han sido naturalmente más atractivos que los nV-exRNAs por diversas razones: 1) Los exRNAs podrían incorporarse de manera selectiva en exosomas y microvesículas[61,62] y se han identificado proteínas que participarían en la regulación de este proceso[63], así como secuencias específicas en ciertos RNAs, particularmente en miRNAs, que facilitarían su empaquetamiento selectivo.[64,65] 2) Al encontrarse protegidos dentro de EV, los exRNAs estarían resguardados de la degradación por nucleasas extracelulares.[66] 3) Las EV están decoradas con proteínas de superficie que, en principio, podrían conferirles tropismo hacia determinadas células u órganos diana.[67] 4) Las EVs facilitarían el ingreso de exRNAs a células receptoras, ya sea por fusión con la membrana plasmática o a través de procesos de endocitosis mediada por receptor al unir proteínas presentes en la superficie de estas vesículas.[54]

Sin embargo, pronto surgió evidencia que sugería que los nV-exRNAs son de hecho más abundantes y, probablemente, más relevantes desde un punto de vista fisiológico de lo que se creyó inicialmente, además como ya fue mencionado, el contenido de RNAs por EVs parece ser extremadamente bajo. En el 2011, dos trabajos publicados de forma independiente demostraron que la mayoría de los miRNAs extracelulares en plasma se encuentran formando complejos con la proteína Argonauta 2 (Ago2) por fuera de EVs.[48,68] Estudios posteriores del grupo de Victor Ambros (Premio Noble de Fisiología y Medicina en el año 2024 por el descubrimiento de los miRNAs) confirmaron estos hallazgos. Mediante estrategias de inmunoprecipitación contra proteínas Ago2 y posterior secuenciación masiva, determinaron que casi el 100% de los miRNAs en plasma están fuera de EVs, y que lo mismo ocurre en otros biofluidos como CSF. Más aún, estos complejos Ago2-miRNAs extracelulares estarían formando unidades de silenciamiento funcionales.[69] En la misma línea, otros investigadores también observaron que el suero de diversos mamíferos (ratón, rata, monos y humanos) es rico en miRNAs y fragmentos de tRNAs extracelulares que no están empaquetados en EVs. Además, los fragmentos de tRNA parecían estar desnudos en este biofluido ya que el tratamiento con proteinasa K no alteraba significativamente sus niveles.[41] En forma temprana, aplicando estrategias de ultra centrifugación diferencial y posterior secuenciación masiva de RNAs pequeños, nuestro grupo observó que algo similar ocurría con los exRNAs provenientes de líneas celulares tumorales. Detectamos diversos tipos de pequeños RNAs en la fracción extracelular no vesicular, como fragmentos de yRNAs, snRNAs y snoRNAs, pero sobre todo una gran cantidad de mitades de tRNAs, principalmente derivados del tRNA de glicina y del tRNA de ácido glutámico[70], los mismos tRNAs que habían sido observado previamente en suero.[41] Posteriormente se observó que la estabilidad de estas mitades de tRNA posiblemente se debiera su capacidad de dimerizar y formar estructuras de RNA doble cadena (dsRNA) resistentes a las RNasas extracelulares[71]. Más recientemente constatamos que estas mitades de tRNA también pueden existir en el espacio extracelular no vesicular como tRNAs que presentan un corte o "nick" en su anticodón. Estas moléculas, que hemos denominado "nicked tRNAs" son sumamente estables en biofluidos como CSF, suero y el medio condicionado de células en cultivo.[49] Cuando se emplean técnicas desnaturalizantes de extracción de RNAs o de secuenciación, estos "nicked tRNAs" se disocian en mitades de tRNA, lo que creemos explica una buena parte de la presencia de mitades de tRNA circulantes en biofluidos humanos, especialmente aquellos que se encuentran fuera de EVs (que, por datos no publicados de nuestro grupo, sabemos que son la mayoría).

b) Biogénesis de los RNAs extracelulares no vesiculares

El origen de los nV-exRNAs y los mecanismos de liberación hacia el espacio extracelular aún no están completamente dilucidados. Una posibilidad es que existan transportadores específicos de RNA en la membrana plasmática que faciliten la secreción de RNAs al exterior. En *C. elegans*, se han identificado proteínas como SID-1 y SID-2[72,73] , localizadas en la membrana plasmática, que participan en la captación y propagación sistémica de RNA de doble cadena desnudo entre células, un proceso clave para la interferencia por RNA en este nematodo. Sin embargo, en mamíferos, la evidencia que vincula a los homólogos de estas proteínas con la liberación o captación de exRNAs aún es poca y controversial.[55]

Recientemente se ha descubierto una nueva población de RNAs glicosilados post transcripcionalmente que se detectan desnudos en el espacio extracelular en asociación a las membranas plasmáticas de las células.[74] Al igual que para las proteínas, el proceso de glicosilación de estos RNAs ocurriría en el retículo endoplasmático (RE)[74], esto plantea la posibilidad de que algunos nV-exRNAs puedan ingresar al RE y ser liberados por las mismas vías de secreción utilizadas por las proteínas extracelulares. Estos RNAs glicosilados se presentan en la superficie celular y la glicosilación parecería jugar un rol en la modulación de las respuestas inmunológicas inducidas por RNAs superficiales liberados por células muertas.[75]

Por último, es posible que la muerte celular represente la principal fuente de nV-exRNAs. De hecho, algunos de estos procesos se caracterizan por la liberación de gran parte del contenido citoplasmático al medio extracelular.[76] En este sentido, durante la activación del inflamasoma y la posterior muerte por piroptosis se generan poros en la membrana celular a través de los cuales se secretan, de forma no canónica, IL-1β e IL-18.[77,78] Es posible que algunos nV-exRNAs escapen también por estos poros. Por otro lado, durante la Netosis se ha visto que los neutrófilos liberan trampas extracelulares que, además de estar compuestas por exDNA, contienen exRNA.[79] A su vez, es posible que la apoptosis y sobre todo la necrosis sean grandes fuentes de nV-exRNAs.[15]

c) Posibles funciones de los RNAs extracelulares no vesiculares

Recientemente se ha observado que una población de nV-exRNAs asociados a la membrana plasmática de neutrófilos regulan la adhesión de estas células a los vasos sanguíneos y su reclutamiento a sitios de infección.[80] A pesar de esta observación, las funciones que podrían desempeñar otros nV-exRNAs, en particular los nV-exRNAs circulantes, no están claras. Es probable que las funciones de estas moléculas estén íntimamente ligadas a la actividad de las RNasas extracelulares, ya que, a priori, los nV-exRNAs, en particular aquellos desnudos, son posibles sustratos de estas enzimas. En este sentido, hipotetizamos que las RNasas extracelulares podrían moldear la composición de los exRNAs en el espacio extracelular no vesicular y regular sus funciones.

Alternativamente, es posible que los nV-exRNA carezcan de función particular y sean simples producto de desecho del metabolismo celular y/o vida de la célula.[15] Por otro lado, los nV-exRNAs podrían desempeñar un rol en la homeostasis metabólica del organismo, siendo completamente degradados por las RNasas extracelulares para liberar nucleótidos o sus precursores, que podrían luego ser reutilizados y redistribuidos hacia otras células del organismo.[15] Una posibilidad intrigante es que la rápida liberación de nV-exRNA constituya un mecanismo para reprogramar la expresión génica de una célula al deshacerse de aquellos transcriptos que no precisa.[15]

Aún más intrigante es la posibilidad de que los nV-exRNAs sí participen activamente en la comunicación célula-célula y que este proceso sea regulado por las RNasas extracelulares. Las RNasas podrían modificar el contenido de nV-exRNAs originalmente liberado al espacio extracelular, generando perfiles moleculares distintivos según el grado de actividad enzimática. Estos perfiles, a su vez, podrían luego ser decodificados por células aceptaras generando distintas respuestas. En este contexto, resulta particularmente relevante la posibilidad de que los nV-exRNAs participen en la comunicación intercelular al ser reconocidos por células del sistema inmune. Estas células poseen sensores especializados en la detección de RNA, que -como se introducirá próximamente- pueden reconocer RNA parcialmente degradado. Considerando que los nV-exRNAs probablemente experimentan algún tipo de fragmentación por nucleasas extracelulares, resulta más plausible postular un mecanismo de comunicación mediado por estos sensores inmunitarios, que uno basado en la transferencia intacta de exRNAs capaces de conservar la función que ejercían en la célula de origen y trasladar esa misma función a una célula aceptora.

En las próximas secciones introduciremos algunos conceptos generales sobre el funcionamiento del sistema inmune para luego focalizarnos en los sensores de RNA.

5. Generalidades sobre el sistema inmune

El sistema inmune (SI) se conforma por diversos órganos, células y componentes solubles que actúan de manera conjunta y coordinada para reconocer, contener y eliminar una noxa (microorganismos patógenos, células tumorales, daño por luz ultravioleta y trauma esteril).[81] Una característica fundamental de este sistema es su capacidad de discriminar entre lo propio y lo ajeno, o bien entre lo “normal” y “lo alterado”. Por lo tanto, el SI cumple un rol esencial en mantener la homeostasis del organismo, con la dificil tarea de proteger lo propio, eliminar el insulto inmunológico y reparar el daño generado[82] . En términos generales, el sistema inmune se divide en dos grandes ramas: el sistema inmune innato (SII) y el sistema inmune adaptativo (SIA), que actúan, en condiciones normales, de manera coordinada.[81]

El SII está constituido por monocitos, macrófagos, neutrófilos, células NK, células dendríticas convencionales y células dendríticas plasmacitoides, así como por componentes solubles, entre ellos el sistema del complemento y péptidos antimicrobiano (solo por mencionar algunos ejemplos). Estas células y moléculas circulan en la sangre y linfa, y además se encuentran en sitios donde comúnmente pueden ingresar patógenos.[81,83] Las células del sistema inmune, en particular aquellas del sistema inmune innato, cuentan con receptores llamados PRRs (del inglés, *pattern recognition receptors*), codificados en la línea germinal y que han sido evolutivamente seleccionados para reconocer un conjunto finito de motivos moleculares llamados señales de peligro.[84] Estas señales de peligro incluyen motivos característicos y conservados en los patógenos denominados PAMPs (del inglés, *pathogen associated molecular patterns*) y motivos que derivan del daño celular denominados DAMPs (del inglés, *damage associated molecular patterns*) que ocurren usualmente en forma secundaria frente a una infección, trauma o proceso tumoral.[85] A través de los PRRs, el SII detecta de manera rápida la presencia de patógenos y daño tisular que estos provocan, activando mecanismos efectores destinados a eliminarlos y a promover la reparación de los tejidos.[81,83] La activación de estos receptores también induce la síntesis y liberación de mediadores químicos, como citoquinas y quimioquinas, que inician el proceso inflamatorio. La inflamación favorece el reclutamiento de células y proteínas desde la sangre hacia el sitio de infección o lesión, y constituye un paso esencial para el establecimiento de la respuesta inmune adaptativa.[81,83] En este proceso, las células dendríticas convencionales desempeñan un papel central ya que son las únicas capaces de activar linfocitos T vírgenes y de esa manera dar comienzo a una respuesta inmune adaptativa específica y especializada. Estas células fagocíticas especializadas internalizan y procesan antígenos, presentando en su superficie fragmentos proteicos -derivados, por ejemplo, de patógenos o células tumorales- que permiten la activación de linfocitos T y B específicos[86] .

El SIA está constituido principalmente por dichas células, los linfocitos B y T. A su vez, los linfocitos T pueden subdividirse en dos grandes poblaciones principales: linfocitos T colaboradores y linfocitos T citotóxicos.[81,83] Tanto los linfocitos B como los T poseen la capacidad de generar un repertorio casi ilimitado de receptores de membrana mediante la recombinación somática de diferentes segmentos génicos presentes en sus genomas. Estos receptores corresponden al BCR (del inglés, *B cell receptor*) y al TCR (del inglés, *T cell receptor*). Ante la presencia de un patógeno o célula tumoral, se activan y expanden clonalmente la población de linfocitos con BCRs y TCRs capaces de reconocer de manera específica antígenos del patógeno o tumor.[81,83]

La acción coordinada de los linfocitos B y T potencia los mecanismos efectores de la inmunidad innata. Los linfocitos B activados secretan anticuerpos específicos (versión soluble del BCR) que facilitan la activación del sistema del complemento, promueven la fagocitosis de patógenos y neutralizan partículas virales.[81,83] Por su parte, los linfocitos T colaboradores estimulan otras células inmunes, potenciando sus funciones efectoras; por ejemplo, favorecen la capacidad de macrófagos y neutrófilos para degradar microorganismos fagocitados. En tanto, los linfocitos T citotóxicos reconocen y eliminan células infectadas por virus o con características tumorales. Una propiedad distintiva del SIA es que su activación genera linfocitos B y T de larga vida, capaces de persistir en el organismo tras la resolución de la infección.[81,83] Gracias a estas células, un segundo encuentro con el mismo agente desencadena una respuesta adaptativa mucho más rápida y eficaz. Este mecanismo exclusivo del SIA, denominado memoria inmunológica, constituye la base de la protección inducida por las vacunas.[81,83]

El sistema inmune está finamente regulado para garantizar el inicio y la finalización adecuada de las respuestas inmunes. La alteración de estos mecanismos puede dar lugar a patologías autoinflamatorias o autoinmunes.[81] Ambas se caracterizan por un funcionamiento defectuoso del sistema inmune que provoca inflamación persistente y daño en órganos y tejidos. No obstante, difieren en que las enfermedades autoinflamatorias suelen originarse por la desregulación de la inmunidad innata[87] , mientras que las autoinmunes involucran también alteraciones en la inmunidad adaptativa.[88] En particular, las enfermedades autoinmunes se caracterizan por la generación de células B y/o T autorreactivas que reconocen antígenos propios.[88] Un ejemplo de esto es el LES, en donde se suelen generar autoanticuerpos contra DNA y contra complejos ribonucleoprotéicos[89] , probablemente como consecuencia de la liberación de nV-exRNAs.[15] Además, como veremos próximamente, la sobre activación da algunos PRRs involucrados en reconocer ácidos nucleicos, en particular RNA, parecería ser uno de los gatillos de esta patología autoinmune.

6. Sensores de RNA del sistema inmune

a) Algunas generalidades sobre los sensores de RNA

Las células del sistema inmune innato, como macrófagos, células dendríticas convencionales y células dendríticas plasmocitoides, están equipadas con un amplio repertorio de PRRs capaces de reconocer ácidos nucleicos.[81] Estos sensores de RNA, a priori, reconocen algunas características moleculares de los ácidos nucleicos presente en virus y bacterias. Nos focalizaremos principalmente en aquellos PRRs que reconocen RNA. Estos PRRs incluyen a los receptores endosomales de la familia Toll: TLR3, TLR7, TLR8 y TLR13 (este último presente solamente en roedores) y a los receptores citosólicos RIG-I y MDA5.[90]

b) Sensores de RNA pertenecientes a la familia de los TLRs

Los TLRs (del inglés, *Toll-like receptors*), que reconocen RNA son estructuralmente muy similares. Además, a diferencia de otros TLRs que se expresan en la membrana plasmática, estos tienden a estar localizados exclusivamente a nivel de la membrana endosomal.[91] Contienen un dominio topológicamente extracelular rico en repetidos de leucina (LLR) que apunta al interior de endosomas y participa en la unión de ligandos internalizados, un dominio helicoidal transmembrana que los ancla a la membrana endosomal y un dominio citosólico Toll/receptor de IL-1 (TIR) involucrado en las casadas de señalización. El reconocimiento de los ligandos por estos TLRs dispara su dimerización, acercando los dominios TIR y desencadenado cascadas de señalización rio abajo (Figura 1). A pesar de su similitud estructural, estos TLRs reconocen ligandos muy diferentes. TLR3 reconoce principalmente RNA doble cadena mayor a 40 pares de bases.[92,93] TLR7 y TLR8 reconocen productos de degradación de RNA simple cadena generados por el procesamiento de RNasas endosomales, en particular RNasa T2, RNasa 2 y posiblemente la RNasa 6.[94–97] Estos sensores cuentan con dos sitios de unión y generalmente ambos son necesarios para su activación. Estudios cristalográficos de ambos sensores indican que el sitio 1 une nucleósidos, mientras que el sitio 2 reconoce pequeños fragmentos de RNA de cadena simple, de generalmente dos o tres nucleótidos. En el caso de TLR7, se requiere la unión de guanosina en el sitio 1 y de trímeros con la secuencia UUX en el sitio 2.[98] Por su parte, TLR8 muestra preferencia por uridina en el primer sitio y por dímeros UG en el segundo.[99] TLR13, que está presente solo en roedores, es el único de estos sensores de RNA que parecería ser secuencia específico ya que reconoce un motivo de 9-12 nucleótidos presente en la subunidad mayor del RNA ribosomal bacteriano.[100,101] (Figura 1) Esta secuencia también ha sido detectada en algunos virus. TLR3 señaliza principalmente vía la proteína adaptadora TRIF (del inglés, *TIR-domain-containing adapter-inducing interferon-β*), mientras que TLR7, TLR8 y TLR13 señalizan vía MyD88 (del inglés, *Myeloid differentiation primary response 88*). El reconocimiento por parte de estos TLRs, gatilla múltiples vías de señalización y la activación de factores de transcripción como NF-κB, IRF3 y IRF7 que, luego de translocar al núcleo, desencadenan la transcripción de citoquinas pro-inflamatorias e interferones de tipo I (Figura 1). En última instancia, los interferones de tipo I (IFN-α e IFN-β) inducen, mediante señalización autocrina y paracrina, la transcripción de múltiples genes de respuesta a interferón (ISGs, del inglés, *Interferon stimulated genes*) (Figura 1). Los TLRs que reconocen RNA están principalmente expresados en células del sistema inmune innato como macrófagos, células dendríticas convencionales y plasmacitoides, aunque TLR3 y TLR7 también se expresan en linfocitos B.[81]

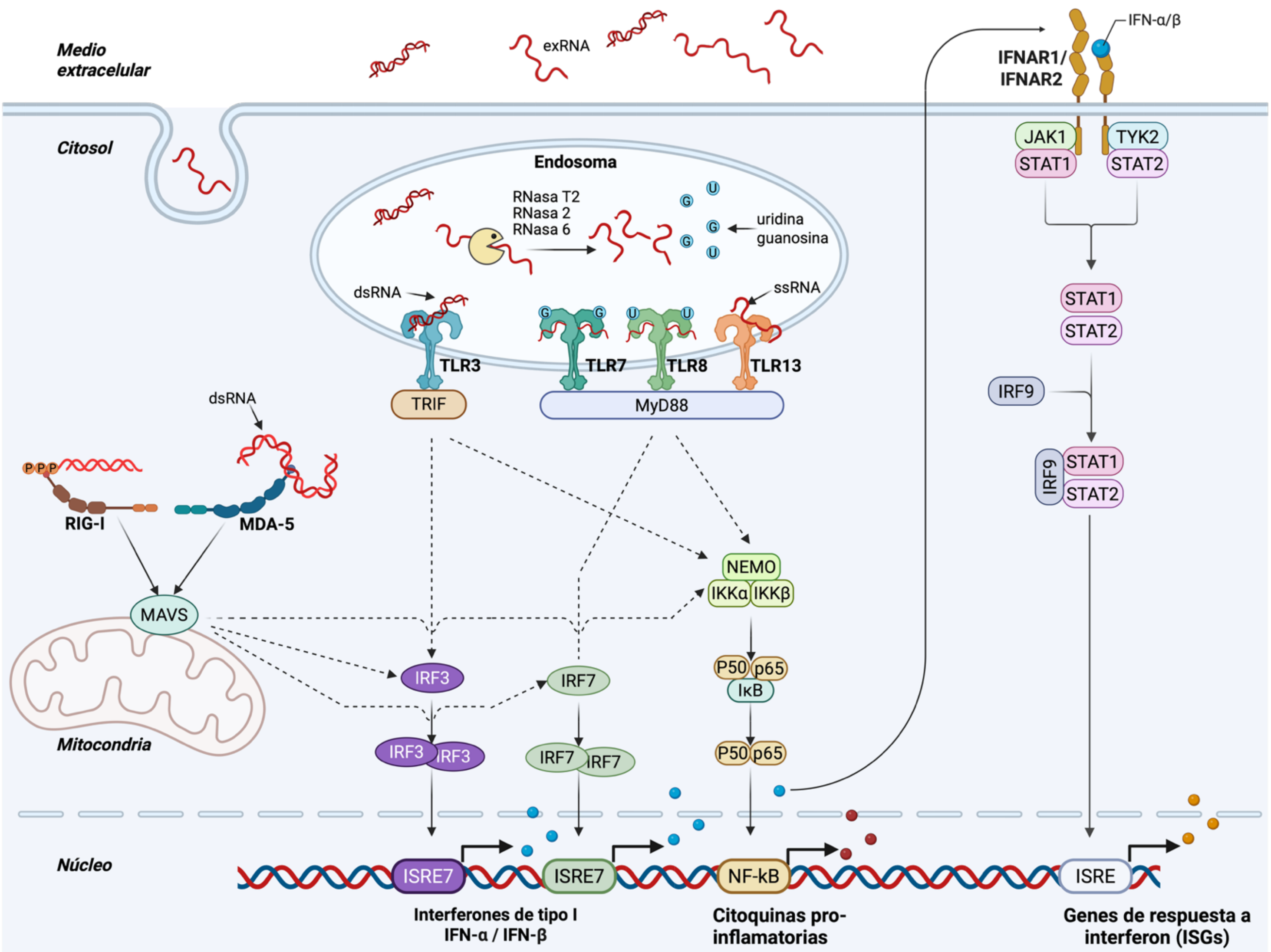

Figura 1. Sensores de RNA de la inmunidad innata y esquema simplificado de las principales vías de señalización que conducen a la producción de citoquinas proinflamatorias e interferones de tipo I tras su activación. Se muestra también la señalización autócrina mediada por interferones de tipo I, que culmina en la inducción de genes de respuesta a interferón. Las flechas punteadas indican la presencia de diversos complejos proteicos implicados en la transducción de señales, que no se representan por motivos de simplicidad. La información sobre las vías de señalización fue tomada de: [102–105]

c) Sensores de RNA pertenecientes a la familia de los RLRs

Existen dos sensores principales que reconocen RNA en el citoplasma y su expresión no depende necesariamente de la presencia de interferones del tipo I en el medio extracelular. Estos PRRs pertenecen a la familia de los RLRs (del inglés, *retinoic acid-inducible gene I like receptors*), que incluye a RIG-I (del inglés, *retinoic acid-inducible gene I*), y a MDA-5 (del inglés, *melanoma differentiation-associated protein 5*).[102] La familia de los RLRs incluye una tercera proteína, LGP2 (del inglés, *laboratory of genetics and physiology 2*) que no es formalmente un sensor de RNA sino que participaría en regular la activación de RIG-I y MDA-5, y, al interactuar con Dicer, en la regulación cruzada entre la vía del interferón y la del RNAi.[106] RIG-I y MDA-5 poseen un dominio carboxi terminal (CTD) seguido de un dominio helicasa y un dominio CARD (del inglés, *caspase activation and recruitment domain*).[102] El dominio CTD y helicasa participan en el reconocimiento de RNAs y el dominio CARD media las vías de señalizaciones una vez activados estos sensores. RIG-I reconoce RNA doble cadena de extremos romos que esté tri- o di-fosforilado en el extremo 5' y en donde la ribosa del primer nucleótido carezca de metilación en el oxígeno de la posición 2' (sin 2'-O-metilación).[102] Estas características son comunes a los RNAs virales y, como veremos más adelante, generalmente está ausentes en transcriptos endógenos. Respecto a MDA-5, inicialmente se creyó que reconocía preferentemente RNA doble cadena largo ya que se activa en respuesta a la transfección de Poly(I:C), sin embargo, hoy no está del todo claro las características moleculares de sus ligandos de RNA.[107] Una vez unen sus ligandos, estos sensores sufren cambios conformacionales, multimerizan, y a través de sus dominios CARD se unen a la proteína MAVS (del inglés, *mitochondrial antiviral signalling protein)*, que desencadena cascadas de señalización que culminan en la activación de IRF3, IRF7 y NF-κB dando lugar a potentes respuestas inflamatorias similares a las que fueron mencionadas para los TLRs.[102] (Figura 1)

d) El reconocimiento aberrante por estos sensores conduce a patologías con componente inflamatorio

Generalmente, los TLRs y RLRs que reconocen RNA se activan en respuesta a virus y bacterias, desencadenando mecanismos efectores destinados a contener la infección, eliminar patógenos y guiar al sistema inmune adaptativo para que generar respuestas específicas contra el patógeno en cuestión.[108] Sin embargo, cada vez se acumula más evidencia respecto a que estos PRRs no distinguen de manera perfecta el RNA propio y el RNA de microorganismos. Esto resulta comprensible si se considera que, a diferencia de otros PAMPs o DAMPs, el RNA no presenta diferencias estructurales drásticas entre bacterias, virus y mamíferos. Además, varios de estos sensores reconocen RNAs cortos que, a priori, podrían provenir de múltiples secuencias diferentes. En línea con esta idea, se ha observado que alteraciones en la expresión de estos PRRs, así como mutaciones en los propios receptores o en proteínas clave para su maduración, se asocian con el desarrollo de enfermedades autoinmunes y autoinflamatorias, como el LES, Psoriasis y diversas interferonopatías como AGS (del inglés, *Aicardi-Goutières syndrome*).[87,109–114] En estas situaciones, el exRNA propio emerge naturalmente como un posible activador de los sensores de RNA, en particular de los TLRs.

En esta línea: el exRNA liberado por cardiomiocitos puede ser reconocido por macrófagos y neutrófilos vía TLR7[115], células necróticas pueden activar macrófagos vía TLR3[116], y la exposición a exRNA promueve la diferenciación a macrófagos de fenotipo pro-inflamatorio.[117] A su vez, la interacción entre exRNA endógenos y proteínas propias como el péptido LL37 facilita la internalización de exRNAs, y la consecuente activación del SI.[118] En células dendríticas estos efectos son dependientes de TLR7 y TLR8.[119] Por otra parte, células dendríticas plasmacitoiodes responden a la transfección de complejos ribonucleoproteicos derivados del spliceosoma, de nuevo por señalización vía TLR7 y TLR8.[120] Estos complejos del spliceosoma también pueden ser reconocidos por linfocitos B autorreactivos vía TLR7.[121]

El reconocimiento de exRNAs por estos sensores también jugaría un rol en la biología tumoral. Se ha observado que la expresión de TLR3 es necesaria para la respuesta antitumoral desencadenada por agentes quimioterapéuticos, probablemente debido a reconocimiento de exRNAs aún no identificados.[122] Salvo en algunas situaciones, no está del todo claro qué tipos de exRNAs propios gatillan estos efectos. Pensamos que en la mayoría de los casos estos sean exRNAs no vesiculares derivados de muerte celular.[123]

e) Estrategias para evitar la sobre activación de los sensores de RNA

Las células del sistema inmune emplearían diversos mecanismos para evitar que los sensores de RNA sean activados por RNAs propios tanto intra como extracelulares y desencadenen respuestas inflamatorias patológicas que contribuyan al desarrollo o agravamiento de enfermedades autoinmunes o autoinflamatorias.[91,124] Estas estrategias incluyen: 1) Compartimentalización de los sensores de RNA. 2) Pequeñas diferencias bioquímicas entre RNAs propios y RNA de patógenos. 3) Regular los niveles de los sensores de RNA y las vías de transducción de señales. 4) Modular la disponibilidad de los ligandos.

La totalidad de los TLRs que reconocen ácidos nucleicos están secuestrados en endosomas. Se piensa que esta estrategia maximiza el reconocimiento de RNAs derivados de patógenos previamente internalizados y evita la activación de estos sensores por ácidos nucleicos propios circulantes. De hecho, mutaciones en UNC93B1, proteína involucrada en el transporte de estos TLRs a los endosomas, está involucrada con el desarrollo de autoinmunidad por sobre-activación de TLR7.[114]

Las diferencias bioquímicas entre el RNA endógeno y el RNA de patógenos también condiciona el reconocimiento por estos sensores. Por ejemplo, los RNAs eucariotas sufren numerosas modificaciones postranscripcionales, habiéndose identificado más de 200 tipos diferentes que regulan múltiples aspectos de su biología.[125] Entre las modificaciones más comunes se encuentran las metilaciones en las bases nitrogenadas, como N6-metiladenosina (m6A) y 5-metilcitidina (m5C); la metilación de la ribosa en la posición 2' (2'-O-metilribosa, 2'-O-me); la isomerización de uridina a pseudouridina (Ψ); y la desaminación de adenosina a inosina (I), entre otras.[126] Gracias a los trabajos pioneros de Katalin Karikó y colaboradores, se conoce que muchas de estas modificaciones influyen en el reconocimiento del RNA por los TLRs, en particular TLR7 y TLR8. De hecho, la presencia de modificaciones como Ψ y m5C impide que RNAs transfectados sea reconocidos por estos sensores y que se desencadenen respuestas pro-inflamatorias.[127] Además, Karikó y colaboradores observaron que los RNAs propios de células eucariotas suelen estar hipermodificados en comparación con los RNAs de patógenos, lo que contribuye a que estos últimos sean más fácilmente detectados por el sistema inmune.[127] De hecho, este hallazgo fue fundamental para el desarrollo de las vacunas basadas en mRNA, las cuales incorporan bases modificadas con el objetivo de evitar respuestas inflamatorias exacerbadas producto del reconocimiento por estos TLRs.[128–131] Muy recientemente Flynn y colaboradores han observado que la glicosilación de RNAs endógenos constituiría otro mecanismo para evitar su reconocimiento, principalmente por TLR3 y TLR7.[75] Por otra parte, la mayoría de los RNAs propios intracelulares maduros carecen o esconden sus extremos 5'PPP y 5'PP evitando así el reconocimiento por parte de los RLRs.[102] En este sentido, las formas maduras de los rRNA 28S, 18S, 5.8S y de los tRNAs presentan extremo 5' monofosfato, los mRNAs y lncRNAs presentan un CAP en su extremo 5'PPP. Otros RNAs no codificantes que sí presentan extremo 5'PPP libre, en particular los transcriptos de la polimerasa III, están metilados en bases claves o asociados a proteínas que esconden sus 5`PPP de estos sensores.[102] Además, los transcriptos eucariotas suelen ser simple cadena evitando tanto el reconocimiento por TLR3 como por los RLRs. La desaminación de adenina a inosina en los mRNAs parecería ser clave en este proceso ya que evita la formación de regiones doble cadena en mRNAs que de lo contrario serían reconocidas por los RLRs, gatillando potentes respuestas inflamatorias.[132–134]

Las células regulan finamente la expresión de los sensores de RNA ya que, como se mencionó anteriormente, alteraciones en los niveles de estos sensores pueden conducir al reconocimiento de ligandos propios y patologías con componente autoinflamatorio o autoinmune. En particular, la expresión de los TLRs suele estar bastante restringida a células del SII y no todos los tipos celulares los expresan en igual medida. A modo de ejemplo, los macrófagos encargados de eliminar cuerpos apoptóticos presentan una baja respuesta frente a ácidos nucleicos, en parte debido a la reducción en la expresión de ciertos TLRs capaces de reconocer este tipo de moléculas.[135]

La disponibilidad y concentración de ligandos probablemente sea uno de los factores más importantes en determinar la activación de estos sensores de RNA. Una forma de evitar que los exRNAs circulantes activen dichos sensores es degradarlos en el espacio extracelular evitando que ingresen a las células. En este sentido, el espacio extracelular y los biofluidos suelen ser ricos en RNasas extracelulares[136], y ya en la década del 80 se postuló que estas enzimas podrían actuar como reguladoras de los niveles de exRNA.[137] De hecho, la sobreexpresión de RNasa 1 atenúa los efectos patológicos en modelos de LES y de isquemia-reperfusión.[138,139] Sin embargo, el papel de estas enzimas en modular los efectos del exRNAs sobre el SI no han sido completamente dilucidados. Ratones *knockout* para RNasa 1 -una de las muchas RNasas extracelulares- tienen mayores niveles de exRNA circulante pero no presenten mayor secreción de citoquinas proinflamatorias ni desarrollan autoinmunidad.[140] Esto podría descartar el rol de las RNasas extracelulares en controlar la disponibilidad de ligandos, pero probablemente se deba a que, como veremos en el próximo capítulo, en el espacio extracelular existen múltiples RNasas. Si bien existe evidencia que sugiere que estas enzimas son importantes para impedir el reconocimiento de los exRNAs propios, su papel en modular la internalización y el reconocimiento de exRNAs -particularmente de exRNAs no vesiculares y exRNAs desnudos- ha sido poco estudiado y no es completamente comprendido.

7. RNasas de la familia A

a) Generalidades sobre esta familia de proteínas

Los vertebrados poseen una superfamilia única de proteínas con actividad ribonucleolítica que son secretadas al espacio extracelular. A estas ribonucleasas se las conoce como RNasas de la familia A. De ahora en más, al utilizar el término RNasa, nos estaremos refiriendo exclusivamente a este grupo de proteínas dejando de lado las múltiples enzimas capaces de cortar el RNA que existen dentro de las células.

El miembro prototípico de esta familia, la RNasa A pancreática -aislada originalmente del páncreas de chanchos[141] y homóloga a la RNasa 1 humana y murina- fue uno de los modelos favoritos de los bioquímicos durante el siglo XX. La RNasa A fue una de las primeras proteínas en secuenciarse (luego de la insulina y hemoglobina)[142,143] , la primera enzima con mecanismo catalítico propuesto (aún sin conocerse su estructura)[144] y la tercera enzima cuya estructura tridimensional fue resuelta.[145] Además, el uso de la RNasa A dio lugar a varios premios Nobel, relacionados al estudio del plegamiento de las proteínas, la secuenciación proteica y la síntesis de proteínas en fase sólida. A pesar de su extenso uso como modelo, como veremos más adelante, recién en la última década se ha tomado conocimiento de que estas proteínas están implicadas en múltiples procesos biológicos adicionales a la digestión del RNA en el aparato digestivo (función inicialmente sugerida para estas proteínas).[146]

El genoma humano codifica 13 genes de RNasas que localizan en un único *cluster* en el cromosoma 14. Ocho de estas proteínas (RNasa 1-RNasa 8) son RNasas prototípicas o canónicas ya que poseen actividad catalítica. Estas incluyen a la RNasa 1 (también llamada RNasa pancreática), RNasa 2 (o EDN, del inglés *eosinophil derived neurotoxin*), RNasa 3 (o ECP, del inglés *eosinophil cationic protein*), RNasa 4, RNasa 5 (también conocida como Angiogenina), RNasa 6, RNAsa 7 y RNasa 8. Por otro lado, las RNasas 9-13 carecen de actividad nucleasa.[147,148] En ratones, el panorama es más complejo, ya que existen dos clústeres genómicos que codifican genes de RNasas: uno ubicado en el cromosoma 14, sinténico con el genoma humano, y otro en el cromosoma 10, que no tiene homología con el genoma humano. Como resultado de múltiples rondas de duplicación génica -particularmente de los genes correspondientes a las RNasas 2, 3 y 5- los ratones expresarían alrededor de 15 o más RNasas funcionales. Sin embargo, carecen de homólogos para RNasa 7 y 8.[147]

Las RNasas de la familia A han experimentado una rápida evolución y divergencia, similar a lo que ocurre para ciertos genes del sistema inmune. A pesar de que existe una baja identidad de secuencia entre algunos miembros de esta familia (menor al 30%), todas presentan similar estructura y el motivo firma CKXXNTF[146] (Figura 2A). Las RNasas de la familia A se caracterizan por ser proteínas pequeñas, monocatenarias, de unos 130 aminoácidos que adquieren un plegamiento globular en forma de riñón, en donde su estructura terciaria está estabilizada por entre 3 y 4 puentes disulfuros (Figura 2B). Estas proteínas son endonucleasas de secreción que degradan preferentemente RNA simple cadena.[149] El mecanismo catalítico, que involucra a los residuos His12, Lis41 e HIS119 (Figura 3A), consiste en una primera reacción de transfosforilación que rompe el enlace P-O^5 entre dos nucleótidos consecutivos del RNA (YpN, [Y:pirimidians y N:cualquier nucléotido]) generado como producto un RNA con fosfato cíclico en el extremo 3´ (Y>p). Posteriormente, la hidrólisis del enlace P-O^2 resuelve el fosfato cíclico.[143,150] Las RNasas de la familia A presentan preferencia por cortar el enlace fosfodiéster del RNA al 3' de residuos de pirimidina y escasa actividad frente a las purinas.[151] Utilizando a la RNasa A pancreática bovina y homopolímeros de RNA simple cadena, se observó que la enzima presenta la siguiente preferencia de sustratos: poly(C) > poly(U) >>> poly(A).[152] Poly(C) es cortado 20 veces más rápido que poly(U) y poly(A) es cortado 10^4-10^5 veces más lento que poly(U).[152] Similares preferencias se han observado para la RNasa 1 humana, homóloga de la RNasa A bovina pancreática.[153,154] Sin embargo, otros miembros de esta familia, como las RNasas 2, 3 y 4 serían catalíticamente más activas frente a poly(U) que a poly(C).[153,154]

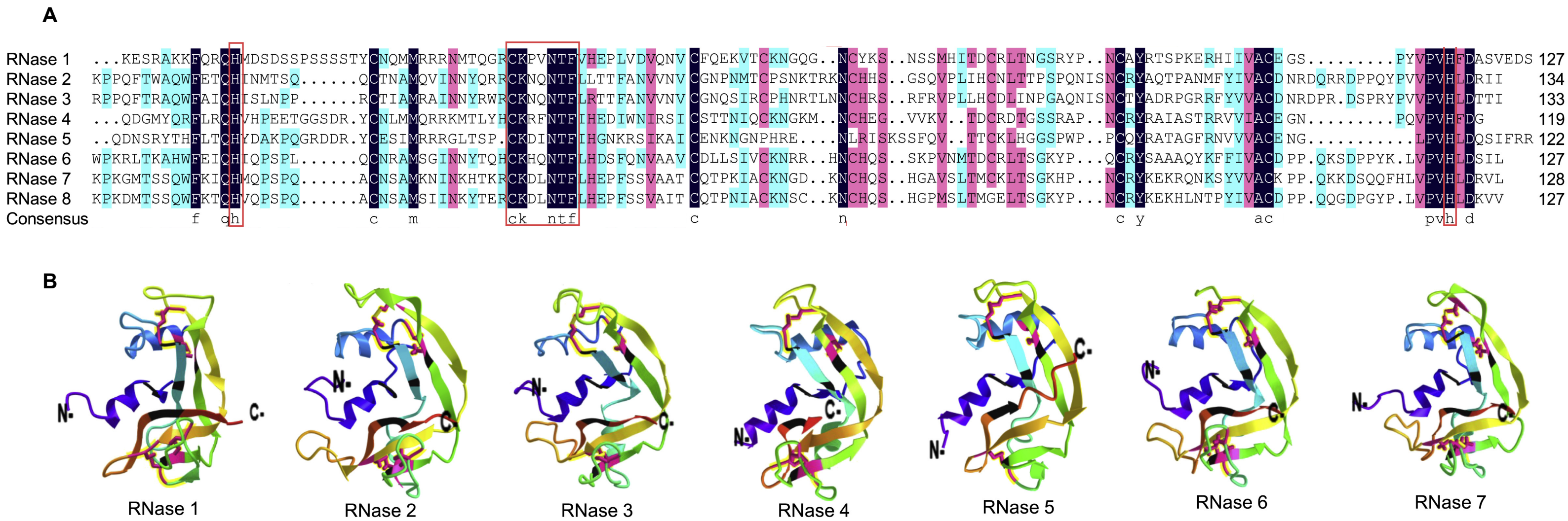

Figura 2. Alineamiento de las secuencias peptídicas (A) y comparación de las estructuras (B) correspondientes a las RNasas canónicas humanas. El sitio catalítico se señala en negro. Los puentes disulfuros se muestran en magenta. Figura adaptada de:[146].

Por otra parte, algunos miembros de la familia de las RNasa A, en particular RNasa 1, pueden degradar -aunque en forma menos eficiente- RNA doble cadena de origen viral, y de origen sintético, como poly(A:U) y poly(I:C).[149,153] La actividad RNasa parecería variar entre los diferentes miembros de esta familia. En humanos, donde se dispone de más información, se observa que las RNasas 1, 2 y 3 presentan elevada actividad catalítica de magnitud comparable. En contraste, las RNasas 4, 6, 7 y 8 son 8-100 veces menos activas, mientras que la RNasa 5 se considera la menos activa de todas siendo 10^5 veces menos activa que RNasa.[146] Sin embargo, recientemente se ha reportado que esta enzima se posiciona en el sitio aceptor vacío de los ribosomas durante el estrés celular, y allí sufre un cambio conformación que aumenta su actividad catalítica, pudiendo cortar tRNAs que se acercan al ribosoma bajo estas condiciones de estrés.[155] También resulta interesante que la actividad de estas enzimas variaría entre diferentes especies de vertebrados, en el caso de la RNasa 1, esta parecería ser más activa en humanos y murciélagos que en roedores y rumiantes.[149]

Las RNasas son proteínas de expresión ubicua, aunque sus niveles varían entre distintos tejidos. Las RNasas 1, 4, 5, se detectan en múltiples órganos y tejidos, mientras que la expresión de las RNasas 2 y 3 está restringida principalmente a la médula ósea y al tracto urinario, donde son secretadas principalmente por eosinófilos y neutrófilos.[156,157] El plasma es especialmente rico en RNasas, en particular RNasa 1, la cual es secretada al torrente sanguíneo principalmente por células endoteliales.[158,159] La expresión ubicua de las RNasas, su rápida evolución y la diversidad de miembros que forman parte de esta familia, sugiere que estas proteínas participan en múltiples procesos biológicos, más allá de su función originalmente propuesta en la digestión de RNA en el aparato digestivo.

b) *Algunas funciones extracelulares de las RNasas de la familia A*

Además de su función clásica en la digestión del RNA de origen dietario, las RNasas de la familia A han sido implicadas en una amplia variedad de procesos biológicos. Estos incluyen: la regulación de los niveles de RNA intra y extracelular, la angiogénesis y reparación de tejidos, la defensa contra patógenos -gracias a la actividad antibacteriana, antiviral y antifúngica de algunas de ellas-, el mantenimiento de la esterilidad en ciertos biofluidos y la generación de pequeños fragmentos de RNA con funciones reguladoras a partir del clivaje selectivo de algunos RNAs no codificantes como tRNAs, entre otras varias funciones.[146,160]

Las RNasas de la familia A serían actores relevantes del sistema inmune innato. Varias de estas proteínas son secretadas por células inmunes como neutrófilos y eosinófilos (RNase 2 y RNase 3), macrófagos y células dendríticas (RNase 4 y RNase 6) y su expresión se induce frente a infecciones.[160] En este contexto, las RNasas favorecerían la eliminación de patógenos por diferentes mecanismos. Por ejemplo, las RNasas 4, 6 y 7 desempeñarían un papel clave en el combate de infecciones bacterianas del tracto urinario.[161–163] Esto se debe, en parte, a su alta carga neta positiva, que les permite comportarse como péptidos antimicrobianos capaces de desestabilizar la membrana y pared de bacterias gram+ y gram- lo cual culmina con la lisis bacteriana. Por otra parte, se ha sugerido que la RNasa 2 podría actuar como quimioquina, y alarmina al unirse directamente a TLR2[164] , esto probablemente esté relacionado a la gran similitud estructural que existe entre RI y los TLRs.[165] Por cuestiones de espacio, nos focalizaremos principalmente en aquellas posibles funciones más directamente relacionadas a la temática de la tesis, en particular el rol de estas enzimas sobre el exRNA.

A finales de 1980, Steven Benner notó que la amplia distribución de las RNasas de la familia A en tejidos y biofluidos sugería que estas enzimas debían desempeñar un rol sobre sustratos extracelulares. Desde su perspectiva, la existencia de RNasas carecería de sentido evolutivo si no existieran RNAs extracelulares sobre los cuales pudieran actuar.[136,137] A partir de esta observación, propuso la hipótesis -en ese momento sin evidencia experimental concluyente- de que una de las funciones principales de las RNasas podría ser la regulación de los niveles de exRNAs circulantes en biofluidos.[137] Esto se basaba en la posibilidad de que dichos RNAs, al igual que las hormonas, contuvieran información relevante para el desarrollo de los organismos y actuasen como agentes en la comunicación intercelular, razón por la cual, regular su concentración por parte de estas enzimas sería central para el correcto funcionamiento del organismo.[136,137] Trabajos más recientes han encontrado evidencia a favor de esta hipótesis. En este sentido, ratones *knockout* en RNasa 1 (la principal RNasa sanguínea) presentan mayores niveles de RNAs extracelulares totales en sangre.[140] Esto tienen sentido ya que, como fue mencionado anteriormente, las células endoteliales secretan grandes niveles de RNasa 1 al torrente sanguíneo.[159] Se ha sugerido que la RNasa 1 actuaría como "scavenger" de RNAs extracelulares, tanto en condiciones de homeostasis como en contextos patológicos, evitando que estas moléculas sean reconocidas por el sistema inmune y que se desencadenen respuestas inflamatorias perjudiciales.[166] En esta línea, en modelos murinos de isquemia/reperfusión, la administración ectópica de RNasa 1 redujo los niveles de TNF-α y atenuó el daño tisular en el corazón, posiblemente al degradar exRNAs proinflamatorios liberados durante el evento isquémico. Por otra parte, en modelos murinos transgénicos que sobreexpresan TLR7 y desarrollan una patología similar al Lupus, la sobreexpresión de RNasa 1 reduce la inflamación sistémica y prolonga la supervivencia de estos animales.[139]

c) las RNasas de la familia A pueden ingresar al interior de las células

Las RNasas de la familia A, pueden ingresar al interior celular por la vía endocítica. Se especula que el ingreso de estas proteínas estaría mediado por su carga neta positiva que permitiría interacciones con proteoglicanos como heparán sulfato.[167] Posteriormente, a través de mecanismos aún no completamente comprendidos, escapan de la vía endocítica e ingresan al citosol. Una vez alcanzan este compartimiento, incluso pueden dirigirse al núcleo.[168] En el interior de las células, estas enzimas retienen su actividad endonucleasa y cumplirían múltiples funciones. En situaciones de estrés celular como daño oxidativo, estrés nutricional e infecciones virales, algunas RNasas, en particular Angiogenina, cortan selectivamente tRNAs a nivel del anticodón y de los bucles T y D generando pequeños fragmentes de tRNA.[13,169] Estos fragmentos de tRNA inducidos por estrés regulan la expresión génica al inhibir la síntesis de proteínas mediante el desplazamiento de los factores de traducción eIF4G/eIF4A de RNAs capeados y no capeados.[11,170] Angiogenina contiene una señal de localización nuclear que media su transporte al núcleo. Dentro del núcleo induce la transcripción de RNA ribosomal y gatilla la proliferación celular.[168] Otras miembros de la familia, en particular RNasa 2 y la RNasa 6, en acción coordinada con otras enzimas con actividad ribonucleolítica como la RNasa T2, actuarían dentro de endosomas mediando el procesamiento parcial de RNAs simple cadena para generar los sustratos necesarios para la activación de TLR8.[95,97]

Si las RNasas de la familia A pueden ingresar a la célula, ¿por qué no degradan indiscriminadamente los RNAs celulares causando muerte celular? Esto no ocurre debido a que las células del organismo expresan una proteína capaz de unirse e inhibir la actividad ribonucleolítica de las RNasas de la familia A. Esta proteína, denominada Inhibidor de RNasas (RI), es una proteína citosólica de unos 50kD rica en repetidos de leucina que adquiere una estructura en forma de herradura.[171] RI une a las RNasas de la familia A con una estequiometria 1:1 e impide que las RNasas puedan unir y degradar RNA.[171,172] (Figura 3B) Esta interacción proteína-proteína es una de las más fuertes que se conocen en la naturaleza, con constantes de disociación del orden del femtomolar, lo que resalta la importancia de inhibir estas enzimas dentro de la célula para asegurar la supervivencia celular.[172] De hecho, RNasas ingenierizadas para evadir RI son tóxicas y conducen a la muerte celular.[173,174] En esta misma línea, células *knockout* para RNH1, el gen que codifica RI, son vulnerables a la acción de RNasa 1 y de Angiogenina extracelular.[175,176] RI es rico en cisteínas y parecería ser un sensor redox. De hecho, la oxidación de algunas de estas cisteínas y la posible formación de puentes disulfuro disminuye la afinidad de RI por las RNasas permitiendo que estas sean liberadas.[177] La oxidación de RI y la fosforilación de algunas RNasa han sido postulados como mecanismos para romper la unión RI:RNasa y permitir la acción regulada de estas enzimas dentro de la célula.[178]

El RI recombinante es ampliamente utilizado en los laboratorios de biología molecular cuando se trabaja con RNA. Por ejemplo, el RI suele añadirse durante la síntesis de cDNA, en diversos tratamientos enzimáticos del RNA y durante la generación de librerías para RNAseq. Si bien las formulaciones más frecuentes de RI comercial se basan en la secuencia humana o porcina, el RI recombinante murino carece de ciertos residuos de cisteína que lo vuelven más resistente a la oxidación, permitiendo que pueda ser utilizado *in vitro* e *in vivo.*[177]

Durante mi maestría, realizada en otro laboratorio, puse a punto un método de detección por RT-qPCR, para lo cual debí usar frecuentemente RI como un reactivo para evitar la degradación de las muestras con las que trabajaba. En aquel momento, no me había percatado que el RI era un inhibidor proteico de preciosa estructura, esencial para protegernos de las RNasas extracelulares, y que un día sería no ya un mero reactivo de laboratorio, sino un componente biológico esencial de mis estudios doctorales.

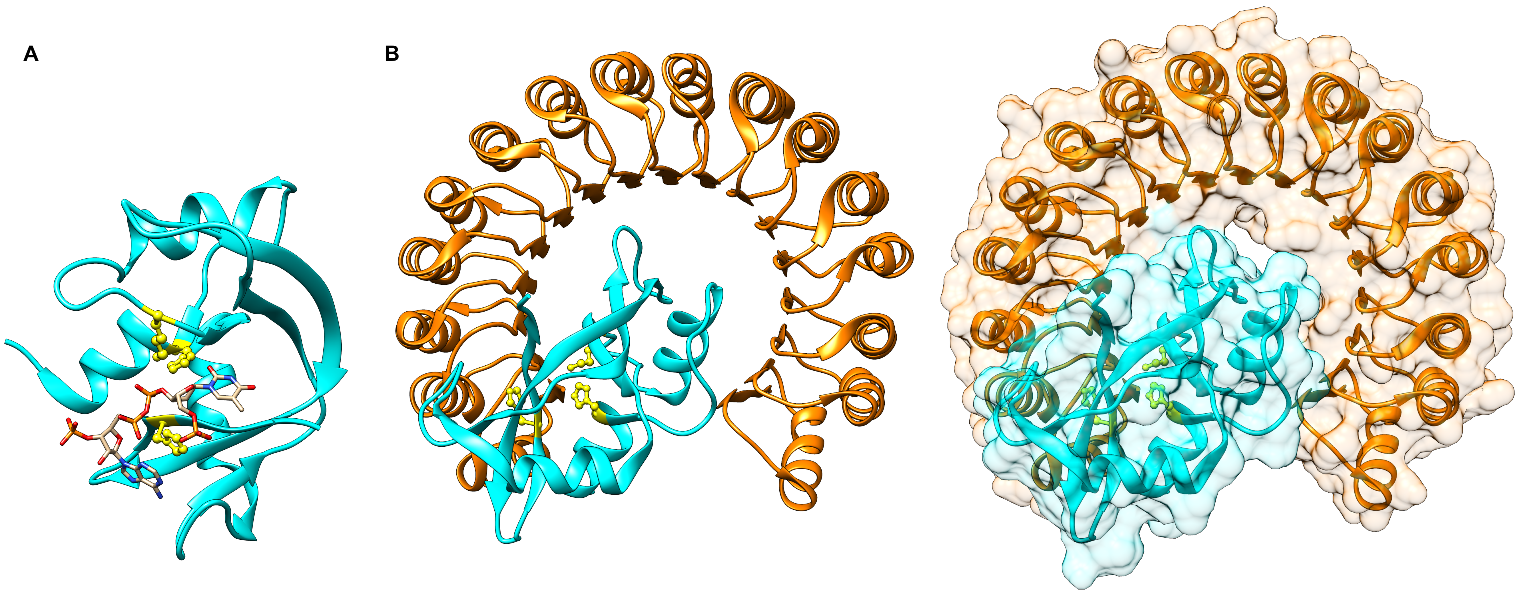

Figura 3. A) Estructura cristalográfica de la RNasa A bovina pancreática homóloga a la RNasa 1 humana y murina en complejo con el análogo de sustrato de ssRNA: 3’-fosfotimidina (3’-5’)-pirofosfato adenosina 3’-fosfato (PDB:1U1B). En Amarillo se muestran los residuos involucrados en la catálisis (Histidina 12, Lisina 41, Histidina 119). B) Estructura cristalográfica del inhibidor de RNasa humano en complejo con la RNasa 1 humana (PDB:1Z7X). En Amarillo se muestran los residuos involucrados en la catálisis que quedan enmascarados por la formación del complejo RI:RNasa 1.

8. exRNAs desnudos: ¿tienen relevancia funcional?

Llegado este punto, resulta pertinente retomar algunas interrogantes que, de forma explícita o implícita, han sido planteadas a lo largo de esta introducción ¿Son los nV-exRNAs, en particular los exRNAs desnudos, moléculas funcionales? Es decir, ¿pueden ser reconocidos, internalizados y modular la expresión génica en células receptoras? En la literatura científica existe una controversia sobre este punto, con evidencia tanto a favor como en contra respecto a su funcionalidad biológica. En lo que refiere a evidencia a favor, por mencionar algunos ejemplos ilustrativos, se ha observado que la administración intravenosa de RNasa 1 atenúa la inflamación en modelos de isquemia/reperfusión[138] y de politraumatismo[179], o que la sobreexpresión de esta enzima reduce la inflamación en un modelo murino de Lupus Eritematoso Sistémico.[139] Dado que las RNasas actuarían principalmente sobre nV-exRNAs, y en particular sobre exRNAs desnudos, estos trabajos sugieren que los exRNA desnudos tienen relevancia funcional, en particular en lo que refiere a su reconocimiento por parte del sistema inmune. Por otra parte, en pacientes con LES y otras enfermedades autoinmunes, se generan autoanticuerpos dirigidos contra complejos ribonucleoproteicos, e incluso contra RNA.[180–182] Dado que la generación de anticuerpos requiere la internalización de antígenos por parte de los linfocitos B, estos hallazgos sugieren que algunos nV-exRNAs podrían ser internalizados por células del sistema inmune en determinados contextos. Sin embargo, la comunidad científica ha asumido casi que como un dogma la idea de que las células son impermeables al exRNA desnudo y que estás moléculas por si solas no pueden atravesar las membranas biológicas, razón por la cual los RNAs terapéuticos (salvo pequeños ASOs modificados) deben si o si ser transfectados y/o encapsulados en nanopartículas lipídicas para poder ingresar a sus células diana.[55,183] En esta misma línea, y por poner un ejemplo muy ilustrativo, la estimulación de macrófagos cultivados *in vitro* con RNA desnudo bacteriano no genera ningún tipo de efecto en este tipo de células fagocíticas. Por el contrario, únicamente cuando el RNA bacteriano es transfectado se desencadena la liberación de múltiples citoquinas pro-inflamatorias.[100,184] Estas y otras observaciones parecerían echar por tierra la idea de que los exRNAs desnudos sean funcionales y/o puedan participar en la comunicación célula-célula.

¿Podemos reconciliar estas discrepancias? Esta tesis de doctorado buscará resolver esto.

Hipótesis

El nV-exRNA, incluyendo a los exRNAs desnudos, son moléculas bioactivas capaces de ser internalizadas y reconocidas por distintos tipos celulares.

Esto no ha sido observado en muchos trabajos debido al hecho de que la mayoría de los estudios en cultivo se realizan en presencia de suero fetal bovino, que es una fuente rica de RNasas extracelulares.

Inhibiendo las RNasas extracelulares, podemos estudiar la biología de la internalización y el reconocimiento de exRNAs desnudos.

La función biológica de las RNasas extracelulares, presentes y abundantes en biofluidos, es precisamente la de regular la biodisponibilidad de exRNAs no vesiculares, a los efectos de contrarrestar sus propiedades biológicas en contextos en los que esto podría dar lugar a respuestas sistémicas perjudiciales para el organismo.

Objetivo General

Estudiar el impacto de las RNasas extracelulares en determinar la composición del RNA extracelular no vesicular, y el elucidar el rol que tendrían estas enzimas en modular el ingreso, el reconocimiento, y la respuesta del sistema inmune al RNA extracelular no vesicular, con particular énfasis en el RNA extracelular desnudo.

Objetivos específicos

1. Caracterizar, mediante secuenciación de RNAs cortos (*small RNA sequencing*), la población de exRNAs no vesiculares liberados al medio extracelular por líneas celulares humanas, y elucidar la contribución de la actividad RNasa extracelular en la composición de los perfiles de RNAs extracelulares no vesiculares. (Artículo científico 1)

2. Estudiar la capacidad de células del sistema inmune innato, principalmente células dendríticas, monocitos y macrófagos, de responder al exRNA desnudo y evaluar el rol de las RNasas en este fenómeno (Artículo científico 2)

3. Elucidar los mecanismos moleculares implicados en el reconocimiento del exRNA desnudo por parte de células del sistema inmune innato (Artículo científico 2)

4. Determinar el rol de las RNasas en regular el ingreso de exRNAs desnudos al citosol y de actuar como moduladores de la captura y traducción de mRNAs desnudos extracelulares. (Artículo científico 2)

5. Estudiar el rol de las RNasa extracelulares en la detección de exRNAs desnudos en modelos *in vivo* (Artículo científico 2)

6. Escritura de un capítulo de libro sobre metodologías experimentales para el estudio de los tRNAs extracelulares vesiculares y no vesiculares. (Artículo científico 3)

Tesis por compendio de artículos

Artículo científico 1: Fragmentation of extracellular ribosomes and tRNAs shapes the extracellular RNAome

En este artículo científico se aborda el objetivo específico 1 de mi tesis doctoral. Mi contribución principal fue la realización completa de los análisis bioinformáticos de *small RNA-seq* sobre fracciones de RNA extracelular no vesicular liberadas por células humanas en cultivo, que fueron recolectadas en presencia o ausencia de inhibidores de RNasas (RI) y luego fraccionadas por tamaño mediante cromatografía de exclusión molecular.

La principal conclusión del estudio es que las células en cultivo liberan al espacio extracelular no vesicular prácticamente todos los biotipos de RNA, probablemente como consecuencia de la muerte celular. Sin embargo, debido a diferencias en la estabilidad intrínseca y en la susceptibilidad a la degradación por RNasas extracelulares, sólo persisten aquellos exRNAs no vesiculares ultrarresistentes, tales como los fragmentos de tRNA y ciertos fragmentos de rRNA. Esta observación se evidenció al comparar los perfiles de secuenciación entre muestras recolectadas con y sin inhibición de la actividad de RNasas. Otra importante observación que surge de este trabajo es que las células liberan ribosomas extracelulares que pueden inducir la maduración de células dendríticas. Lo que fue de hecho el primer paso de nuestro laboratorio hacia el estudio de las propiedades inmunológicas de los exRNAs, y constituyó el primer caso de colaboración entre mis dos tutores, siendo este el antecedente inmediato y principal sobre el que se constituyó mi proyecto de tesis de doctorado.

12874–12888 *Nucleic Acids Research, 2020, Vol. 48, No. 22* *Published online 12 August 2020*
doi: 10.1093/nar/gkaa674

Fragmentation of extracellular ribosomes and tRNAs shapes the extracellular RNAome

Juan Pablo Tosar[1,2,3,4,*], Mercedes Segovia[5], Mauricio Castellano[1,2], Fabiana Gámbaro[2,6], Yasutoshi Akiyama[3,4], Pablo Fagúndez[1,2], Álvaro Olivera[7], Bruno Costa[1,2], Tania Possi[2], Marcelo Hill[5], Pavel Ivanov[3,4,8] and Alfonso Cayota[2,9,*]

[1]Analytical Biochemistry Unit. Nuclear Research Center. Faculty of Science. Universidad de la República, Uruguay, [2]Functional Genomics Unit, Institut Pasteur de Montevideo, Uruguay, [3]Division of Rheumatology, Immunology and Allergy, Brigham and Women's Hospital, Boston, MA, USA, [4]Department of Medicine, Harvard Medical School, Boston, MA, USA, [5]Laboratory of Immunoregulation and Inflammation, Institut Pasteur de Montevideo, Uruguay. Immunobiology Department, Faculty of Medicine, Universidad de la República, Uruguay, [6]Molecular Virology Laboratory, Nuclear Research Center. Faculty of Science. Universidad de la República, Uruguay, [7]Centro Universitario Regional Este, Universidad de la República, Uruguay, [8]The Broad Institute of Harvard and M.I.T., Cambridge, MA, USA and [9]Department of Medicine, University Hospital, Universidad de la República, Uruguay

Received April 18, 2020; Revised July 19, 2020; Editorial Decision July 27, 2020; Accepted July 31, 2020

ABSTRACT

A major proportion of extracellular RNAs (exRNAs) do not copurify with extracellular vesicles (EVs) and remain in ultracentrifugation supernatants of cell-conditioned medium or mammalian blood serum. However, little is known about exRNAs beyond EVs. We have previously shown that the composition of the nonvesicular exRNA fraction is highly biased toward specific tRNA-derived fragments capable of forming RNase-protecting dimers. To solve the problem of stability in exRNA analysis, we developed a method based on sequencing the size exclusion chromatography (SEC) fractions of nonvesicular extracellular samples treated with RNase inhibitors (RI). This method revealed dramatic compositional changes in exRNA population when enzymatic RNA degradation was inhibited. We demonstrated the presence of ribosomes and full-length tRNAs in cell-conditioned medium of a variety of mammalian cell lines. Their fragmentation generates some small RNAs that are highly resistant to degradation. The extracellular biogenesis of some of the most abundant exRNAs demonstrates that extracellular abundance is not a reliable input to estimate RNA secretion rates. Finally, we showed that chromatographic fractions containing extracellular ribosomes are probably not silent from an immunological perspective and could possibly be decoded as damage-associated molecular patterns.

INTRODUCTION

Extracellular RNA (exRNA) profiling in biofluids such as urine, plasma or serum is a promising approach for early disease detection and monitoring in minimally invasive liquid biopsies (1). Although plasma cell-free DNA analysis has proven powerful to detect cancer-associated mutations (2) or altered DNA methylation events (3), exRNA analysis has the potential to inform about transcript expression, post-transcriptional modifications and splicing variants (4). Additionally, it was reported that cells use exRNAs to communicate and reciprocally regulate their gene expression, even in distant tissues (5–7).

Because RNA is widely recognized as unstable in biofluids such as plasma due to their high RNase content (8), exRNAs are typically studied in the context of lipid membrane-containing extracellular vesicles (EVs) (7,9,10) or lipoprotein particles (LPPs) (11,12). Alternatively, exRNAs can achieve high extracellular stability by their association with proteins (13,14). However, extracellular soluble ribonucleoproteins remain the least studied exRNA carriers (15), with most attention thus far placed at the level of EVs.

Strikingly, a major proportion of extracellular small RNAs are found outside EVs (13,16). Furthermore, nonvesicular exRNA profiles are highly biased toward glycine and glutamic acid 5′ tRNA halves. This has been extensively documented both in cell culture media (16,17) and in biofluids such as urine, blood serum, saliva or cerebrospinal fluid (18–21). The abundance of these species in the extracellular,

*To whom correspondence should be addressed. Tel: +598 2522 0910; Email: jptosar@pasteur.edu.uy
Correspondence may also be addressed to Alfonso Cayota. Email: cayota@pasteur.edu.uy

nonvesicular fraction (16,20,21)challenges the widespread belief that exRNAs are unstable when not present inside EVs and raise the question on the origin of their remarkable extracellular stability.

A possible answer to this question arises from our recent report that glycine and glutamic acid 5′ tRNA halves can form homo- or heterodimeric hybrids, which render them resistant to single-stranded RNases (22). The RNAs with predicted dimer-forming capacity are those of 30 or 31 nucleotides, which are slightly shorter than the 5′ tRNA halves generated by endonucleolytic cleavage of the anticodon loop (typically 34–35 nt) during the stress response (23–25). Interestingly, nonvesicular extracellular fractions are usually enriched in glycine and glutamic acid tRNA halves of precisely 30–31 nt (16,18), suggesting a causal link between extracellular stability and abundance (18). As a consequence, the enrichment of glycine and glutamic acid tRNA halves in extracellular samples does not necessarily imply that these sequences are released at higher rates from cells when compared to other small RNAs. Differential extracellular stability might as well produce the same outcome. Furthermore, the possibility that these fragments could be generated by extracellular fragmentation of tRNA precursors has not been sufficiently explored.

We hypothesized that extracellular RNA degradation is a major force shifting what cells release to the extracellular space toward those species with higher extracellular stability. Consequently, we speculated that conventional exRNA profiling fails to capture the complete set of RNAs released from cells to the extracellular space, frustrating attempts to infer RNA secretion mechanisms from comparisons between intracellular and extracellular RNA profiles. To study this, we compared exRNAs in cell-conditioned media obtained with or without addition of recombinant ribonuclease inhibitor (RI). Surprisingly, addition of RI greatly increased the complexity of exRNA profiles, stabilizing extracellular ribosomes and tRNAs which rapidly decay to rRNA- and tRNA-derived fragments in the absence of RNase inhibitors. Some of these fragments are highly stable and can accumulate in samples with high RNase activity, even when present outside EVs. Overall, we provide a dynamic and comprehensive characterization of the nonvesicular RNAome which can impact biomarker discovery in biofluids.

MATERIALS AND METHODS

Reagents

A full list of reagents including antibodies, primers and probes used in this study are reported in SI Materials and Methods.

Preparation of cell-conditioned medium

Cells were cultured in DMEM + 10% fetal bovine serum (S+ medium) at 37°C and 5% CO_2 or in different serum-free formulations as depicted in SI Materials and Methods. Recombinant ribonuclease inhibitor (RI; NEB) was added in selected experiments at a final concentration of 4–8 U/ml, either at the time of medium renewal or following collection of cell-conditioned media.

Preparation of the nonvesicular extracellular fraction by ultracentrifugation

The cell-condtioned medium already spinned at 2000 × g was centrifuged for 2.5 h at 100 000 × g and 4°C in a Beckman Coulter Optima XPN-90 ultracentrifuge using a SW40 Ti rotor. The supernatant was concentrated to ∼250 μl with 10 000 MWCO ultrafiltration units (Vivaspin 20, Sartorious Stedim Biotech) and subjected to size-exclusion chromatography or RNA extraction with TRIzol (according to manufacturer's instructions).

Size exclusion chromatography

The 100 000 × g supernatants of the cell-conditioned medium were concentrated by ultrafiltration by successive dilutions with PBS to remove phenol red and small molecules. Concentrated EV-depleted fractions (500 μl) were injected in a Superdex S200 10/300 column (Amersham, GE) and size exlusion chromatography (SEC) was performed at 0.9 ml/min in 0.22 μm-filtered 1× PBS with an Äkta Pure (GE healthcare) FPLC system. All samples were centrifuged at 16 000 × g for 10 min at 4°C before injection in the columns. Fractions of 0.25 ml were collected while monitoring the absorbance at 260 and 280 nm. Chromatograms were deconvoluted *in silico* using empirically determined 260/280 ratios from pure bovine serum albumin (BSA) and synthetic $tRNA^{Gly}{}_{GCC}$ 5′ halves (of 30 nt).

Sequencing of small RNAs

RNA was purified from selected chromatographic peaks using TRIzol LS and following manufacturer's instructions. The obtained RNA was diluted in 8 μl of ultra-pure RNase-free water, and 7 μl were used as input for NGS library preparation using the NEBNext Small RNA Library Prep Set for Illumina (New England Biolabs). Sequencing was performed in a MiSeq benchtop sequencer for 200 cycles. The analysis was performed as depicted in SI Materials and Methods. FastQ files containing sequences of at least 15 nt after 3' adapter identification and removal are available at NCBI SRA.

Northern blotting

Northern blots (10% denaturing gels transferred to positively-charged nylon membranes) were performed based on digoxigenin-labeled DNA probes and an alkaline phosphatase-labeled anti-digoxigenin antibody (Roche). Signals were visualized with CDP-Star ready-to-use (Roche) and detected using ChemiDoc imaging system (BioRad). A detailed protocol and probe sequences are provided in SI Materials and Methods.

Differentiation of dendritic cells and flow-cytometry.

Adherent mouse bone marrow-derived dendritic cells (BMDC) were prepared as described in (26). Selected chromatographic fractions or synthetic RNAs were added to 1×10^6 BMDCs. At $t = 24$ hs, cells were harvested and analyzed by flow cytometry using a CyAn ADP Analyzer (Dako). A detailed protocol is provided in SI Materials and Methods.

RESULTS

Inhibition of extracellular ribonucleases dramatically alters exRNA profiles

We have previously shown that the most abundant non-vesicular exRNAs have the capacity to form homo- and heterodimers and are therefore highly stable against the action of extracellular RNases (16,22). Consequently, we reasoned that conventional experimental approaches to assess exRNAs could be biased toward the most stable entities and miss most of the RNAs actually released from cells due to their low extracellular half-life.

In order to understand exRNA dynamics and capture both stable and unstable RNAs, we developed a method based on size-exclusion chromatography (SEC) fractionation of RNase inhibitor (RI)-treated cell-conditioned medium (RI-SEC-seq). Briefly, MCF-7 cell-conditioned medium (CCM) was treated (or not) with a recombinant RNase A family inhibitor, and EVs were later removed by ultracentrifugation to obtain the 'EV-depleted' extracellular fraction. Next, SEC separation was used to identify major RNA populations, which were subjected to standard small RNA sequencing procedures.

Under basal (-RI) conditions, chromatographic analysis of the EV-depleted fraction of MCF-7 CCM consistently showed two peaks with Abs 260 > Abs 280 which we termed P1 (V_e = 15.0 ml) and P2 (V_e = 16.5 ml) (Figure 1 A; top). The elution volume of P1 corresponds to that obtained when injecting yeast full-length $tRNA^{Phe}$ or RNA dimers of 30 nt (Supplementary Figure S1, A and (22)). In contrast, synthetic ssRNAs of 30 nt elute in P2. Treatment of the CCM with exogenous RNase A prior to SEC depleted the P1 peak and degradation products were evident with V_e ≥ 19 ml (Figure 1A, middle). However, absorbance in the P2 region was only modestly affected. Addition of the recombinant RNase A-family inhibitor (RI) to the CCM precluded the formation of P2 (Figure 1A, bottom), demonstrating that the P2 peak also contains RNA. In this situation, the P1 peak was still prominent, but similar amounts of nucleic acids now eluted in the exclusion volume of the column (V_e = 7.5 ml; apparent MW ≥ 800 kDa). For simplicity, we will term this new peak 'P0'.

The high MW RNA-containing complex in P0 was mutually exclusive with the P2 peak (Figure 1B). Furthermore, P2 could be reconstituted by RNase A treatment of the purified P0 fraction (Figure 1C). Taken together, these results suggest that P2 contains a highly resistant small RNA population formed by partial fragmentation of long RNAs within P0 (and possibly P1 as well).

RI-SEC-seq offers an unbiased and dynamic view of the extracellular RNAome.

Small RNA sequencing of the different chromatographic fractions showed that P0 is mainly composed of rRNAs (Figure 1D). Sequencing of P1 obtained with or without addition of RI was previously published by our group (22) and showed a predominance of 5′ tRNA halves derived from $tRNA^{Gly}_{GCC}$ and $tRNA^{Glu}_{CUC}$. However, tRNA-derived fragments in the '+RI' library tended to be longer than in '–RI' (33–35 versus 30–31) (Figure 1E and Supplementary Figure S1B). On top of that, PI – RI was highly enriched in glycine tRNA halves of 30 nt when compared to PI + RI (Figure 1F). The ability of these fragments to form RNase-resistant homodimers is consistent with their detection in the absence of RI and their elution in the P1 peak. Interestingly, addition of RI recovered a higher diversity of small RNAs in the P1 peak, including fragments of rRNA and full-length snoRNAs (Supplementary Figure S1C). It is remarkable that the main rRNA-derived fragments and snoRNAs sequenced in P1 + RI are known to interact (Supplementary Figure S1D). Thus, it is possible to speculate that dsRNA hybrids tend to accumulate in extracellular nonvesicular samples due to their intrinsic resistance to extracellular single-stranded ribonucleases. Nevertheless, the stabilities of glycine tRNA halves are outstanding since these are virtually the only species identified in the absence of RI.

Sequencing of full-length mature tRNAs is challenging due to the abundance of modified ribonucleotides and their strong self-complementarity. Therefore, specific protocols for tRNA sequencing and analysis have been developed in recent years (27–30). Despite using conventional ligation-based library preparation methods, we obtained a low but nonnegligible number of reads corresponding to two full-length $tRNA^{Glu}$ isoacceptors (Supplementary Figure S1E). These sequences were exclusively detected in the 'P1 + RI' library and contained the 3′ terminal nontemplated CCA addition indicative of mature tRNAs. Analysis of the P1 + RI fraction in a denaturing RNA gel showed that, indeed, most RNAs migrated like full length tRNAs (Figure 1, G). In contrast, the majority of RNAs in 'P1 –RI' were < 33 nt, consistent with tRNA halves. Altogether, these results suggest that exRNA profiles are biased toward highly stable tRNA halves by the action of extracellular ribonucleases and they do not necessarily reflect the composition of RNAs actually released by cells.

The P0 peak contains mostly high-MW RNA, as evidenced by denaturing gel electrophoresis (Figure 1, G) and because reinjection of the purified RNA from the P0 peak still eluted in the void volume (Figure 1C). Small RNA sequencing showed the same tRNA-derived fragments found in P1, but overwhelmingly higher levels of rRNA fragments (Figure 1D, H–I). The majority of these were 28S rRNA 5′ fragments of 20–40 nucleotides. Our size-selected libraries were too short (<200 nt) to capture the complete 28S (5070 nt) or 18S (1869 nt) rRNAs, although sequences spanning the entire 28S rRNA were detectable (Supplementary Figure S1F). Nevertheless, the entire 5.8S rRNA could be read (156 nt; Figure 1I and Supplementary Figure S1G).

To demonstrate the presence of full-length rRNAs in P0 we performed random-primed reverse transcription and qPCR amplification with primers spanning different regions of 28S, 18S and 5.8S rRNAs (Figure 1J). All primer sets amplified comparably and exclusively in P0, while $tRNA^{Gly}_{GCC}$ 5′ tRNA halves peaked in P1 and P2 as expected. This evidence, together with sequencing of the entire 5.8S rRNA, strongly suggests the release of intact rRNAs from both ribosomal subunits to the extracellular space and outside EVs.

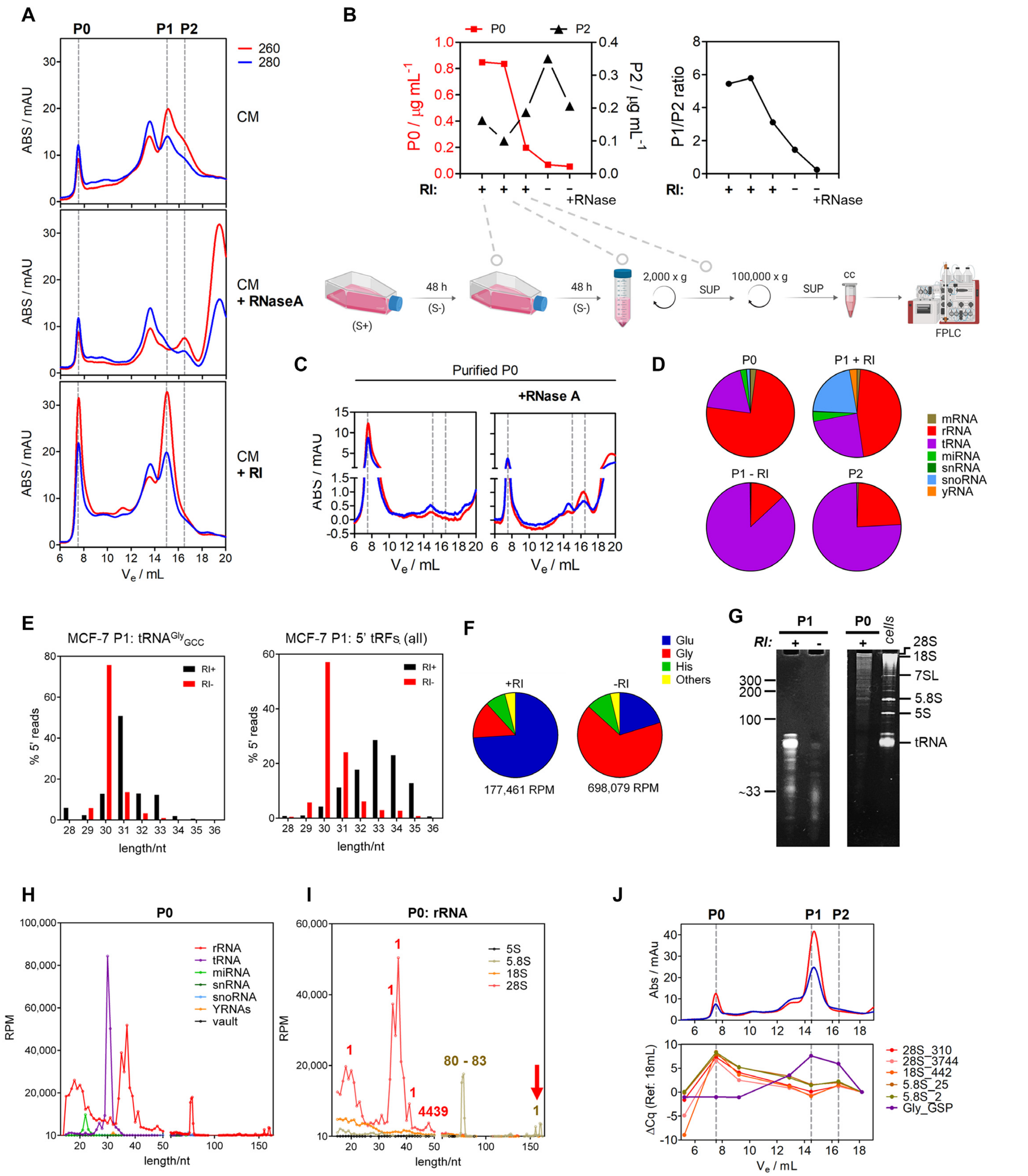

Figure 1. RNase inhibition stabilizes full-length extracellular rRNAs and tRNAs. (**A**) Size exclusion chromatography (SEC) of 100 000 × g supernatants of MCF-7 cell-conditioned medium (CM) following addition of RNase A (middle) or Ribonuclease Inhibitor (RI, bottom). Red, Blue: absorbance at 260 and 280 nm, respectively. (**B**) The earlier RI was added to the CCM during sample preparation, the higher the P0/P2 (left) and P1/P2 (right) ratios. S+, S–: serum-containing and serum-free media, respectively. SUP: supernatant. (**C**) The P0 peak was purified after SEC and treated with RNase A, which partially reconstituted the P2 peak. (**D**) Pie charts showing relative representations of different RNA biotypes in RI-SEC-seq datasets. (**E**) Size distribution of reads mapping to the 5' half of glycine tRNA (left) or to all tRNAs (right) in the P1 peak from MCF-7 cells either with (black) or without (red) addition of RI. (**F**) Relative representation of reads mapping to different tRNA isoacceptors in the P1 peak of cells treated (top) or not (bottom) with RI. (**G**) Analysis of the P1 peak either with (+) or without (–) RI treatment (left gel) or the P0 peak (right gel) in a denaturing polyacrylamide gel. (**H**) Size distribution of small RNA sequencing reads mapping to different ncRNAs (see legend) in the P0 peak of MCF-7 cells. RPM: reads per million mapped reads. (**I**) As in (H) but showing only the reads aligning to rRNAs. Numbers indicate starting position of most reads. (**J**) Amplification of different rRNA regions by random-primed RT-qPCR in fractions collected after SEC. Gly_GSP: amplification of glycine 5' halves using a gene-specific primer during RT. Numbers after underscores represent the 5' position of the expected amplicon.

Release of rRNAs and tRNAs occurs promptly after 30 seconds of medium renewal

To clearly differentiate between RNAs directly released from cells and fragments generated by extracellular processing of longer precursors, we combined RI treatment with exRNA profiling shortly after medium renewal. To do this, we performed four sequential washes of cells with PBS and analyzed the RNA content in the cell-conditioned PBS, with a conditioning time as short as 30 s (Figure 2A). Strikingly, both the rRNA-associated P0 and the tRNA-associated P1 peaks were consistently detected in the four washes (Figure 2B). Similar results were obtained when washing with serum-free chemically defined growth medium (MEGM; Supplementary Figure S2A), albeit with a higher wash-to-wash variability**.** Thus, detection of rRNAs and tRNAs in the fourth PBS or MEGM wash was not a consequence of carry-over from previously longer incubations. Instead, fast release of these RNAs occurred every time the cells were washed. Increasing incubation time from 30 s to 10 min did not increase extracellular RNA levels (Figure 2C). This phenomenon was highly reproducible in a variety of adherent cell lines, including primary normal cell lines such as BJ fibroblasts (Figure 2D and Supplementary Figure S2B).

As expected, the vast majority of cells were not affected by the washing protocol and retained their anchorage (Supplementary Figure S2C). Induction of cell stress was not evident based on eIF2α phosphorylation levels (Figure 2E). However, floating nuclei were observable after the washes when serum-free media or different buffers were used (data not shown), questioning the source of the exRNAs detected in the media. Estimated RNA levels in each wash were 0.1–0.5% of the total RNA present in the culture.

Extracellular nonvesicular RNAs mirror the intracellular transcriptome

To distinguish between selective and nonselective release of cytoplasmic contents, we scaled up our cultures in an attempt to detect less abundant nonvesicular exRNAs. Surprisingly, denaturing PAGE analysis of TRIzol-purified RNA from extracellular, RI-treated fractions showed all RNA bands typically found in cellular extracts and respecting their relative intensities (Figure 2F). This was observed also in the DU145 cell line which is deficient in ATG5 and therefore in autophagy (31) (Figure 2G) suggesting that the release mechanism operating herein is unrelated to the recently described autophagy-dependent secretion of cytoplasmic nucleic acids (32).

Identification of ribosomes and oligoribosomes in the extracellular space

We could identify features with size and morphology consistent with the presence of ribosomal particles by negative-stain transmission electron microscopy of the concentrated P0 peak or unfractionated PBS washes of different adherent cell lines (Figure 3A). To confirm the presence of extracellular ribosomes, we resort to study concentrated extracellular fractions by velocity sedimentation in sucrose gradients optimized for polysome preparations (Figure 3B). Analysis of the velocity gradients showed three clearly defined 254 nm peaks in the region corresponding to ribosomal subunits or ribosomes (Figure 3C). These peaks corresponded to the small ribosomal subunit 40S (low levels of 28S, 5.8S and 5S rRNA, high levels of 18S rRNA, low levels of RPL7a, high levels of RPS6), 80S monosomes (all rRNAs and all ribosomal proteins detectable with the expected stoichiometry), and, considering a lack of detectable ribosomal proteins in fraction #10 and their reappearance in fraction #11, two ribosomes (2×). Interestingly, a small 254 nm peak in fraction #14 was accompanied by a faint but detectable band for RPL7a and RPS6 and was indicative of oligoribosomes or polysomes. These were further stabilized by treating cells with the translation elongation blocker cycloheximide (but not with the premature terminator puromycin) straight before HBSS+ washes (Figure 3D).

Because polysomes are formed by ribosomes sitting on messenger RNAs, we wondered whether the extracellular fractions also contained mRNAs. A reanalysis of our small RNA sequencing in the P0 peak from MCF-7 cells revealed a variety of reads unambiguously mapping to coding sequences. Considering only reads of 19 nt or longer, we could detect 125 unique mRNAs supported by at least five counts each. In many cases, reads mapped to different exons and were long enough (30–40 nt) to discard the possibility of ambiguous mapping. Once again, their extracellular representation was positively correlated ($r = 0.416$, $P < 0.0001$) to their expected intracellular levels, and included mRNAs transcribed from the mitochondrial genome (Figure 3E). One of the most abundantly detected mRNAs in our sequencing study, HSP90B1, could be amplified from the P0 peak of different cells using an oligo dT reverse transcription primer and PCR primers aligning to its 5′ end (Figure 3F). Thus, complete, nondegraded mRNAs are detectable in the extracellular space and co-purify with extracellular ribosomes. Long reads representing full-length, spliced mRNAs were also identified by direct RNA sequencing of extracellular samples using an Oxford Nanopore MinION sequencer (data not shown). RNA inputs were too low to obtain a reliable and representative description of extracellular mRNAs. Nevertheless, the presence of full-length mRNAs in these extracellular fractions is strongly supported.

Next, we addressed whether extracellular ribosomes/polysomes contained attached polypeptides. To do so, we incubated concentrated extracellular samples with puromycin (an analog of the 3′ end of aminoacyl-tRNA) and evaluated incorporation of the antibiotic to nascent peptides by Western blot. Interestingly, puromycin incorporation was independent of added ATP/GTP (Figure 3G) but was dependent on temperature (Figure 3H), consistent with the energy independency (33) but temperature dependency (34) of the puromycylation reaction. These results also suggest that extracellular ribosomes contain preformed polypeptides (considering elongation unlikely under these experimental conditions) and were therefore engaged in translation before their release to the extracellular space. To the best of our knowledge, this is the first evidence of the peptidyl transferase reaction occurring in extracellular samples obtained without deliberated cell lysis steps.

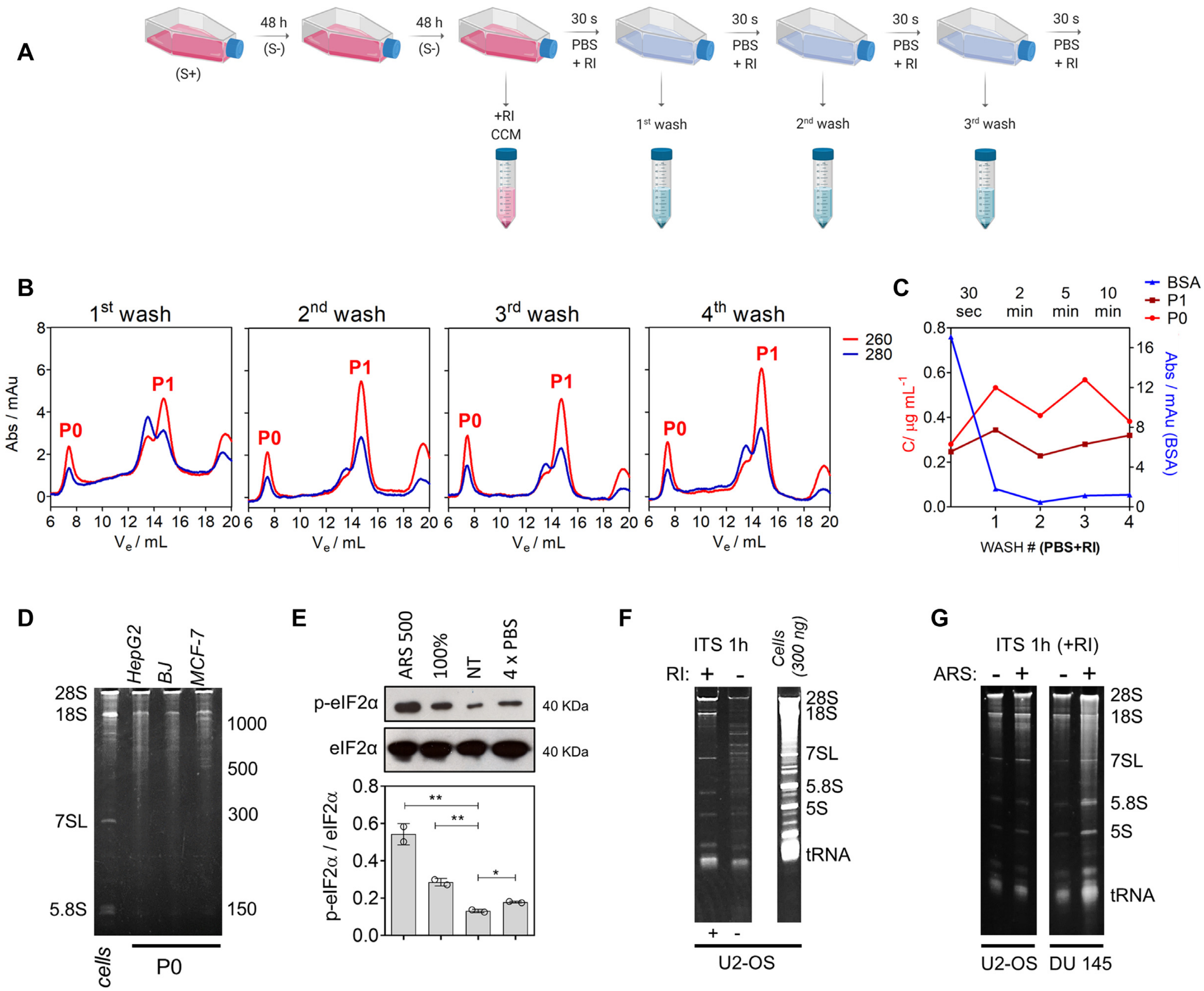

Figure 2. rRNAs and tRNAs are rapidly released to the extracellular space. (**A**) Schematic representation of the experimental protocol used in panels B–E. S+: DMEM + 10% FBS. S–: serum-free MEGM medium. (**B**) RNA analysis by SEC in PBS washes #1 to #4 of MCF-7 cells. Conditions identical to those used in Figure 1. (**C**) Variation of RNA concentration corresponding to the P0 (light red) and P1 (dark red) peaks in PBS washes #1 to #4. The variation in the Abs 280 nm of the BSA peak is plotted in the right axis. Initial values correspond to those present in the CCM. (**D**) Denaturing electrophoresis (6% PAGE) of the concentrated P0 peak from the fourth PBS wash of HepG2, BJ and MCF-7 cell lines. No RNA purification was performed. 'Cells': MCF-7 RNA lysate. (**E**) Analysis of eIF2 alpha phosphorylation (Wblot) in nontreated (NT) MCF-7 cells, in cells exposed to four consecutive PBS washes (4× PBS), in cells cultured after confluency (100%) or exposed to 500 μM sodium arsenite for 1 h (ARS 500). Bottom: densitometry analysis in two independent biological replicates of the experiment. (**F**) Denaturing electrophoresis (10% PAGE) of purified extracellular RNA from U2-OS cells incubated for 1 h in a serum-free medium (DMEM + ITS, ± RI; 5×10^6 cells), ran alongside 300 ng of purified U2-OS intracellular RNA. (**G**) Purified RNA from U2-OS (left) or DU 145 (right) cell-conditioned medium (ITS + RI, 1 h) obtained in the presence (+) or absence (–) of 200 μM sodium arsenite.

Nonvesicular ribosomal RNAs co-purify with extracellular vesicles

Isopycnic centrifugation of exRNAs obtained after short washes of U2-OS cells with HBSS+ confirmed that virtually all RNAs detectable by SYBR gold staining were not associated with EVs (Figure 3I). However, sequential ultracentrifugation of cell-conditioned HBSS (either with or without divalent cations) showed sedimentation of rRNA- and tRNA-containing complexes at speeds usually used to purify small EVs (100 000 × g; Figure 3J). Strikingly, presence of divalent ions favored rRNA sedimentation at speeds typically used to collect large EVs (16 000 × g). This effect was not observed for tRNAs (Figure 3K). These observations are consistent with the involvement of magnesium ions in the stabilization of ribosomes (35) and demonstrate that the most frequently used method for EV purification (i.e. ultracentrifugation) does not allow separation of EVs from nondegraded extracellular ribosomes.

Extracellular biogenesis of extracellular tRNA halves

As shown above (Figure 1), full-length tRNAs comprise the majority of RNAs present in the P1 peak in RI-treated CCM, but this profile shifted toward RNase-resistant glycine tRNA halves (30–31 nt) in the absence of RI. One

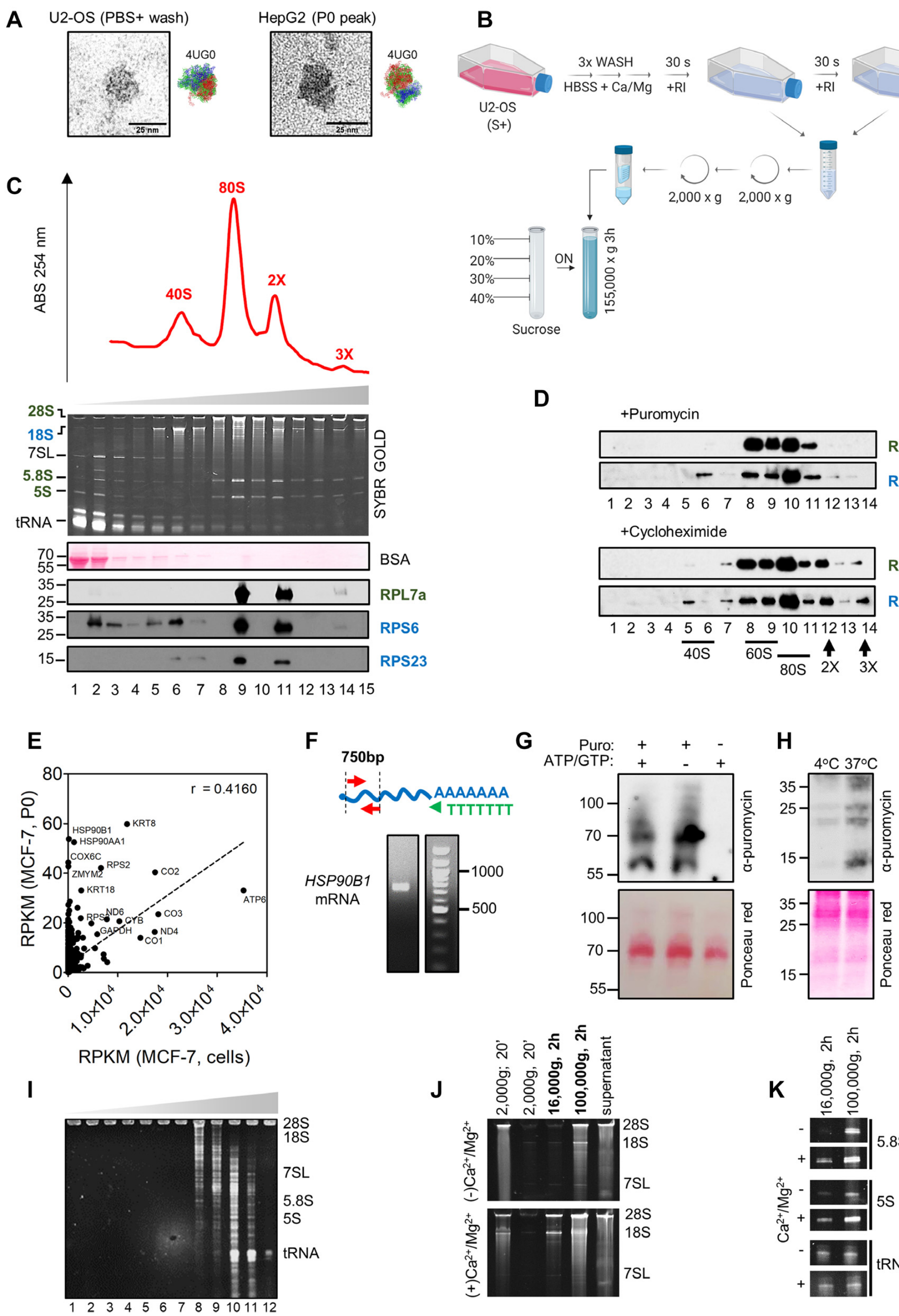

Figure 3. The extracellular space contains ribosomes. (**A**) Negative-stain TEM images of ribosome-like particles in concentrated cell-conditioned PBS or chromatographic P0 peak from U2-OS and Hep G2 cells, respectively. Scale bar: 25 nm. A Cryo-EM structure of the human ribosome (PDB: 4UG0) is shown for comparison, with 28S and 18S rRNAs colored red and blue, respectively. (**B**) Schematic representation of the experimental protocol used in panels C and D. (**C**) Velocity gradient (10–40% sucrose, 3 h at 155 000 × g) of cell-conditioned HBSS (plus divalent cations and RI) from U2-OS cells. Fractions of 0.5 ml were taken out from the top of the tube and treated with TRIzol. RNA was analyzed in a denaturing 10% PAGE and proteins were analyzed by western blot using antibodies specific to human ribosomal proteins. (**D**) Same as (C), but cells were treated with puromycin (2 μg /ml; 10 min) or cycloheximide (10 μg/ml; 30 min) before washes. (**E**) Analysis of mRNAs in the P0 peak of MCF-7 cells. Relative abundances (expressed as reads per kilobase of transcript, per million mapped reads, RPKM) assume random fragmentation of parental mRNAs. Intracellular abundances in MCF-7 cells were based on transcriptomic data from the Human Protein Atlas. (**F**) RT-PCR of human HSP90B1 mRNA with an oligo-dT primer and PCR primers complementary to exons 5 and 9 (2229 bp from 3' end). (**G**) U2-OS cell-conditioned buffer (+RI, + divalent cations) was concentrated by ultrafiltration and treated with 5 μg/ml puromycin for 2 h at 37°C with or without addition or ATP/GTP. Extracted proteins were analyzed by Western blot with an anti-puromycin antibody. (**H**) Same as (G), but incubating samples at either 37°C or 4°C. (**I**) Isopycnic centrifugation in a 12–36% iodixanol gradient of the concentrated fourth wash of U2-OS cells (HBSS+). Twelve fractions of 1 ml were collected from the top of the tube. Densities in each fraction were comparable to ref 32. (**J, K**) U2-OS cells were washed with HBSS with/without divalent ions for 30 s. Samples were centrifuged twice at 2000 × g, followed by sequential ultracentrifugation. Pellets were resuspended in water and, together with the concentrated 100 000 × g supernatant, ethanol precipitated, resuspended, and analyzed by denaturing electrophoresis. Panels I and J show different regions of the same gel.

possibility is that these tRNA halves were released directly from cells and accumulated because of their resistance to degradation. Alternatively, they could be generated by the fragmentation of extracellular tRNAs.

To distinguish between both possibilities, we developed different protocols where the activity of extracellular ribonucleases could be experimentally modulated. These protocols allowed us to obtain exRNAs with virtually no degradation (short washes in the presence of RI), or in the presence of FBS, which contains highly active RNase A.

As an intermediate situation between both extremes, a third protocol was optimized where cells were washed and incubated in serum-free medium (DMEM + ITS supplement, hereafter 'ITS') for 1 h and in the absence of RI (protocol 3, SI Materials and Methods). Under these experimental conditions, RNase activity relies mostly on endogenous secreted ribonucleases. Cell-conditioned medium was later incubated at 37°C for 24 h in order to amplify the effects of endogenous RNases ('cell-free maturation step', Figure 4A).

Iodixanol density gradient centrifugation confirmed that most of the RNAs were present in the nonvesicular fractions after an incubation of U2-OS cells in ITS for 1 h (Figure 4B). Endogenous RNase activity was evident when comparing exRNA profiles with or without RI, irrespectively of the cell-free maturation step (Figures 2F and 4C). When including this step, rRNA bands were no longer detectable, but the tRNAs were affected to a much lower extent (Figure 4C). Surprisingly, Northern blot analysis showed marked differences in tRNA stability (with $tRNA^{Lys}{}_{UUU}$ > $tRNA^{iMet}{}_{CAU}$ > $tRNA^{Gly}{}_{GCC}$), which were inversely correlated to their corresponding 5′ tRNA halves (Figure 4D). This strongly suggest that extracellular tRNA halves are generated by extracellular cleavage of tRNAs. This cleavage is dependent on extracellular RNase A family members because it can be modulated by exogenously added RI, but Angiogenin is dispensable or redundant based on almost identical results in wild-type (Figure 4C) or ANG knock-out cells (Figure 4D).

Two bands were observed in the case of glycine 5′ tRNA halves. These were 33–35 nt (i.e. 5′ tRNA halves cleaved at the anticodon loop) or 30–31 nt (Figure 4D and Supplementary Figure S3A). For simplicity, we will call these fragments long tRNA halves (L-tRNAh) and short tRNA halves (S-tRNAh), respectively. Both species are detectable inside U2-OS cells stressed with sodium arsenite but L-tRNAh are produced at much higher levels (36). In contrast, only the S-tRNAh are predicted to form RNase-resistant homodimers according to our previous study (22). Strikingly, only the S-tRNAh was detectable in the extracellular milieu in the absence of RI (Figure 4D) confirming the enhanced extracellular stability of this specific fragment.

Five prime tRNA halves were termed 'stress-induced tRNA-derived fragments' or tiRNAs (24) because their production is induced by cellular stress. Loading of one microgram of intracellular RNA from U2-OS cells did not show production of these tRNA halves or tiRNAs above the assay's sensitivity (Supplementary Figure S3, A). Despite the full-length $tRNA^{Gly}{}_{GCC}$ was not detectable after 24 h of cell-free maturation of the CCM (Figure 4D), the full-length tRNA as well as the L-tRNAh and S-tRNAh were clearly present if this cell-free maturation step was omitted (Supplementary Figure S3A). Interestingly, 3′ tRNA-derived fragments were also detectable in the same samples although they are rarely found intracellularly, even in arsenite-treated U2-OS cells (24). The higher the degradation state of the exRNA population, the higher the fragment-to-tRNA ratio for both 5′ and 3′ fragments (Supplementary Figure S3B).

To obtain direct evidence for the conversion of extracellular tRNAs into tRNA halves, we briefly washed U2-OS cells with HBSS+ in the absence of RI and divided the cell-conditioned buffer into four aliquots. These aliquots were incubated for 0, 1 or 5 h at 37°C before addition of RI and subsequent analysis by Northern blot (Figure 4E). The fourth aliquot was mixed 1:1 with S+ medium (to obtain a final serum concentration of 5%) and incubated for 1 h at 37°C. The full-length $tRNA^{Gly}{}_{GCC}$ and the L-tRNAh (but not the S-tRNAh) were present at $t = 0$. Incubation for 5 h at 37°C showed a slight decrease in the intensity of the full-length band and a concomitant increase in L-tRNAh. Strikingly, incubation for only 1 h in the presence of serum (RNase-rich sample) entirely converted the full-length tRNA band to S-tRNAh. The L-tRNAh band was also lost. Thus, RNases present in serum perform a highly efficient conversion of glycine tRNAs into 5′ tRNA halves of precisely 30 or 31 nt, which then accumulate due to their capacity to form RNase-resistant homodimers (22). It remains to be determined whether S-tRNAh are generated by an alternative cleavage site at glycine tRNAs (Figure 4F) or whether they are generated by cleavage or trimming of L-tRNAh. Note that the concentration of tRNA-derived fragments in S+ is below the limit of detection of our assay (Figure 4G). Thus, FBS is solely serving as a source of RNases while not supplying RNAs at a concentration that could interfere with these studies.

EVs contain full-length ncRNAs while the EV-depleted fraction is enriched in ncRNA fragments.

To evaluate exRNA profiles under standard serum-containing growth conditions (S+; protocol: 1, SI Materials and Methods), we collected CCM at different time points, separated vesicles from nonvesicular RNAs by density gradients and analyzed exRNAs by northern blot.

One striking difference in respect to what was previously observed in ITS incubations (protocol: 3; Figure 4A) or HBSS+ washes (protocol: 4; Figure 3A) was that the tRNA and the 7SL RNA bands were enriched according to what could be expected by rRNA band intensities (Supplementary Figure S3C). Here, addition of RI (120 U; 12 U/ml) did not have any observable effect on exRNA profiles.

Having observed that $tRNA^{Gly}{}_{GCC}$ is particularly susceptible to the action of serum RNases (Figure 4E), we were surprised to detect it by northern blot in the extracellular space of U2-OS cells incubated in the presence of 10% serum (Figure 4G). Furthermore, the intensity of the full-length tRNA band was positively correlated to the length of the incubation. However, density gradient analysis later confirmed that extracellular tRNAs and 7SL RNAs were exclusively associated with EVs (Figure 4H). Conversely,

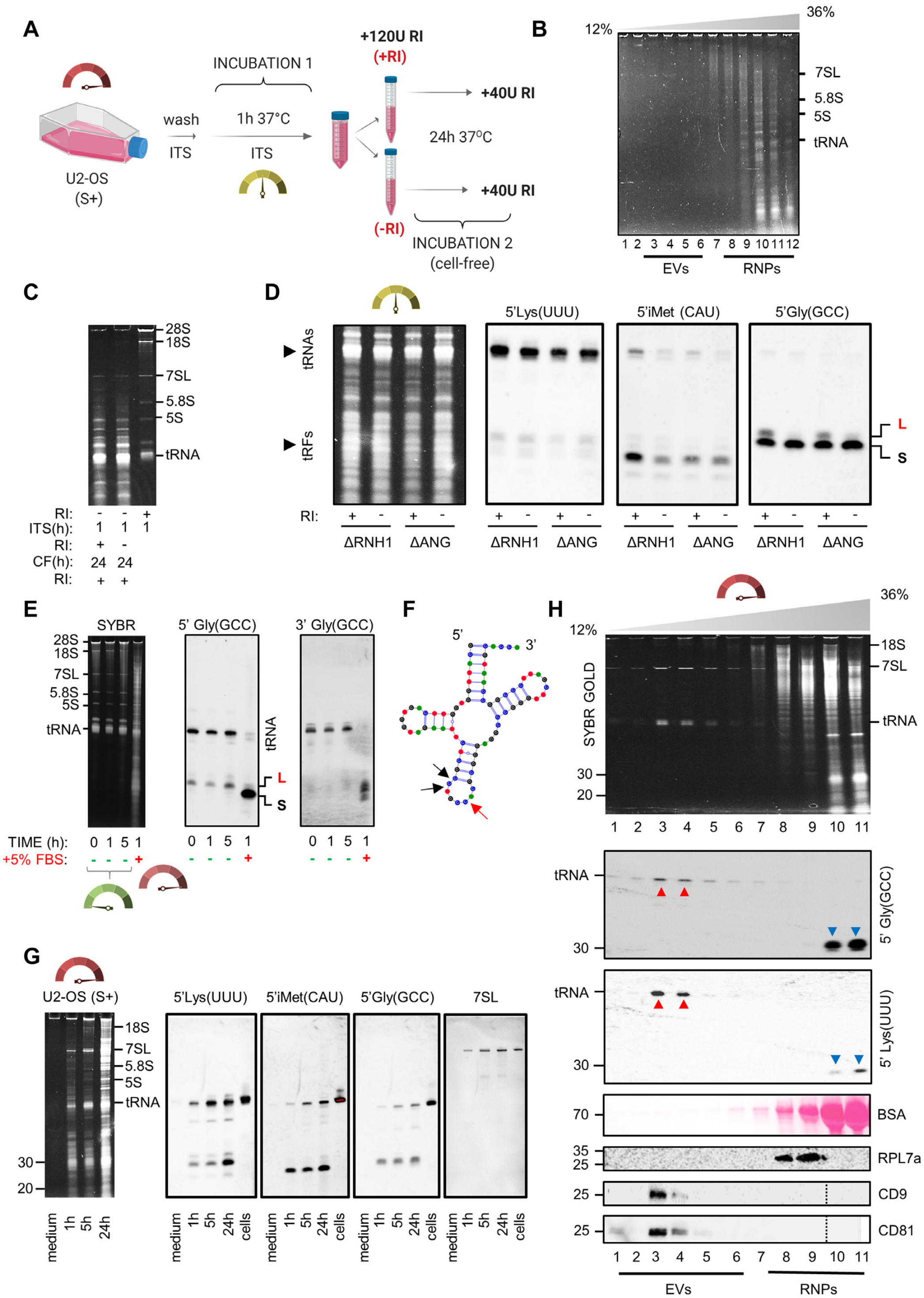

Figure 4. Extracellular tRNAs are processed to extracellular tRNA-derived fragments. (**A**) Schematic representation of the experimental setup used in panels B–D. (**B**) Iodixanol gradient showing most exRNAs were present in the nonvesicular fractions (RNPs) in the input sample (before cell-free processing). (**C**) Analysis of exRNAs by denaturing electrophoresis before and after the cell-free (CF) maturation step. (**D**) Northern blot analysis with probes targeting the 5' region of different tRNAs in samples obtained as explained in (A). L: 5' tRNA halves of 33–34 nt; S: 5' tRNA halves of 30–31 nt. (**E**) Samples were obtained after a short (30 s) wash of U2-OS cells with HBSS+ (without RI addition), and incubated cell-free at 37°C for 0, 1 or 5 h, or for 1 h after addition of S+ medium in a 1:1 ratio. Northern blot was performed with two different probes targeting both halves of $tRNA^{Gly}{}_{GCC}$. (**F**) Cloverleaf representation of glycine tRNA (GCC anticodon, isodecoder #2) with red arrow showing predicted cleavage at the anticodon loop (sequence CpCpA), rendering a 33 or 34 nt 5' fragment, and black arrows showing a putative alternative cleavage site (sequence CpCpU), generating 30–31 nt 5' fragments. (**G**) Analysis of exRNAs in U2-OS CCM (1, 5 and 24 h, S+ medium). The concentrated nonconditioned medium was run as a control. Northern blot was done with the same probes as in panel (D), plus a 7SL RNA-specific probe. (**H**) Isopycnic centrifugation of U2-OS CCM ($t = 24$ h in S+ medium). Color code (dials): green (short wash with RI; low RNase activity), yellow (endogenous RNases, released during 1 h incubation in serum-free medium without RI), red (FBS-derived RNases).

tRNA-derived fragments (glycine S-tRNAh in particular) were only present outside EVs. A similar tendency was found for other RNA polymerase III transcripts like YRNAs and their fragments (Supplementary Figure S3D), in agreement with previous reports in nematodes (37).

In summary, long transcripts (including tRNAs) cannot resist prolonged incubation in samples with high RNase activity such as those containing serum except when protected inside EVs. However, some of their fragments are much more resistant and are consistently detected in the EV-depleted fraction. These fragments define the extracellular nonvesicular RNAome in the absence of added RI, although many of them are not directly released from cells.

Immunoregulatory potential of extracellular nonvesicular RNAs

We wondered whether dendritic cells (DCs) could sense and react to nonvesicular exRNAs. These cells are regarded as the sentinels of the immune system and link innate and adaptive immune responses (38). Thus, we reasoned that if exRNAs are nonsilent from an immunological perspective, they should be sensed by DCs in the first place.

ExRNAs obtained from MCF-7 cells were either treated or not with RNase A and later separated by SEC in order to obtain the following samples/fractions: P0, P0 post RNase-treatment and P1. These fractions were concentrated, filtered and added directly to the media of freshly prepared non-primed bone marrow-derived murine dendritic cells (BMDC) (Figure 5A, B). The synthetic dsRNA analogue Poly (I:C) was used as a positive control. After incubation for 24 h, BMDC maturation was evaluated by flow cytometry monitoring the percentage of CD11c-positive cells expressing high levels of the activation-induced markers MHC class II and CD80 (Figure 5C and Supplementary Figure S4). Interestingly, the purified P0 peak diluted to an RNA concentration as low as 12 ng/ml was sufficient to trigger BMDC maturation, at levels comparable to those obtained when adding micrograms of Poly (I:C) (Figure 5D). Undiluted P0 (1.2 μg/ml) was highly cytotoxic, with more than 90% of cells staining positive for PI. Furthermore, high levels of the pro-inflammatory cytokine IL-1β were found in the media of these cells (Figure 5E). Altogether, these observations suggest that components in the P0 peak can be sensed by DCs when present in the extracellular space. They can trigger DC maturation and, at higher concentrations, a form of cell death presumably related to over activation or pyroptosis. The latter effect is dependent on RNA because undiluted RNase-treated P0 did not induce IL-1β release nor triggered significant BMDC maturation in viable cells. These observations strongly argue against potential endotoxin contamination of the P0 fraction that may have led to DC maturation and/or IL-1β secretion. These results afford new avenues in the biological characterization of exRNAs, suggesting at least some of these RNAs are immunologically nonsilent. This supports the possibility of an immune surveillance mechanism involving exRNAs or RNP complexes such as extracellular ribosomes.

DISCUSSION

A substantial fraction of exRNAs are not encapsulated inside EVs, yet the extracellular nonvesicular RNAome has not been studied in a comprehensive manner yet. By inhibiting extracellular RNases, our results highlight that the nonvesicular exRNA fraction is highly dynamic. This experimental approach enabled us to obtain exRNA profiles with an unprecedented level of detail and with temporal resolution. Furthermore, we succeeded in stabilizing extracellular full-length tRNAs and ribosomes, which have not been identified before outside EVs due to their susceptibility to extracellular ribonucleases. In contrast, some of their fragments were found to be highly stable and they collectively define the nonvesicular RNAome under standard conditions, especially in the presence of serum. These results have profound implications on the way we understand the mechanisms responsible for RNA release.

The presence of ribosomal aggregates in the extracellular EV-depleted fraction is further supported by the co-isolation of rRNAs, ribosomal proteins and polyA+ mRNAs from the same chromatographic fractions. Extracellular ribosomes were described in the 70's in the blowfly *Calliphora vicina* (39) but subsequently linked to an experimental artefact (40) and have received little attention since then. However, we have demonstrated that extracellular ribosomes exist at least transiently in the media of cultured mammalian cells and possibly also in body fluids. In support of the latter, a modified small-RNA sequencing method has been recently reported that permits the identification of mRNA fragments in blood plasma or serum (41). Strikingly, the authors found that the distribution and length of reads mapping to mRNAs was reminiscent of ribosome profiling, suggesting that the sequenced fragments could be the footprints of ribosomes circulating in biofluids.

There is an increasing body of evidence showing that EVs actually contain more full-length ncRNAs than microRNAs or ncRNA fragments. For instance, Bioanalyzer's peaks corresponding to intact 18S and 28S rRNAs have been identified in purified EVs (32,42–45), while full-length YRNAs and other ncRNAs have been identified by sequencing, RT-qPCR and/or Northern blot (17,46). The use of thermostable group II intron reverse transcriptases (TGIRT-seq) has allowed the identification of full-length tRNAs in EVs, which greatly outnumber tRNA-derived fragments (47–49). Our results are consistent with these reports, and clearly show the presence of tRNAs and 7SL RNAs in EVs purified by buoyant density flotation in linear iodixanol gradients. At the level of sensitivity achievable by DIG-based Northern blotting, tRNA-derived fragments were not detectable in EVs (Figure 4H). Therefore, TGIRT-seq does not seem to be biasing results toward full-length tRNAs (48), and gives a picture of the RNA content of EVs which is in good agreement with our Northern blot results. This can change, however, when EVs are purified from stressed cells. Considering stressed cells upregulate tRNA-derived fragments (23,24) and that changes in intracellular RNA profiles are mirrored in EVs (50), it is reasonable to speculate that EVs coming from stressed cells could contain higher payloads of stress-induced tRNA halves (51).

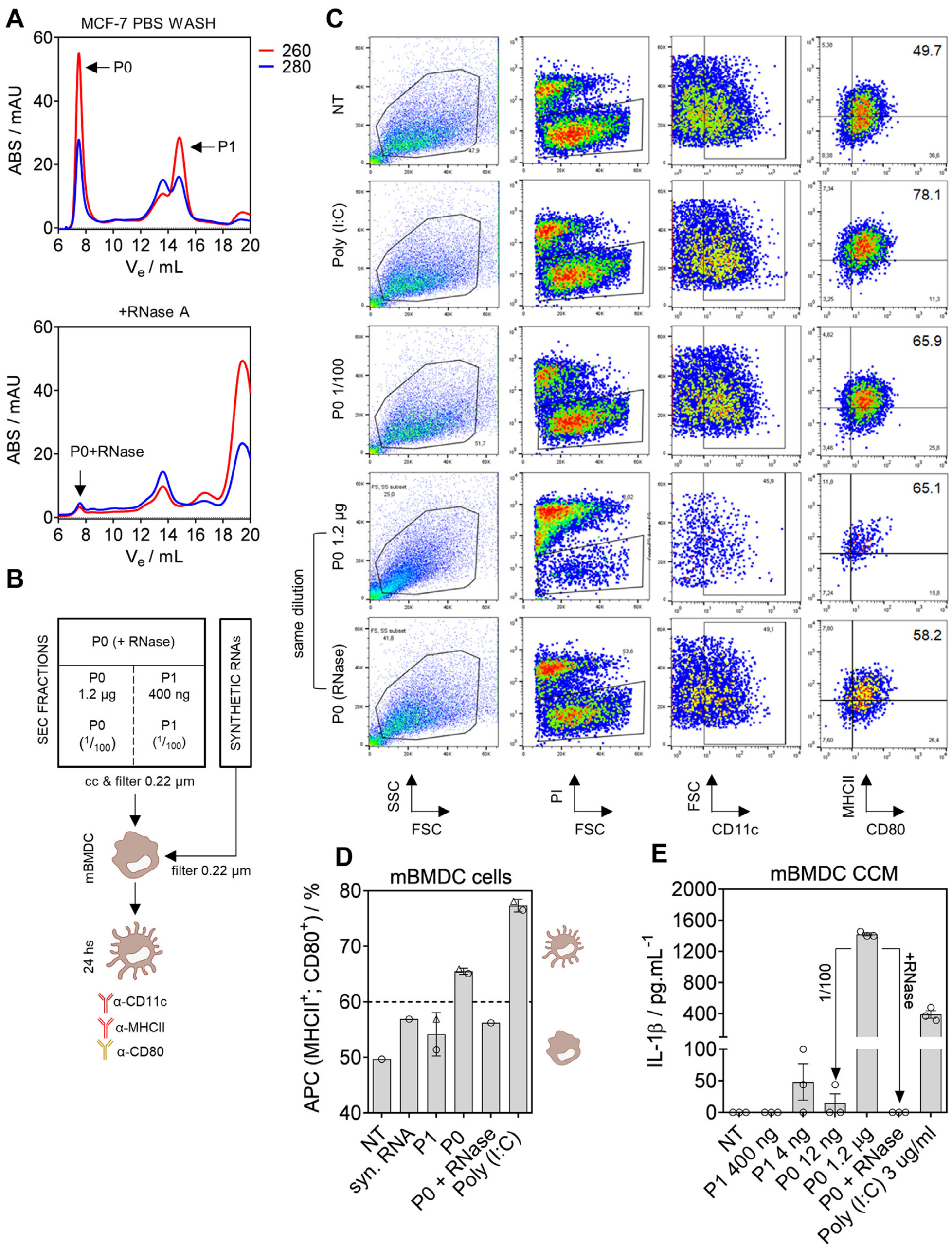

Figure 5. The contents of the P0 peak can trigger dendritic cell maturation in an RNA-dependent manner. (**A**) SEC separation of the P0 and P1 peaks used for dendritic cell maturation assays. Cell-conditioned PBS was concentrated and separated into two aliquots, one of which was treated with RNase A before SEC. (**B**) Concentrated and sterilized SEC fractions were incubated with nonprimed murine bone marrow-derived dendritic cells (BMDC). The TLR3 agonist Poly (I:C) was used as a positive control. (**C**) Flow cytometry analysis of BMDC at $t = 24$ h post exposure to the P0 and P1 peaks (or synthetic RNAs). PI: propidium iodide. FSC: forward scatter. SSC: side scatter. Numbers to the right correspond to the percentage of viable (PI negative), CD11c-positive cells expressing high levels of class II MHC and CD80. (**D**) Percentage of matured BMDC (considered as antigen-presenting cells, APC) at $t = 24$ h post exposure. Triangles correspond to diluted fractions (P0: 1/100; P1: 1/100; Poly [I:C]: 1/10). E) Quantitation by ELISA of IL-1β levels in the media of BMDC analyzed by flow cytometry in the previous panel.

Nonvesicular exRNAs have received very little attention (15) until recently (32). In the past, we have compared the small RNA content between EVs and 100,000 x g supernatants of cell-conditioned medium and found that the EV-depleted fraction was highly enriched in 5′ tRNA halves of precisely 30 or 31 nucleotides and almost exclusively derived from glycine or glutamic acid tRNAs (16). Similar results were obtained by other groups working on primary cultures of glioblastoma (17). Furthermore, glycine tRNA halves are predominantly found outside EVs in serum (20) and are ubiquitous in many biofluids including serum, urine, saliva and bile (18). We are now showing that these fragments are not directly released from cells *in vitro*. Instead, they are generated in the extracellular space (Figure 6). Enrichment of these fragments, especially when found in the EV-depleted fraction, is probably a consequence of their dif-

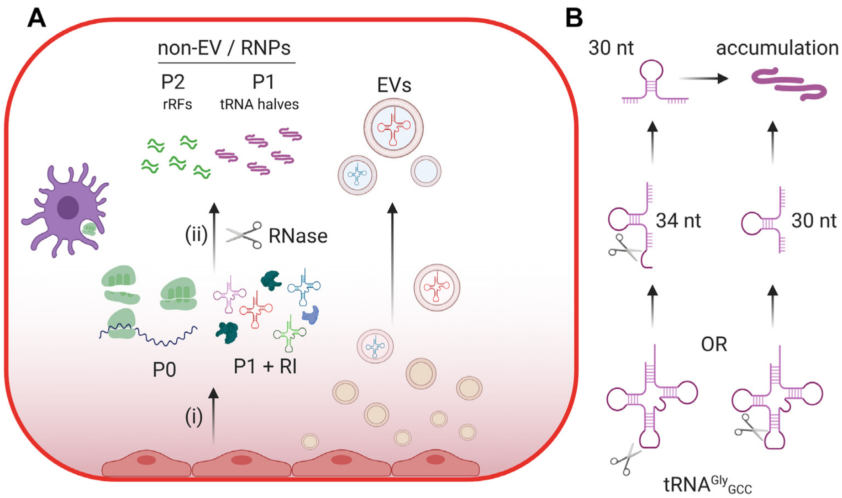

Figure 6. Proposed model. (**A**) Cells in culture release tRNAs, ribosomal subunits or ribosomes to the extracellular space, even outside EVs. When the CCM is analyzed by SEC, these RNAs define the P0 and P1 peaks, respectively (i). However, their detection is only possible after addition of RI to the medium. Active secretion (e.g., autophagy-dependent) might contribute to nonvesicular exRNA profiles, but damaged or dead cells with compromised plasma membrane integrity may be quantitatively more important. Extracellular RNases degrade nonvesicular RNAs and generate stable fragmentation products like glycine tRNA halves (ii), which can assemble into dimers and elute in the chromatographic P1 peak even in the absence of RI. The P2 peak is probably composed of rRNA-derived fragments (rRFs) forming tightly bound dsRNAs which are not amenable to standard small RNA sequencing techniques. While full-length tRNAs and YRNAs are not detected in the non-EV fraction in the absence of RI, those which are present inside EVs are protected from degradation. Thus, EVs are probably the only source of full-length ncRNAs in RNase-rich extracellular samples. Overall, this diagram represent the remarkable differences between what is sequenced in the extracellular space in the absence of RI and what cells actually release, as revealed by RI-SEC-seq. (**B**) A diagram explaining possible biogenetic routes for extracellular, nonvesicular tRNA$^{Gly}{}_{GCC}$ 5' halves.

ferential extracellular stability rather than their preferential or selective secretion. This is further supported by the recent observation that circular RNAs, which are known to be highly stable, are increased in nearly all human biofluids when compared to matched tissues (52).

Live cells can release a representative fraction of their cytoplasm by mechanisms such as cytoplasmic extrusion (53) or amphisome fusion with the plasma membrane (32), and these mechanisms could be involved in the release of nonvesicular ribosomes and tRNAs to the extracellular space. However, a few events of cellular damage or death might be quantitatively more important in defining exRNA profiles as has been discussed above. In support of this, it has been shown that extracellular rRNA levels correlate with extracellular lactate dehydrogenase (LDH) activity, which is widely used as a marker of cell death (54). Even though exRNA analysis derived from dead cells can be considered as an artifact of cell culture, there are situations where nonapoptotic, immunogenic cell death (ICD) occurs at abnormal frequencies in an organism. These situations include aging (55), trauma (56), ischemia-reperfusion injury (57), infectious diseases and cancer. In the latter, ICD can occur because of the hypoxic inner mass characteristic of solid tumors or following treatment with cytotoxic agents (58). In all cases, dying cells release intracellular components which are sensed by innate immune cells and interpreted as damage-associated molecular patterns (DAMPs). Furthermore, the therapeutic activity of several anticancer drugs eliciting ICD involves an autocrine and paracrine circuit which depends at least in part on the release of self RNAs by stressed or dying cancer cells (59). Because rRNAs and tRNAs are highly abundant intracellularly and they are exposed in the extracellular space in cases of damage, and considering RNAs are actively sensed by the innate immune system (60,61), we hypothesized that exRNA-containing nonvesicular complexes could be endowed with immunomodulatory abilities. The high turnover of these complexes as a consequence of extracellular RNases could prevent activation under physiological conditions.

As for the ribonuclease responsible for extracellular, nonvesicular tRNA cleavage, it is clearly a serum-derived ribonuclease in FBS-containing samples (probably RNase A itself). When serum is not present or highly diluted, such as after thoroughly washing cells with serum-free media or buffers, it is possible that endogenous secreted RNases are responsible for shaping nonvesicular exRNA profiles. Stressed cancer cells secrete enzymes to perform some metabolic reactions in the extracellular space and then uptake the enzymatic products to fuel cellular energetics (62). By analogy, we are tempted to speculate that secreted RNases such as ANG could play a role in extracellular RNA metabolism, preventing the toxicity associated with their intracellular activity in nonstressed cells (63). Although the function of ANG in tRNA cleavage seems to be partially redundant (36,64), its implications in extracellular RNA cleavage under physiological conditions remains to be elucidated. Redundancy might be lower in serum-free environments as the nervous system, where several mutations in ANG have been functionally linked to neurodegenerative diseases (65). We have provided preliminary evidence suggesting an involvement of extracellular, nonvesicular RNAs or RNPs in immune surveillance. Thus, a link between mutations in ANG and deregulated extracellular RNA fragmentation patterns is feasible in diseases such as ALS whose etiology or evolution is deeply connected to inflammation (66).

Bacterial rRNA and tRNAs induce Toll-like receptor (TLR)-dependent DC maturation and IL-1β secretion, and are therefore considered pathogen-associated molecular patterns. However, to elicit such a response, addition of the purified RNAs with cationic lipids seems to be essential (67). In contrast, we have obtained high extracellular levels of IL-1β when incubating BMDC with approximately one microgram of RNA obtained from the P0 peak of MCF-7 cells (composed mainly of ribosome particles) in the absence of any transfection reagent. Strikingly, this effect was lost when incubating DCs with RNase A-pretreated P0. It remains to be elucidated whether RNA itself or any potentially associated RNA-binding proteins are responsible for these effects. We address some limitations in our experimental design, including the incubation of human-derived RNAs with murine dendritic cells. Thus, these results should be interpreted with caution. Follow-up studies will confirm whether or not extracellular nonvesicular RNAs are active players in immune surveillance.

Although extracellular ribosomes are not predicted to resist extracellular RNases they might still achieve functionally relevant concentrations *in vivo* in extracellular microenvironments. The identification of a RNase-resistant peak (P2) derived from partial fragmentation of P0 (and possibly P1 as well) suggests that, similarly to what we have shown for 30–31 nt tRNA halves, rRNA-derived fragments may accumulate in the extracellular space and their extracellular concentration may increase in situations of abnormal cell death. A new method has been recently described enabling RNA sequencing from a few microliters of human serum (68). With this method, almost perfect separation between normal and breast cancer patients was possible based on rRNA or mitochondrial tRNA sequences.

In conclusion, ribonuclease inhibition dramatically shapes extracellular RNA profiles and uncovers a population of extracellular ribosomes, tRNAs and other coding and noncoding RNAs. These RNAs, which are not protected by encapsulation inside EVs, are rapidly degraded by extracellular RNases. However, some of their fragments resist degradation and can accumulate in cell culture media and in biofluids. This dynamic view of exRNAs impacts our understanding of RNA secretion mechanisms and may offer a window to new molecules with biomarker potential. These include intrinsically stable ncRNA fragments and extracellular RNPs stabilized by addition of RI immediately upon collection of samples.

NOTE ADDED IN REVISION

During the review process of this manuscript, an article has been accepted for publication in Nucleic Acids Research which has shown that human RNase 1 generates tRNA- and YRNA-derived fragments in the extracellular space and outside EVs (69). This report supports many of our findings. Taken together, the support for the extracellular biogenesis of extracellular small RNAs seems to be strong.

DATA AVAILABILITY

Data is available at NCBI SRA under the BioProject ID: PRJNA633249.

SUPPLEMENTARY DATA

Supplementary Data are available at NAR Online.

ACKNOWLEDGEMENTS

J.P.T., M.S., M.H. and A.C. are members of the Sistema Nacional de Investigadores (SNI, ANII). The authors want to thank the following core facilities at the Pasteur Institute of Montevideo: Flow cytometry (UBC), Recombinant Proteins (UPR) and the Analytical Biochemistry and Proteomics Unit (UByPA) for their technical assistance. TEM images were obtained in Centro Universitario Regional Este (CURE, Universidad de la República). The authors also want to thank Eric Westhof (Strasbourg University), Marco Li Calzi (IPMon), Laura Fornaro (CURE/UdelaR), Kenneth W. Witwer (Johns Hopkins University), Paul Anderson, Shawn Lyons, Nancy Kedersha, Prakash Kharel and Vivek M. Advani (BWH/HMS) for helpful suggestions, experimental help and insightful scientific discussions.

FUNDING

Agencia Nacional de Investigación e Innovación (ANII, Uruguay) [FCE_3_2018_1_148745]; Comisión Sectorial de Investigación Científica (CSIC-UdelaR, Uruguay) [MIA_PAS2019_2_99]; National Institutes of Health, USA [RO1GM126150 and UG3CA241694, supported by the NIH Common Fund, through the Office of Strategic Coordination/Office of the NIH Director]. Funding for open access charge: NIH [UG3CA241694].

Conflict of interest statement. None declared.

REFERENCES

1. Heitzer,E., Haque,I.S., Roberts,C.E.S. and Speicher,M.R. (2019) Current and future perspectives of liquid biopsies in genomics-driven oncology. *Nat. Rev. Genet.*, **20**, 71–88.
2. Sacher,A.G., Paweletz,C., Dahlberg,S.E., Alden,R.S., O'Connell,A., Feeney,N., Mach,S.L., Jänne,P.A. and Geoffrey,O. (2016) Prospective validation of rapid plasma genotyping for the detection of EGFR and kras mutations in advanced lung cancer. *JAMA Oncol.*, **2**, 1014–1022.
3. Warren,J.D., Xiong,W., Bunker,A.M., Vaughn,C.P., Furtado,L.V., Roberts,W.L., Fang,J.C., Samowitz,W.S. and Heichman,K.A. (2011) Septin 9 methylated DNA is a sensitive and specific blood test for colorectal cancer. *BMC Med.*, **9**, 133.
4. Antoury,L., Hu,N., Balaj,L., Das,S., Georghiou,S., Darras,B., Clark,T., Breakefield,X.O. and Wheeler,T.M. (2018) Analysis of extracellular mRNA in human urine reveals splice variant biomarkers of muscular dystrophies. *Nat. Commun.*, **9**, 3906.
5. Thomou,T., Mori,M.A., Dreyfuss,J.M., Konishi,M., Sakaguchi,M., Wolfrum,C., Rao,T.N., Winnay,J.N., Garcia-Martin,R., Grinspoon,S.K. *et al.* (2017) Adipose-derived circulating miRNAs regulate gene expression in other tissues. *Nature*, **542**, 450–455.
6. Zomer,A., Maynard,C., Verweij,F.J., Kamermans,A., Schafer,R., Beerling,E., Schiffelers,R.M., de Wit,E., Berenguer,J., Ellenbroek,S.I.J. *et al.* (2015) In vivo imaging reveals extracellular vesicle-mediated phenocopying of metastatic behavior. *Cell*, **161**, 1046–1057.
7. Valadi,H., Ekstrom,K., Bossios,A., Sjostrand,M., Lee,J.J. and Lotvall,J.O. (2007) Exosome-mediated transfer of mRNAs and microRNAs is a novel mechanism of genetic exchange between cells. *Nat. Cell Biol.*, **9**, 654–659.
8. Tsui,N.B.Y., Ng,E.K.O. and Lo,Y.M.D. (2002) Stability of endogenous and added RNA in blood specimens, serum, and plasma. *Clin. Chem.*, **48**, 1647–1653.

9. Ratajczak,J., Miekus,K., Kucia,M., Zhang,J., Reca,R., Dvorak,P. and Ratajczak,M.Z. (2006) Embryonic stem cell-derived microvesicles reprogram hematopoietic progenitors: evidence for horizontal transfer of mRNA and protein delivery. *Leukemia*, **20**, 847–856.
10. Skog,J., Wurdinger,T., van Rijn,S., Meijer,D.H., Gainche,L., Sena-Esteves,M., Curry,W.T.J., Carter,B.S., Krichevsky,A.M. and Breakefield,X.O. (2008) Glioblastoma microvesicles transport RNA and proteins that promote tumour growth and provide diagnostic biomarkers. *Nat. Cell Biol.*, **10**, 1470–1476.
11. Tabet,F., Vickers,K.C., Cuesta Torres,L.F., Wiese,C.B., Shoucri,B.M., Lambert,G., Catherinet,C., Prado-Lourenco,L., Levin,M.G., Thacker,S. *et al.* (2014) HDL-transferred microRNA-223 regulates ICAM-1 expression in endothelial cells. *Nat. Commun.*, **5**, 3292.
12. Vickers,K.C., Palmisano,B.T., Shoucri,B.M., Shamburek,R.D. and Remaley,A.T. (2011) MicroRNAs are transported in plasma and delivered to recipient cells by high-density lipoproteins. *Nat. Cell Biol.*, **13**, 423–435.
13. Arroyo,J.D., Chevillet,J.R., Kroh,E.M., Ruf,I.K., Pritchard,C.C., Gibson,D.F., Mitchell,P.S., Bennett,C.F., Pogosova-Agadjanyan,E.L., Stirewalt,D.L. *et al.* (2011) Argonaute2 complexes carry a population of circulating microRNAs independent of vesicles in human plasma. *Proc. Natl. Acad. Sci. U.S.A.*, **108**, 5003–5008.
14. Turchinovich,A., Weiz,L., Langheinz,A. and Burwinkel,B. (2011) Characterization of extracellular circulating microRNA. *Nucleic Acids Res.*, **39**, 7223–7233.
15. Li,K., Rodosthenous,R.S., Kashanchi,F., Gingeras,T., Gould,S.J., Kuo,L.S., Kurre,P., Lee,H., Leonard,J.N., Liu,H. *et al.* (2018) Advances, challenges, and opportunities in extracellular RNA biology: insights from the NIH exRNA strategic workshop. *JCI insight*, **3**, 98942.
16. Tosar,J.P., Gámbaro,F., Sanguinetti,J., Bonilla,B., Witwer,K.W. and Cayota,A. (2015) Assessment of small RNA sorting into different extracellular fractions revealed by high-throughput sequencing of breast cell lines. *Nucleic Acids Res.*, **43**, 5601–5616.
17. Wei,Z., Batagov,A.O., Schinelli,S., Wang,J., Wang,Y., El Fatimy,R., Rabinovsky,R., Balaj,L., Chen,C.C., Hochberg,F. *et al.* (2017) Coding and noncoding landscape of extracellular RNA released by human glioma stem cells. *Nat. Commun.*, **8**, 1145.
18. Srinivasan,S., Yeri,A., Cheah,P.S., Chung,A., Danielson,K., De Hoff,P., Filant,J., Laurent,C.D., Laurent,L.D., Magee,R. *et al.* (2019) Small RNA sequencing across diverse biofluids identifies optimal methods for exRNA isolation. *Cell*, **177**, 446–462.
19. Godoy,P.M., Bhakta,N.R., Barczak,A.J., Cakmak,H., Fisher,S., MacKenzie,T.C., Patel,T., Price,R.W., Smith,J.F., Woodruff,P.G. *et al.* (2018) Large differences in small RNA composition between human biofluids. *Cell Rep.*, **25**, 1346–1358.
20. Dhahbi,J.M., Spindler,S.R., Atamna,H., Yamakawa,A., Boffelli,D., Mote,P. and Martin,D.I.K. (2013) 5′ tRNA halves are present as abundant complexes in serum, concentrated in blood cells, and modulated by aging and calorie restriction. *BMC Genomics*, **14**, 298.
21. Zhang,Y., Zhang,Y., Shi,J., Zhang,H., Cao,Z., Gao,X., Ren,W., Ning,Y., Ning,L., Cao,Y. *et al.* (2014) Identification and characterization of an ancient class of small RNAs enriched in serum associating with active infection. *J. Mol. Cell Biol.*, **6**, 172–174.
22. Tosar,J.P., Gambaro,F., Darre,L., Pantano,S., Westhof,E. and Cayota,A. (2018) Dimerization confers increased stability to nucleases in 5′ halves from glycine and glutamic acid tRNAs. *Nucleic Acids Res.*, **46**, 9081–9093.
23. Fu,H., Feng,J., Liu,Q., Sun,F., Tie,Y., Zhu,J., Xing,R., Sun,Z. and Zheng,X. (2009) Stress induces tRNA cleavage by angiogenin in mammalian cells. *FEBS Lett.*, **583**, 437–442.
24. Yamasaki,S., Ivanov,P., Hu,G.-F. and Anderson,P. (2009) Angiogenin cleaves tRNA and promotes stress-induced translational repression. *J. Cell Biol.*, **185**, 35–42.
25. Thompson,D.M., Lu,C., Green,P.J. and Parker,R. (2008) tRNA cleavage is a conserved response to oxidative stress in eukaryotes. *RNA*, **14**, 2095–2103.
26. Segovia,M., Cuturi,M.C. and Hill,M. (2011) Preparation of mouse bone marrow-derived dendritic cells with immunoregulatory properties. *Methods Mol. Biol.*, **677**, 161–168.
27. Cozen,A.E., Quartley,E., Holmes,A.D., Hrabeta-Robinson,E., Phizicky,E.M. and Lowe,T.M. (2015) ARM-seq: AlkB-facilitated RNA methylation sequencing reveals a complex landscape of modified tRNA fragments. *Nat. Methods*, **12**, 879–884.
28. Gogakos,T., Brown,M., Garzia,A., Meyer,C., Hafner,M. and Tuschl,T. (2017) Characterizing expression and processing of precursor and mature human tRNAs by hydro-tRNAseq and PAR-CLIP. *Cell Rep.*, **20**, 1463–1475.
29. Torres,A.G., Reina,O., Attolini,C.S.O. and De Pouplana,L.R. (2019) Differential expression of human tRNA genes drives the abundance of tRNA-derived fragments. *Proc. Natl. Acad. Sci. USA*, **116**, 8451–8456.
30. Zheng,G., Qin,Y., Clark,W.C., Dai,Q., Yi,C., He,C., Lambowitz,A.M. and Pan,T. (2015) Efficient and quantitative high-throughput tRNA sequencing. *Nat. Methods*, **12**, 835–837.
31. Ouyang,D.Y., Xu,L.H., He,X.H., Zhang,Y.T., Zeng,L.H., Cai,J.Y. and Ren,S. (2013) Autophagy is differentially induced in prostate cancer LNCaP, DU145 and PC-3 cells via distinct splicing profiles of ATG5. *Autophagy*, **9**, 20–32.
32. Jeppesen,D.K., Fenix,A.M., Franklin,J.L., Higginbotham,J.N., Zhang,Q., Zimmerman,L.J., Liebler,D.C., Ping,J., Liu,Q., Evans,R. *et al.* (2019) Reassessment of Exosome Composition. *Cell*, **177**, 428–445.
33. Aviner,R. (2020) The science of puromycin: From studies of ribosome function to applications in biotechnology. *Comput. Struct. Biotechnol. J.*, **18**, 1074–1083.
34. Semenkov,Y., Shapkina,T., Makhno,V. and Kirillov,S. (1992) Puromycin reaction for the A site-bound peptidyl-tRNA. *FEBS Lett.*, **296**, 207–210.
35. Nolan,R.D. and Arnstein,H.R.V. (1969) The dissociation of rabbit reticulocyte ribosomes with EDTA and the location of messenger ribonucleic acid. *Eur. J. Biochem.*, **9**, 445–450.
36. Akiyama,Y., Lyons,S., Fay,M.M., Abe,T., Anderson,P. and Ivanov,P. (2019) Multiple ribonuclease A family members cleave transfer RNAs in response to stress. bioRxiv doi: https://doi.org/10.1101/811174, 21 October 2019, preprint: not peer reviewed.
37. Buck,A.H., Coakley,G., Simbari,F., McSorley,H.J., Quintana,J.F., Le Bihan,T., Kumar,S., Abreu-Goodger,C., Lear,M., Harcus,Y. *et al.* (2014) Exosomes secreted by nematode parasites transfer small RNAs to mammalian cells and modulate innate immunity. *Nat. Commun.*, **5**, 5488.
38. Banchereau,J. and Steinman,R.M. (1998) Dendritic cells and the control of immunity. *Nature*, **392**, 245–252.
39. Sridhara,S. and Levenbook,L. (1973) Extracellular ribosomes during metamorphosis in the blowfly Calliphora erythrocephala. *Biochem. Biophys. Res. Commun.*, **53**, 1253–1259.
40. Levenbook,L., Sridhara,S. and Lambertsson,A. (1976) Extracellular ribosomes during metamorphosis of the blowfly Calliphora vicina R. D. – a reappraisal of their authenticity. *Biochem. Biophys. Res. Commun.*, **70**, 15–21.
41. Akat,K.M., Lee,Y.A., Hurley,A., Morozov,P., Max,K.E.A., Brown,M., Bogardus,K., Sopeyin,A., Hildner,K., Diacovo,T.G. *et al.* (2019) Detection of circulating extracellular mRNAs by modified small-RNA-sequencing analysis. *JCI Insight*, **4**, 127317.
42. Lunavat,T.R., Cheng,L., Einarsdottir,B.O., Bagge,R.O., Muralidharan,S.V., Sharples,R.A., Lässer,C., Gho,Y.S., Hill,A.F., Nilsson,J.A. *et al.* (2017) BRAFV600 inhibition alters the microRNA cargo in the vesicular secretome of malignant melanoma cells. *Proc. Natl. Acad. Sci. U.S.A.*, **114**, E5930–E5939.
43. Lunavat,T.R., Cheng,L., Kim,D.K., Bhadury,J., Jang,S.C., Lässer,C., Sharples,R.A., López,M.D., Nilsson,J., Gho,Y.S. *et al.* (2015) Small RNA deep sequencing discriminates subsets of extracellular vesicles released by melanoma cells – evidence of unique microRNA cargos. *RNA Biol.*, **12**, 810–823.
44. Lässer,C., Shelke,G.V., Yeri,A., Kim,D.K., Crescitelli,R., Raimondo,S., Sjöstrand,M., Gho,Y.S., Van Keuren Jensen,K. and Lötvall,J. (2017) Two distinct extracellular RNA signatures released by a single cell type identified by microarray and next-generation sequencing. *RNA Biol.*, **14**, 58–72.
45. Chiou,N.T., Kageyama,R. and Ansel,K.M. (2018) Selective export into extracellular vesicles and function of tRNA fragments during T cell activation. *Cell Rep.*, **25**, 3356–3370.
46. Driedonks,T.A.P., van der Grein,S.G., Ariyurek,Y., Buermans,H.P.J., Jekel,H., Chow,F.W.N., Wauben,M.H.M., Buck,A.H., ’t Hoen,P.A.C. and Nolte-’t Hoen,E.N.M. (2018) Immune stimuli shape the small non-coding transcriptome of extracellular vesicles released by dendritic cells. *Cell. Mol. Life Sci.*, **75**, 3857–3875.

47. Qin,Y., Yao,J., Wu,D.C., Nottingham,R.M., Mohr,S., Hunicke-Smith,S. and Lambowitz,A.M. (2016) High-throughput sequencing of human plasma RNA by using thermostable group II intron reverse transcriptases. *RNA*, **22**, 111–128.
48. Shurtleff,M.J., Yao,J., Qin,Y., Nottingham,R.M., Temoche-Diaz,M.M., Schekman,R. and Lambowitz,A.M. (2017) Broad role for YBX1 in defining the small noncoding RNA composition of exosomes. *Proc. Natl. Acad. Sci. U.S.A.*, **114**, E8987–E8995.
49. Temoche-Diaz,M.M., Shurtleff,M.J., Nottingham,R.M., Yao,J., Fadadu,R.P., Lambowitz,A.M. and Schekman,R. (2019) Distinct mechanisms of microrna sorting into cancer cell-derived extracellular vesicle subtypes. *Elife*, **8**, 47544.
50. Gámbaro,F., Li Calzi,M., Fagúndez,P., Costa,B., Greif,G., Mallick,E., Lyons,S., Ivanov,P., Witwer,K., Cayota,A. *et al.* (2020) Stable tRNA halves can be sorted into extracellular vesicles and delivered to recipient cells in a concentration-dependent manner. *RNA Biol.*, **17**, 1168–1182.
51. Tosar,J.P. and Cayota,A. (2020) Extracellular tRNAs and tRNA-derived fragments. *RNA Biol.*, **17**, 1149–1167.
52. Hulstaert,E., Morlion,A., Cobos,F.A., Verniers,K., Nuytens,J., Eynde,E.V, Yigit,N., Anckaert,J., Geerts,A., Hindryckx,P. *et al.* (2019) Charting extracellular transcriptomes in The Human Biofluid RNA Atlas. bioRxiv doi: https://doi.org/10.1101/823369, 05 November 2019, preprint: not peer reviewed.
53. Lee,K.-Z., Lestradet,M., Socha,C., Schirmeier,S., Schmitz,A., Spenlé,C., Lefebvre,O., Keime,C., Yamba,W.M., Bou Aoun,R. *et al.* (2016) Enterocyte purge and rapid recovery is a resilience reaction of the gut epithelium to pore-forming toxin attack. *Cell Host Microbe*, **20**, 716–730.
54. Böttcher,K., Wenzel,A. and Warnecke,J.M. (2006) Investigation of the origin of extracellular RNA in human cell culture. In: *Annals of the New York Academy of Sciences*. Blackwell Publishing Inc., Vol. **1075**, pp. 50–56.
55. Franceschi,C., Garagnani,P., Vitale,G., Capri,M. and Salvioli,S. (2017) Inflammaging and 'Garb-aging'. *Trends Endocrinol. Metab.*, **28**, 199–212.
56. Zhang,Q., Raoof,M., Chen,Y., Sumi,Y., Sursal,T., Junger,W., Brohi,K., Itagaki,K. and Hauser,C.J. (2010) Circulating mitochondrial DAMPs cause inflammatory responses to injury. *Nature*, **464**, 104–107.
57. Slegtenhorst,B.R., Dor,F.J.M.F., Rodriguez,H., Voskuil,F.J. and Tullius,S.G. (2014) Ischemia/reperfusion injury and its consequences on immunity and inflammation. *Curr. Transplant. Rep.*, **1**, 147–154.
58. Galluzzi,L., Buqué,A., Kepp,O., Zitvogel,L. and Kroemer,G. (2017) Immunogenic cell death in cancer and infectious disease. *Nat. Rev. Immunol.*, **17**, 97–111.
59. Sistigu,A., Yamazaki,T., Vacchelli,E., Chaba,K., Enot,D.P., Adam,J., Vitale,I., Goubar,A., Baracco,E.E., Remédios,C. *et al.* (2014) Cancer cell–autonomous contribution of type I interferon signaling to the efficacy of chemotherapy. *Nat. Med.*, **20**, 1301–1309.
60. Gong,T., Liu,L., Jiang,W. and Zhou,R. (2020) DAMP-sensing receptors in sterile inflammation and inflammatory diseases. *Nat. Rev. Immunol.*, **20**, 95–112.
61. Dhir,A., Dhir,S., Borowski,L.S., Jimenez,L., Teitell,M., Rötig,A., Crow,Y.J., Rice,G.I., Duffy,D., Tamby,C. *et al.* (2018) Mitochondrial double-stranded RNA triggers antiviral signalling in humans. *Nature*, **560**, 238–242.
62. Loo,J.M., Scherl,A., Nguyen,A., Man,F.Y., Weinberg,E., Zeng,Z., Saltz,L., Paty,P.B. and Tavazoie,S.F. (2015) Extracellular metabolic energetics can promote cancer progression. *Cell*, **160**, 393–406.
63. Thomas,S.P., Hoang,T.T., Ressler,V.T. and Raines,R.T. (2018) Human angiogenin is a potent cytotoxin in the absence of ribonuclease inhibitor. *RNA*, **24**, 1018–1027.
64. Su,Z., Kuscu,C., Malik,A., Shibata,E. and Dutta,A. (2019) Angiogenin generates specific stress-induced tRNA halves and is not involved in tRF-3-mediated gene silencing. *J. Biol. Chem.*, **294**, 16930–16941.
65. van Es,M.A., Schelhaas,H.J., van Vught,P.W.J., Ticozzi,N., Andersen,P.M., Groen,E.J.N., Schulte,C., Blauw,H.M., Koppers,M., Diekstra,F.P. *et al.* (2011) Angiogenin variants in Parkinson disease and amyotrophic lateral sclerosis. *Ann. Neurol.*, **70**, 964–973.
66. Trias,E., King,P.H., Si,Y., Kwon,Y., Varela,V., Ibarburu,S., Kovacs,M., Moura,I.C., Beckman,J.S., Hermine,O. *et al.* (2018) Mast cells and neutrophils mediate peripheral motor pathway degeneration in ALS. *JCI Insight*, **3**, 123249.
67. Sha,W., Mitoma,H., Hanabuchi,S., Bao,M., Weng,L., Sugimoto,N., Liu,Y., Zhang,Z., Zhong,J., Sun,B. *et al.* (2014) Human NLRP3 inflammasome senses multiple types of bacterial RNAs. *Proc. Natl. Acad. Sci. U.S.A.*, **111**, 16059–16064.
68. Zhou,Z., Wu,Q., Yan,Z., Zheng,H., Chen,C.J., Liu,Y., Qi,Z., Calandrelli,R., Chen,Z., Chien,S. *et al.* (2019) Extracellular RNA in a single droplet of human serum reflects physiologic and disease states. *Proc. Natl. Acad. Sci. U.S.A.*, **116**, 19200–19208.
69. Nechooshtan,G., Yunusov,D., Chang,K. and Gingeras,T.R. (2020) Processing by RNase 1 forms tRNA halves and distinct Y RNA fragments in the extracellular environment. *Nucleic Acids Res.*, doi:10.1093/nar/gkaa526.

Figuras y métodos suplementarios correspondientes al artículo 1

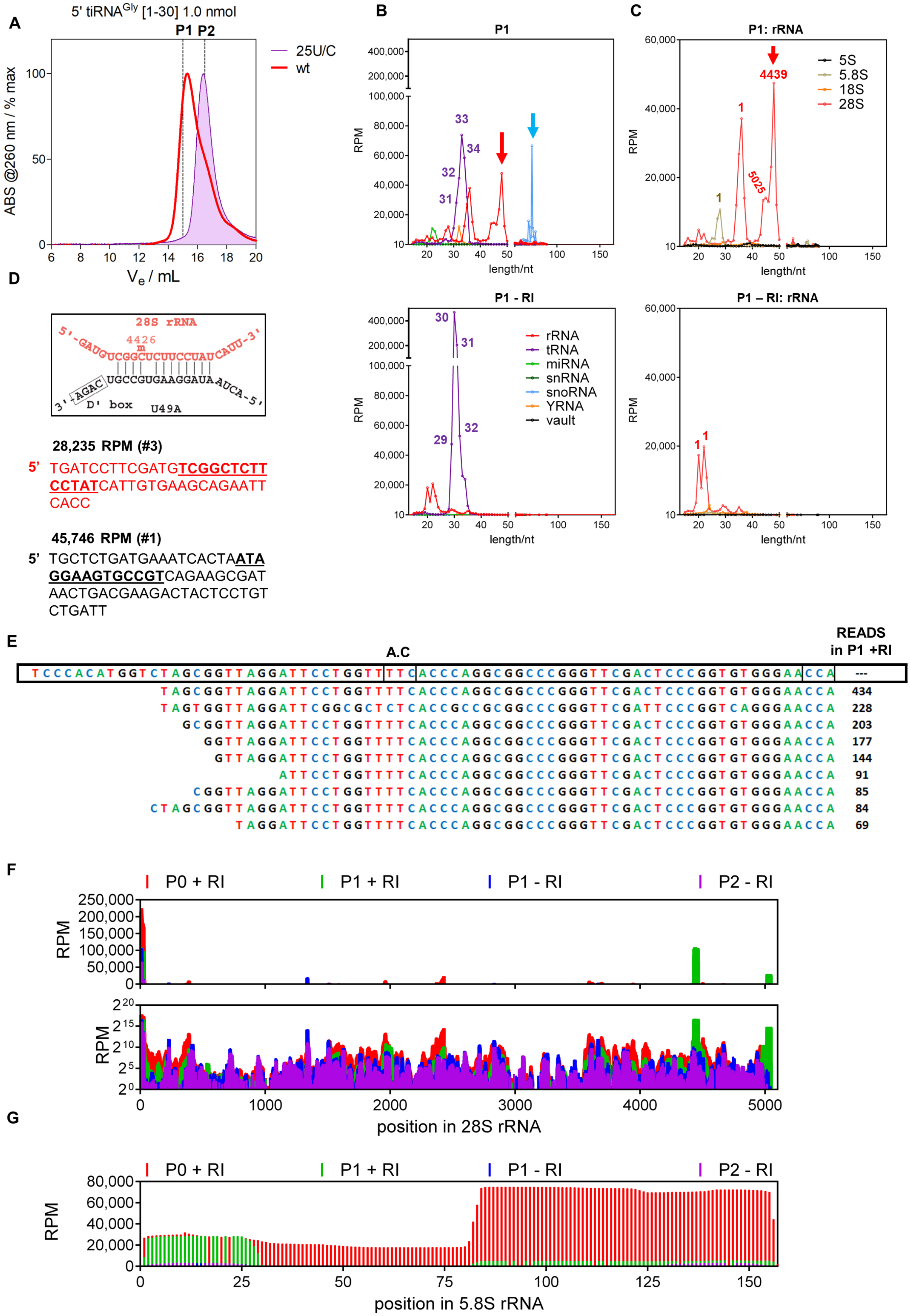
A
5' tiRNAGly [1-30] 1.0 nmol
P1 P2
25U/C
wt
ABS @260 nm / % max
Ve / mL
B
P1
P1 - RI
RPM
length/nt
rRNA
tRNA
miRNA
snRNA
snoRNA
YRNA
vault
C
P1: rRNA
P1 – RI: rRNA
5S
5.8S
18S
28S
4439
5025
D
28S rRNA
5'-GAUGUCGGCUCUUCCUAUCAUU-3'
4426
m
3'-AGACUGCCGUGAAGGAUAAUCA-5'
D' box
U49A
28,235 RPM (#3)
5' TGATCCTTCGATGTCGGCTCTT CCTATCATTGTGAAGCAGAATT CACC
45,746 RPM (#1)
5' TGCTCTGATGAAATCACTAATA GGAAGTGCCGTCAGAAGCGAT AACTGACGAAGACTACTCCTGT CTGATT
E
A.C
READS in P1 +RI
TCCCACATGGTCTAGCGGTTAGGATTCCTGGTTTTCACCCAGGCGGCCCGGGTTCGACTCCCGGTGTGGGAACCA ---
TAGCGGTTAGGATTCCTGGTTTTCACCCAGGCGGCCCGGGTTCGACTCCCGGTGTGGGAACCA 434
TAGTGGTTAGGATTCGGCGCTCTCACCGCCGCGGCCCGGGTTCGATTCCCGGTCAGGGAACCA 228
GCGGTTAGGATTCCTGGTTTTCACCCAGGCGGCCCGGGTTCGACTCCCGGTGTGGGAACCA 203
GGTTAGGATTCCTGGTTTTCACCCAGGCGGCCCGGGTTCGACTCCCGGTGTGGGAACCA 177
GTTAGGATTCCTGGTTTTCACCCAGGCGGCCCGGGTTCGACTCCCGGTGTGGGAACCA 144
ATTCCTGGTTTTCACCCAGGCGGCCCGGGTTCGACTCCCGGTGTGGGAACCA 91
CGGTTAGGATTCCTGGTTTTCACCCAGGCGGCCCGGGTTCGACTCCCGGTGTGGGAACCA 85
CTAGCGGTTAGGATTCCTGGTTTTCACCCAGGCGGCCCGGGTTCGACTCCCGGTGTGGGAACCA 84
TAGGATTCCTGGTTTTCACCCAGGCGGCCCGGGTTCGACTCCCGGTGTGGGAACCA 69
F
P0 + RI
P1 + RI
P1 - RI
P2 - RI
RPM
position in 28S rRNA
G
P0 + RI
P1 + RI
P1 - RI
P2 - RI
RPM
position in 5.8S rRNA

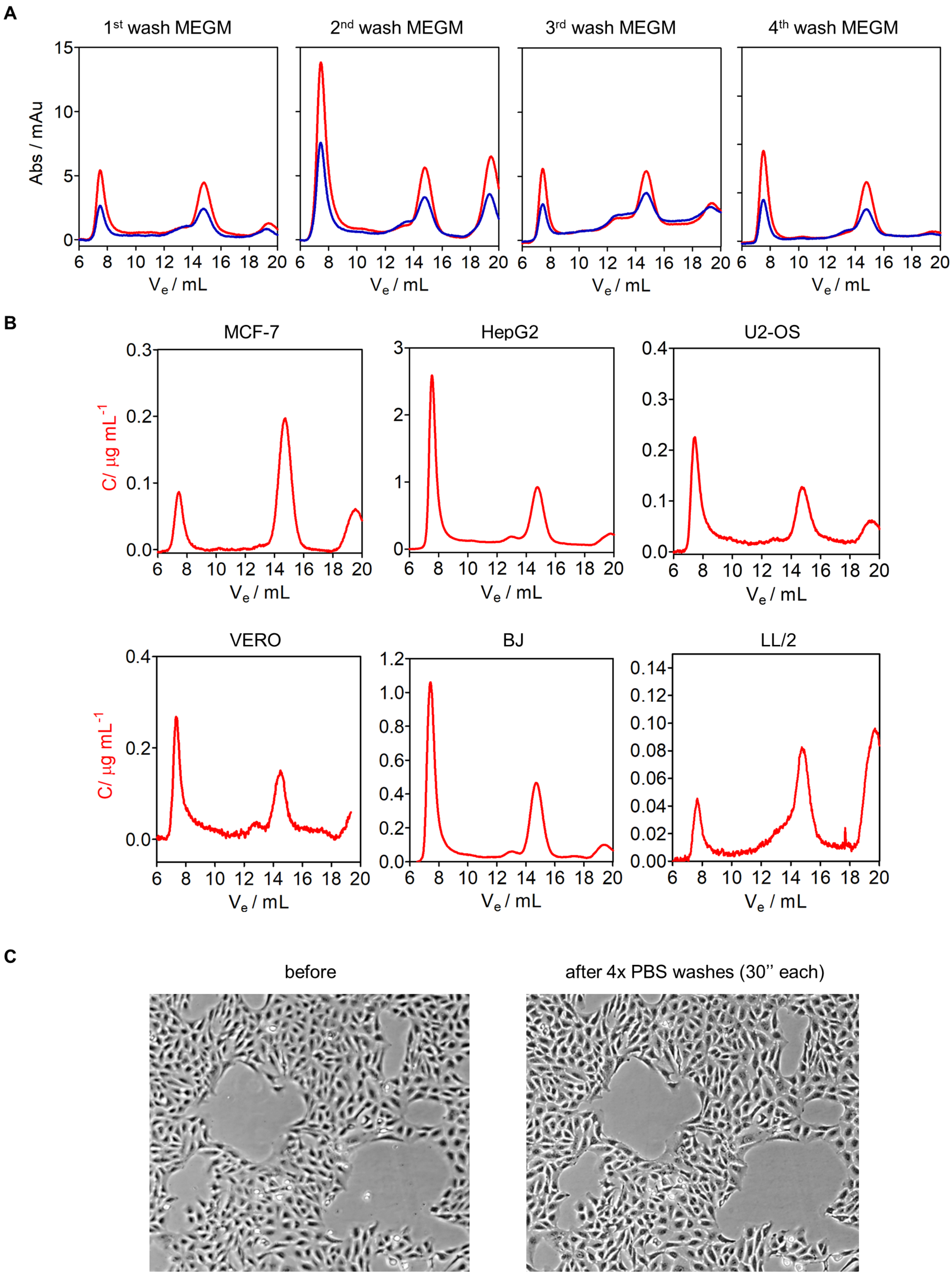

A
1st wash MEGM
2nd wash MEGM
3rd wash MEGM
4th wash MEGM
Abs / mAu
15
10
5
0
6 8 10 12 14 16 18 20
V_e / mL
B
MCF-7
HepG2
U2-OS
VERO
BJ
LL/2
C/ µg mL-1
V_e / mL
C
before
after 4x PBS washes (30'' each)

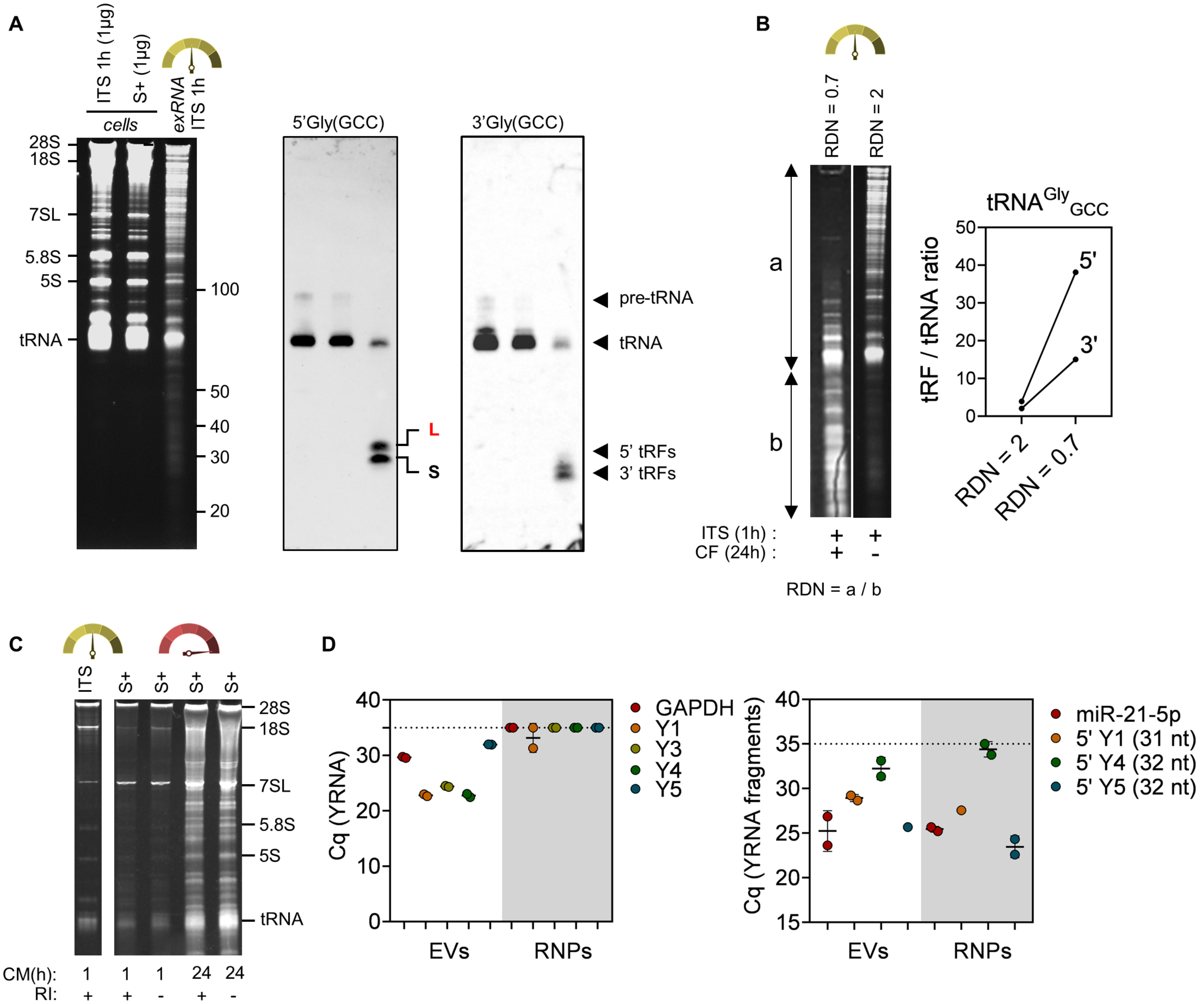

A
ITS 1h (1µg)
S+ (1µg)
cells
exRNA ITS 1h
28S
18S
7SL
5.8S
5S
tRNA
100
50
40
30
20
5'Gly(GCC)
3'Gly(GCC)
pre-tRNA
tRNA
L
S
5' tRFs
3' tRFs
B
RDN = 0.7
RDN = 2
a
b
ITS (1h) :
CF (24h) :
RDN = a / b
tRNA^Gly_GCC
tRF / tRNA ratio
5'
3'
RDN = 2
RDN = 0.7
C
ITS
S+
28S
18S
7SL
5.8S
5S
tRNA
CM(h):
RI:
D
Cq (YRNA)
GAPDH
Y1
Y3
Y4
Y5
EVs
RNPs
Cq (YRNA fragments)
miR-21-5p
5' Y1 (31 nt)
5' Y4 (32 nt)
5' Y5 (32 nt)

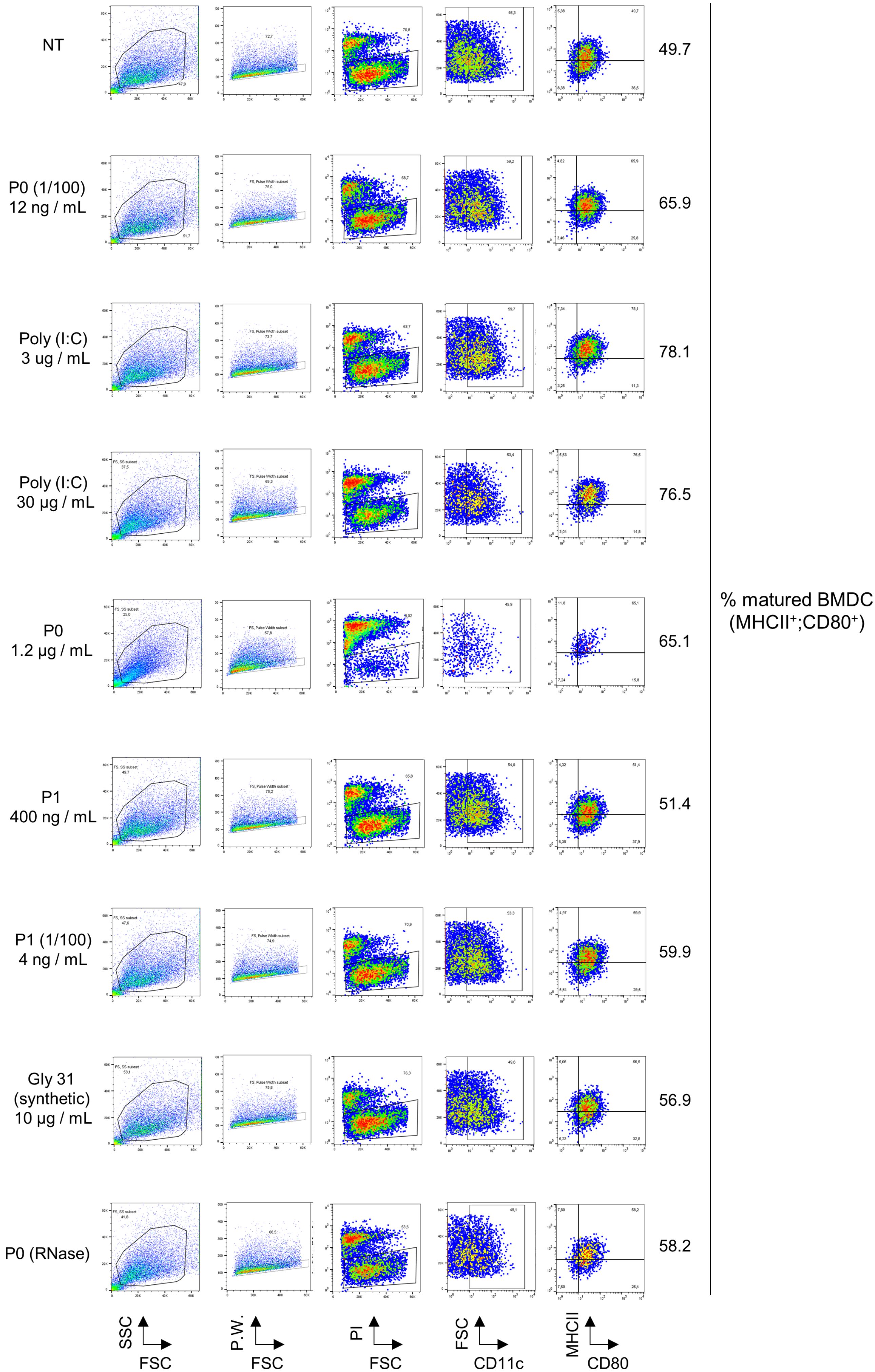
NT
49.7
P0 (1/100)
12 ng / mL
65.9
Poly (I:C)
3 ug / mL
78.1
Poly (I:C)
30 µg / mL
76.5
P0
1.2 µg / mL
65.1
P1
400 ng / mL
51.4
P1 (1/100)
4 ng / mL
59.9
Gly 31
(synthetic)
10 µg / mL
56.9
P0 (RNase)
58.2
% matured BMDC
(MHCII+;CD80+)
SSC
FSC
P.W.
FSC
PI
FSC
FSC
CD11c
MHCII
CD80

Fragmentation of extracellular ribosomes and tRNAs shapes the extracellular RNAome

Juan Pablo Tosar[1,2,3]*; Mercedes Segovia[4]; Mauricio Castellano[1,2]; Fabiana Gámbaro[2,5]; Yasutoshi Akiyama[3], Pablo Fagúndez[1,2], Álvaro Olivera[6], Bruno Costa[1,2], Tania Possi[2], Marcelo Hill[4], Pavel Ivanov[3,7], Alfonso Cayota[2,8]*.

[1]Analytical Biochemistry Unit. Nuclear Research Center. Faculty of Science. Universidad de la República, Uruguay. [2]Functional Genomics Unit, Institut Pasteur de Montevideo, Uruguay. [3]Division of Rheumatology, Immunology and Allergy, Brigham and Women's Hospital, Boston, MA, USA. Department of Medicine, Harvard Medical School, Boston, MA, USA. [4]Laboratory of Immunoregulation and Inflammation, Institut Pasteur de Montevideo, Uruguay. Immunobiology Department, Faculty of Medicine, Universidad de la República, Uruguay. [5]Molecular Virology Laboratory, Nuclear Research Center. Faculty of Science. Universidad de la República, Uruguay. [6]Centro Universitario Regional Este, Universidad de la República, Uruguay. [7]The Broad Institute of Harvard and M.I.T., Cambridge, MA, USA. [8]Department of Medicine, University Hospital, Universidad de la República, Uruguay.

*To whom correspondence should be addressed. Email: jptosar@pasteur.edu.uy; cayota@pasteur.edu.uy

SUPPLEMENTARY INFORMATION: MATERIALS AND METHODS

LEGENDS TO SUPPLEMENTARY FIGURES

Supplementary Figure 1: data associated to Figure 1. A) Injection of synthetic RNAs of 30 nt corresponding to 5' tiRNA$^{Gly}_{GCC}$ (which forms RNA dimers as reported in Tosar et al. (2018) [22]; red) and a mutant with a 25U/C substitution (which is not able to dimerize; violet) in a Superdex 200 10/300 column with PBS 1x as the mobile phase. B-C) same as Figure 1(H) and Figure 1(I) but in the P1 peak of MCF-7 CCM either treated (top) or not treated (bottom) with RI. D) Representation of the predicted SNORD49A (U49A; black)/28S rRNA (red) interaction, as depicted in snoRNABase (www-snorna.biotoul.fr). Below is the sequence with the highest number of reads. Its relative abundance is expressed as reads per million mapped reads (RPM). Its ranking in the "P1 + RI" dataset is also shown. E) Alignment of reads mapping to tRNA^{Glu} (anticodons CUC and UUC) and the genomic sequence for tRNA$^{Glu}_{UUC}$ with manual addition of the 3' CCA sequence. "A.C": anticodon. F) Coverage plots of sequences mapping to 28S rRNA in P0 (red), "P1 + RI" (green), "P1 – RI" (violet) and P2 (blue), either in linear scale (top) or Log2 scale (bottom). G) Coverage plot of sequences mapping 5.8 S rRNA.

Supplementary Figure 2: data associated to Figure 2. A) Same as Figure 2(B) but washing cells with MEGM instead of PBS. B) Deconvolution of chromatograms obtained by SEC analysis of PBS washes of different adherent malignant and nonmalignant cell lines, derived from different mammalian species. C) U2-OS cells before (left) and after (right) four consecutive washes with HBSS for 30 seconds.

Supplementary Figure 3: data associated to Figure 4. A) Experimental conditions were similar to those used in Figure 4 A-D, but the cell-free processing step was omitted. Control lanes include RNA lysates from U2-OS cells incubated in

DMEM + 10% FBS (S+) or in the same cells used for exRNA analysis (ITS, 1 hour). L: 5' tRNA halves of 33 – 34 nt; S: 5' tRNA halves of 30 – 31 nt. B) Comparison of SYBR gold-stained denaturing 10% PAGE gels from Figure 4, C and Supplementary Fig. 4, A. A parameter named the RNA Degradation Number (RDN) was defined as the ratio between SYBR gold intensities above and below the tRNA band. The lower the RDN (the higher extent of extracellular fragmentation), the higher the fragment-to-full-length-tRNA ratio (estimated by densitometric analysis of Northern blot bands). C) Effect of RI addition (120 U in 10 mL) in exRNA profiles from U2-OS CCM (1 hour in ITS medium or 1 – 24 hours in S+ medium). D) Analysis of YRNAs (left) or some selected 5' fragments (right) by RT-qPCR (left) or SL-RT-qPCR (right) in 100,000 x g pellets (EVs) or concentrated 100,000 x g supernatants (RNPs) of U2-OS ΔANG conditioned medium (t = 48 hs; MEGM).

Supplementary Figure 4: data associated to Figure 5C. Complete flow cytometry analysis in all the samples included in Figure 5, D-E. Gly (31): a synthetic single-stranded RNA of 31 nucleotide with the sequence of glycine 5' tRNA halves.

<u>SUPPLEMENTARY METHODS</u>

Reagents

RI (ribonuclease inhibitor, murine; 40U / µL) was purchased from New England Biolabs. Sterile Phosphate buffered saline, PBS (10x DPBS for chromatographic separations, 1x DPBS with or without calcium and magnesium for cell culture), DMEM, trypsin–EDTA solution, fetal bovine serum (FBS), 100x Insulin-Transferrin-Selenium solution (ITS) and nuclease-free distilled water were obtained from Gibco. Hank's Balanced Salt Solution (HBSS, no phenol red), either with or without calcium and magnesium were obtained from Corning as 1x sterile solutions. Trizol and Trizol LS reagents were from Invitrogen (Thermo). The 60% Optiprep solution used to prepare iodixanol gradients was obtained from Sigma.

Cell lines and preparation of cell-conditioned medium/buffers.

Cell lines were obtained from ATCC. Creation and characterization of U2-OS ΔANG and U2-OS ΔRNH1 cells was described in Akiyama et al. 2019 (doi: 10.1101/811174). The gene-edited cells were clonally selected and genotyped.

Conditioned medium was typically derived from one 75 cm^2 flask for chromatographic analysis or from one 150 cm^2 flask for electrophoresis. Cells were plated at a density which was adjusted to obtain a confluency of 80% at the endpoint of the experiment.

Extracellular samples containing RNAs were prepared based on the following protocols:

Preparation of serum-containing conditioned medium (protocol 1): cells were grown in DMEM + 10% FBS ("S+" medium). They were washed with S+ medium, and incubated in S+ for variable periods of time which ranged from 1 to 48 hours.

Preparation of serum-free conditioned medium (protocol 2): cells were plated on day zero and grown in S+ for 24 hours. Later, they were washed with PBS, grown in Mammary Epithelial Growth Medium without antibiotics and without bovine pitutary extract (MEGM, Lonza) for 48 hours, washed again with PBS, and grown in MEGM for additional 48 hours.

Preparation of serum-free conditioned medium (protocol 3): cells were grown in S+, washed with DMEM and incubated with DMEM + 1x Insulin-Transferrin-Selenium solution ("ITS" medium) for one hour.

ExRNA analysis after short washes in PBS or Hank's Balanced Salt Solution (HBSS) (protocol 4): cells were grown in S+ medium until 80% confluent, washed three times with warm buffer (5 seconds per wash), and washed a forth time for 30 seconds with 5 mL (in T75 flasks) or 10 mL (in T150 flasks) of warm buffer plus 20 – 40 U RI (respectively). Buffers could correspond to PBS, PBS plus divalent cations (PBS+), HBSS or HBSS plus divalent cations (HBSS+) depending on the experiment. Flasks were gently tilted from side to side during washes.

For protocols 1-4: conditioned media or conditioned-buffers were centrifuged at 800 x g at room temperature to remove detached cells and then spinned twice at 4°C and 2,000 x g. The supernatants were either processed immediately or stored at -20°C for later use. If frozen, media was spinned again at 4°C and 2,000 x g upon thaw.

Antibodies

The following primary antibodies were used for Western blot: anti-Puromycin (Millipore, cat # MABE343, clone 12D10); anti-RPS6 (Santa Cruz Biotechnology; cat # sc-74459; clone C-8); anti-RPS23 (Santa Cruz Biotechnology; cat # sc-100837; clone SJ-K2); anti-RPL7a (Cell Signaling; cat # 2415; clone E109); anti-CD63 (BD Biosciences; cat # 556019; clone H5C6); anti-CD9 (Millipore; cat # CBL162; clone MM2/57); anti-CD81 (R&D; cat # MAB4615; clone 454720); anti-eIF2α (Cell Signaling: cat # 9722); anti-(p)eIF2α (Ser51; Cell Signaling; cat # 9721). Antibodies for flow cytometry where from BD and directed to mouse proteins CD11c (clone HL3), CD80 (clone 16-10A1), I-Ab (clone AF6-120.1).

Primers and RT-qPCR

In figure 1J: cDNA was obtained with SuperScript II (Thermo) using random hexamers and following manufacturer's instructions. For glycine 5' halves a gene-specific primer (GSP) was used (the sample was heated at 65ºC, following by primer annealing and extension at 42ºC). Input material: 2 µL of each chromatographic fraction. Quantitative real-time PCR was performed with a Kapa SYBR Fast qPCR Master Mix (2x) from Kapa Biosystems.

$tRNA^{Gly}$ 5' halves (RT GSP): TGCCATCCACCACCCTGTTGCTGTAGCGAGAATT
$tRNA^{Gly}$ 5' halves (F-primer): ccCCGCATTGGTGGTTCAGTGGTA
$tRNA^{Gly}$ 5' halves (R-primer): TCCACCACCCTGTTGCTGTA
28S rRNA (position 310; F-primer): GGGTGGTAAACTCCATCTAAGG
28S rRNA (position 310; R-primer): GCCCTCTTGAACTCTCTCTTC
28S rRNA (position 3744; F-primer): GTAAACGGCGGGAGTAACTATG

28S rRNA (position 3744; R-primer): GACAGTGGGAATCTCGTTCATC
18S rRNA (position 442; F-primer): CTGAGAAACGGCTACCACATC
18S rRNA (position 442; R-primer): GCCTCGAAAGAGTCCTGTATTG
5.8S rRNA (position 25; F-primer): CTCGTGCGTCGATGAAGAA
5.8S rRNA (position 25; R-primer): TCGAAGTGTCGATGATCAATGT
5.8S rRNA (position 2; F-primer): ACTCTTAGCGGTGGATCACT
5.8S rRNA (position 2; R-primer): GATGATCAATGTGTCCTGCAATTC

In Figure 3E: Chromatographic fractions corresponding to the P0 peak from BJ cells were concentrated to 50 µL by ultrafiltration (Vivaspin 500; MWCO 5 kDa). One microliter was used as input. cDNA was obtained with SuperScript II (Thermo) using an oligo$(dT)_{18}$ primer and following manufacturer's instructions. End-point PCR was performed with recombinant Taq DNA Polymerase (Thermo) for 35 cycles. Annealing temperature: 58ºC. Expected amplicon length: 731 bp (> 2200 bp from predicted mRNA 3' end)

HSP90B1 (F-primer): GGTGTAGGAATGACCAGAGAAG
HSP90B1 (R-primer): GGAGCAGATGTGGGTACAAATA

In Supplementary Figure S4, F: cDNA for full-length YRNA analysis was obtained with SuperScript II (Thermo) using random hexamers and following manufacturer's instructions. cDNA for YRNA fragments was obtained based on the stem-loop RT-qPCR method which was described in detail in our previous publication (Tosar et al. 2018; *Nucleic Acids Research* 46, 9081-9093).

Full-length YRNAs (conventional RT with random hexamers):

RNA Y1 (F-primer): TGGTCCGAAGGTAGTGAGTTA
RNA Y1 (R-primer): GTCAAGTGCAGTAGTGAGAAGG
RNA Y3 (F-primer): CCGAGTGCAGTGGTGTTTA
RNA Y3 (R-primer): AGGGCTAGTCAAGTGAAGCAG
RNA Y4 (F-primer): GTCCGATGGTAGTGGGTTATC
RNA Y4 (R-primer): AAAGCCAGTCAAATTTAGCAGT
RNA Y5 (F-primer): GTCCGAGTGTTGTGGGTTATT
RNA Y5 (R-primer): ACAGCAAGCTAGTCAAGCG

YRNA fragments (SL-RT-qPCR; as described in Tosar et al. 2018):

Stem-loop RT primer ("X" denotes assay-specific 3' overhangs):
GTCGTATCCAGTGCAGGGTCCGAGGTATTCGCACTGGATACGACXXXXXX

RNA Y1 (5' fragment; 31 nt; 3' overhang): ATTGAG
RNA Y4 (5' fragment; 32 nt; 3' overhang): AGTTCT
RNA Y5 (5' fragment; 32 nt; 3' overhang): CTTAAC
miR-21-5p (3' overhang): GTCAAC
RNA Y1 (5' fragment; 31 nt; F-primer): caagTGGTCCGAAGGTAGTGAGT
RNA Y4 (5' fragment; 32 nt; F-primer): tgGTCCGATGGTAGTGGGTT
RNA Y5 (5' fragment; 32 nt; F-primer): agttgGTCCGAGTGTTGTGG
miR-21-5p (F-primer): gccccgTAGCTTATCAGACTGATGT
Universal reverse primer: GTGCAGGGTCCGAGGT

All primers were obtained from Integrated DNA Technologies (IDT, USA).

Density gradient separations

For separation of ribosomal subunits and ribosomes, a linear gradient composed of 10 – 40 % RNase-free sucrose was used. The gradients were prepared in 20 mM Tris-Cl buffer (pH = 8), 4 mM $MgCl_2$, 50 mM KCl and 1mM DTT (added fresh). Layers of 40%, 30% 20% and 10% sucrose were added sequentially to a 12 mL polypropylene tube and frozen at -80ºC in between. The whole gradient was thawed overnight in the cold-room and used the next day. Extracellular samples were obtained from U2-OS cells using protocol 4 and washing with HBSS+ in the presence of RI. Washes four and five were pooled, concentrated by ultrafiltration and stored at -80°C until use. Concentrated extracellular fractions (0.5 mL) were thawed, layered gently on top of the gradient, and centrifuged at 186,000 x g for 3 hours at 4ºC using a SW 40 Ti rotor (acceleration: max; break: min). A density gradient analyzer and fractionator equipped with a Teledyne ISCO UA-6 UV/Vis detector was used to collect fractions of 0.5 mL, starting from the top of the gradient. Collected fractions were treated with 0.5 mL TRIzol to purify both RNA and proteins according to the manufacturer's instructions.

To separate extracellular vesicles from ribonucleoproteins (RNPs) or other high-density components of the non-EV fraction, high-resolution (12 – 36 %) iodixanol gradients were used following the protocol described in [23]. Briefly, samples were layered on the bottom of a 12 mL polypropylene tube, and layers of ice-cold 36%, 30%, 24%, 18% and 12% iodixanol (prepared in PBS) were added sequentially on top. The gradients were centrifuged for 15 h at 120,000 x g and 4ºC, using a SW40 Ti rotor. Twelve fractions of 1 mL were obtained from the top of the gradient and transferred to new tubes. One half of each fraction was treated with an equal volume of TRIzol and used for RNA and protein purification following manufacturer's instructions. The other half was twice precipitated with cold (-20ºC) 60% acetone, and the pellets were resuspended in 1x loading buffer for Western blot analysis. Loading buffer contained reducing agents or not depending on the primary antibodies intended to use.

Sequencing data analysis

After sample demultiplexing and adapter trimming (only sequences > 15 bases which contained an identifiable 3′ adaptor were analyzed), FastQ files containing sequencing information were mapped to the human genome (hg38) with RNA STAR (--outFilterMultimapNmax=2000, to allow mapping to repetitive tRNA and rRNA genes, --outFilterMismatchNoverLmax=0.25, --alignIntronMax=30, and default settings). To determine read length distribution counts for RNA biotypes across experimental samples, mapped reads were filtered with BAM-filter (-mapped=TRUE, -include bed and default settings) using small nuclear RNA, small nucleolar RNA, vault RNA, YRNA (Ensemble release 100), mature miRNA (miRbase release V22), tRNAs (UCSC) and ribosomal RNA (custom GTF) genomic coordinates. Filter reads were extracted, converted to Fasta and the length of each individual read was computed. The relative abundance of reads with a given length was expressed as reads per million (RPM) mapped reads by dividing its absolute count number by the total amount of mapped reads in the data set and multiplying by a million. rRNA 28s coverage was determined with bamCoverage (--minMappingQuality=0, --region=chr21:8213887:8218941 and default settings). The relative abundance of reads mapping to different tRNA isoacceptors was determined with feature counts (-M, --fraction=TRUE, default settings). Data was submitted to NCBI’s small read archive (SRA) under the BioProject ID: PRJNA633249.

Northern blotting

RNA samples were run on 10% TBE-urea polyacrylamide gels (ThermoFisher Scientific), transferred to positively charged nylon membranes (Roche). The membranes were cross-linked by UV irradiation. After cross-linking, the membranes were hybridized overnight at 40°C with digoxigenin (DIG)-labeled DNA probes in DIG Easy Hyb solution (Roche). After low stringency washes (washing twice with 2× SSC/0.1% SDS at room temperature) and a high stringency wash (1× SSC/0.1% SDS at 40ºC), the membranes were blocked in blocking reagent (Roche) for 30 min at room temperature, probed with alkaline phosphatase-labeled anti-digoxigenin antibody (Roche) for 30 min, and washed with 1x TBS-T. Signals were visualized with CDP-Star ready-to-use (Roche) and detected using ChemiDoc imaging system (BioRad) according to the manufacturer’s instructions. Oligonucleotide probes were synthesized by IDT. DIG-labeled probes were prepared using the DIG Oligonucleotide tailing kit (2nd generation; Roche) according to the manufacturer’s instructions. The sequences of the probes were as follows:

probe for 5'-tRNA$^{Lys}_{UUU}$: 5' CTGATGCTCTACCGACTGAGCTATCCGGGC 3';
probe for 5'-tRNA$^{iMet}_{CAU}$: 5' CTTCCGCTGCGCCACTCTGCT 3';
probe for 5'-tRNA$^{Gly}_{GCC}$: 5' CTACCACTGAACCACCCATGC 3';
probe for 3'-tRNA$^{Gly}_{GCC}$: 5' GCCGGGAATCGAACCCGGGCCTCCCGCG 3';
probe for 7SL RNA: 5' CACTACAGCCCAGAACTCCTGGACT 3'.

Protein puromycilation assays

Extracellular samples were obtained from four T150 flasks of U2-OS cells (70% confluency) based on protocol 4 (PBS+ in Figure 3, G and HBSS+ in Figure 3, H) and concentrated by ultra-filtration (cut-off: 10 kDa) to 300 µL, which were then separated in three identical aliquots. Each aliquot received 40 U RI and 80 mM KCl. Puromycin was added to two aliquots at a final concentration of 5 µg / mL. Two aliquots also received ATP and GTP at 1mM each. All samples were incubated at 37ºC for two hours. Proteins were then precipitated with cold acetone, washed with cold acetone at 60%, and analyzed by Western blot using an anti-puromycin antibody (1 / 1000, overnight, in PBS, BSA 5%, Tween 0.1 %). In a separate experiments, samples were incubated at either 37ºC or 4ºC.

Transmission electron microscopy

Two T75 flasks containing cells grown in S+ at 80% confluency were washed twice with serum-free DMEM, once with PBS, and once with PBS + 40U RI. This last wash was concentrated and subjected to size exclusion chromatography as previosuly described. The fractions corresponding to the P0 peak were concentrated to 20 µL by ultrafiltration and frozen. Once thawed, samples were incubated on carbon-coated grids for 1.5 min. The grids were washed by touching a miliQ water drop and blotted with filter paper (twice), then two series of touching a 1% phosphotungstic acid drop and blotting with filter paper before air drying. Grids were imaged in a JEOL JEM-2100 electron microscope at 200 kV.

Extracellular samples from U2-OS cells were obtained following protocol #4, concentrated to 20 µL by ultrafiltration and frozen. Once thawed, samples were incubated on carbon-coated grids for 10 min. The grids were washed once by touching and blotting a miliQ water drop, placed inverted on top of a droplet containing 1% uranyl acetate for 1 minute, then grids were washed by touching and blotting a miliQ water drop, air dried and imaged in a JEOL JEM-2100 electron microscope at 200 kV.

Sample preparation for dendritic cell maturation assays

Bone marrow cells were obtained from the leg bones of C57BL/6 mice and differentiated in culture for eight days in the presence of 0.4 ng / mL GM-CSF as described in [26].

Two T75 flasks containing MCF-7 cells were grown in MEGM for 48 hours (80% confluency) and then washed with PBS + 40U RI for 30 seconds. The cell-conditioned PBS was separated into two aliquotes. One aliquot was treated with 320 ng RNase A and incubated at 37ºC for 30 min. Both aliquotes were then subjected to SEC in order to obtain the following fractions/samples: P0, RNase-treated P0 and P1. Each of these fractions were concentrated to 100 µL by ultrafiltration (MWCO 5 kDa) and filter-sterilized in the cell culture room. P0 and P1 were also diluted 100-fold with sterile PBS. All samples (100 µL) were added directly to the media of 1 x 10^6 BMDCs grown in 900 µL of complete media (RPMI + 10% FBS, 0.05 mM 2-mercaptoethanol, 2mM L-glutamine, 1mM sodium pyruvate, 1% HEPES, 100 U/mL penicillin, 0.1 mg/mL streptomycin ; 6-well plates) and incubated for 24 hours at 37ºC and 5% CO_2. Control wells contained: 100 µL PBS (NT; nontreated cells), synthetic $tRNA^{Gly}_{GCC}$ 5' halves or a mutated version of this RNA ($25^{U/C}$; both at 10 µg / mL final concentration), or the synthetic dsRNA analogue Poly(I:C) (Invivogen) at either 30 µg / mL or 3 µg / mL, diluted in PBS.

At that time, cells were harvested and resuspended in PSA (PBS, 0.2% fetal bovine serum, 0.1 sodium azide) to stain them with antibodies against CD11c, CD80 and I-Ab for 20 minutes on light-protected ice. After two washes with PBS, propidium iodide was added. The samples were acquired in the CyAN ADP Analyzer (Dako) and the data analyzed with the FlowJo vX.0.7 software (FlowJo, LLC)

Levels of IL-1β in the media were measured using a commercial ELISA kit from Biolegend.

Artículo científico 2: Ribonuclease activity undermines immune sensing of naked extracellular RNA

Este es el artículo científico central de la tesis de doctorado en donde se abordan los objetivos específicos 2-5. En este trabajo demostramos que las RNasas extracelulares condiciona la internalización, reconocimiento y escape endosomal de los exRNAs desnudos indicando que las membranas biológicas no son totalmente impermeables a estas moléculas. La inhibición de las RNasas extracelulares permite que los exRNAs desnudos ingresen a células dendríticas y macrófagos, desencadenen potentes respuestas proinflamatorias principalmente a través de la activación de TLRs endosomales. Además, estos exRNAs pueden escapar del compartimento endosomal y activar sensores de RNA en el citosol. También observamos que mRNAs extracelulares desnudos pueden ser internalizados espontáneamente y traducidos por diversos tipos celulares en presencia de RI. En modelos *in vivo*, la coinyección intravenosa de exRNAs desnudos inflamatorios junto a RI potencia la activación de linfocitos esplénicos. Asimismo, se evidencia que el exRNA desnudo presenta una actividad proinflamatoria intrínseca en compartimentos pobres en RNasas, como la cavidad peritoneal. En conjunto, estos hallazgos demuestran que el exRNA desnudo posee actividad biológica intrínseca sin necesidad de ser encapsulado en vesículas extracelulares o nanopartículas lipídicas. Los resultados de este artículo respaldan la existencia de un rol del exRNA desnudo en la comunicación intercelular y abren la puerta a posibles desarrollos biotecnológicos.

Ribonuclease activity undermines immune sensing of naked extracellular RNA

Graphical abstract

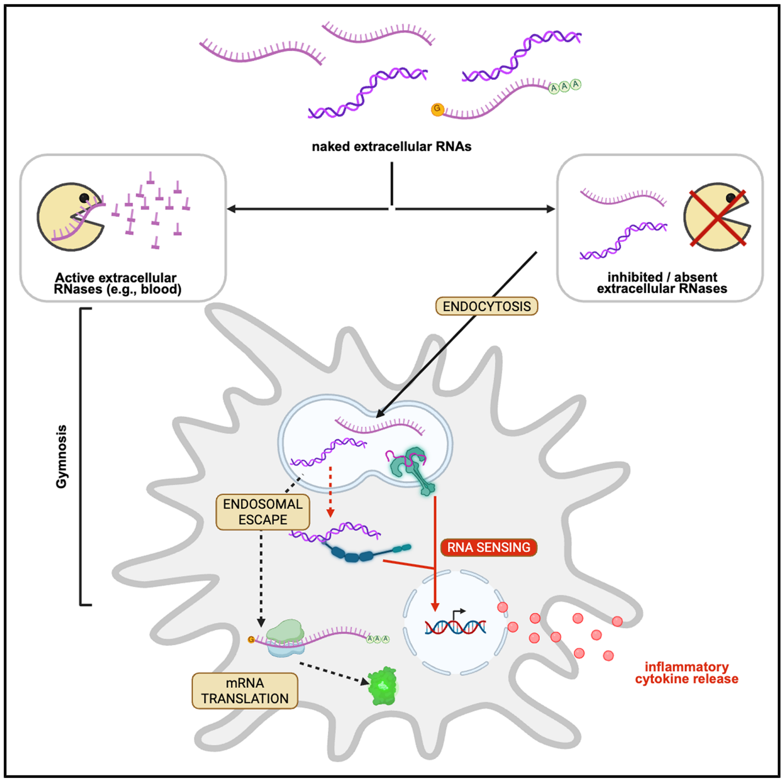

Highlights

- Naked extracellular RNA (exRNA) is bioactive when RNases are inhibited/absent
- Internalized naked exRNA activates endosomal TLRs as well as cytosolic RLRs
- Naked extracellular mRNAs can be translated in recipient cells
- Extracellular RNases avoid naked-exRNA-induced systemic inflammation

Authors

Mauricio Castellano, Valentina Blanco, Marco Li Calzi, ..., Alfonso Cayota, Mercedes Segovia, Juan Pablo Tosar

Correspondence

msegovia@pasteur.edu.uy (M.S.),
jptosar@pasteur.edu.uy (J.P.T.)

In brief

Castellano et al. show that when extracellular RNases are inhibited or absent, naked extracellular RNA is internalized spontaneously by cells, inducing inflammation mediated by endosomal TLRs or cytosolic RLRs. Extracellular ribonucleases counteract this effect. The authors also show translation of naked extracellular mRNAs upon ribonuclease inhibition.

Castellano et al., 2025, Cell Genomics *5*, 100874
May 14, 2025 © 2025 The Authors. Published by Elsevier Inc.
https://doi.org/10.1016/j.xgen.2025.100874

Cell Genomics

CellPress
OPEN ACCESS

Article

Ribonuclease activity undermines immune sensing of naked extracellular RNA

Mauricio Castellano,[1,2,3] Valentina Blanco,[1] Marco Li Calzi,[1] Bruno Costa,[1,3] Kenneth Witwer,[4,5,6] Marcelo Hill,[2,7] Alfonso Cayota,[1,8] Mercedes Segovia,[2,7,*] and Juan Pablo Tosar[1,3,9,*]

[1]Functional Genomics Laboratory, Institut Pasteur de Montevideo, Montevideo 11400, Uruguay
[2]Immunoregulation and Inflammation Laboratory, Institut Pasteur de Montevideo, Montevideo 11400, Uruguay
[3]Analytical Biochemistry Unit, School of Science, Universidad de la República, Montevideo 11400, Uruguay
[4]Department of Molecular and Comparative Pathobiology, Johns Hopkins University School of Medicine, Baltimore, MD 21205, USA
[5]EV Core Facility "EXCEL," Institute for Basic Biomedical Sciences, Johns Hopkins University School of Medicine, Baltimore, MD 21205, USA
[6]The Richman Family Precision Medicine Center of Excellence in Alzheimer's Disease, Johns Hopkins University School of Medicine, Baltimore, MD 21205, USA
[7]Academic Unit of Immunobiology, School of Medicine, Universidad de la República, Montevideo 11800, Uruguay
[8]Hospital de Clínicas, Universidad de la República, Montevideo 11600, Uruguay
[9]Lead contact
*Correspondence: msegovia@pasteur.edu.uy (M.S.), jptosar@pasteur.edu.uy (J.P.T.)
https://doi.org/10.1016/j.xgen.2025.100874

SUMMARY

Cell membranes are thought of as barriers to extracellular RNA (exRNA) uptake. While naked exRNAs can be spontaneously internalized by certain cells, functional cytosolic delivery has been rarely observed. Here, we show that extracellular ribonucleases (RNases)—primarily from cell culture supplements—have obscured the study of exRNA functionality. When ribonuclease inhibitor (RI) is added to cell cultures, naked exRNAs can trigger pro-inflammatory responses in dendritic cells and macrophages, largely via endosomal Toll-like receptors (TLRs). Moreover, naked exRNAs can escape endosomes, engaging cytosolic RNA sensors. In addition, naked extracellular mRNAs can be spontaneously internalized and translated by various cell types in an RI-dependent manner. *In vivo*, RI co-injection amplifies naked-RNA-induced activation of splenic lymphocytes and myeloid leukocytes. Furthermore, naked RNA is inherently pro-inflammatory in RNase-poor compartments like the peritoneal cavity. These findings demonstrate that naked RNA is bioactive without requiring vesicular encapsulation, making a case for nonvesicular-exRNA-mediated intercellular communication.

INTRODUCTION

Lipid bilayers are considered to be impermeable to negatively charged RNA molecules. However, cells can pack and release RNA inside biological lipid nanoparticles called extracellular vesicles (EVs).[1–3] These vesicles can be internalized by recipient cells enabling the intercellular exchange of genetic information.[4,5] Similarly, therapeutic delivery of messenger RNA (mRNA) or double-stranded small interfering RNA (siRNA) also requires RNA encapsulation inside synthetic lipid nanoparticles (LNPs).

The spontaneous uptake of naked RNA molecules is less studied and considered highly inefficient. Nevertheless, some pharmaceutical preparations containing antisense oligonucleotides (ASOs) lack cationic lipids or any other transfection reagents.[6] These drugs manage to enter cells and gain access to the cytosol or even the nucleus through an endocytosis-dependent naked-RNA-specific uptake process referred to as gymnosis.[7] Although the molecular mechanism(s) responsible for this functional uptake route are still obscure, gymnosis might depend on the increased hydrophobicity conferred by phosphorothioate bonds, a frequent modification in therapeutic ASOs.[8]

Gymnotic uptake and subsequent translation of naked mRNA vaccines has been reported, usually following intramuscular, intradermal, or intralymphatic administration in mice.[9–12] These studies have also shown that dendritic cells are the main cell type responsible for gymnotic mRNA uptake, probably through a macropinocytosis-dependent mechanism. However, intranodal injection of naked mRNA vaccines in humans failed to show a response compared with placebo.[13] The clinical success of LNPs as delivery vectors for mRNAs and siRNAs[14,15] has consolidated the view that cationic or ionizable lipids are required for efficient RNA uptake, as supported by analysis of delivery methods in clinical trials.[13]

Compared with lipofection, gymnotic uptake is considered a slower and less efficient process.[7] Currently, its study is mostly restricted to the context of short and highly modified therapeutic ASOs. Several factors explain the disadvantage of this uptake route for longer or unmodified RNAs. For example, endosomal escape, the rate-limiting step in RNA therapeutics,[16] is facilitated by an LNP-induced endosomal rupture mechanism that would not apply in the case of gymnosis. Immunological studies also argue against extracellular naked RNAs being functional. For

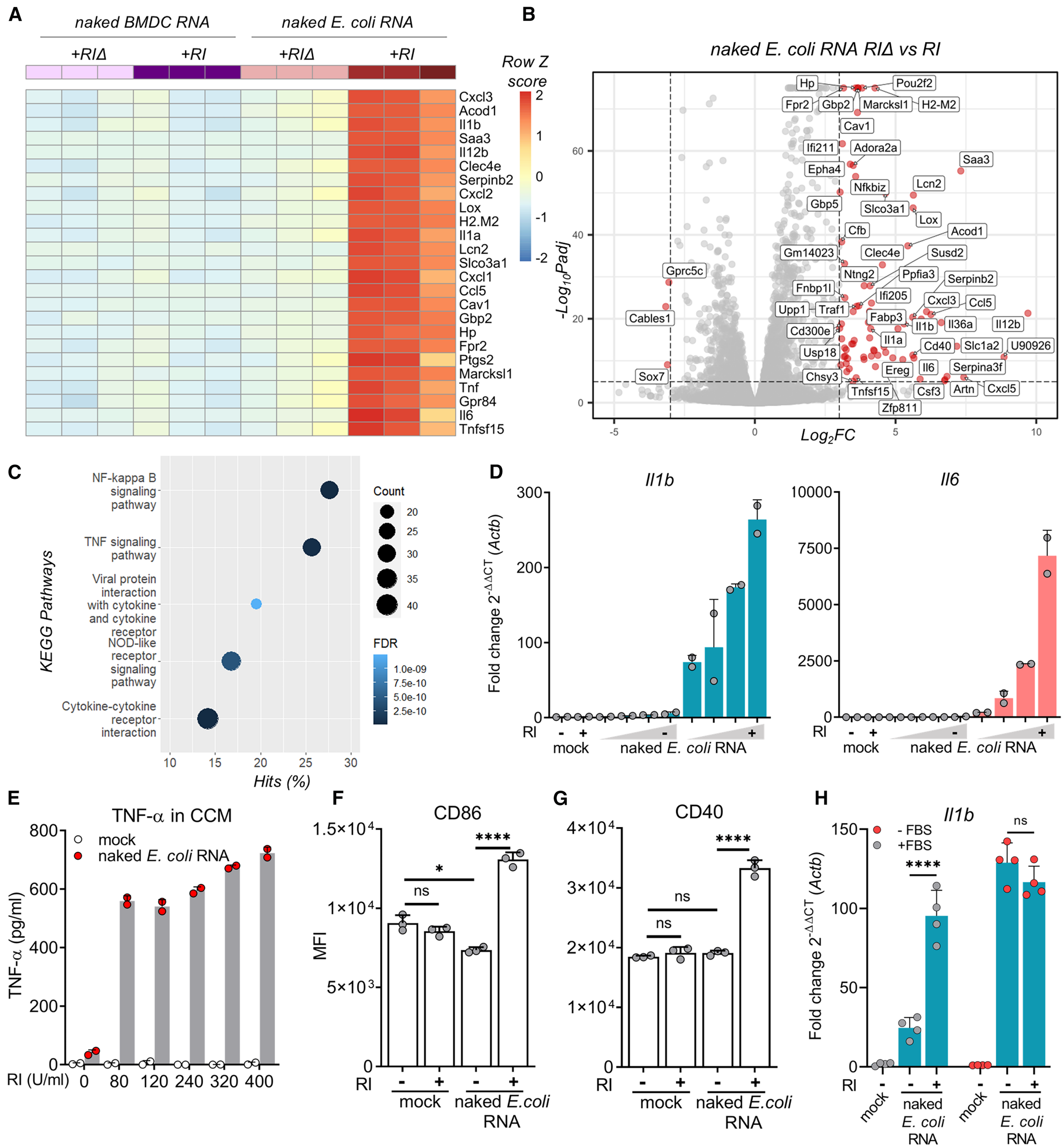

Figure 1. Naked bacterial exRNA activates BMDCs in an RI-dependent manner

(A) Heatmap showing top 25 most differentially regulated genes in BMDCs stimulated for 6 h with 100 ng/mL naked RNA from *E. coli* or from BMDCs in the presence of RNase inhibitors (+RI) or a thermally inactivated RI instead (+RIΔ).

(B) Volcano plot of differentially expressed genes (adjusted p [p-adj] $< 1 \times 10^{-3}$, $|\log_2 FC| \geq 3$) between BMDCs stimulated with naked total *E. coli* RNA (+RI vs. +RIΔ).

(C) Pathway enrichment analysis corresponding to BMDCs stimulated with naked *E. coli* RNA + RI.

(D) *Il-1b* and *il-6* expression measured by RT-qPCR in BMDCs stimulated with varying doses (1, 5, 10, or 25 μg/mL) of naked *E. coli* RNA, with or without RI. DPBS was used as negative control.

(E) TNF-α secreted by BMDCs after stimulation (6 h) with 1 μg/mL naked *E. coli* RNA (or DPBS) with varying doses of RI.

(legend continued on next page)

67

instance, transfection of bacterial RNAs using cationic lipids triggers immune cell activation in human and murine macrophages,[17,18] but this response is abrogated when the RNA is spiked into the media in the absence of lipofection reagents.[17]

Finally, naked RNA is highly unstable in biofluids and extracellular samples, which tend to contain high quantities of active ribonucleases (RNases). This fact, coupled with the low efficiency of gymnotic uptake,[7] and the apparent lack of immune cell activation induced by naked extracellular bacterial RNAs,[17] explains why RNA-mediated intercellular communication is mostly—and almost exclusively—studied in the context of EVs.[19]

We have recently shown that some RNAs are intrinsically stable in the extracellular space and act as stable reservoirs of shorter RNA fragments that can enter cells spontaneously.[20] In addition, when adding a broad-range ribonuclease inhibitor (RI) to human cancer cell-conditioned medium, we stabilized a previously unknown population of extracellular ribosomes that induced dendritic cell maturation.[21] These results suggest that extracellular, nonvesicular RNAs, comprising both naked RNAs and ribonucleoprotein complexes, can interact with recipient cells and induce downstream signaling responses. Importantly, to observe any functional interaction involving nonvesicular extracellular RNAs (exRNAs), strict control of extracellular RNase activity is required. This is impossible in typical cell culture experiments, in which 10% fetal bovine serum (FBS) is usually employed. We hypothesize that failure to control for serum-derived RNase activity has so far precluded the study of intercellular communication pathways mediated by nonvesicular RNAs, hence underestimating the efficiency of gymnosis as a functional and efficient RNA uptake process.

Here, using a broad-spectrum RI, we show that both single-stranded and double-stranded long and short RNAs can be spontaneously internalized by different murine and human cell types in the absence of any transfection reagents. Internalized RNAs can be sensed by Toll-like receptors (TLRs) inside endosomal compartments. Furthermore, at least some RNA molecules can escape the endosomes into the cytosol and regulate or modify gene expression in recipient cells. Intravenous administration of RI enhances the inflammatory responses triggered by naked exRNA *in vivo*. In contrast, compartments with low RNase activity, such as the peritoneal cavity, seem to be inherently prone to nonvesicular exRNA recognition. Altogether, these results suggest that naked or nonvesicular exRNAs and extracellular RNases might work as antagonistic inducers and regulators of compartment-specific inflammatory responses.

RESULTS

Naked bacterial exRNA activates BMDCs in an RI-dependent manner

Earlier studies showed lack of exRNA recognition by innate immune cells when bacterial RNA, a well-known pro-inflammatory molecule, was spiked into the medium instead of transfected.[17,22] This suggests that the spontaneous uptake of naked exRNA is inefficient, possibly due to the fact that cells are refractory to internalizing negatively charged nucleic acids.[8] Alternatively, it could simply be a consequence of RNA stability. Because cell-culture experiments are typically done in the presence of FBS, a rich source of RNases, we hypothesized that this could explain the apparent lack of naked-exRNA bioactivity seen in earlier studies.[19–21] To study this, we worked with primary cultures of murine bone-marrow-derived cells (BMDCs), differentiated into antigen-presenting cells.[23,24] We incubated these BMDCs with purified *Escherichia coli* RNA in the absence of any transfection reagents, but adding either a broad-range extracellular RNase inhibitor (+RI) or a thermally inactivated inhibitor (+RIΔ), lacking any protective activity (Figure S1A). Consistent with our hypothesis, naked bacterial exRNA induced a highly pro-inflammatory transcriptional signature only in the presence of RI (Figures 1A–1C, S1B, and S1C). Of note, BMDC-derived self-RNA was immunologically silent regardless of RI addition (Figures 1A and S2).

Previous results were further confirmed by RT-qPCR. All tested genes (*Cxcl10*, *Ifit2*, *Il1a*, *Il1b*, *Il6*, *Oas3*) showed a dose-dependent induction in the presence of RI (Figures 1D and S3). Additionally, pretreatment of naked *E. coli* RNA with RNAse1 completely abrogated the observed effects regardless of RI addition (Figures S1B and S1C). Interestingly, BMDCs exposed to naked *E. coli* RNA released high levels of tumor necrosis factor (TNF)-α (Figure 1E) and increased the expression of cell surface markers associated with DC activation, such as CD40 and CD86 (Figures 1F and 1G), only in the presence of RI.

Interestingly, when previous experiments were repeated in serum-deprived medium (−FBS), the response elicited by BMDCs to naked *E. coli* RNA was as strong as previously observed but now completely independent of RI (Figure 1H). Overall, these results demonstrate that naked bacterial RNA can be specifically sensed by murine BMDCs, but this recognition cannot be observed if extracellular RNases are not previously inhibited or removed.

RI enhances the endocytic uptake of naked RNA by exRNA stabilization

To understand whether naked-exRNA sensing requires prior internalization, we incubated BMDCs with Dynasore, a dynamin inhibitor that blocks clathrin-dependent endocytosis and macropinocytosis,[25] before the addition of naked exRNAs. Upregulation of *Il6*, *Il1b*, *Cxcl10*, and *Ifit2* in response to bacterial exRNA was strongly inhibited in the presence of the drug (Figure 2A). Of note, although *Il6*, *Il1b*, *Cxcl10*, and *Ifit2* induction was strongly dependent on RI (as previously observed; Figures 1D and S3), endocytosis of Dextran-AF647 was independent of RI (Figure 2B). These results demonstrate that the main mechanism by which RI facilitates naked-exRNA uptake is by stabilizing RNA

(F and G) Flow cytometry analysis of CD40 and CD86 in BMDCs stimulated for 24 h with 50 μg/mL naked *E. coli* RNA with or without RI. Median fluorescence intensity of CD86 (F) and CD40 (G) are shown.

(H) *Il1b* expression (RT-qPCR) in BMDCs stimulated with 1 μg/mL naked *E. coli* RNA with or without RI, in either serum-deprived medium (−FBS) or serum-containing medium (+FBS) for 6 h. RPMI was used as mock.

(F–H) ns, not significant; *$p < 0.05$, ****$p < 0.0001$; one-way ANOVA with Tukey's multiple comparison test.

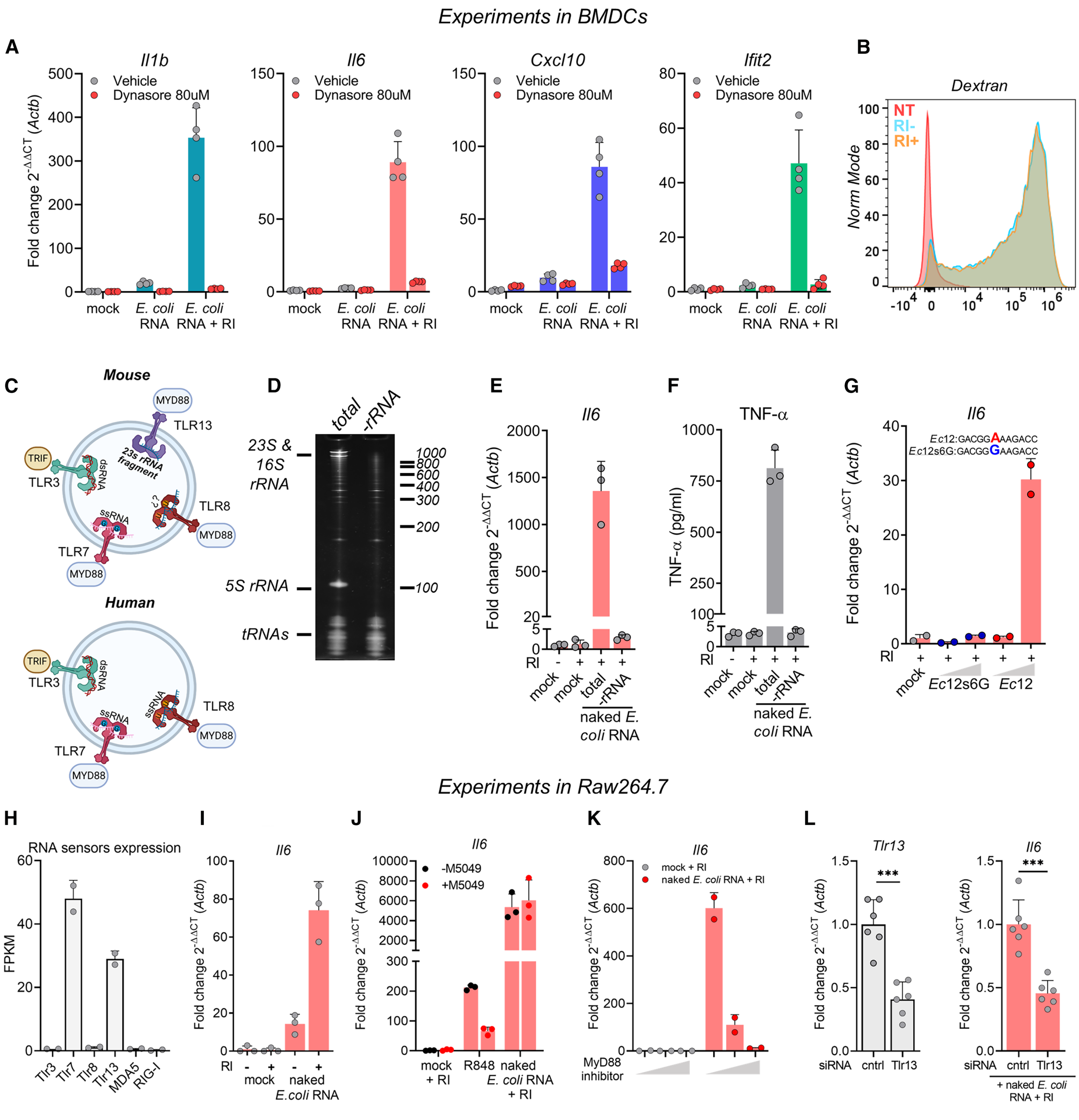

Figure 2. TLR13 senses naked bacterial ribosomal RNA in BMDCs and Raw264.7 macrophages

(A) *il6*, *Il1b*, *Cxcl10*, and *Ifit2* expression by RT-qPCR in BMDCs stimulated for 6 h with 1 μg/mL of naked *E. coli* RNA, with or without RI, in the presence of Dynasore (red circles) or vehicle (gray circles).

(B) Flow cytometry analysis of BMDCs untreated or incubated with Dextran-AF647 for 1 h, with or without RI.

(C) Diagram of RNA-sensing endosomal TLRs in mouse (top) and human (bottom). TLR3 senses double-stranded RNA (dsRNA) larger than 40 bp, TLR7 and TLR8 (in humans) sense short single-stranded RNA (ssRNA) in the presence of guanosine (G) or uridine (U), respectively, and TLR13 recognizes an ssRNA fragment derived from 23S bacterial rRNA.

(D) Denaturing PAGE of total and ribosomal RNA-depleted (−rRNA) RNA from *E. coli*.

(E and F) *Il-6* expression (RT-qPCR) and levels of secreted TNF-α (ELISA) of BMDCs stimulated with 1 μg/mL of naked total or rRNA-depleted *E. coli* RNA, in the presence of RI.

(G) *Il6* expression (RT-qPCR) in BMDCs stimulated with 1 or 5 μg/mL of synthetic unmodified naked Ec12 RNA (a known agonist of TLR13), or its mutated version (Ec12s6G), both in the presence of RI. Mock: RPMI.

(legend continued on next page)

in the extracellular space, and not by increasing endocytosis rates.

Naked bacterial RNA is sensed by TLR13 in BMDCs and murine macrophages

The requirement of endocytosis (Figure 2A), and the potential role of the nuclear factor (NF)-κB pathway in BMDC response to naked exRNA (Figure 1C), suggests the involvement of endosomal pattern recognition receptors (PRRs) in these processes (Figure 2C).

To infer which receptor-ligand interaction is mostly responsible for the observed effects, we separated total *E. coli* RNA into a small (<200 nt) and a large (>200 nt) fraction (Figure S4A) and observed that only naked RNAs longer than 200 nt triggered the production of pro-inflammatory cytokines at both the RNA and the protein levels (Figures S4B and S4C). Considering that RNAs longer than 200 nt are mainly ribosomal RNAs (rRNAs), we speculated that extracellular bacterial rRNAs were triggering these effects. Indeed, probe-based selective depletion of bacterial rRNAs (Figure 2D) abrogated both *Il6* transcription and TNF-α release, despite using equal RNA concentrations across conditions (Figures 2E and 2F). This suggests the involvement of TLR13, a mouse-specific endosomal PRR that recognizes bacterial 23S ribosomal RNA and that is expressed in dendritic cells.[22,26]

A 23S rRNA segment, encompassing 12 nucleotides, was previously identified as the ligand of TLR13 in *Staphylococcus aureus*.[22] We first corroborated that this sequence, named here as *Ec12*, is conserved in *Escherichia coli*. Interestingly, BMDCs stimulated with a synthetic and unmodified naked RNA comprising the sequence of *Ec12* triggered *Il6* expression (Figure 2G). Strikingly, this response was completely abrogated when adenosine in position six of *Ec12* was substituted for guanosine (*Ec12s6G)*, a substitution that is known to affect TLR13 recognition.[22]

To gain further insights into the potential role of TLR13 in the recognition of naked bacterial RNA, we leveraged the fact that the murine macrophage cell line Raw264.7 expresses TLR7 and TLR13 as the only RNA sensors (Figure 2H). Like BMDCs, Raw264.7 cells can recognize and respond to naked *E. coli* RNA in an RI-dependent manner (Figure 2I and S4D–S4F). Of note, in agreement with previous observations,[27] the human monocytic cell line THP-1, which lacks TLR13, did not respond (Figures S4G–S4I). This lack of response was not due to lack of uptake, as we found that 100% of cells were positive for labeled Ec12 RNA, even when testing concentrations as low as 1 nM (Figure S5).

Interestingly, the response to naked *E. coli* RNA remained unchanged when macrophages were incubated with M5049, a TLR7/8 specific inhibitor. As expected, M5049 significantly reduced the response to R848, a TLR7/8 agonist (Figure 2J). On the other hand, inhibiting MyD88 in these cells completely abolished the observed response (Figure 2K). Taken together, these results strongly suggest the involvement of the TLR13/MyD88 axis in the response of murine macrophages to naked bacterial RNA. Furthermore, siRNA-mediated knockdown of TLR13 (50% reduction) reduced the response by an almost identical amount (Figure 2L).

Overall, using BMDCs and Raw264.7 macrophages as models, we have shown that naked exRNAs can gain access to the endocytic pathway and trigger activation of endosomal RNA sensors when extracellular RNases are inhibited.

Naked double-stranded RNA is also recognized by BMDCs

To study whether other nonvesicular exRNAs could also activate BMDCs, we used poly(I:C) as a model to understand naked double-stranded RNA (dsRNA) recognition. This molecule is known to be recognized by TLR3 at the endosomal level and by the RIG-I-like receptors (RLRs) RIG-I and MDA5 in the cytosol when dsRNAs are transfected[28,29] (Figure 3A). Interestingly, when BMDCs were incubated with naked extracellular poly(I:C), there was a strong, RI-dependent increment in the expression of *Cxcl10* and *Ifit2* (Figures 3B and 3C). These two genes were tested since they are known to be induced by poly(I:C) in human DCs (Figures S6A and S6B), and we also validated their induction with naked poly(I:C) in the murine dendritic cell line, JawsII (Figure S6C). In contrast, Raw264.7 macrophages did not respond to naked poly(I:C) (Figures S4D–S4F), in agreement with these cells not expressing any of the above-mentioned RNA sensors (Figure 2H).

Naked double-stranded RNA is recognized by mitochondrial antiviral-signaling protein-dependent cytosolic RNA sensors in human macrophages

We could not easily determine whether poly(I:C) was being recognized at the endosomal or cytosolic level in BMDCs because these cells express all of the sensors involved in dsRNA recognition (Figure 3D). Human THP-1 monocytes and macrophages could serve as a better model to understand the molecular basis of naked dsRNA recognition because they lack TLR3 but express high levels of RIG-I and MDA5 (Figure 3E). Hence, any response to poly(I:C) in these cells can be attributed, at least in theory, to either of these RLRs.

First, using flow cytometry, we observed that RI enhanced naked fluorescein-labeled poly(I:C) uptake in THP-1 monocytes without altering endocytosis rates, as measured by

(H) Expression of cytosolic and endosomal RNA-specific PRRs in Raw264.7 cells. Data were obtained from GEO: GSE103958.
(I) *il6* expression (RT-qPCR) in Raw264.7 stimulated for 6 h with 2 μg/mL of naked *E. coli* RNA, with or without RI.
(J) *il6* expression (RT-qPCR) in Raw264.7 preincubated with or without the TLR7/8 inhibitor M5049 at 1 μM for 3 h and later stimulated for 6 h with 1 μg/mL of naked *E. coli* RNA, with or without RI. The TLR7/8 agonist, R848 at 1 μg/mL, was used as a positive control.
(K) *il6* expression (RT-qPCR) in Raw264.7 preincubated with a Myd88 inhibitory peptide (at 0, 1, or 10 μM) for 4 h, and later stimulated for 6 h with 1 μg/mL of naked *E. coli* RNA, with or without RI.
(L) siRNA-mediated *Tlr13* knockdown in Raw264.7. Left: *Tlr13* expression (RT-qPCR) 48 h post transfection with either a control siRNA at 50 nM or a mix containing two siRNAs directed against *Tlr13* (25 nM each). Right: 48 h post siRNA transfection, Raw264.7 cells were stimulated for 6 h with 1 μg/mL of naked *E. coli* RNA with RI and *il6* expression was measured by RT-qPCR. ***$p < 0.001$; unpaired two-tailed t test.

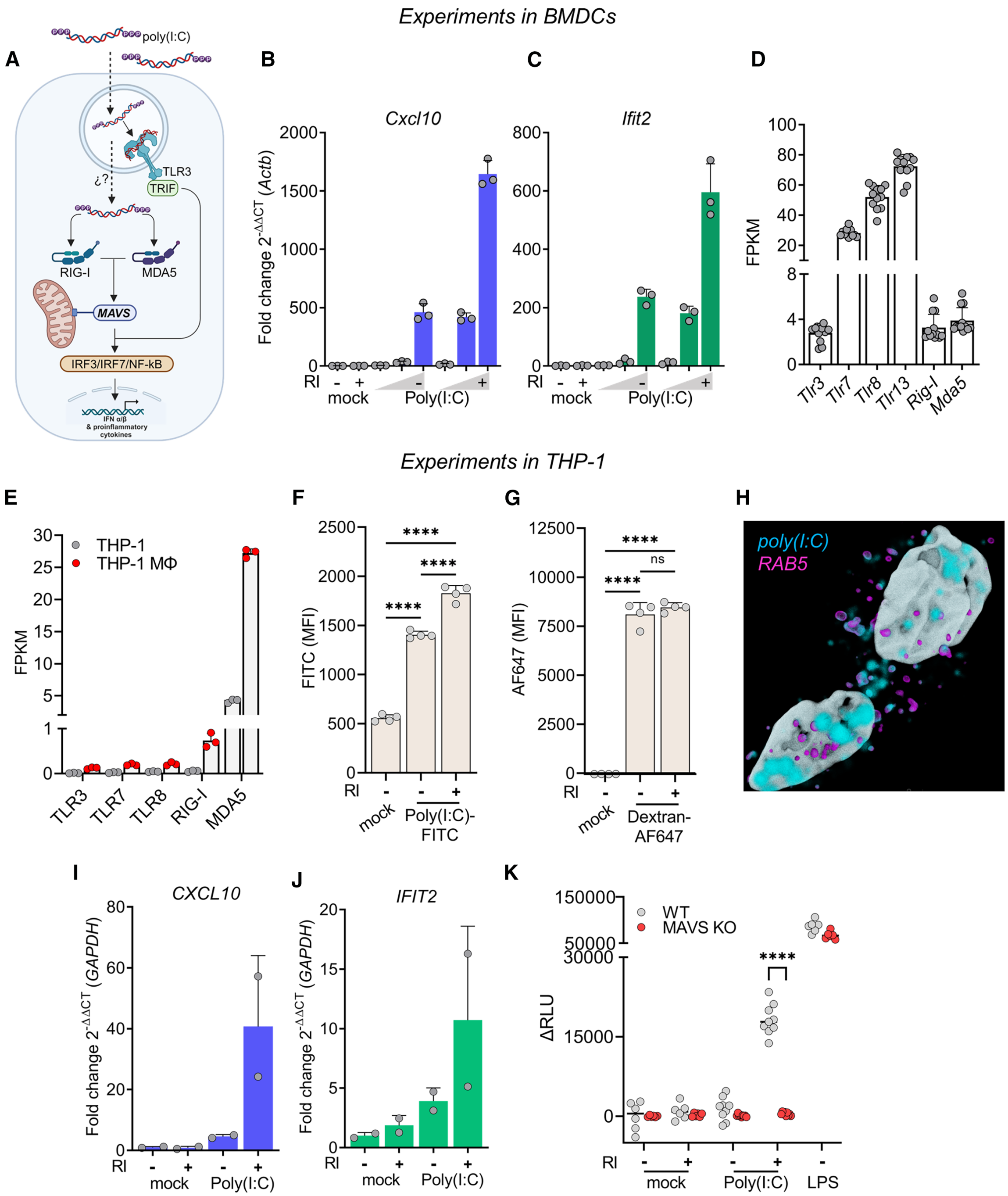

Figure 3. Naked exRNA triggers MAVS-dependent cytosolic RNA sensors in human macrophages

(A) Diagram of RNA-sensing endosomal and cytosolic receptor capable of recognizing naked poly(I:C) in BMDCs and THP-1 cells.

(B and C) BMDC expression of *Cxcl10* (B) and *Ifit2* (C) by RT-qPCR after 6-h stimulation with varying doses (0.1, 1, 10 μg/mL) of naked poly(I:C), with (+) or without (−) RI. RPMI was used as negative control.

(D) Expression (fragments per kilobase per million [FPKM]) of cytosolic and endosomal RNA PRRs in BMDCs.

(E) Expression of cytosolic and endosomal RNA-specific PRRs in THP-1 cells or in THP-1-derived macrophages (GEO: GSE130011).

(F and G) Flow cytometry of THP-1 monocytes stimulated for 3 h with naked fluorescein-labeled poly(I:C) at 0.5 μg/mL (F) or dextran conjugated to AF647 (G), both with and without 160 U/mL RI. ns: not significant; $****p < 0.0001$; one-way ANOVA with Tukey's multiple comparison test.

(H) Confocal microscopy (z stack) and 3D rendering of THP-1 macrophages stimulated for 30 min with naked fluorescein-labeled poly(I:C) at 0.5 μg/mL. Nuclei (white), dsRNA (cyan), and Rab5 (purple) are represented.

(legend continued on next page)

AF647-Dextran (Figures 3F, 3G, S7A, and S7B). These cells showed, by confocal microscopy, a labeling pattern consistent with endosomal localization of the labeled RNA (Figure S7C). A similar pattern was also observed in BMDCs (Figure S7D). Importantly, the endosomal localization of internalized poly(I:C) was confirmed in THP-1 macrophages co-stained for Rab5, a well-established early endosome marker (Figures 3H and S7E). Last, in these cells, we also observed a strong *CXCL10* and *IFIT2* induction upon stimulation with naked poly(I:C), but only in the presence of RI (Figures 3I and 3J).

Considering that THP-1 cells lack endosomal TLR3 (Figure 3E), the above results make a strong case for naked poly(I:C) being internalized by endocytosis and then escaping from endosomal compartments into the cytosol to engage cytosolic RLRs. To test this, we used a reporter THP-1 cell line that expresses a secreted luciferase under the control of the interferon regulatory factor (IRF) transcription factors. The IRF pathway is activated in response to type I interferons or several PRR agonists, including RIG-I and MDA5, which are both dependent on the mitochondrial antiviral-signaling protein (MAVS). In agreement with previous results (Figures 3I and 3J), only naked extracellular poly(I:C) in the presence of RI triggered the IRF pathway (Figure 3K). Furthermore, this response was completely abrogated in *MAVS* knockout (KO) cells. This behavior cannot be attributed to a non-responsive KO cell line, as they behaved similarly to wild-type cells when using lypopolysaccharide (LPS), a MAVS-independent IRF pathway inductor.

Overall, these results demonstrate that naked exRNAs can also reach the cytosol, where the MAVS pathway is located, presumably by endosomal escape.

RI facilitates protein translation after gymnotic uptake of mRNA

Our previous observations suggest that naked exRNA can, in the presence of RI, be internalized by cells and reach the cytosol after escaping the endosomal network. To assess the generalizability of this phenomenon, we studied gymnotic uptake of mRNAs in different human and murine cell types. Because translation occurs exclusively in the cytosol, observation of protein synthesis would provide conclusive evidence of gymnotic uptake, possibly involving endosomal RNA escape. We synthesized capped and polyadenylated *nanoLuc* mRNA by *in vitro* transcription (IVT) and confirmed its translatability using a rabbit reticulocyte extract (Figure 4A). Then, purified *nanoLuc* mRNA was added to murine BMDCs either with or without RI. Surprisingly, when extracellular RNases were inhibited, the intracellular levels of intact full-length mRNA molecules increased by 40-fold (Figure 4B). After 24 h, we detected nanoLuc protein exclusively in BMDCs when extracellular RNases were inhibited (Figure 4C). To further underscore the influence of extracellular RNases on *nanoLuc* mRNA uptake and translation, we subjected BMDCs to varying concentrations of FBS and RI prior to their incubation with naked extracellular mRNA. As expected, increasing doses of RI stimulated translation, while increasing percentages of FBS had the opposite effect (Figure 4D). Beyond 10% FBS, RNase activity was sufficiently high to abolish *nanoLuc* translation, even in the presence of RI (Figure 4D).

Since BMDCs are professional phagocytic cells, we sought to determine whether gymnosis also occurred in other cell types. Interestingly, several human epithelial cell lines could uptake and translate nanoLuc mRNA in the presence of RI (Figures 4E and 4F). As previously observed in murine BMDCs, nanoLuc translation in human epithelial cells was abrogated in the presence of endocytosis inhibitors (Figure 4G). Additionally, using confocal microscopy, we could detect that U-2 OS cells are also able to capture and translate naked eGFP mRNA, but only if cells are cultured in the absence of FBS and RI is added to the medium (Figures 4H and 4I).

Compartment-specific RNase activity modulates naked-exRNA-induced inflammation

We have observed that naked exRNA induces pro-inflammatory responses in cultures of human and murine immune cells and that these responses are modulated by extracellular RNase activity. To assess whether naked exRNAs could also induce inflammatory responses *in vivo*, we intravenously injected both naked *E. coli* RNA and poly(I:C) (Figure 5A) with or without 480 units of RI, a dose sufficient to inhibit mouse serum RNases (Figure S8A). Naked exRNAs increased the percentage of activated ($CD86^{+}MHCII^{+}$) pDCs and macrophages in the spleen (Figure S9), and, more surprisingly, the percentage of activated splenic B cells ($CD86^{+}CD69^{+}$) and T cells ($CD69^{+}$) (Figures 5B and S10), with minor or no changes in total cell numbers. Importantly, despite the lower RNase activity observed in mouse serum compared with FBS (Figure S8B), we could still recapitulate the effect of RI addition, which was stronger in the case of poly(I:C). These results are in good agreement with previous findings using LNP-formulated RNAs.[30] We cannot currently determine whether B and T cell activation was cell autonomous due to exRNA recognition by their own innate sensors[31] or requires prior activation of myeloid cells (Figure S9). Nevertheless, these results highlight that naked exRNAs can trigger systemic inflammation *in vivo*.

Our *in vitro* experiments in BMDCs showed that RI is not required for naked-exRNA-induced inflammation when cells are cultured in serum-deprived medium (Figure 1H). This made us wonder whether naked exRNA alone could be sufficient to induce inflammatory responses when released into tissues or compartments with low RNase activity. Using a highly sensitive fluorometric assay, we found that the RNase activity of mouse peritoneal fluid is approximately 4.5-fold lower than an equivalent dilution of mouse serum (Figure 6B). In agreement with this observation, intraperitoneal injection of either naked

(I and J) The expression of *CXCL10* (I) and *IFIT2* (J) in THP-1 macrophages, measured by RT-qPCR after 22-h stimulation with naked poly(I:C) at 10 μg/mL, with (+) or without (−) RI. RPMI was used as a negative control.

(K) Relative luciferase activity corresponding to IRF pathway activation in reporter THP-1 dual wild-type or *MAVS* knockout cells after stimulation for 24 h with 5 μg/mL of naked poly(I:C), with or without RI. RPMI and 200 ng/mL LPS were used as negative and positive controls, respectively.

****$p < 0.0001$ Welch ANOVA with multiple comparison Dunnett T3 test.

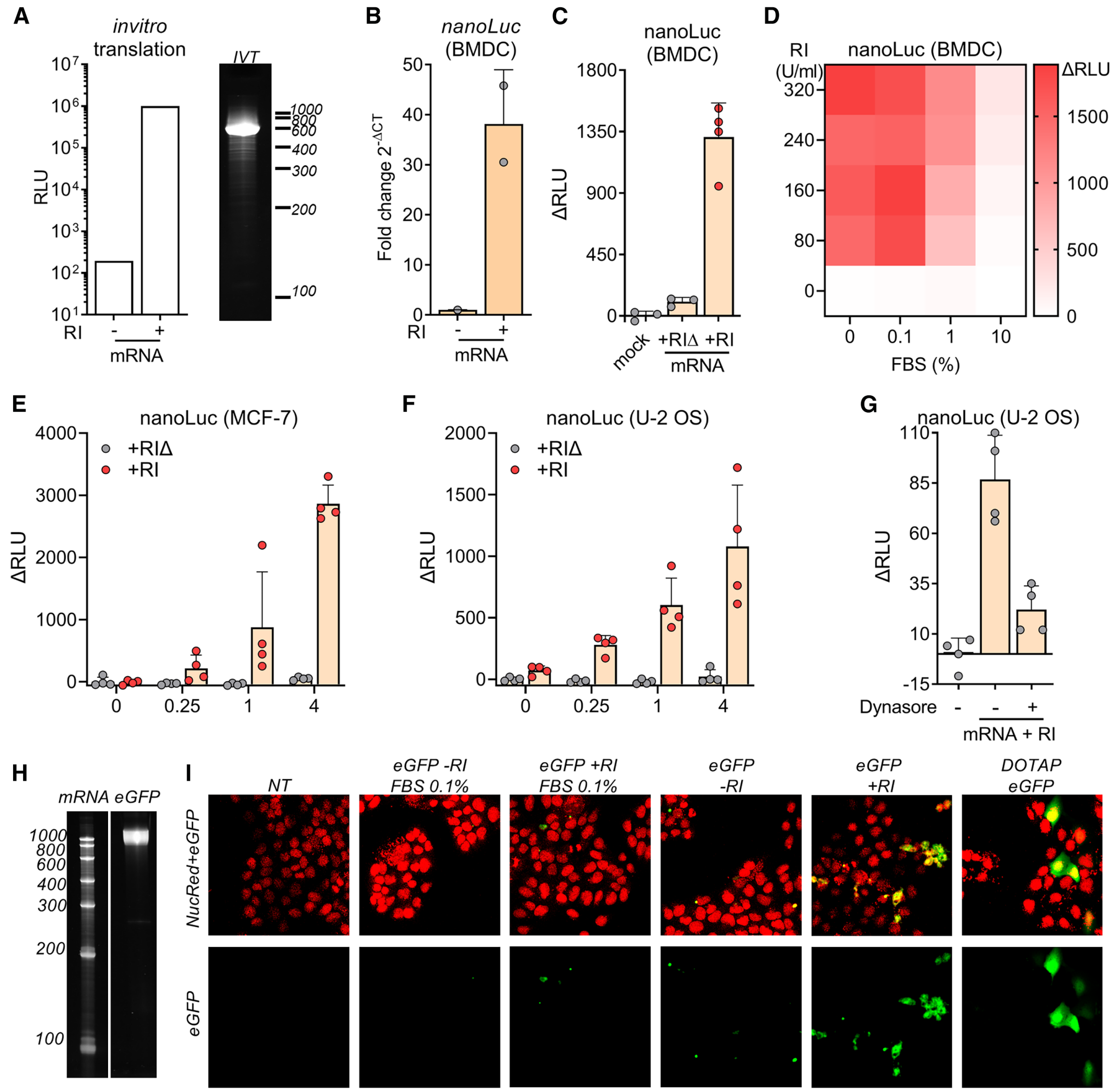

Figure 4. RI facilitates protein translation after gymnotic uptake of mRNA

(A) Bioluminescence of *in vitro* translated nanoLuc protein (left) and denaturing PAGE of *in vitro*-transcribed nanoLuc mRNA (right).

(B) BMDCs cultured without FBS were incubated with 1 μg/mL naked nanoLuc mRNA with or without 80 U/mL RI. After 6 h, intact intracellular nanoLuc mRNA was quantified by RT-qPCR.

(C) After 24 h, nanoLuc protein levels were quantified by bioluminescence.

(D) Heatmap showing nanoLuc intracellular protein levels detected by bioluminescence in BMDCs (cultured with varying doses of FBS) as a function of RI concentration.

(E and F) MCF-7 (E) and U-2 OS (F) cells cultured in 0.1% FBS were incubated with increasing doses of nanoLuc mRNA (0, 0.25, 1, 4 μg/mL) with 80 U/mL RI. After 24 h, NanoLuc protein levels were quantified by bioluminescence.

(G) U-2 OS cells cultured in 0.1% FBS were incubated with nanoLuc mRNA and RI in the presence of 80 μM Dynasore or vehicle. After 24 h, nanoLuc protein levels were determined by bioluminescence.

(H) Denaturing PAGE corresponding to *in vitro*-transcribed eGFP mRNA.

(I) Confocal microscopy of U-2 OS cells incubated with 5 μg/mL naked eGFP mRNA with or without 80 U/mL RI at the indicated FBS dose. Non-treated cells and DOTAP-transfected cells were used as negative and positive controls, respectively. Green channel, eGFP; red channel, nuclei.

E. coli RNA or poly(I:C) (Figure 6A) triggered a strong inflammatory response that was completely independent of RI (Figures 6C, 6D, and S11). This response was characterized by a strong, dose-dependent disappearance of resident large peritoneal macrophages (LPMs) and recruitment of myeloid cells (comprising monocytes and/or neutrophils) and inflammatory macrophages (iMFs) at 24 h, a hallmark of peritoneal inflammation.[32] Of note, the recruitment of monocytes/neutrophils was not observed in the case of poly(I:C) treatment, which deserves further investigation.

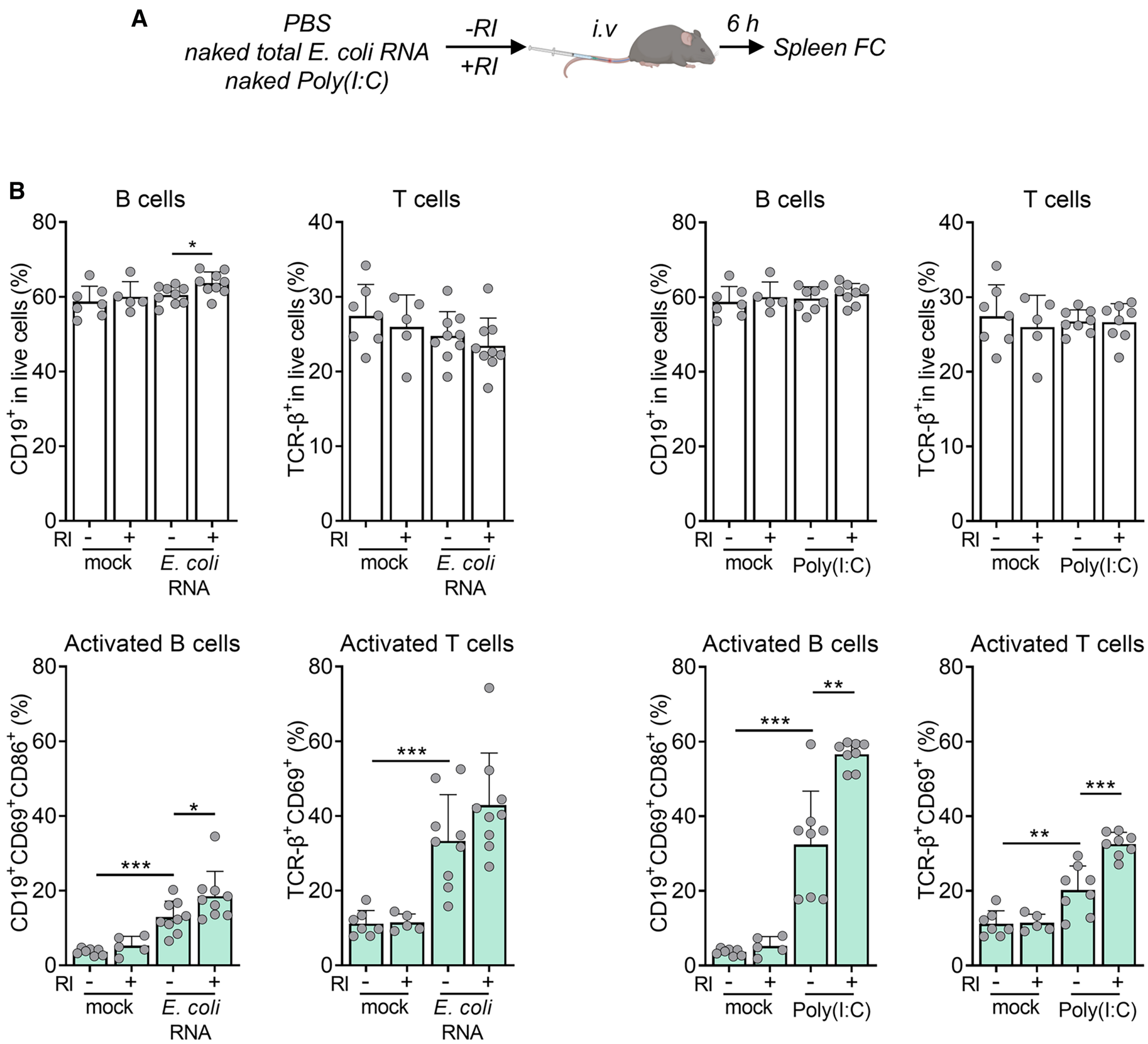

Figure 5. RI enhances the immunostimulatory effects of naked exRNAs circulating in the blood

(A) Experimental scheme.

(B) Flow cytometry analysis of splenic total B cells (defined as CD19$^+$), total T cells (defined as T cell receptor [TCR]-β^+), activated B cells (defined as CD19$^+$CD69$^+$CD86$^+$), and activated T cells (defined as TCR-β^+CD69$^+$) 6 h after intravenous administration of naked poly(I:C) (1 μg) or naked total *E. coli* RNA (10 μg), with or without 480 U of RI. Mock: DPBS. Total cells are shown in the top panel, and activated cells are shown in the bottom panel. *$p < 0.05$, **$p < 0.01$, ***$p < 0.001$; unpaired two-tailed t test (if normally distributed data) or unpaired two-tailed Mann-Whitney test (when data had no normal distribution) [naked RNA - RI vs. naked RNA + RI], [naked RNA − RI vs. mock − RI]. See also Figures S9 and S10.

In summary, naked exRNA is inherently bioactive in RNase-poor environments such as the peritoneal cavity, while RI is needed for maximum activity in the bloodstream. Altogether, these results suggest a key role for bloodborne extracellular RNases in the regulation of exRNA-induced systemic inflammation.

DISCUSSION

RNA-mediated intercellular communication has been almost exclusively studied in the context of EVs,[5] despite most exRNAs being present outside EVs in human biofluids,[33,34] cell-conditioned media,[21,35,36] and even in plants.[37,38] A bias against the study of nonvesicular exRNAs can be explained by the widespread assumption that exRNA is unstable unless protected inside EVs. Additionally, EVs provide a mechanism for functional RNA delivery into recipient cells.[5] In contrast, naked RNA is assumed to be incapable of penetrating the "billion-year-old barrier" comprising the plasma membrane and the membrane of endocytic vesicles.[8] By being refractory to the uptake of exRNAs, cells could protect themselves from selfish genetic elements such as viroids and positive-stranded RNA viruses, while preserving their transcriptional identity.

However, several RNA species are stable in the extracellular space even when not associated with EVs. These resilient exRNAs include ribonucleoprotein particles (RNPs) such as Ago2/miRNA complexes,[33,34,39] protein-protected RNA

74

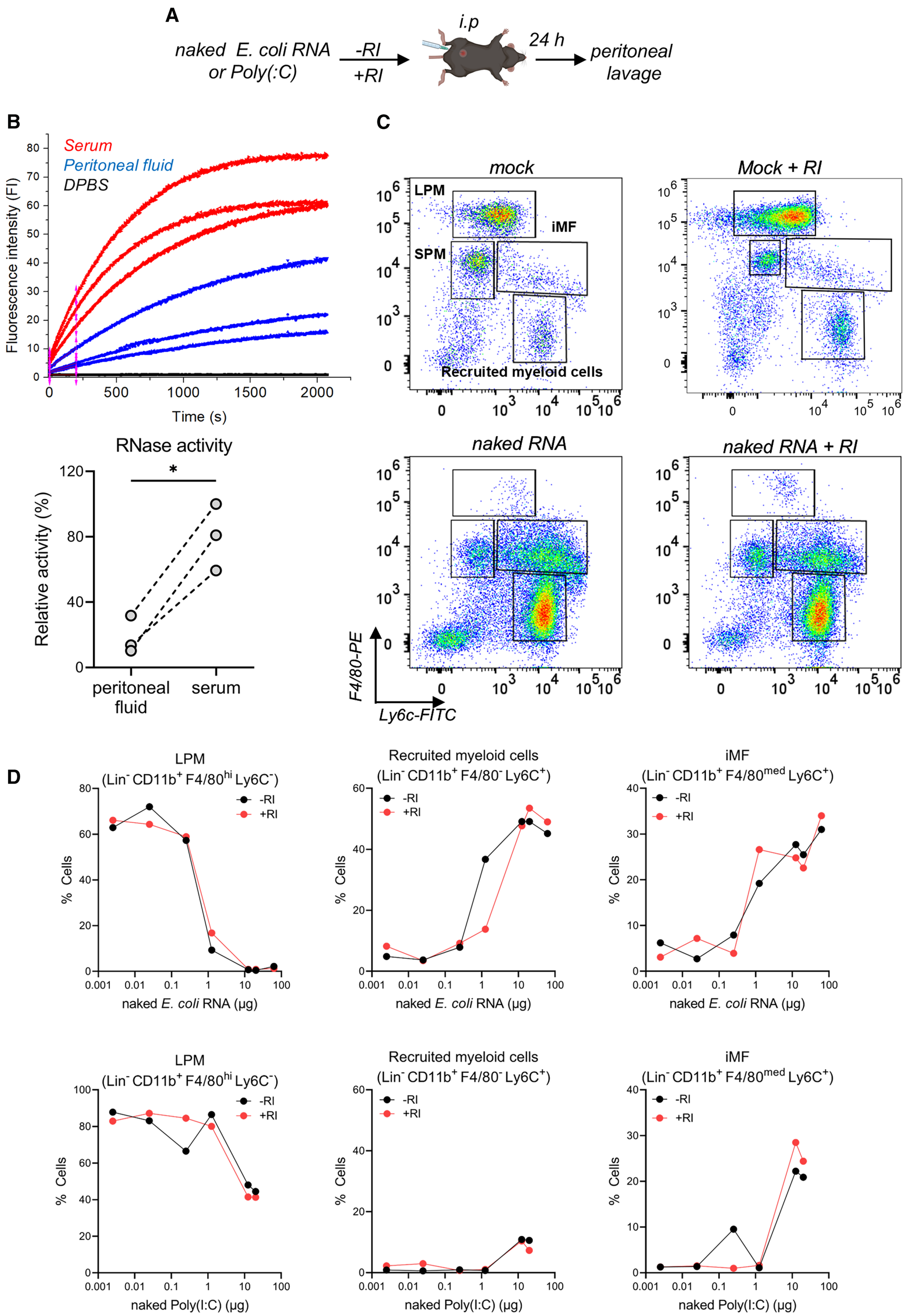

(legend on next page)

75

fragments[40] derived from the ribosome,[20,21,41] U2 snRNPs,[41] and possibly Xist RNPs.[42] Additionally, a population of intrinsically stable nicked tRNAs circulates in human biofluids, probably unprotected or naked.[20]

Rather than being inert, naked exRNAs can enter cells by gymnosis. It should be noted that this term was not defined in the context of a precise molecular mechanism[7]; the name axiomatically refers to functional naked RNA delivery into the cytosol.[43] Since best results in the original publication were obtained with locked nucleic acid (LNA)-containing phosphorothioate ASOs,[7] gymnotic uptake was later considered as an emerging property of phosphorothioate-containing oligonucleotides.[8] Unmodified and longer naked RNAs are thought to lack any biological activity.

In this work, we provide a different interpretation: any naked RNA can enter cells by endocytosis, and even reach the cytosol, as long as its extracellular stability is sufficiently high. The main factor limiting the concentration of naked exRNAs are extracellular RNases, which are highly abundant and active in biofluids such as the human blood.[20,44] Phosphorothioate-containing ASOs are resistant to degradation, and this may be why gymnotic uptake can occur for ASO-based biotherapeutics.[6] By adding a broad-range RNase inhibitor to cell culture medium, we demonstrated that uptake can be extended to naked bacterial rRNAs, synthetic short oligonucleotides (e.g., the Ec12 sequence), poly(I:C), and *in vitro*-transcribed mRNAs. This was shown in a variety of different cell types, including primary cultures of professional phagocytes and human epithelial cell lines.

It should be noted that we used the term "naked RNA" throughout this study because all stimuli were added in the absence of proteins or transfection reagents, including lipid nanoparticles. However, we cannot rule out the possibility that these naked RNAs might form a complex with one or more soluble extracellular protein(s) or other binding partners before cellular uptake. Having said that, the fact that similar responses were obtained in experiments performed in FBS-containing and FBS-free fresh media (Figure 1H) argues against this possibility.

We have shown that naked exRNAs, when stabilized by RI, are intrinsically bioactive in recipient cells. They can engage with endosomal RNA sensors such as TLR13 (in BMDCs and Raw264.7 macrophages), but they can also escape from endosomes into the cytosol, where they can be recognized by MAVS-dependent cytosolic RNA sensors (at least in human THP-1 macrophages). More strikingly, two different mRNAs encoding reporter proteins could be internalized by gymnosis and still be capable of serving as templates for protein synthesis in both BMDCs and human epithelial cell lines. This suggests their capacity to perform endosomal escape because ribosomes are present only in the cytosol. It is important to mention that these mRNA translation assays are highly sensitive to extracellular RNases, because a single cleavage event would render an mRNA untranslatable. Hence, the effect of RI was more pronounced in these assays and was potentiated by FBS depletion.

RNA endosomal escape in the absence of LNPs means that the billion-year-old barrier[8] may actually be leaky under certain circumstances. Interestingly, while efficient translation of our GFP-encoding mRNA required the use of modified nucleotides to avoid recognition by TLR7,[45] nanoLuc mRNA was translated even with unmodified uridine. These results encourage further basic research in naked mRNA therapies and vaccines. Although positive results were obtained after localized naked mRNA injections in organs with presumably low extracellular RNase activity,[9–11] co-administration of RI could enable more systemic delivery routes.

If pathogen-derived naked exRNAs are potent pro-inflammatory molecules, how are potentially life-threatening systemic inflammatory responses avoided? For example, the complement system could induce bacterial lysis in the bloodstream, releasing high loads of pro-inflammatory bacterial rRNAs that could activate circulating leukocytes. This study strongly suggests that extracellular RNases are highly abundant in the bloodstream to avoid RNA-induced systemic inflammation. We showed this by demonstrating that RI co-administration enhances immune cell activation in the spleen after intravenous injection of naked RNA. Interestingly, RI was dispensable when a similar assay was performed in the peritoneal cavity, an important site of immune surveillance with much lower RNase activity. Thus, naked exRNAs might convey important information for immune cells residing in tissues with relatively low blood irrigation and hence with low extracellular RNase content.

The immune system has multiple regulatory layers to ensure an optimal response to the different stimuli that immune cells could encounter. One key challenge is to differentiate self from non-self nucleic acids, which is achieved by regulating both the affinity[46] and the subcellular localization of endosomal TLRs.[47,48] Indeed, we observed a dramatically different response when comparing bacterial and murine RNAs incubated at the same concentration, both in the presence of RI. Surprisingly, the effect of RI itself was as dramatic as the capacity of BMDC RNA sensors (predominantly TLR13) to discriminate self from non-self RNAs. Thus, RNase-mediated control of exRNA stability lies on top of a series of layers comprising control of endocytosis, TLR loading and recognition, endosomal escape, and engagement with cytosolic RNA sensors.

Figure 6. Naked exRNA is intrinsically bioactive in the peritoneal cavity

(A) Experimental scheme.

(B) Comparison of RNase activity in serum and peritoneal fluid of three mice using a fluorometric assay. Top: kinetic curves. Bottom: the relative RNase activity derived from initial reaction velocities. $^{*}p < 0.05$; paired two-tailed t test.

(C) Representative flow cytometry dot plots showing expression of F4/80 and Ly6c (gated on lineage^{-} CD11b^{+}) to characterize immune cell populations in the peritoneal cavity 24 h after intraperitoneal (i.p.) injection of DPBS or 25 μg of naked total *E. coli* RNA, with or without 40 U of RI. Resident large (LPM) and small (SPM) peritoneal macrophages, recruited myeloid cells and inflammatory macrophages (iMFs) are shown. See also Figure S11.

(D) Graphs showing the percentage of resident large peritoneal macrophages (LPMs) defined as Lin^{-}CD11b^{+}F40/80^{hi}Ly6c^{-}, recruited myeloid cells defined as Lin^{-}CD11b^{+}F4/80^{-}Ly6c^{+}, and inflammatory macrophages defined as Lin^{-}CD11b^{+}F4/80^{med}Ly6c^{+}, 24 h after i.p. injections of increasing doses of naked total *E. coli* RNA (top panel, 0.025, 0.250, 1.25, 12.5, 25, and 62.5 μg) or naked poly(I:C) (bottom panel, 0.0025, 0.025, 0.250, 1.25, 12.5, and 20 μg) in the presence or absence of 40U of RI. The lowest concentration of naked *E. coli* RNA corresponds to DPBS, adjusted to fit the log scale.

One interesting finding that deserves further discussion is that the uptake of Ec12 RNA, unlike poly(I:C), did not depend on RI addition (Figures S5 and 3F, respectively). Moreover, the uptake efficiency in FBS-containing medium was almost identical when the Ec12 sequence was presented in the context of a single-stranded RNA or a double-stranded DNA, although the latter is presumably more stable (Figure S5). These results imply that the Ec12 RNA is inherently stable against RNase A family members, which might be explained by its pyrimidine-poor sequence composition, lacking any uridine residues. This observation made us wonder about the evolution of RNA sensors. For example, TLR13 is known to recognize a conserved sequence motif in bacterial 23S rRNA,[22] but our results suggest that this specific sequence might have also been selected based on its extracellular stability. This conclusion would be consistent with RNA-sensing TLRs recognizing mainly cell-free exRNAs.

There are several lines of evidence pointing to a role of enhanced and sustained exRNA sensing as a trigger of systemic inflammation or autoimmunity.[31,42,46,47,49–51] It is striking that all single-stranded endosomal RNA sensors (i.e., TLR7, TLR8, and TLR13) are codified in the X chromosome, possibly explaining sex-biased autoimmunity due to defects in dosage compensation.[52] These studies demonstrate that endosomal RNA sensing must be exquisitely fine-tuned[48] and that the control of TLR expression and localization is an effective way of doing so. Our study strongly suggests that extracellular RNases may act as an additional regulatory layer to control the levels of pro-inflammatory exRNAs and that they should therefore be considered as a regulatory arm of the innate immune system.

Supporting the role of extracellular RNases in the regulation of inflammatory responses, several reports have shown that ectopic administration of extracellular RNases reduces inflammation in mouse models of lupus-like disease,[53] traumatic brain injury,[54] and myocardial infarction.[55] In humans, sterile inflammation causing cell death and the release of RNPs into the extracellular space seems to be an important trigger of systemic lupus erythematosus.[42,56] In this and other autoimmune diseases, clinical trials using RNase-based drugs have shown evidence of efficacy.[57,58]

On a more technical note, we would like to emphasize that intents to understand exRNA biology using cell-culture-based assays will inevitably fail if fetal or calf serum is used without RI supplementation. This technical problem has led to the wrong assumption that exRNA biology is relevant only in the context of EVs, or that the study of intracellular nucleic acid sensors requires the use of transfection reagents.[17] We envision that this study will renovate interest in nonvesicular exRNAs in intercellular communication, particularly in the context of inflammatory and autoimmune diseases.

In conclusion, this study clearly demonstrates that naked exRNA is intrinsically bioactive both *in vitro* and *in vivo*. Moreover, in the absence of RNases, exRNA can spontaneously enter cells and even escape from endosomal compartments, engaging both endosomal and cytosolic RNA sensors. Earlier studies may have failed to observe these phenomena due to the confounding effect of extracellular RNases. Furthermore, this study suggests that the multiple RNases that exist in the extracellular space may have evolved to avoid potentially harmful systemic inflammatory responses triggered by either host- or pathogen-derived naked or nonvesicular exRNAs.

Limitations of the study

Although this study has several strengths, including the use of diverse cellular models, multiple naked RNA species, and the combination of *in vitro* and *in vivo* results, a key limitation is the reliance on exogenous RNAs (lacking RNA modifications) for *in vivo* studies. Future work should complement these findings by modulating endogenous exRNA levels. Additionally, findings on TLR13 activation in murine cell lines may not directly translate to humans, as this RNA sensor is not expressed in primates.

RESOURCE AVAILABILITY

Lead contact

Further information and requests for resources and reagents should be directed to and will be fulfilled by the corresponding author, Juan Pablo Tosar (jptosar@pasteur.edu.uy).

Materials availability

This study did not generate new unique reagents.

Data and code availability

The sequencing data generated in this study can be accessed at NCBI under BioProject PRJNA1120732 (SRA: SRP512141).

ACKNOWLEDGMENTS

The authors gratefully acknowledge the following core facilities and technological platforms at the Institut Pasteur of Montevideo for their support and assistance in the present work: Advanced Bioimaging Unit (UBA), Animal Biotechnology Unit (UBAL), and the Cell Biology Unit (UBC), with special thanks to Karen Perelmuter and Paula Céspedes. The authors want to thank María Elena Márquez, Sofía Russo, Daniela Olivera, Germán Galliussi, and Valentina Perez for helpful suggestions, experimental help, and insightful scientific discussions. This study was funded by Agencia Nacional de Investigación e Innovación (ANII, Uruguay) (FCE_1_2021_1_166344; PEC_3_2019_1_158011), Fondo para la Convergencia Estructural del Mercosur (FOCEM) (COF 03/11), Comisión Sectorial de Investigación Científica (CSIC, UdelaR, Uruguay) (22620220100069UD), Comisión Académica de Posgrado (CAP, CSIC, UdelaR, Uruguay) (BDDX_2020_1#50810037; BFPD_2023_1#50810037), the National Institutes of Health (NIH, USA) (R21CA263424), and the NIH Office of the Director (UH3CA241694).

AUTHOR CONTRIBUTIONS

J.P.T. and M.S. led and oversaw the study. J.P.T., M.S., and M.C. conceived the project and designed experiments. M.C. performed and analyzed most *in vitro* and *in vivo* experiments. M.C. carried out bioinformatic analysis. V. B., B.C., and M.L.C. conducted and analyzed naked mRNA capture experiments, RNA stability experiments, and confocal microscopy experiments, respectively. K.W., M.H., and A.C. contributed to data interpretation and evaluation. J.P.T. and M.C. wrote the manuscript with input from all authors.

DECLARATION OF INTERESTS

J.P.T., M.S., M.H., and A.C. are members of the Sistema Nacional de Investigadores (SNI) and Programa de Desarrollo de las Ciencias Básicas (PEDECIBA, MEC-UdelaR). K.W. has a sponsored research agreement with Ionis Pharmaceuticals; is or has been an advisory board member of ShiftBio, Exopharm, NeuroDex, NovaDip, and ReNeuron; and performs *ad hoc* consulting as Kenneth Witwer Consulting. J.P.T. is a founder of B4-RNA, a startup involved in exRNA-based diagnosis. J.P.T., B.C., A.C., and K.W. have filed patents on RNA repair and sequencing for biomarker/diagnostic applications.

After submitting the initial version of this manuscript, J.P.T. was contacted and later became a member of the advisory board of Resolve Therapeutics, a company employing synthetic RNases to treat human diseases. This company had no involvement in this study.

STAR★METHODS

Detailed methods are provided in the online version of this paper and include the following:

- KEY RESOURCES TABLE
- EXPERIMENTAL MODEL DETAILS
  - Animals
  - Cell lines
  - Primary cell culture
- METHOD DETAILS
  - Total E. coli RNA purification and fractionation
  - RNA-seq and bioinformatic analysis
  - Bioinformatic analysis of publicly available datasets
  - Cell stimulation
  - RT-qPCR
  - Tlr13 knockdown in Raw264.7
  - *In vitro* transcription
  - *In vitro* translation
  - RNase activity in mouse serum and peritoneal wash
  - nanoLuc mRNA internalization and translation assays
  - Naked eGFP internalization and translation assays
  - *In vivo* experiments
  - Flow cytometry
  - RNA polyacrylamide electrophoresis
- QUANTIFICATION AND STATISTICAL ANALYSIS

SUPPLEMENTAL INFORMATION

Supplemental information can be found online at https://doi.org/10.1016/j.xgen.2025.100874.

Received: April 27, 2024
Revised: February 26, 2025
Accepted: April 10, 2025
Published: May 6, 2025

REFERENCES

1. Valadi, H., Ekström, K., Bossios, A., Sjöstrand, M., Lee, J.J., and Lötvall, J.O. (2007). Exosome-mediated transfer of mRNAs and microRNAs is a novel mechanism of genetic exchange between cells. Nat. Cell Biol. *9*, 654–659. https://doi.org/10.1038/ncb1596.
2. Ratajczak, J., Miekus, K., Kucia, M., Zhang, J., Reca, R., Dvorak, P., and Ratajczak, M.Z. (2006). Embryonic stem cell-derived microvesicles reprogram hematopoietic progenitors: evidence for horizontal transfer of mRNA and protein delivery. Leukemia *20*, 847–856. https://doi.org/10.1038/sj.leu.2404132.
3. Skog, J., Würdinger, T., van Rijn, S., Meijer, D.H., Gainche, L., Sena-Esteves, M., Curry, W.T., Jr., Carter, B.S., Krichevsky, A.M., and Breakefield, X.O. (2008). Glioblastoma microvesicles transport RNA and proteins that promote tumour growth and provide diagnostic biomarkers. Nat. Cell Biol. *10*, 1470–1476. https://doi.org/10.1038/ncb1800.
4. Kalluri, R., and LeBleu, V.S. (2020). The Biology, Function, and Biomedical Applications of Exosomes (American Association for the Advancement of Science). https://doi.org/10.1126/science.aau6977.
5. O'Brien, K., Breyne, K., Ughetto, S., Laurent, L.C., and Breakefield, X.O. (2020). RNA delivery by extracellular vesicles in mammalian cells and its applications. Nat. Rev. Mol. Cell Biol. *21*, 585–606. https://doi.org/10.1038/s41580-020-0251-y.
6. Levin, A.A. (2019). Treating Disease at the RNA Level with Oligonucleotides. N. Engl. J. Med. *380*, 57–70. https://doi.org/10.1056/NEJMra1705346.
7. Stein, C.A., Hansen, J.B., Lai, J., Wu, S., Voskresenskiy, A., Høg, A., Worm, J., Hedtjärn, M., Souleimanian, N., Miller, P., et al. (2010). Efficient gene silencing by delivery of locked nucleic acid antisense oligonucleotides, unassisted by transfection reagents. Nucleic Acids Res. *38*, e3. https://doi.org/10.1093/nar/gkp841.
8. Dowdy, S.F. (2017). Overcoming Cellular Barriers for RNA Therapeutics (Nature Publishing Group). https://doi.org/10.1038/nbt.3802.
9. Wolff, J.A., Malone, R.W., Williams, P., Chong, W., Acsadi, G., Jani, A., and Felgner, P.L. (1990). Direct gene transfer into mouse muscle in vivo. Science *247*, 1465–1468. https://doi.org/10.1126/science.1690918.
10. Kreiter, S., Selmi, A., Diken, M., Koslowski, M., Britten, C.M., Huber, C., Türeci, O., and Sahin, U. (2010). Intranodal vaccination with naked antigen-encoding RNA elicits potent prophylactic and therapeutic antitumoral immunity. Cancer Res. *70*, 9031–9040. https://doi.org/10.1158/0008-5472.CAN-10-0699.
11. Diken, M., Kreiter, S., Selmi, A., Britten, C.M., Huber, C., Türeci, Ö., and Sahin, U. (2011). Selective uptake of naked vaccine RNA by dendritic cells is driven by macropinocytosis and abrogated upon DC maturation. Gene Ther. *18*, 702–708. https://doi.org/10.1038/gt.2011.17.
12. Selmi, A., Vascotto, F., Kautz-Neu, K., Türeci, Ö., Sahin, U., von Stebut, E., Diken, M., and Kreiter, S. (2016). Uptake of synthetic naked RNA by skin-resident dendritic cells via macropinocytosis allows antigen expression and induction of T-cell responses in mice. Cancer Immunol. Immunother. *65*, 1075–1083. https://doi.org/10.1007/s00262-016-1869-7.
13. Bitounis, D., Jacquinet, E., Rogers, M.A., and Amiji, M.M. (2024). Strategies to reduce the risks of mRNA drug and vaccine toxicity. Nat. Rev. Drug Discov. *23*, 281–300. https://doi.org/10.1038/s41573-023-00859-3.
14. Akinc, A., Maier, M.A., Manoharan, M., Fitzgerald, K., Jayaraman, M., Barros, S., Ansell, S., Du, X., Hope, M.J., Madden, T.D., et al. (2019). The Onpattro Story and the Clinical Translation of Nanomedicines Containing Nucleic Acid-Based Drugs (Nature Publishing Group). https://doi.org/10.1038/s41565-019-0591-y.
15. Hou, X., Zaks, T., Langer, R., and Dong, Y. (2021). Lipid Nanoparticles for mRNA Delivery (Nature Publishing Group). https://doi.org/10.1038/s41578-021-00358-0.
16. Dowdy, S.F. (2023). Endosomal escape of RNA therapeutics: How do we solve this rate-limiting problem? RNA *29*, 396–401. https://doi.org/10.1261/rna.079507.122.
17. Sha, W., Mitoma, H., Hanabuchi, S., Bao, M., Weng, L., Sugimoto, N., Liu, Y., Zhang, Z., Zhong, J., Sun, B., and Liu, Y.J. (2014). Human NLRP3 Inflammasome senses multiple types of bacterial RNAs. Proc. Natl. Acad. Sci. USA *111*, 16059–16064. https://doi.org/10.1073/pnas.1412487111.
18. Kailasan Vanaja, S., Rathinam, V.A.K., Atianand, M.K., Kalantari, P., Skehan, B., Fitzgerald, K.A., and Leong, J.M. (2014). Bacterial RNA:DNA hybrids are activators of the NLRP3 inflammasome. Proc. Natl. Acad. Sci. USA *111*, 7765–7770. https://doi.org/10.1073/pnas.1400075111.
19. Tosar, J.P., Witwer, K., and Cayota, A. (2021). Revisiting Extracellular RNA Release, Processing, and Function (Elsevier Ltd). https://doi.org/10.1016/j.tibs.2020.12.008.
20. Costa, B., Li Calzi, M., Castellano, M., Blanco, V., Cuevasanta, E., Litvan, I., Ivanov, P., Witwer, K., Cayota, A., and Tosar, J.P. (2023). Nicked tRNAs are stable reservoirs of tRNA halves in cells and biofluids. Proc. Natl. Acad. Sci. USA *120*, e2216330120. https://doi.org/10.1073/pnas.2216330120.
21. Tosar, J.P., Segovia, M., Castellano, M., Gámbaro, F., Akiyama, Y., Fagúndez, P., Olivera, Á., Costa, B., Possi, T., Hill, M., et al. (2020). Fragmentation of extracellular ribosomes and tRNAs shapes the extracellular RNAome. Nucleic Acids Res. *48*, 12874–12888. https://doi.org/10.1093/nar/gkaa674.
22. Oldenburg, M., Krüger, A., Ferstl, R., Kaufmann, A., Nees, G., Sigmund, A., Bathke, B., Lauterbach, H., Suter, M., Dreher, S., et al. (2012). TLR13 recognizes bacterial 23S rRNA devoid of erythromycin resistance - Forming

modification. Science *337*, 1111–1115. https://doi.org/10.1126/science.1220363.

23. Helft, J., Böttcher, J., Chakravarty, P., Zelenay, S., Huotari, J., Schraml, B. U., Goubau, D., and Reis e Sousa, C. (2015). GM-CSF Mouse Bone Marrow Cultures Comprise a Heterogeneous Population of CD11c +MHCII+ Macrophages and Dendritic Cells. Immunity *42*, 1197–1211. https://doi.org/10.1016/j.immuni.2015.05.018.
24. Na, Y.R., Jung, D., Gu, G.J., and Seok, S.H. (2016). GM-CSF grown bone marrow derived cells are composed of phenotypically different dendritic cells and macrophages. Mol. Cells *39*, 734–741. https://doi.org/10.14348/molcells.2016.0160.
25. Preta, G., Cronin, J.G., and Sheldon, I.M. (2015). Dynasore - Not just a dynamin inhibitor. Cell Commun. Signal. *13*, 1–7. https://doi.org/10.1186/s12964-015-0102-1.
26. Hidmark, A., von Saint Paul, A., and Dalpke, A.H. (2012). Cutting Edge: TLR13 Is a Receptor for Bacterial RNA. J. Immunol. *189*, 2717–2721. https://doi.org/10.4049/jimmunol.1200898.
27. Fieber, C., Janos, M., Koestler, T., Gratz, N., Li, X.-D., Castiglia, V., Aberle, M., Sauert, M., Wegner, M., Alexopoulou, L., et al. (2015). Innate immune response to Streptococcus pyogenes depends on the combined activation of TLR13 and TLR2. PLoS One *10*, e0119727. https://doi.org/10.1371/journal.pone.0119727.
28. Dauletbaev, N., Cammisano, M., Herscovitch, K., and Lands, L.C. (2015). Stimulation of the RIG-I/MAVS Pathway by Polyinosinic:Polycytidylic Acid Upregulates IFN-β in Airway Epithelial Cells with Minimal Costimulation of IL-8. J. Immunol. *195*, 2829–2841. https://doi.org/10.4049/jimmunol.1400840.
29. McCartney, S., Vermi, W., Gilfillan, S., Cella, M., Murphy, T.L., Schreiber, R.D., Murphy, K.M., and Colonna, M. (2009). Distinct and complementary functions of MDA5 and TLR3 in poly(I:C)-mediated activation of mouse NK cells. J. Exp. Med. *206*, 2967–2976. https://doi.org/10.1084/jem.20091181.
30. Nelson, J., Sorensen, E.W., Mintri, S., Rabideau, A.E., Zheng, W., Besin, G., Khatwani, N., Su, S.V., Miracco, E.J., Issa, W.J., et al. (2020). Impact of mRNA chemistry and manufacturing process on innate immune activation. Sci. Adv. *6*, eaaz6893. https://doi.org/10.1126/sciadv.aaz6893.
31. Hwang, S.-H., Lee, H., Yamamoto, M., Jones, L.A., Dayalan, J., Hopkins, R., Zhou, X.J., Yarovinsky, F., Connolly, J.E., Curotto de Lafaille, M.A., et al. (2012). B cell TLR7 expression drives anti-RNA autoantibody production and exacerbates disease in systemic lupus erythematosus-prone mice. J. Immunol. *189*, 5786–5796. https://doi.org/10.4049/jimmunol.1202195.
32. Louwe, P.A., Badiola Gomez, L., Webster, H., Perona-Wright, G., Bain, C. C., Forbes, S.J., and Jenkins, S.J. (2021). Recruited macrophages that colonize the post-inflammatory peritoneal niche convert into functionally divergent resident cells. Nat. Commun. *12*, 1770. https://doi.org/10.1038/s41467-021-21778-0.
33. Arroyo, J.D., Chevillet, J.R., Kroh, E.M., Ruf, I.K., Pritchard, C.C., Gibson, D.F., Mitchell, P.S., Bennett, C.F., Pogosova-Agadjanyan, E.L., Stirewalt, D.L., et al. (2011). Argonaute2 complexes carry a population of circulating microRNAs independent of vesicles in human plasma. Proc. Natl. Acad. Sci. USA *108*, 5003–5008. https://doi.org/10.1073/pnas.1019055108.
34. Turchinovich, A., Weiz, L., Langheinz, A., and Burwinkel, B. (2011). Characterization of extracellular circulating microRNA. Nucleic Acids Res. *39*, 7223–7233. https://doi.org/10.1093/nar/gkr254.
35. Tosar, J.P., Gámbaro, F., Sanguinetti, J., Bonilla, B., Witwer, K.W., and Cayota, A. (2015). Assessment of small RNA sorting into different extracellular fractions revealed by high-throughput sequencing of breast cell lines. Nucleic Acids Res. *43*, 5601–5616. https://doi.org/10.1093/nar/gkv432.
36. Sork, H., Conceicao, M., Corso, G., Nordin, J., Lee, Y.X.F., Krjutskov, K., Orzechowski Westholm, J., Vader, P., Pauwels, M., Vandenbroucke, R.E., et al. (2021). Profiling of extracellular small rnas highlights a strong bias towards non-vesicular secretion. Cells *10*, 1543. https://doi.org/10.3390/cells10061543.
37. Borniego, M.L., and Innes, R.W. (2023). Extracellular RNA: mechanisms of secretion and potential functions. J. Exp. Bot. *74*, 2389–2404. https://doi.org/10.1093/jxb/erac512.
38. Zand Karimi, H., Baldrich, P., Rutter, B.D., Borniego, L., Zajt, K.K., Meyers, B.C., and Innes, R.W. (2022). Arabidopsis apoplastic fluid contains sRNA- and circular RNA-protein complexes that are located outside extracellular vesicles. Plant Cell *34*, 1863–1881. https://doi.org/10.1093/plcell/koac043.
39. Geekiyanage, H., Rayatpisheh, S., Wohlschlegel, J.A., Brown, R., and Ambros, V. (2020). Extracellular microRNAs in human circulation are associated with miRISC complexes that are accessible to anti-AGO2 antibody and can bind target mimic oligonucleotides. Proc. Natl. Acad. Sci. USA *117*, 24213–24223. https://doi.org/10.1073/pnas.2008323117.
40. LaPlante, E.L., Stürchler, A., Fullem, R., Chen, D., Starner, A.C., Esquivel, E., Alsop, E., Jackson, A.R., Ghiran, I., Pereira, G., et al. (2023). exRNA-eCLIP intersection analysis reveals a map of extracellular RNA binding proteins and associated RNAs across major human biofluids and carriers. Cell Genom. *3*, 100303. https://doi.org/10.1016/j.xgen.2023.100303.
41. Tosar, J.P., Cayota, A., and Witwer, K. (2022). Exomeres and supermeres : Monolithic or diverse. J. Extracell. Biol. *1*, e45. https://doi.org/10.1002/jex2.45.
42. Dou, D.R., Zhao, Y., Belk, J.A., Zhao, Y., Casey, K.M., Chen, D.C., Li, R., Yu, B., Srinivasan, S., Abe, B.T., et al. (2024). Xist ribonucleoproteins promote female sex-biased autoimmunity. Cell *187*, 733–749.e16. https://doi.org/10.1016/j.cell.2023.12.037.
43. Zhang, X., Castanotto, D., Liu, X., Shemi, A., and Stein, C.A. (2018). Ammonium and arsenic trioxide are potent facilitators of oligonucleotide function when delivered by gymnosis. Nucleic Acids Res. *46*, 3612–3624. https://doi.org/10.1093/nar/gky150.
44. Lomax, J.E., Eller, C.H., and Raines, R.T. (2017). Comparative functional analysis of ribonuclease 1 homologs: Molecular insights into evolving vertebrate physiology. Biochem. J. *474*, 2219–2233. https://doi.org/10.1042/BCJ20170173.
45. Karikó, K., Buckstein, M., Ni, H., and Weissman, D. (2005). Suppression of RNA recognition by Toll-like receptors: The impact of nucleoside modification and the evolutionary origin of RNA. Immunity *23*, 165–175. https://doi.org/10.1016/j.immuni.2005.06.008.
46. Brown, G.J., Cañete, P.F., Wang, H., Medhavy, A., Bones, J., Roco, J.A., He, Y., Qin, Y., Cappello, J., Ellyard, J.I., et al. (2022). TLR7 gain-of-function genetic variation causes human lupus. Nature *605*, 349–356. https://doi.org/10.1038/s41586-022-04642-z.
47. Mishra, H., Schlack-leigers, C., Lim, E.L., Thieck, O., Magg, T., Raedler, J., Wolf, C., Klein, C., Ewers, H., Lee-Kirsch, M.A., et al. (2024). Disrupted degradative sorting of TLR7 is associated with human lupus. Sci. Immunol. *9*, eadi9575. https://doi.org/10.1101/2023.04.03.535356.
48. Lind, N.A., Rael, V.E., Pestal, K., Liu, B., and Barton, G.M. (2022). Regulation of the nucleic acid-sensing Toll-like receptors. Nat. Rev. Immunol. *22*, 224–235. https://doi.org/10.1038/s41577-021-00577-0.
49. Suen, A.O., Chen, F., Wang, S., Li, Z., Zhu, J., Yang, Y., Conn, O., Lopez, K., Cui, P., Wechsler, L., et al. (2023). Extracellular RNA Sensing Mediates Inflammation and Organ Injury in a Murine Model of Polytrauma. J. Immunol. *210*, 1990–2000. https://doi.org/10.4049/jimmunol.2300103.
50. Christensen, S.R., Shupe, J., Nickerson, K., Kashgarian, M., Flavell, R.A., and Shlomchik, M.J. (2006). Toll-like Receptor 7 and TLR9 Dictate Autoantibody Specificity and Have Opposing Inflammatory and Regulatory Roles in a Murine Model of Lupus. Immunity *25*, 417–428. https://doi.org/10.1016/j.immuni.2006.07.013.
51. Majer, O., Liu, B., Kreuk, L.S.M., Krogan, N., and Barton, G.M. (2019). UNC93B1 recruits syntenin-1 to dampen TLR7 signalling and prevent autoimmunity. Nature *575*, 366–370. https://doi.org/10.1038/s41586-019-1612-6.
52. Souyris, M., Cenac, C., Azar, P., Daviaud, D., Canivet, A., Grunenwald, S., Pienkowski, C., Chaumeil, J., Mejía, J.E., and Guéry, J.-C. (2018). TLR7

escapes X chromosome inactivation in immune cells. Sci. Immunol. *3*, eaap8855. https://doi.org/10.1126/sciimmunol.aap8855.

53. Sun, X., Wiedeman, A., Agrawal, N., Teal, T.H., Tanaka, L., Hudkins, K.L., Alpers, C.E., Bolland, S., Buechler, M.B., Hamerman, J.A., et al. (2013). Increased Ribonuclease Expression Reduces Inflammation and Prolongs Survival in TLR7 Transgenic Mice. J. Immunol. *190*, 2536–2543. https://doi.org/10.4049/jimmunol.1202689.

54. Krämer, T.J., Hübener, P., Pöttker, B., Gölz, C., Neulen, A., Pantel, T., Goetz, H., Ritter, K., Schäfer, M.K.E., and Thal, S.C. (2022). Ribonuclease-1 treatment after traumatic brain injury preserves blood–brain barrier integrity and delays secondary brain damage in mice. Sci. Rep. *12*, 5731. https://doi.org/10.1038/s41598-022-09326-2.

55. Cabrera-Fuentes, H.A., Ruiz-Meana, M., Simsekyilmaz, S., Kostin, S., Inserte, J., Saffarzadeh, M., Galuska, S.P., Vijayan, V., Barba, I., Barreto, G., et al. (2014). RNase1 prevents the damaging interplay between extracellular RNA and tumour necrosis factor-α in cardiac ischaemia/reperfusion injury. Thromb. Haemost. *112*, 1110–1119. https://doi.org/10.1160/TH14-08-0703.

56. Doedens, J.R., Jones, W.D., Hill, K., Mason, M.J., Gersuk, V.H., Mease, P. J., Dall'Era, M., Aranow, C., Martin, R.W., Cohen, S.B., et al. (2016). Blood-Borne RNA Correlates with Disease Activity and IFN-Stimulated Gene Expression in Systemic Lupus Erythematosus. J. Immunol. *197*, 2854–2863. https://doi.org/10.4049/jimmunol.1601142.

57. Burge, D.J., Werth, V.P., Boackle, S.A., and Posada, J. (2024). Evaluation of RNase therapy in systemic lupus erythematosus: a randomised phase 2a clinical trial of RSLV-132. Lupus Sci. Med. *11*, e001113. https://doi.org/10.1136/lupus-2023-001113.

58. Posada, J., Valadkhan, S., Burge, D., Davies, K., Tarn, J., Casement, J., Jobling, K., Gallagher, P., Wilson, D., Barone, F., et al. (2021). Improvement of Severe Fatigue Following Nuclease Therapy in Patients With Primary Sjögren's Syndrome: A Randomized Clinical Trial. Arthritis Rheumatol. *73*, 143–150. https://doi.org/10.1002/art.41489.

59. Segovia, M., Russo, S., Jeldres, M., Mahmoud, Y.D., Perez, V., Duhalde, M., Charnet, P., Rousset, M., Victoria, S., Veigas, F., et al. (2019). Targeting TMEM176B Enhances Antitumor Immunity and Augments the Efficacy of Immune Checkpoint Blockers by Unleashing Inflammasome Activation. Cancer Cell *35*, 767–781.e6. https://doi.org/10.1016/j.ccell.2019.04.003.

60. Dobin, A., Davis, C.A., Schlesinger, F., Drenkow, J., Zaleski, C., Jha, S., Batut, P., Chaisson, M., and Gingeras, T.R. (2013). STAR: Ultrafast universal RNA-seq aligner. Bioinformatics *29*, 15–21. https://doi.org/10.1093/bioinformatics/bts635.

61. Okonechnikov, K., Conesa, A., and García-Alcalde, F. (2016). Qualimap 2: Advanced multi-sample quality control for high-throughput sequencing data. Bioinformatics *32*, 292–294. https://doi.org/10.1093/bioinformatics/btv566.

62. Liao, Y., Smyth, G.K., and Shi, W. (2014). FeatureCounts: An efficient general purpose program for assigning sequence reads to genomic features. Bioinformatics *30*, 923–930. https://doi.org/10.1093/bioinformatics/btt656.

63. Love, M.I., Huber, W., and Anders, S. (2014). Moderated estimation of fold change and dispersion for RNA-seq data with DESeq2. Genome Biol. *15*, 550. https://doi.org/10.1186/s13059-014-0550-8.

64. Ge, S.X., Jung, D., Yao, R., and Yao, R. (2020). ShinyGO: A graphical gene-set enrichment tool for animals and plants. Bioinformatics *36*, 2628–2629. https://doi.org/10.1093/bioinformatics/btz931.

65. Green, I.D., Pinello, N., Song, R., Lee, Q., Halstead, J.M., Kwok, C.T., Wong, A.C.H., Nair, S.S., Clark, S.J., Roediger, B., et al. (2020). Macrophage development and activation involve coordinated intron retention in key inflammatory regulators. Nucleic Acids Res. *48*, 6513–6529. https://doi.org/10.1093/nar/gkaa435.

66. Johnson, J.S., De Veaux, N., Rives, A.W., Lahaye, X., Lucas, S.Y., Perot, B.P., Luka, M., Garcia-Paredes, V., Amon, L.M., Watters, A., et al. (2020). A Comprehensive Map of the Monocyte-Derived Dendritic Cell Transcriptional Network Engaged upon Innate Sensing of HIV. Cell Rep. *30*, 914–931.e9. https://doi.org/10.1016/j.celrep.2019.12.054.

67. Das, A., Yang, C.-S., Arifuzzaman, S., Kim, S., Kim, S.Y., Jung, K.H., Lee, Y.S., and Chai, Y.G. (2018). High-Resolution Mapping and Dynamics of the Transcriptome, Transcription Factors, and Transcription Co-Factor Networks in Classically and Alternatively Activated Macrophages. Front. Immunol. *9*, 22. https://doi.org/10.3389/fimmu.2018.00022.

68. Zhang, W., Lohman, A.W., Zhuravlova, Y., Lu, X., Wiens, M.D., Hoi, H., Yaganoglu, S., Mohr, M.A., Kitova, E.N., Klassen, J.S., et al. (2017). Optogenetic control with a photocleavable protein, Phocl. Nat. Methods *14*, 391–394. https://doi.org/10.1038/nmeth.4222.

69. Hartveit, F., and Thunold, S. (1966). Peritoneal fluid volume and the oestrus cycle in mice. Nature *210*, 1123–1125. https://doi.org/10.1038/2101123a0.

70. Galaxy Community (2022). The Galaxy platform for accessible, reproducible and collaborative biomedical analyses: 2022 update. Nucleic Acids Res. *50*, W345–W351. https://doi.org/10.1093/nar/gkac247.

71. Schneider, C.A., Rasband, W.S., and Eliceiri, K.W. (2012). NIH Image to ImageJ: 25 years of image analysis. Nat. Methods *9*, 671–675. https://doi.org/10.1038/nmeth.2089.

STAR★METHODS

KEY RESOURCES TABLE

REAGENT or RESOURCE	SOURCE	IDENTIFIER
Antibodies		
FITC anti-mouse CD40	BioLegend	Cat# 124607; RRID:AB_1134090
PE anti-mouse CD86	BD Biosciences	Cat# 553692; RRID:AB_394994
APC anti-mouse MHCII(I-A/I-E)	BioLegend	Cat# 107614; RRID:AB_313329
APC/Cyanine7 anti-mouse CD19	BioLegend	Cat# 115529; RRID:AB_830706
APC/Cyanine7 anti-mouse TCR beta chain	BioLegend	Cat# 109220; RRID:AB_893624
Brilliant Violet 711(TM) anti-mouse Ly-6G	BioLegend	Cat# 127643; RRID:AB_2565971
PE-Cy7 anti-mouse CD11c	BD Biosciences	Cat# 558079; RRID:AB_647251
PerCP/Cyanine5.5 anti-mouse/human CD45R/B220	BioLegend	Cat# 103236; RRID:AB_893354
PE anti-mouse F4/80	BD Biosciences	Cat# 565410; RRID:AB_2687527
Alexa Fluor(R) 700 anti-mouse/human CD11b	BioLegend	Cat# 101222; RRID:AB_493705
FITC anti-mouse CD86	BioLegend	Cat# 105006; RRID:AB_313149
PerCP/Cyanine5.5 anti-mouse/human CD11b	BioLegend	Cat# 101228; RRID:AB_893232
PE-Cy7 anti-mouse CD69	BD Biosciences	Cat# 552879; RRID:AB_394508
Anti-human RAB5A	Cell Signaling	Cat# 46449; RRID:AB_2799303
Alexa Fluor(R) 488 anti-mouse IgG (H + L)	Invitrogen	Cat# A-11029; RRID:AB_2534088
Alexa Fluor(R) 647 anti-mouse IgG (H + L)	Invitrogen	Cat# A-21236; RRID:AB_2535805
Chemicals, peptides, and recombinant proteins		
3′-*O*-Me-m7G(5′)ppp(5′)G RNA Cap Structure Analog	New England Biolabs	Cat #S1411
Acetone	Dorwill	Cat #UN1090
Albumin fraction V pH = 7.0	AppliChem	Cat #A1391
Ammonium chloride	Sigma-Aldrich	Cat #A9434
Blasticidine	Invivogen	Cat #ant-bl
Chloroform	Droguería Industrial Uruguay	Cat #41191
Collagenase D	Roche	Cat #11088858001
DAPI	Sigma-Aldrich	Cat #D9542
Dextran conjugated to Alexa Fluor 647	Invitrogen	Cat #D22914
DMEM, high glucose, pyruvate	Gibco	Cat #11995065
DMSO	Sigma-Aldrich	Cat #D2650
DNasa I	Roche	Cat #04716728001
DOTAP	Roche	Cat #11202375001
DPBS without Ca^{2+} Mg^{2+}	Gibco	Cat #14190086
Dithiothreitol	Sigma-Aldrich	Cat #D0632
EDTA disodium salt	Sigma-Aldrich	Cat #E6635
EDTA for molecular biology	New England Biolabs	Cat #7011V
Ethanol absolute anhydrous	Carlo Erba	Cat #4146052
FastStart Universal SYBR Green Master	Roche	Cat #FSUSGMMRO
Fetal bovine serum, qualified Brazil	Gibco	Cat #12657029
HEPES	Gibco	Cat #15630130
L-Glutamine	Gibco	Cat #A2916801
LIVE/DEAD^{TM} Fixable Violet Dead Cell Stain	Invitrogen	Cat #L34964
Lipopolysaccharides from Escherichia coli O111:B4	Sigma-Aldrich	Cat #L4391
MEGM	Lonza	Cat #CC-4136
MEM Non-Essential Amino Acids Solution	Gibco	Cat #11140035
N1-Methylpseudouridine-5′-Triphosphate	TriLink Biotechnologies	Cat #*N*-1081

(*Continued on next page*)

Continued

REAGENT or RESOURCE	SOURCE	IDENTIFIER
Normal rat serum	Invitrogen	Cat #10710C
Normicin	Invivogen	Cat #ant-nr
NucRed Live 647 ReadyProbes Reagent	Invitrogen	Cat #R37106
Optimem	Gibco	Cat #51985091
Penicillin-Streptomycin	Gibco	Cat #15140148
Phorbol 12-Myristate 13-Acetate	Sigma-Aldrich	Cat #P8139
Phusion Polymerase	Thermo Fischer	Cat #F-530XL
Polymyxin B	Sigma-Aldrich	Cat #P4932
Potassium bicarbonate	Sigma-Aldrich	Cat #60339
QuantiLuc	Invivogen	Cat #rep-qlc
R848	Invivogen	Cat #tlrl-r848
Recombinant Human Ribonuclease, Pancreatic/RNASE1	Bon Opus Biosciences	Cat #CA30-10UG
RLT buffer	Qiagen	Cat #79216
RNA loading dye	New England Biolabs	Cat #B0363
RNase Inhibitor, Murine	New England Biolabs	Cat #M0314
RPMI 1640 glutaMax	New England Biolabs	Cat #M0314
Sodium acetate	Sigma-Aldrich	Cat #S2889
Sodium pyruvate	Gibco	Cat #11360070
SYBR. Gold Nucleic Acid Gel Stain	Invitrogen	Cat #S11494
Trizol	Invitrogen	Cat #15596026
Trypsin-EDTA 0.05%	Gibco	Cat #25300062
Turbo DNase I	Invitrogen	Cat #AM2238
UltraPure TBE Buffer, 10X	Invitrogen	Cat #15581044
Zeocine	Invivogen	Cat #ant-zn
β-mercaptoethanol	Sigma-Aldrich	Cat #M3148
Critical commercial assays		
NEBNext rRNA Depletion Kit	New England Biolabs	Cat #E7850
Bio-Glo-NL Luciferase Assay System	Promega	Cat #J3081
Compensation Beads	Biolegend	Cat #424602
HiScribe T7 High Yield RNA Synthesis Kit	New England Biolabs	Cat #E2040
M-MLV reverse transcriptase	Thermo Fischer	Cat #28025013
Monarch RNA Cleanup Kit	New England Biolabs	Cat #T2040
NEBNext rRNA Depletion Kit	New England Biolabs	Cat #E7850
PureLink quick gel extraction kit	Invitrogen	Cat #K210012
Retic Lysate IVT Kit	Thermo Fischer	Cat #AM1200
TNF-α mouse ELISA Kit	Biolegend	Cat #430904
RNaseAlert Lab Test Kit	Thermo Fischer	Cat #AM1964
Deposited data		
Raw and processed bulk RNA-seq data	This paper	SRA: SRP512141
Raw and processed bulk RNA-seq data	Zhang et al.[68]	GEO: GSE130011
Raw and processed bulk RNA-seq data	Hartveit and Thunold[69]	GEO: GSE125817
Raw and processed bulk RNA-seq data	Galaxy Community[70]	GEO: GSE103958
Experimental models: Cell lines		
MCF-7	ATCC	Cat#HTB-22
U2-OS	ATCC	Cat#HTB-96
THP-1	ATCC	Cat#TIB-202
JAWSII	ATCC	Cat#CRL-3612
RAW 264.7	ATCC	Cat#TIB-71
THP-1 Dual wild type	Invivogen	Cat#thpd-nfis

(*Continued on next page*)

Continued		
REAGENT or RESOURCE	SOURCE	IDENTIFIER
THP-1 Dual Mavs knockout	Invivogen	Cat#thpd-komavs
Experimental models: Organisms/strains		
E. coli 5-alpha Competent cells	New England Biolabs	Cat #C2987H
Oligonucleotides		
RNA sequence Ec12: 5′-GrArCrGrGrArArArGrArCrC-3′	This paper	N/A
RNA sequence Ec12s6G: 5′-GrArCrGrGrGrArArGrArCrC-3′	This paper	N/A
RNA sequence Ec12 conjugated toTye665: 5’-/Tye665/-GrArCrGrGrArArArGrArCrC-3′	This paper	N/A
Ec12 ssDNA forward sequence conjugated to Cy5: 5’-/Cy5/-GACGGAAAGACC-3′	This paper	N/A
Ec12 ssDNA reverse sequence: 5′-GGTCTTTCCGTC-3′	This paper	N/A
DsiRNA negative control siRNA	IDT	Cat# 51-01-14-04
DsiRNA 1 against TLR13: 5′-GrCrCrCrCrArArCrUrUrArArArArGrCrUrU-3′ 5′-CrArGrArUrUrCrArArGrCrUrUrUrArArG-3′	IDT	Cat#mm.Ri.Tlr13.13.1
DsiRNA 2 against TLR13: 5′-CrUrUrGrArArGrGrUrCrArUrUrArArUrCrA-3′ 5′-ArUrGrArCrUrUrUrGrArUrUrArArUrGrArC-3′	IDT	Cat#mm.Ri.Tlr13.13.2
Poly(I:C) (HMW) Fluorescein	Invivogen	Cat#tlrl-picf
Poly(I:C) HMW	Invivogen	Cat#tlrl-pic
DNA primer sequences for qPCR	This paper	See Table S1
DNA primer sequences for IVT template amplification	This paper	See Table S2
Recombinant DNA		
pEGFP-N2 plasmid	Clontech TaKaRa	N/A
pUAS-NanoLuc plasmid	Zhang et al.[68]	Addgene Cat #87696
Software and algorithms		
FlowJo v10.8.1	LLC	https://www.flowjo.com
SnapGene	N/A	https://www.snapgene.com/
Prism 9	Graphpad	https://www.graphpad.com
ImageJ	Galaxy Community[70]	https://imagej.net/ij/
Galaxyproject	Schneider et al.[71]	https://usegalaxy.eu/
Qualimap	Okonechnikov et al.[61]	N/A
FastQC	N/A	http://www.bioinformatics.babraham.ac.uk/projects/fastqc/
RNA Star	Dobin et al.[60]	N/A
FeatureCounts	Liao et al.[62]	N/A
DESeq2	Love et al.[63]	N/A
Pheatmap	N/A	https://cran.r-project.org/web/packages/pheatmap/pheatmap.pdf
Ggpubr	N/A	https://cran.r-project.org/package=ggpubr
Enhanced volcano plots	N/A	https://bioconductor.org/packages/release/bioc/vignettes/EnhancedVolcano/inst/doc/EnhancedVolcano.html
ShinyGO v0.77	Ge et al.[64]	http://bioinformatics.sdstate.edu/go77/
PhotoScapeX	N/A	http://x.photoscape.org/

(*Continued on next page*)

CellPress
OPEN ACCESS

Continued

REAGENT or RESOURCE	SOURCE	IDENTIFIER
Other		
Novex TBE-Urea Gels, 10%	Invitrogen	Cat #EC68755BOX
Novex TBE-Urea Gels, 6%	Invitrogen	Cat #EC6865BOX

EXPERIMENTAL MODEL DETAILS

Animals

Male and female C57BL/6 mice, aged between 8 and 12 weeks, were used (Jackson Lab; Bar Harbor, ME). Mice were bred for up to 20 generations in a pathogen-free environment at the Laboratory Animal Biotechnology Unit of the Pasteur Institute of Montevideo. All experiments were performed under strict adherence to the guidelines set by the National Commission for Animal Experimentation. Experimental procedures were approved by the Ethics Committee on Laboratory Animals of the Pasteur Institute of Montevideo (protocol: 022-22). For primary cell cultures both male and female C57BL/6 mice were used. For *in vivo* experiments, C57BL/6 female mice were used.

Cell lines

U-2 OS and MFC-7 cells were cultured in DMEM supplemented with 10% FBS. Raw264.7 cells were cultured in DMEM (high glucose) supplemented with 10% FBS, 1 mM sodium pyruvate and 100 U/mL penicillin-streptomycin. THP-1 cells were cultured in RPMI with glutaMAX supplemented with 10% FBS, non-essential amino acids, 1 mM sodium pyruvate, 10 mM HEPES and 100 U/mL Penicillin-Streptomycin. THP-1-Dual and THP-1 Dual *MAVS* knockout reporter cell lines (Invivogen, USA) were cultured in RPMI with glutaMAX, supplemented with 10% FBS, 25 mM HEPES, 2mM Glutamine, 100 U/mL Penicillin-Streptomycin and 100 μg/mL Normocin. Selection pressure was maintained with 10 μg/mL Blasticidin and 100 μg/mL Zeocin. THP-1, THP-1-Dual and THP-1 Dual *MAVS* knockout monocytes were differentiated to macrophages by 3 h stimulation with 40 nM Phorbol 12-myristate 13-acetate (PMA), followed by 48–72 h incubation without PMA.

Primary cell culture

Differentiated Bone Marrow Derived Cells, containing dendritic cells, were cultured from bone marrow cell precursors as described in.[59] Briefly, bone marrow cells were collected form 8–12 weeks-old C57Bl/6 mice and differentiated with 0.4 ng/mL GM-CSF for 8 days in RPMI supplemented with 10% heat-inactivated FBS, 2mM glutamine, non-essential amino acids, 1 mM sodium pyruvate, 10 mM HEPES, 0.05 mM *β-mercaptoethano*l and 100 U/mL Penicillin-Streptomycin. At day 8, BMDCs were harvested and used as needed.

METHOD DETAILS

Total E. coli RNA purification and fractionation

Total RNA was extracted from exponentially growing *E. coli* DH5α cells with OD = 0.6. Cells were lysed in RLT buffer supplemented with 20 mM DTT using a bullet blender homogenizer (Next Advance). The homogenate was precipitated with 2.5 volumes of 100% acetone. The resulting pellet was resuspended in TRIzol, and total RNA was purified from the aqueous phase using a Monarch RNA cleanup kit. To isolate large (>200 nt) and small (<200 nt) RNAs, total RNA was sequentially bound to Monarch spin columns using binding buffer with 33% ethanol (allows binding of only >200 bp RNAs) and 66% ethanol (binds all RNAs). Additionally, 23S, 16S and 5S ribosomal RNAs were selectively removed with a NEBNext rRNA Depletion Kit for bacteria. When required, total *E. coli* RNA was degraded with recombinant human RNase 1.

RNA-seq and bioinformatic analysis

BMDCs (300,000 cells per well) cultured in growth medium with 10% FBS and supplemented with 10 μg/mL Polymyxin B were stimulated with 100 ng/mL naked total RNA from *E. coli* or naked total self-RNA from BMDCs (isolated from cultures at day 8), in the presence of either 80 U/mL RI or heat-inactivated RI (RIΔ) for 6 h. Afterward, cells were lyzed with TRIzol and RNA present in the aqueous phase after addition of chloroform was purified with a Monarch RNA cleanup kit. RNA integrity was confirmed by electrophoresis in 10% TBE-urea polyacrylamide gels. RNA was precipitated with 0.1 volumes of 3M sodium acetate pH = 3.2 and 2 volumes of 100% ethanol and shipped to Macrogen (Korea) for paired-end mRNA sequencing (TruSeq Stranded mRNA, Illumina). Then, FastQ files containing paired-end sequencing information were mapped to the mouse genome (GRCm39) using STAR[60] (default settings). Mapping quality was assessed with QualiMap[61] (default settings). Expression of mRNAs across samples was analyzed with FeatureCounts[62] (default settings and paired-end reads counted as a single fragment) using Ensembl mouse annotation (Release v109). Differential expression across samples was computed with DESeq2[63] (default settings). Heatmaps showing topmost differentially expressed genes were calculated using rlog-transformed counts and the pheatmap R package and row-scaled. Volcano plots and MA-plots were constructed using EnhancedVolcano and ggpubr R packages, respectively. Differentially expressed genes between conditions of naked *E. coli* RNA with RI and naked *E. coli* RNA with inactivated RI having fold change >2, adjusted *p*p-value < $1x10^{-5}$ and base mean >16 were used for pathway enrichment analysis using ShinyGO (v0.77).[64] To determine expression differences between RNA sensors, fragments per kilobase per million (FPKM) were calculated for *Tlr3*, *Tlr7, Tlr8, Tlr13, Rig-I, Mda-5.* Raw sequencing data can be accessed at NCBI under BioProject: PRJNA1120732; SRA: SRP512141.

Bioinformatic analysis of publicly available datasets

Publicly available transcriptomic datasets of THP-1 cells differentiated to THP-1 macrophages with PMA (GEO: GSE130011),[65] human monocyte-derived dendritic cells stimulated with different TLR agonists (GEO: GSE125817)[66] and Raw264.7 macrophages (GEO: GSE103958)[67] were downloaded from the NCBI SRA repository and subjected to a similar bioinformatic pipeline as previously described.

Cell stimulation

BMDCs seeded in 24 well plates (300,000 cells/well) cultured with growth medium containing 10% FBS were stimulated for either 6 or 24 h with the following RNAs at the indicated dose: total *E coli* RNA, rRNA-depleted *E coli* RNA, size-fractionated *E. coli* RNA, synthetic RNAs Ec12 and Ec12s6G (sequences provided in the key resources table) and high molecular weight poly(I:C), together with 80 U/mL RI, thermally inactivated RI (RIΔ), or without RI. RPMI or Dulbecco's phosphate-buffered saline (DPBS) were used as negative controls and 100 ng/mL R848 was used as a positive control. Whenever bacterial RNA was used, cells were cultured with 10 μg/mL Polymyxin B to quench any endotoxins remaining after RNA purification. After 6 h, the expression of *Il1b*, *Il1a*, *Il6, Cxcl10, Ifit2,* and *Oas3* was analyzed by RT-qPCR (See primers in Table S1). Secreted TNF-α was quantified in cell-conditioned medium by ELISA. After 24 h, cell surface expression of CD40 and CD86 was analyzed by flow cytometry. To study involvement of dynamin-dependent endocytosis on internalization and responses of naked inflammatory RNAs, BMDCs were stimulated for 6 h with 1 μg/mL naked total RNA with or without 80 U/mL RI in the presence of 80μM Dynasore or vehicle (DMSO). Dynasore was preincubated for 1 h before the addition of the stimuli. In other experiments, BMDCs were stimulated with 0.5 μg/mL naked fluorescein-labeled poly(I:C) or Dextran-AF647 in the presence or absence of 120 U/mL RI for 1 h, and analyzed by confocal microscopy and flow cytometry.

Raw264.7 cells, seeded in 24 well adherent plates (at 200.000–300.000 cells/well) and cultured in 10% FBS-containing medium, were stimulated for 6 h with naked total *E. coli* RNA at 1 or 2 μg/mL, naked poly(I:C) at 10 μg/mL or R848 at 1 μg/mL. When indicated, 80 U/mL RI was added. M0549, a TLR7/8 selective inhibitor, was used at 1 μM and preincubated for 3 h before stimuli. A MyD88 inhibitory peptide was used at 1 or 10 μM and preincubated for 4 h before stimuli.

THP-1 cells, seeded in 24 well adherent plates (250.000–350.000 cell/well) and cultured in 10% FBS-containing medium, were differentiated to THP-1 macrophages with 100 nM PMA for 48 h. THP-1 monocytes or THP-1 macrophages were stimulated for 22 h with naked *E. coli* RNA at 1 μg/mL, naked poly(I:C) at 10 μg/mL, or R848 at 1 μg/mL. RI was added at 80 U/mL. In other experiments, THP-1 cells, cultured in 10% FBS, were seeded in 96 well plates (100.000 cells/well) and stimulated with 0.5 μg/mL naked fluorescein-labeled poly(I:C) or Dextran-AF647 in the presence or absence of 160 U/mL RI for 180 min and analyzed by flow cytometry.

THP-1 dual wild type and *Mavs* knockout cells (Invivogen) seeded in 96 well adherent plates and cultured with growth medium containing 10% FBS were differentiated to macrophages with PMA. Then THP-1 derived macrophages were stimulated for 24 h with 5 μg/mL naked poly(I:C), with or without 80U/mL RI. RPMI and 200 ng/mL LPS were used as negative and positive controls, respectively. After 24 h, luciferase activity in the medium was detected following manufacturer's instructions using a LUMIstar Optima luminometer.

RT-qPCR

BMDC RNA was extracted with TRIzol following manufacturer's instructions and quantified spectrophotometrically. cDNA was synthesized from 300 to 1000 ng total RNA using M-MLV reverse transcriptase (Thermo). Briefly, total RNA was treated with 2 units of DNase I for 20 min at 25°C to eliminate genomic DNA, in a reaction volume of 10 μL. DNase I was inactivated by addition of EDTA at a final concentration of 4.5 mM and heating at 75°C for 10 min. Then, RNA was reverse-transcribed in a 20-μL reaction volume using oligo$(dT)_{18}$ primers, following manufacturer's instructions and employing a two-step PCR program: 52 min at 37°C, followed by 15 min at 70°C. Then, cDNA was diluted 1/5 and stored at −20°C until use. Gene expression was quantified by qPCR in a QuantStudio 3 Real-Time PCR System (Applied Biosystems) employing a FastStart Universal SYBR Green Master Mix. Briefly, a 10-μL reaction was carried out using 2 μL of cDNA, a primer mix at 0.3 μM final concentration, and 5 μL of an SYBR Green Master Mix. The qPCR program was: 2 min at 50°C, followed by 10 min at 95°C, followed by 40 cycles of 15 s at 95°C and 1 min annealing/extension at 60°C–65°C, and a final melt curve stage. Comparative gene expression analysis was calculated using the $2^{-\Delta\Delta CT}$ method. Data was normalized against mock treatment (RPMI or DPBS) and *actb* was used as a housekeeping, reference gene.

Tlr13 knockdown in Raw264.7

Tlr13 knockdown was carried out in Raw264.7 cells with DsiRNAs (IDT) and RNAiMAX as transfecting agent. 80.000 cells seeded in 24 well adherent plates were cultured in complete growth medium for 24 h. Afterward, fresh growth medium (450 μL; without antibiotics) containing 50 μL of preformed DsiRNA-lipid complexes was added to each well. Cells were incubated for 24 h with DsiRNA-lipid complexes containing either control DsiRNA or an equimolar mixture of two DsiRNAs targeting TLR13. Afterward, the medium was replaced for 1,000 μL of fresh growth medium containing antibiotics and cells were cultured for additional 24 h. To assess *Tlr13* silencing, cells were lyzed with TRIzol and *Tlr13* was measured by RT-qPCR. To assess the functional involvement of TLR13 in the recognition of naked exRNAs, cells were stimulated with naked *E. coli* RNA for 6 h in the presence of 80 U/ml RI and 20 μg/mL Polymyxin B. The levels of *Il6* were measured by RT-qPCR. DsiRNA-lipid complexes were made using lipofectamine RNAiMAX according to manufacturer's instructions. Briefly, a ratio of 2.5 μL of DsiRNA at 10 μM, 0.8 μL RNAiMAX, and 50 μL Opti-MEM (Thermo), was used for each well. DsiRNAs were used at a final concertation of 50 nM. Using a fluorescent DsiRNA-tye563, we confirmed transfection efficiencies of 80%, and minimal cell death.

In vitro transcription

mRNAs coding for *nanoLuc* or *eGFP* were synthesized by *in vitro* transcription: nanoLuc and eGFP coding sequences were amplified by PCR from the pUAS-NanoLuc[68] and pEGFP-N2 plasmids, using primers shown in Table S2. Forward and reverse primers were designed to incorporate a T7 RNA polymerase sequence and a Kosak sequence, and a 30–31 nt polyA tail, respectively. PCR reactions were carried out with Phusion Polymerase. The amplification program was: 30 s at 98°C, followed by 30–35 amplification cycles, each comprising 10 s at 98°C, 10 s at 60°C, and 30 s at 72°C. A final extension step of 10 min at 72°C was included. PCR products were analyzed by 1% agarose gel electrophoresis and purified with PureLink quick gel extraction kit directly from the PCR solution (for *nanoLuc*) or from excised gel bands (for *eGFP*). DNA was concentrated by overnight ethanol precipitation and used as template for mRNA synthesis. *nanoLuc* and *eGFP* mRNAs were synthesized and co-transcriptionally capped using HiScribe T7 High Yield RNA Synthesis Kit. Briefly, reactions were performed in a 20-μL reaction volume at 37°C for 2 h using 1 μg of template and a 3′-*O*-Me-m7G (5′)ppp(5')G RNA Cap Structure Analog, with 4:1 CAP:GTP ratio, and following manufacturer's instructions. For *eGFP*, UTP was substituted with N1-Methylpseudouridine-5′-Triphosphate. Afterward, DNA templates were digested with Turbo DNase I. In vitro-synthesized mRNAs were purified with a Monarch RNA Cleanup Kit and stored at −80°C until use.

In vitro translation

NanoLuc mRNA was translated *in vitro* with Retic Lysate IVT Kit following manufacturer's instructions. Briefly, 100 ng of *NanoLuc* mRNA was incubated for 45 min at 30°C with a rabbit reticulocyte extract. Afterward, nanoLuc bioluminescence was measured using a Bio-Glo-NL Luciferase Assay System and detected in a LUMIstar Optima luminometer.

RNase activity in mouse serum and peritoneal wash

Blood from three female mice was collected from the submandibular vein and allowed to clot for 45 min at room temperature. Serum was obtained by centrifuging the blood for 15 min at 4°C. A cell-free peritoneal wash was collected from the same mice. To that end, 3.3 mL DPBS was introduced into the peritoneal cavity, collecting 2.5 mL of peritoneal wash fluid. To remove peritoneal cells and debris, the peritoneal wash was centrifuged four times: 5 min at 300 g, 6 min at 450 g, 6 min at 500 g, and 10 min at 2,000 g. RNase activity in both serum and peritoneal wash was measured using a continuous fluorometric assay with the RNaseAlert Lab Test kit (Thermo). Briefly, 5 μL serum (diluted 1/100 in DPBS) and 5 μL of an identical effective dilution of peritoneal wash (1/3 in DPBS; assuming a peritoneal volume of 100 μL[69] that was previously diluted to 3.4 mL with DPBS) were assayed, following the manufacturer's instructions. Fluorescence was measured using a Varioskan fluorimeter for over 35 min, with excitation at 490 nm and emission at 520 nm. RNase activity was determined based on the initial reaction velocities and expressed as a percentage relative to the sample with the highest RNase activity.

nanoLuc mRNA internalization and translation assays

Naked nanoLuc mRNA capture and translation was assessed in murine primary cells (BMDCs) and two human epithelial cell lines (U-2 OS and MCF-7). To quantify *nanoLuc* mRNA levels and nanoLuc protein in BMDCs (Figures 4B and 4C), cells were seeded in 24 (250.000 cells/well) or 48 (120,000 cells/well) well plates and cultured for 2 h to allow adhesion. Then, growth medium containing FBS was removed, cells were washed, incubated in growth medium without FBS and stimulated for 2 h with 1 μg/mL naked *nanoLuc* mRNA with 80 U/mL RI, thermally inactivatedRI, or without RI. To investigate the impact of varying concentrations of FBS and RI on *nanoLuc* translation by BMDCs (Figure 4D), cells were seeded in 48 well plates (120,000 cells/well) and cultured for 2 h to allow adhesion. Then, growth medium containing FBS was removed, cells were washed, incubated in growth medium containing varying concentration of FBS (0, 0.1, 1, 10%) and RI (0, 80, 120, 240, 320 U/mL) and stimulated with 1 μg/mL naked *nanoLuc* mRNA for 2 h. Subsequently, the medium containing the stimuli was removed and fresh growth medium with 10% FBS was added. After 6 h, *nanoLuc* mRNA was quantified by RT-qPCR. The RT-qPCR protocol was specifically designed to enable detection of full-length, undegraded *nanoLuc* mRNA. This was achieved by designing primers that selectively amplified the transcript 5′ end, which had been previously reverse-transcribed using oligo(dT) primers. After 24 h, nanoLuc protein translation in BMDCs was detected with Bio-Glo-NL Luciferase Assay System using a LUMIstar Optima luminometer. MCF-7 and U-2 OS cells were seeded in 48 well adherent plates. After reaching 80% confluence, growth medium was replaced with growth medium containing 0.1% FBS. Then, cells were incubated with varying concentration of *nanoLuc* mRNA (0, 0.25, 1, 4μg/mL), with either 80 U/mL RI or thermally inactivated RI for 2 h. To assess the involvement of dynamin-dependent endocytosis in naked *nanoLuc* mRNA capture, U-2 OS cells were incubated for 2 h with

86

80 μM Dynasore or DMSO, before addition of 1 μg/mL *nanoLuc* mRNA, with or without 80 U/mL RI. After 2 h, media was replaced with growth medium containing 10% FBS. Cells were cultured for additional 24 h, and nanoLuc protein levels were measured as previously described.

Naked eGFP internalization and translation assays

U-2 OS cells were seeded onto 35-mm glass bottom dishes (100,000 cells) and incubated overnight with growth medium. The next day, cells were washed 3 times with MEGM (Lonza), and MEGM either without or with 0.1% FBS was added. Cells were incubated for 2 h with 5 μg/mL naked eGFP mRNA in the presence or absence of 80 U/mL RI, or with a DOTAP-eGFP mRNA complex. After the incubation, cells were washed 3 times and cultured for an additional 24 h in complete growth medium, containing 10% FBS. To visualize and analyze eGFP translation, cells were imaged using a Zeiss LSM 880 confocal microscope. Nuclei were stained with NucRed (Thermo). Imaging was performed utilizing a 63× oil immersion objective with a numerical aperture of 1.4, employing a Plan Apochromat configuration. The imaging acquisition parameters were set with a pixel dwell time of 4.10 μs and size of 0.55 microns, utilizing bidirectional scanning. The total scanning duration for each acquisition was 1 min and 20 s, with an image size of 655.8 x 655.8 microns. Images were subsequently processed and analyzed using ImageJ. The segmentation was conducted on both the green (eGFP) and red (nuclei) fluorescence channels. Quantitative analysis of the cellular responses was executed through Integrated Density calculations. Prior to calculations, a noise subtraction step was implemented to ensure data integrity. The resultant processed images were subjected to total image calculations, facilitating the extraction of Integrated Density values indicative of cellular responses. The image in the GFP channel (488 nm) was processed by setting the minimum value at 3 and the maximum value at 8. Then, a Gaussian blur filter of value 2 was applied. The same was done for data visualization and figure creation. Images were cropped to aid visualization.

In vivo experiments

For intraperitoneal administration of RNAs, female mice were *i.p* inoculated with 250 μL of varying doses (0.025–62.5 μg) of naked total *E. coli* RNA with or without 40, 200 or 400 units of RI in DPBS. DPBS and 62.5 μg LPS were used as positive and negative controls, respectively. After 24 h, animals were euthanized and 4–5 mL of DPBS supplemented with 3 mM EDTA was injected into the peritoneal cavity to extract peritoneal cells. Peritoneal cells were pelleted at 375 g for 5 min at 4°C, resuspended in FACS buffer (0.5% w/v BSA, 2 mM EDTA in DPBS), counted, and stained for flow cytometry analysis. For systemic administration of RNAs, female mice were retro-orbitally inoculated with 100 μL of either high molecular weight naked poly(I:C) (200 ng or 1000 ng) or naked total *E. coli* RNA 10 μg in the presence or absence of 480 units of RI in DPBS. DPBS with or without RI was used as control. After 6 h, mice were euthanized, and spleens were collected. To obtain spleen cells, spleens were incubated in 1mL of collagenase solution (2 mg/mL Collagenase D, 2% v/v FBS in RPMI), cut on ice with a bistoury and incubated for 20 min at 37°C. The reaction was stopped with 100 μL of 100 mM EDTA. Spleen cells were passed through a 100 μm filter and resuspended in 40 mL of PES buffer (0.7 mM EDTA, 2% v/v FBS in DPBS). Cells were pelleted at 1500 rpm for 15 min at 4°C, resuspended in 5 mL RBCL buffer (154 mM NH_4Cl, 10 mM $KHCO_3$, 0.1 mM EDTA; pH = 7.2–7.4), and incubated for 10 min at room temperature to lyse red blood cells. Then, spleen cells were washed two times with PES solution, resuspended in FACS buffer, counted, and stained for flow cytometry analysis.

Flow cytometry

Cells suspended in FACs buffer were seeded in V-shaped 96 well plates (200,000–500,000 cells/well). When live/dead viability dye was used, cells were stained with 200 μL of 1/200 live/dead violet in FACS buffer and incubated on ice for 30 min in the dark. If viability was assessed with DAPI, the previous step was not performed. Then, cells were pelleted at 2200 rpm for 2 min and blocked with 25 μL of 10% normal rat serum in FACS buffer for 30 min on ice. For cell surface antibody staining, 25 μL of 2x antibody mix (see Table S3) in FACS buffer was added, and cells were stained for 30 min on ice in the dark. Stained cells were washed 2 times with FACS buffer, resuspended in 200 μL FACS buffer, and analyzed by flow cytometry. To assess viability, 0.5 μg/mL final concentration of DAPI was added immediately before sample analysis. Myeloid and lymphoid spleen cells were analyzed in a Cytek Aurora spectral flow cytometer. Peritoneal immune cells were analyzed in an Attune NxT flow cytometer or in a Cytek Aurora spectral flow cytometer. BMDCs cells were analyzed in a BD Accuri C6 flow cytometer or in a Cytek Aurora spectral flow cytometer.

RNA polyacrylamide electrophoresis

RNAs were analyzed by polyacrylamide gel electrophoresis under denaturing conditions using 6–10% acrylamide TBE-urea gels. Briefly, RNA samples were mixed with 2x RNA loading dye, heated at 65°C for 5 min, cooled on ice and analyzed on an XCell *SureLoc* Mini-Cell Electrophoresis system (Invitrogen) using 0.5x TBE as running buffer. Gels were run at constant voltage (160V) for 60–80 min. Gels were stained for 15 min with 1/10000 SYBR Gold in 0.5x TBE and imaged with a transilluminator (Loccus biotecnologia) with a coupled imaging platform (Carestream). When needed, images were cut and contrasted using PhotoScapeX.

QUANTIFICATION AND STATISTICAL ANALYSIS

Statistical analysis was performed using R or GraphPad Prism 9. For RNA-seq experiments, 3 biological replicates for all 4 experimental conditions were performed. Significant differences in gene expression across samples was computed with DESeq2 and multiple hypothesis testing was controlled for using the Benjamini-Hochberg method to estimate false discovery rates (FDR). Differentially expressed genes with adjusted *p*p-values lower than 0.001 were reported. For *in vitro* experiments, each dot in bar plots represents a biological replicate. For *in vivo* experiments, each dot in bar plots represents a different mouse. Bar plots correspond to mean, error bars to standard deviation. For microscopy experiments, each dot in violin plots represents an individual cell. When statistical analysis was performed, normal distribution of data was assessed using Shapiro-Wilk and Kolmogorov-Smirnov tests. For statistical comparisons between two conditions, unpaired two-tailed t-test was used when the data followed a normal distribution, and unpaired two-tailed Mann-Whitney test was applied when the data did not follow a normal distribution. For multiple comparisons, if data was normally distributed and had variance homogeneity, one-way ANOVA was used. If data was normally distributed but had no variance homogeneity, Welch ANOVA test was used. If data had no normal distribution, Kruskal-Wallis test was used. Mouse serum and peritoneal wash RNase activity was compared using a paired two-tailed t test. Statistically significant differences are indicated with asterisks (*, p-value < 0.05, **: p-value < 0.01, ***: p-value < 0.001, ****: p-value < 0.0001).

Cell Genomics, Volume *5*

Supplemental information

Ribonuclease activity undermines immune sensing of naked extracellular RNA

Mauricio Castellano, Valentina Blanco, Marco Li Calzi, Bruno Costa, Kenneth Witwer, Marcelo Hill, Alfonso Cayota, Mercedes Segovia, and Juan Pablo Tosar

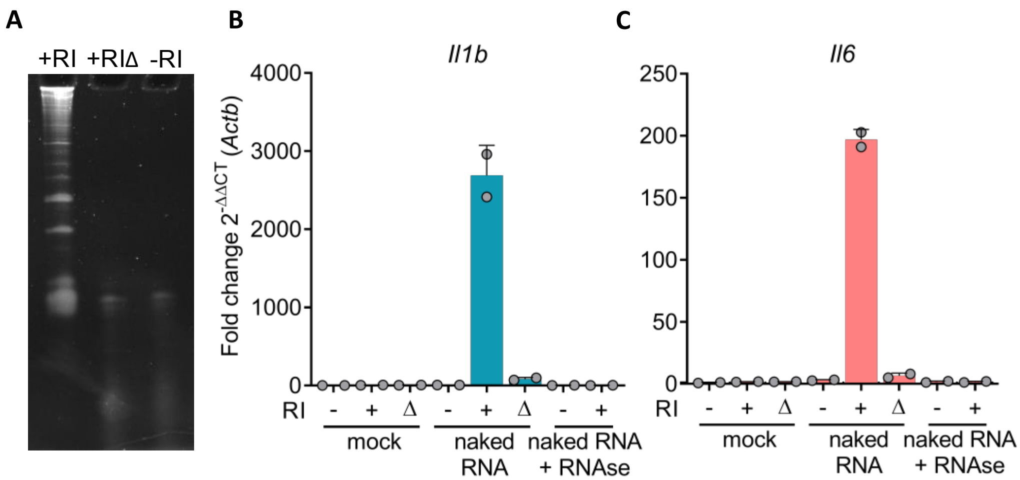

Figure S1. Naked exRNA recognition is completely dependent on RI enzymatic activity, related to Figure 1. A) Denaturing PAGE of U-2 OS total RNA incubated in 10% fetal bovine serum together with 400 U / mL RI (+RI), heat inactivated RI (+RIΔ), or without RI (-RI), for 45 minutes. B,C) *Il1b* (B) and *il6* (C) expression by RT-qPCR in BMDCs stimulated for 6 hs with 1 µg / mL naked total RNA from *E. coli* with 80 U / mL RI (+RI), heat-inactivated RI (+RIΔ), or without RI (-). RNAse1-treated *E. coli* RNA with (+RI) or without RI (-) were used as controls, as well as DPBS (mock).

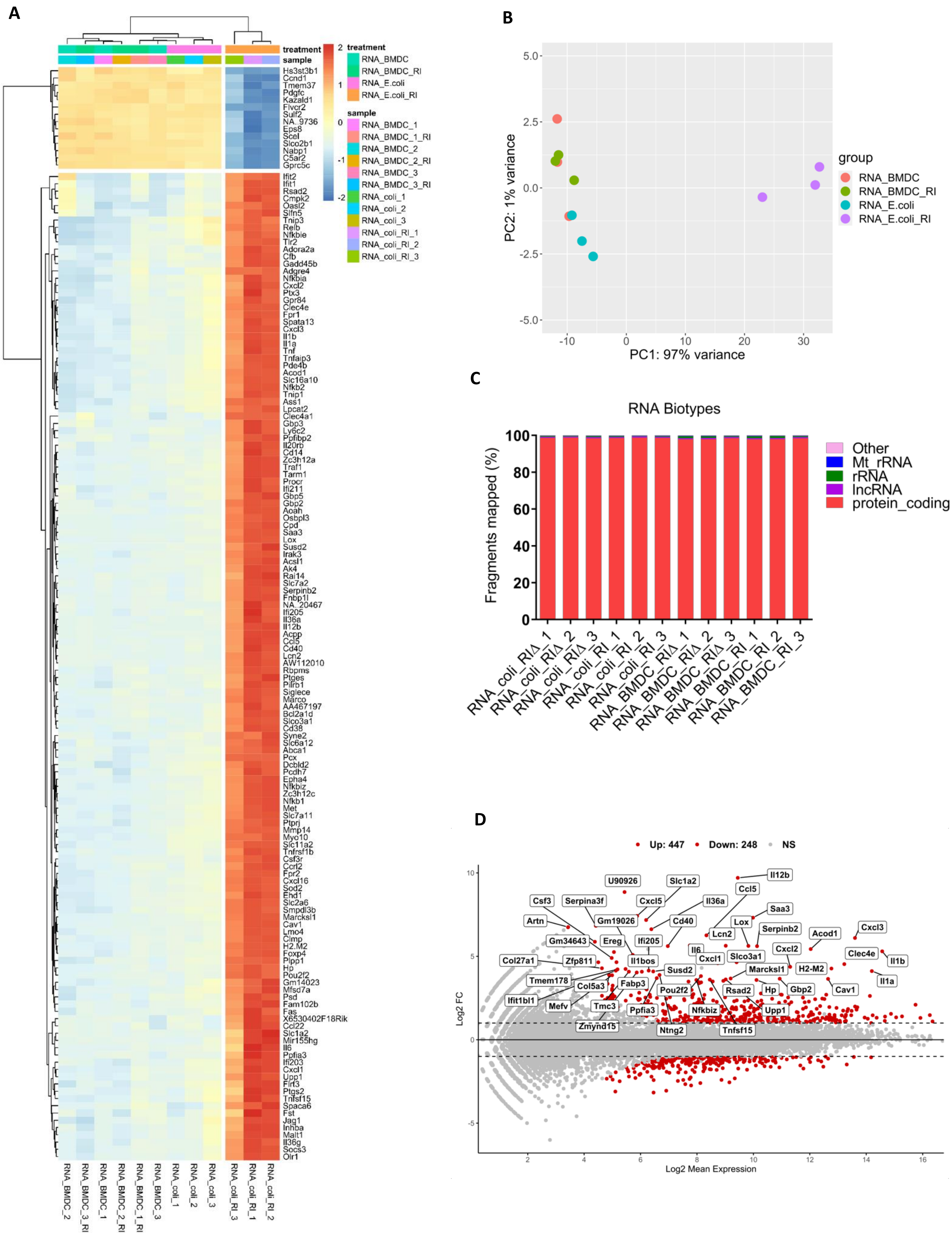

Figure S2. Additional results corresponding to the BMDC RNA-seq experiment, related to Figure 1. A) Heatmap showing top 150 most differentially regulated genes in BMDCs stimulated for 6hs with 100 ng / ml naked total RNA from *E. coli* or 100 ng / mL total RNA from BMDCs in the presence of 80 U / mL RI (+RI) or thermally inactivated RI (+RIΔ). B) PCA plots corresponding to all experimental conditions. C) Abundance of RNA biotypes across samples. D) MA-plot of BMDCs stimulated with 100 ng / mL naked total RNA (RIΔ vs. RI).

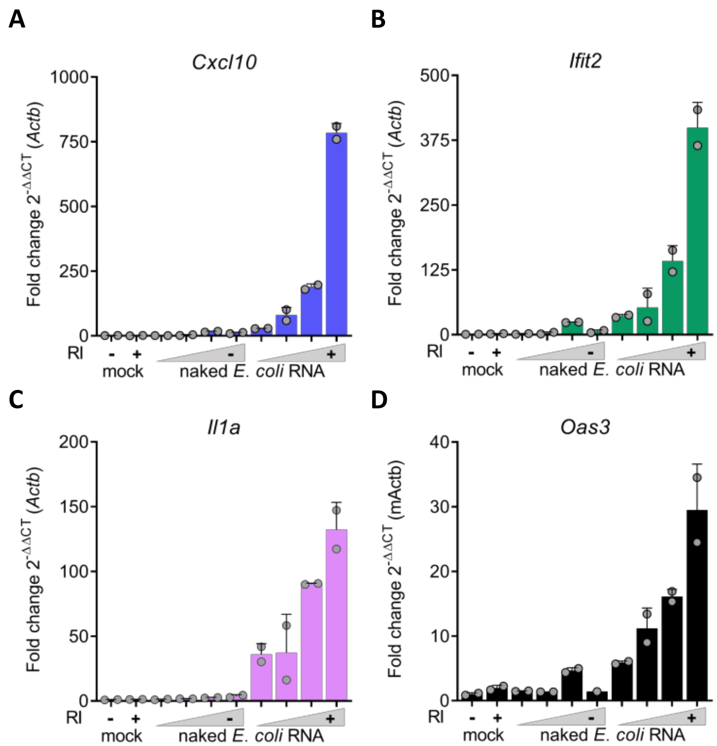

Figure S3. Induction of several pro-inflammatory cytokines and chemokines in BMDCs, related to Figure 1. Expression (RT-qPCR) of *Cxcl10* (A) *ifit2* (B) *Il1a* (C) *and Oas3* (D) in BMDCs stimulated for 6 h with varying doses (1; 5; 10; 25 µg / mL) of naked total RNA with or without 80 U / mL RI. DPBS was used as negative control.

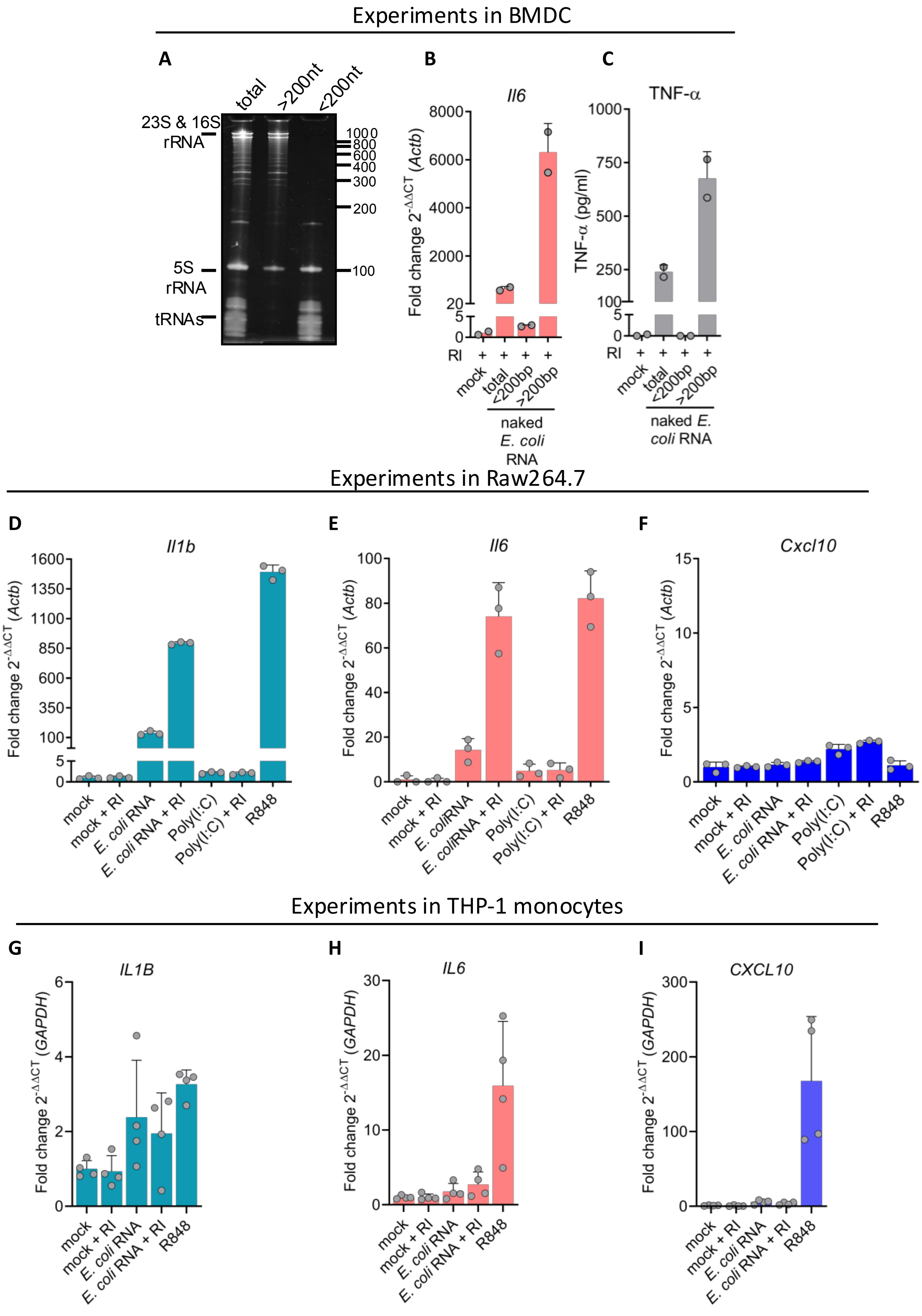

Figure S4. Response of BMDCs, Raw264.7 and THP-1 cells to different naked exRNAs, related to Figures 2 and 3. A) Denaturing PAGE of *E. coli* total RNA (total) or fractioned into "small RNAs" of less than 200 nt (< 200nt) or "large RNAs" of more than 200 nt (> 200nt). B,C) *Il6* expression (RT-qPCR) and levels of secreted TNF-α (ELISA) of BMDCs stimulated with 1 μg / mL of naked total *E. coli* RNA, "small RNAs" or "large RNAs", all in the presence of RI. Mock: DPBS. D,E,F) *Il1b* (D)*, Il6* (E) and *Cxcl10* (F) expression (RT-qPCR) in Raw264.7 stimulated for 6 h with 2 μg / mL naked *E. coli* RNA, 10 μg / mL naked Poly(I:C), DMEM as mock and 1 μg / mL R848 as a positive control. When indicated, 80 U / mL RI was added. G,H,I,) *IL1B* (G)*, IL6* (H) and *CXCL10* (I) expression (RT-qPCR) in THP-1 cells stimulated for 18 h with 1 μg / mL naked *E. coli* RNA, RPMI as mock and 1 μg / mL R848 as a positive control. When indicated, 80 U / mL RI was added.

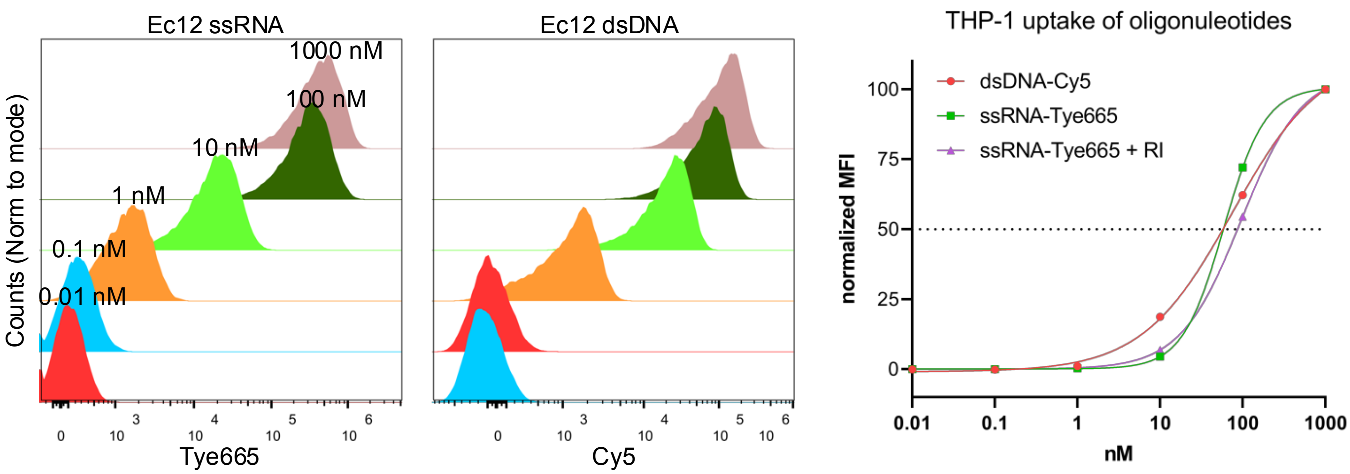

Figure S5. Uptake efficiency of Ec12 with an RNA or DNA backbone, related to Figure 3. A,B) Flow cytometry of THP-1 monocytes stimulated for 3 h with Tye665-labeled naked Ec12 ssRNA or Cy5-labeled naked Ec12 dsDNA at 0.01; 0.1; 1; 10; 100 or 1000 nM. When indicated, 160 U / mL RI was added. The histogram plots display oligonucleotide uptake at each concentration (left and center panels). A curve representing the normalized mean fluorescence intensity (MFI) is plotted against the concentration for each oligonucleotide (right panel). Data was fitted to sigmoidal curves, and the EC50 values were determined.

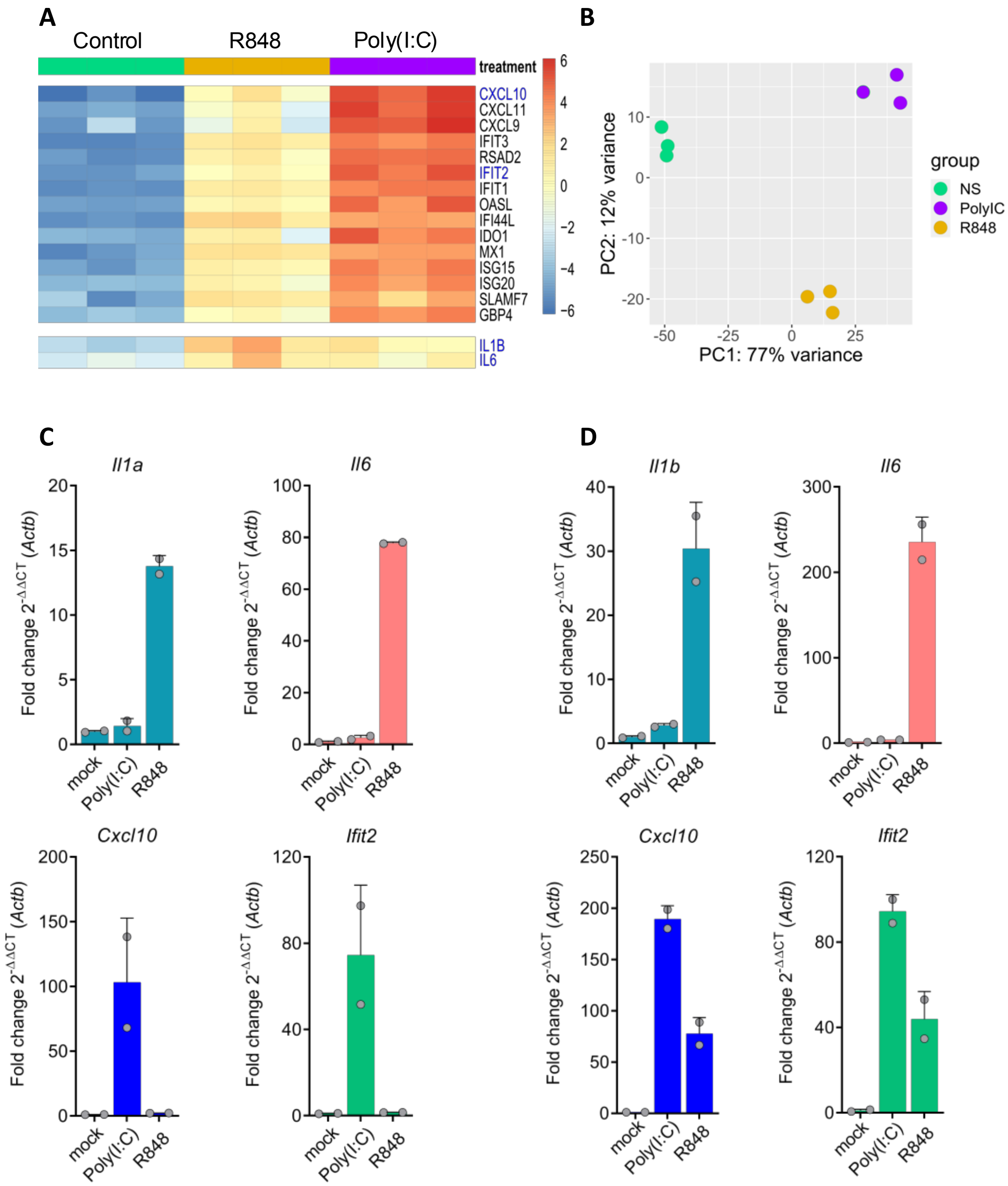

Figure S6. Transcriptional signature of Mo-DCs and JawsII dendritic cell line in response to R848 and poly(I:C), related to Figure 3. A,B) Data mining and differential gene expression analysis of a transcriptomic dataset[S1] (GEO:GSE125817) from monocyte derived dendritic cells stimulated with Poly(I:C) or R848 for 6 h. A, B) Heatmap (A) with the top 15 most upregulated genes (including *Il1b* and *Il6*) and the corresponding PCA (B) plot. C,D) Expression (RT-qPCR) of *Il1b (or Il1a), il6, Cxcl10 and Ifit2* in JawsII dendritic cell line (C) or in BMDCs (D), stimulated for 6 h with 10 µg / mL poly(I:C) or 100 ng / mL R848. DPBS was used as negative control.

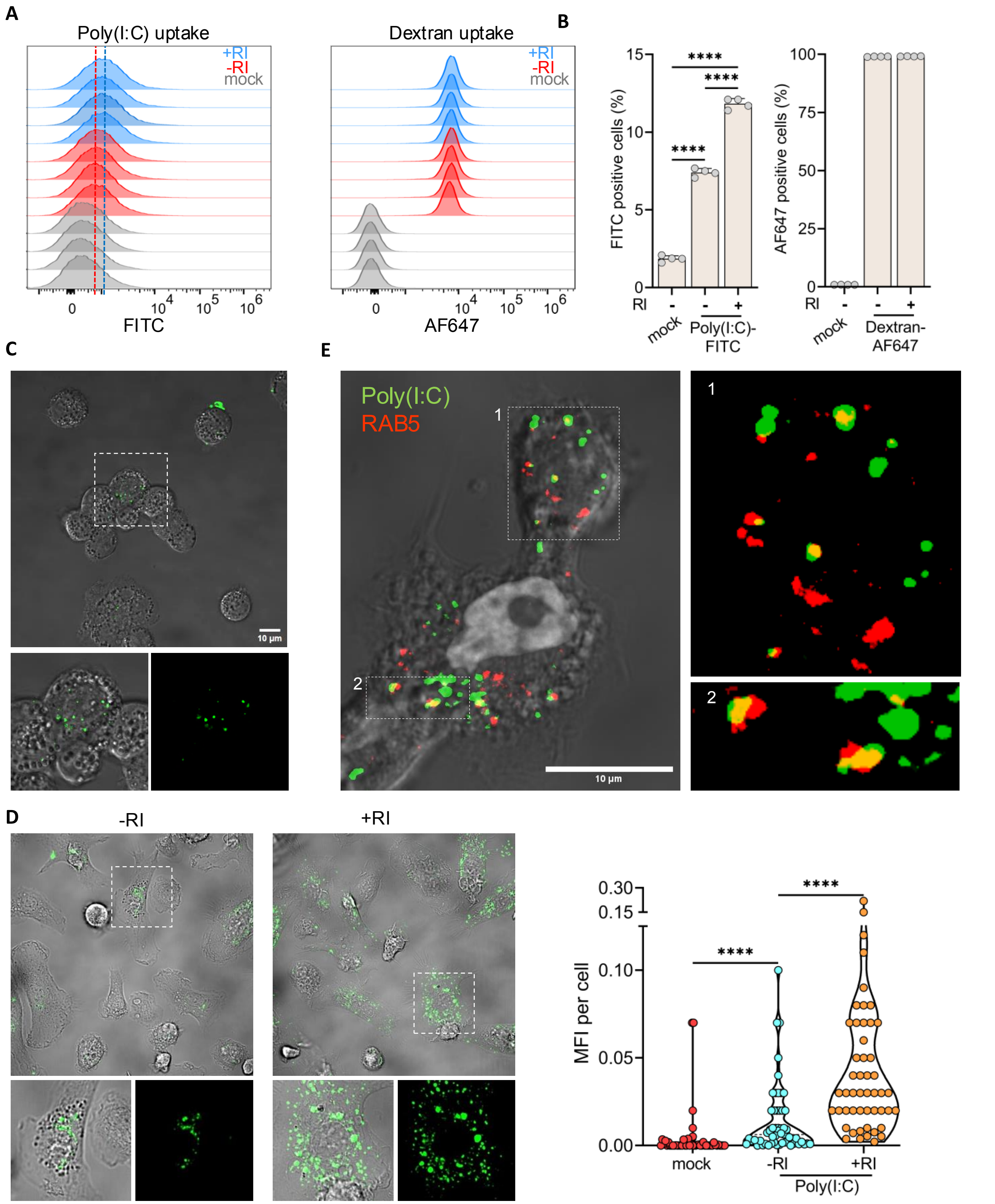

Figure S7. Uptake of labeled dsRNA by THP-1 and BMDCs, related to Figure 3. A,B) Flow cytometry of THP-1 monocytes stimulated for 3 h with naked fluorescein-labeled poly(I:C) at 0.5 µg / mL or AF647-Dextran, with or without 160 U / mL RI. Histograms (A) and bar plots (B) with the percentage of positive cells are shown. C,D) Confocal microscopy of THP-1 monocytes (C) or BMDCs (D) stimulated for 1 h with naked fluorescein-labeled poly(I:C) at 0,5 µg / mL. For BMDCs, experiments were carried out with or without 80 U / mL RI. E) Confocal microscopy of THP-1 macrophages stimulated for 30 min with naked fluorescein-labeled poly(I:C) at 0,5 µg / mL. Nuclei (white), dsRNA (green) and RAB5 (red) are visualized. Colocalization of dsRNA with RAB5 is depicted in yellow in the merged image. **** $p < 0.001$; Kruskal-Wallis with Dunn`s test.

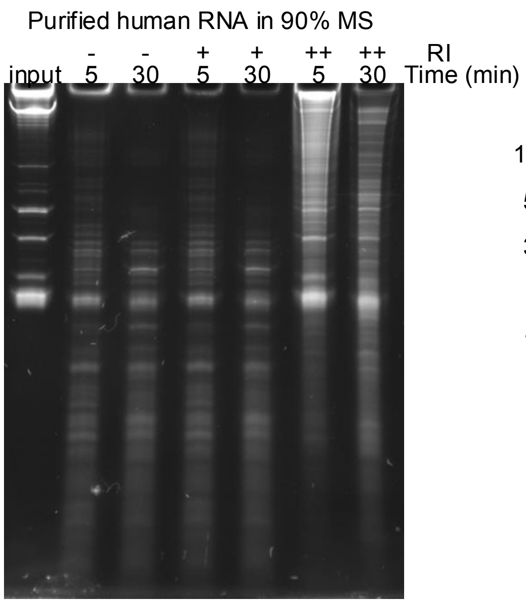

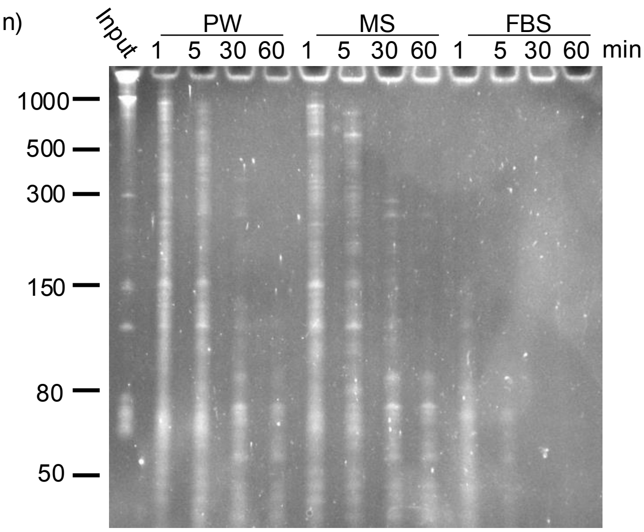

Figure S8. RNA stability in different fluids assessed by PAGE, related to Figure 5 and 6. A) Denaturing PAGE of human total RNA incubated in 90% mouse serum for either 5 or 30 min in the presence of 160 U / mL (++), 40 U / mL (+), or without RI (-). B) RNA stability assays in different biofluids. Denaturing PAGE of U-2 OS RNA incubated ex vivo in peritoneal wash (PW), mouse serum (MS) or fetal bovine serum (FBS). RNA degradation was analyzed after 1, 5, 30 or 60 min. All biofluids were diluted to 3.33 % (v/v) in DPBS.

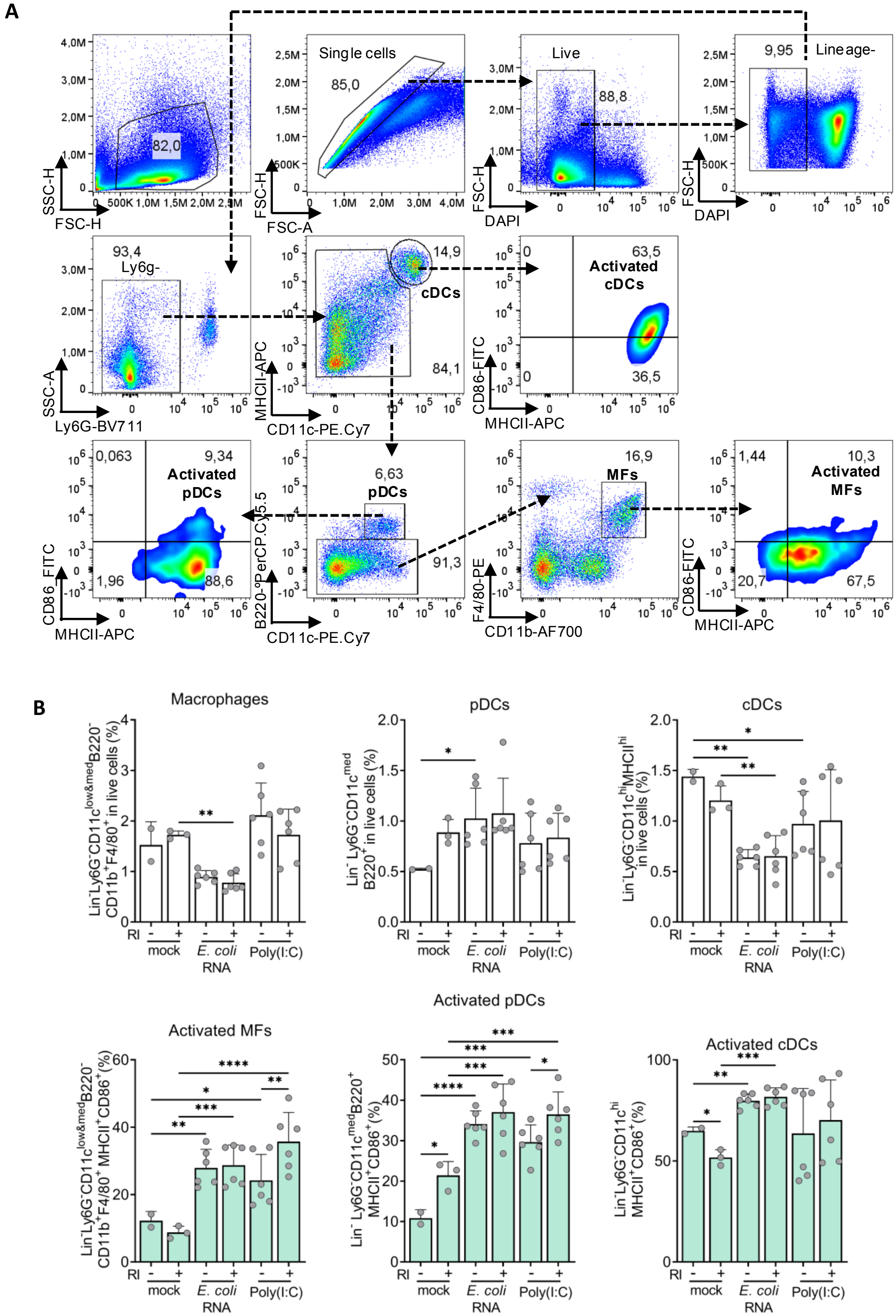

Figure S9. Gating strategy and the effect of naked exRNAs on splenic myeloid cells, related to Figure 5. A) Flow cytometry gating strategy to study splenic cDC, pDC and macrophages after intravenous administration of naked RNA stimuli. Percentages correspond to the parental gates. B) Flow cytometry analysis of spleen cells 6 h after intravenous administration of either 200ng naked Poly(I:C), or 10 µg of naked total *E. coli* RNA, with or without 480 U RI. PBS was used as mock. The percentage of total macrophages ($Lin^-Ly6G^-CD11c^{low\&med}B220^-CD11b^+F4/80^+$), pDCs ($Lin^-Ly6G^-CD11c^{med}B220^+$), cDCs ($Lin^-Ly6G^-CD11c^{hi}MHCII^{hi}$), gated in live cells is shown in top panels. The percentage of activated macrophages, pDCs, cDCs, (defined as $MHCII^+CD86^+$) gated under their corresponding cell type is shown in bottom panels with bar plots shaded in green. ∗p < 0.05, ∗∗p < 0.01, ∗∗∗p < 0.001; ∗∗∗∗p < 0.0001; one-way ANOVA with Fisher's test (if data had normal distribution and variance homogeneity) or Welch ANOVA (if data had normal distribution but lacked variance homogeneity).

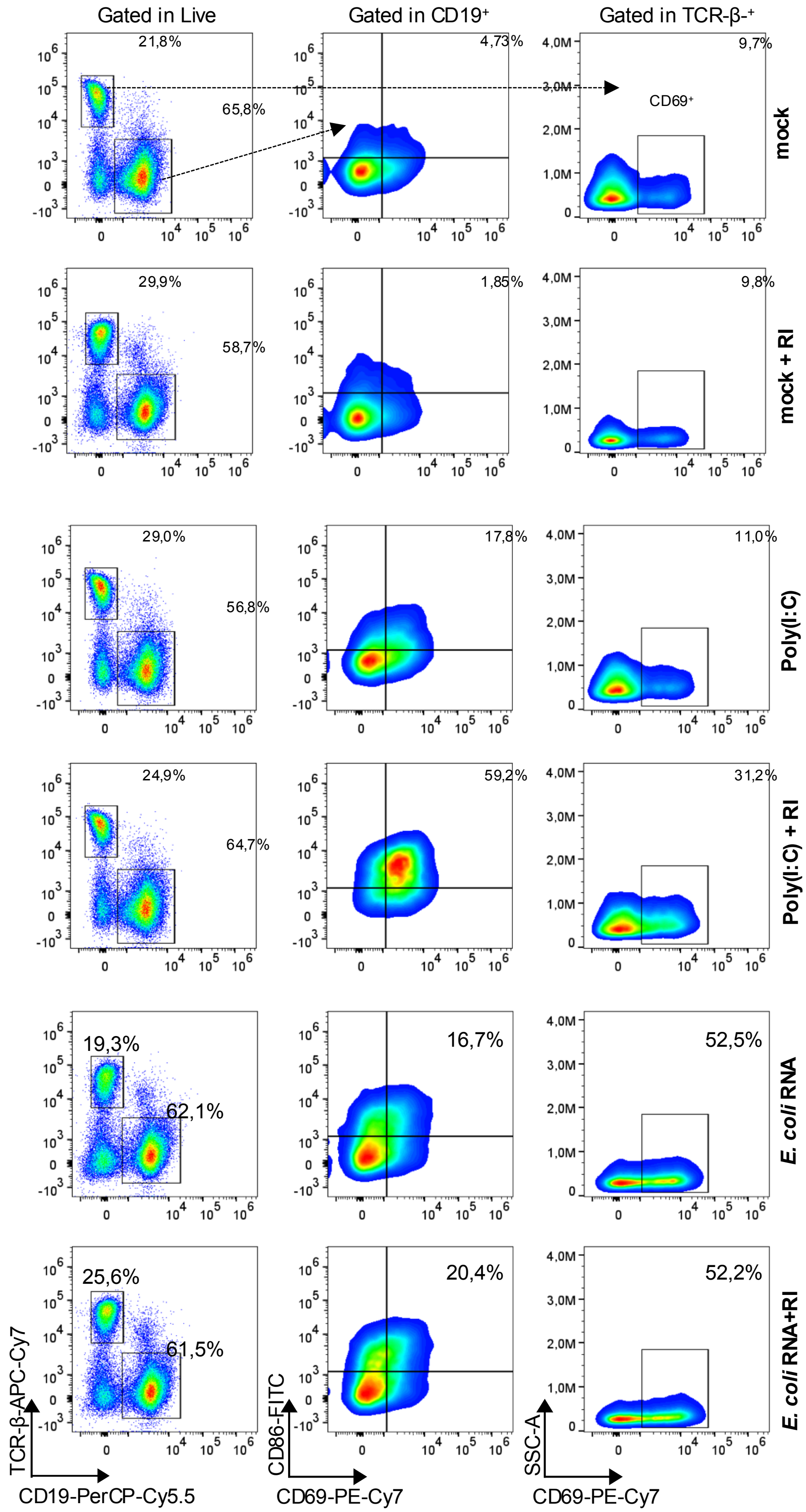

Figure S10. Effect of naked exRNA on splenic lymphoid cells, related to Figure 5. A) Flow cytometry gating strategy to study splenic B and T cells populations after intravenous administration of RNA. B) Dot plots showing flow cytometry analysis of spleen cells 6 h after intravenous administration of 10 µg naked total *E. coli* RNA, 1 µg naked poly(I:C), or DPBS, with or without 480 U RI. Percentages correspond to the parental gates.

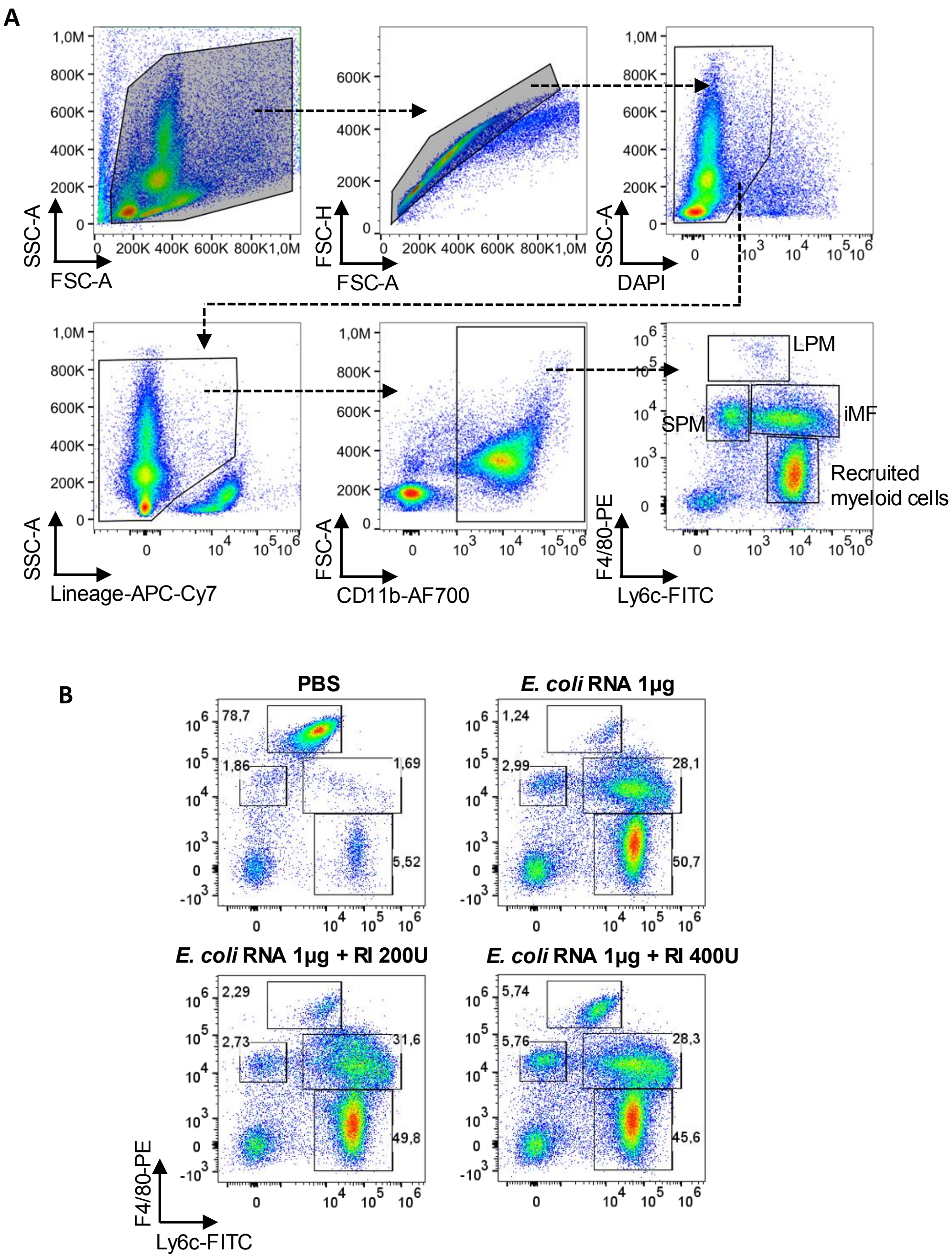

Figure S11. Gating strategy to study mice peritoneal cells, related to Figure 6. A) Gating strategy used for analyzing resident large (LPM) and small (SPM) peritoneal macrophages, recruited myeloid cells, and inflammatory macrophages (iMF) by flow cytometry. Cells were analyzed 24 hours after i.p. administration of 12.5 µg of total naked *E. coli* RNA. B) Peritoneal cell populations gated on Lineage-CD11b+ cells, 24 h after administration of DPBS or 1 µg of naked *E. coli* RNA with the indicated RI doses. Cell percentages are based on the parental gates.

Table S1. Primers for RT-qPCR, related to Star Methods		
Gene	Forward Primer	Reverse Primer
murine *Il6*	5'-AAGCCAGAGTCCTTCAGAGAG-3'	5'-GTCTTGGTCCTTAGCCACTCC-3'
murine *Il1a*	5'-AGTCAACTCATTGGCGCTTG-3'	5'-AGAGAGAGATGGTCAATGGCAG-3'
murine *Cxcl10*	5'-AGTGCTGCCGTCATTTTCTG-3'	5'-GCAGGGATGATTTCAAGCTTCC-3'
murine *Ifit2*	5'-TGCTTTGAGCGCTTTGACAC-3'	5'-TCGCAGATTGCTCTCCAGTG-3'
murine *Oas3*	5'-AGGCTACCGTGTACGCATC-3'	5'-CTTCACACAGCGGCCTTTACC-3'
murine *Il1b*	5'-TGCCACCTTTTGACAGTGATG-3'	5'-ATGTGCTGCTGCGAGATTTG-3'
murine *Actb*	5'-TGGCTCCTAGCACCATGAAG-3'	5'-AACGCAGCTCAGTAACAGTCC-3'
NanoLuc	5'-ATGGTCTTCACACTCGAAGATTTCG-3'	5'-CTGGACACACCTCCCTGTTC-3'
human *IL6*	5'-CCTGAACCTTCCAAAGATGGC-3'	5'-TTCACCAGGCAAGTCTCCTCA-3'
human *IL1B*	5'-ATGATGGCTTATTACAGTGGCAA-3'	5'-GTCGGAGATTCGTAGCTGGA-3'
human *CXCL10*	5'-GTGGCATTCAAGGAGTACCTC-3'	5'-TGATGGCCTTCGATTCTGGATT-3'
human *GAPDH*	5'-CGGAGTCAACGGATTTGGTC-3'	5'-TTCCCGTTCTCAGCCTTGAC-3'

Table S2. Primers for in vitro transcription template amplification, related to Star Methods		
Gene	Forward Primer	Reverse Primer
NanoLuc	5'-ACGACGTAATACGACTCACTATAGG GTATCCGCCACCATGGTCTTCACACTCG-3'	5'-TTTTTTTTTTTTTTTTTTTTTTTTTTTTTT CGACTCTAGAATTATTACGCCAGAATG-3'
eGFP	5'- ACGACGTAATACGACTCACTATAGGGTATC CGCCACCATGGTGAGC-3'	5'-TTTTTTTTTTTTTTTTTTTTTTTTTTTTTTT ACTTGTACAGCTCGTCCATGC-3'

Table S3. Antibodies mixes used, related to Star Methods		
.	Antibodies	Concentration
BMDCs	CD40-FITC	1/500
	CD86-PE	1/200
	MHCII-APC	1/200
Spleen myeloid cells	CD19-APC-Cy7	1/200
	TCR-B-APC-Cy7	1/200
	Ly6G-BV711	1/200
	CD11c PE-Cy7	1/200
	MHC-II-APC	1/200
	B220-PerCP-Cy5.5	1/200
	F4/80-PE	1/200
	CD11b-AF700	1/200
	CD86-FITC	1/500
Spleen lymphoid cells	CD19-PerCP-Cy5.5	1/200
	TCR-B-APC-Cy7	1/200
	CD69-PECy7	1/200
	CD86-FITC	1/500
Peritoneal macrophages and monocytes	CD19-APC-Cy7	1/200
	TCR-B-APC-Cy7	1/200
	CD11b-AF700	1/200
	F4/80-PE	1/200
	Ly6c-FITC	1/500

Supplemental references

[S1] Johnson, J.S., De Veaux, N., Rives, A.W., Lahaye, X., Lucas, S.Y., Perot, B.P., Luka, M., Garcia-Paredes, V., Amon, L.M., Watters, A., et al. (2020). A Comprehensive Map of the Monocyte-Derived Dendritic Cell Transcriptional Network Engaged upon Innate Sensing of HIV. Cell Rep *30*, 914–931. https://doi.org/10.1016/j.celrep.2019.12.054.

Artículo científico 3: Discrimination between vesicular and nonvesicular extracellular tRNAs and their fragments

El artículo 3 de esta tesis de doctorado consiste en el desarrollo de un protocolo, en parte extraído del artículo 1, que resulta de gran utilidad para separar exRNAs vesiculares de exRNAs no vesiculares. Este protocolo permite obtener fracciones que facilita el estudio de nV-exRNAs.

CHAPTER TEN

Discrimination between vesicular and nonvesicular extracellular tRNAs and their fragments

Mauricio Castellano[a,b,c], **Marco Li Calzi**[a], **Maria Rosa Garcia**[a], **Alfonso Cayota**[a,d], **and Juan Pablo Tosar**[a,c,*]

[a]Functional Genomics Laboratory, Institut Pasteur de Montevideo, Montevideo, Uruguay
[b]Immunoregulation and Inflammation Laboratory, Institut Pasteur Montevideo, Montevideo, Uruguay
[c]Analytical Biochemistry Unit, Center for Nuclear Research, School of Science, Universidad de la Republica, Montevideo, Uruguay
[d]Hospital de Clínicas, Universidad de la República, Montevideo, Uruguay
*Corresponding author. e-mail address: jptosar@pasteur.edu.uy

Contents

Abstract

The extracellular space contains RNAs both inside and outside extracellular vesicles (EVs). Among RNA types, tRNAs and tRNA-derived small RNAs (tDRs) tend to be abundant and are frequently detected when performing small RNA sequencing of extracellular samples. For several applications, including answering basic biology questions and biomarker discovery, it is important to understand which specific extracellular tRNAs and tDRs are inside EVs and which are not.

We have observed that EVs contain mainly full-length tRNAs, while cells also release full-length tRNAs into nonvesicular fractions. However, these nonvesicular tRNAs are fragmented by extracellular ribonucleases into nicked tRNAs, which can dissociate

Methods in Enzymology, Volume 711
ISSN 0076-6879, https://doi.org/10.1016/bs.mie.2024.11.042

into tDRs both in extracellular samples and in the laboratory. It is therefore crucial to separate EVs from other nonvesicular RNA-containing extracellular carriers to prevent cross-contamination. Otherwise, extracellular tDR profiling may mix up signals coming from structurally and functionally different carrier types.

Here, we provide two protocols that achieve this by: (a) density gradient separation and, (b) the use of commercial, pre-packed size-exclusion chromatography columns. The first protocol is time-consuming but achieves high resolution, while the second protocol is faster, simpler, and recommended for routine separations. Taken together, they form a solid experimental toolkit for addressing different questions related to extracellular tRNA biology or biomarker discovery.

1. Introduction

Small, non-coding RNAs (sncRNAs) are important regulators of gene expression and genome integrity. They are involved in key cellular processes such as cell differentiation, proliferation, migration and death, acting at both the transcriptional and posttranscriptional levels. The best-known members of this family are microRNAs (miRNAs), small interfering RNAs (siRNAs), Piwi-interacting RNAs (piRNAs), and tRNA-derived small RNAs (tDRs). The latter have been observed across various cells, tissues, and organisms (Fu et al., 2009; Garcia-Silva, Fruiger et al., 2010; Garcia-Silva, Tosar et al., 2010; Haiser, Karginov, Hannon, & Elliot, 2008; Jöchl et al., 2008; Lee & Collins, 2005; Li et al., 2008; Thompson, Lu, Green, & Parker, 2008; Yamasaki, Ivanov, Hu, & Anderson, 2009), and are also present in extracellular samples and biofluids such as cerebrospinal fluid, urine or blood serum (Dhahbi et al., 2013; Garcia-Silva et al., 2014; Godoy et al., 2018; Hulstaert et al., 2020; Nolte'T Hoen et al., 2012; Tosar et al., 2015; Wei et al., 2017; Wu et al., 2023; Zhang et al., 2014).

Over the past decade, our group has focused on the role of non-coding RNAs in intercellular communication. Searching for new small RNA families in the protozoan parasite Trypanosoma cruzi, we discovered a population of tDRs that was induced by stress and recruited to cytoplasmic granules (Garcia-Silva, Fruiger et al., 2010; Garcia-Silva, Tosar et al., 2010). These tDRs were potential substrates of TcPIWI-tryp, the only Argonaute protein present in these parasites (Garcia-Silva, Fruiger et al., 2010; Garcia-Silva, Tosar et al., 2010). Surprisingly, we later found that *T. cruzi* releases extracellular vesicles (EVs) containing these tDRs into the extracellular space (Fernandez-Calero et al., 2015; Garcia-Silva et al., 2014). In addition, these EVs could be internalized by both human and *T. cruzi* cells, affecting parasitic proliferation and infection rates (Garcia-Silva et al., 2014). These results suggested that tDRs could be involved in non-cell autonomous functions mediating host-pathogen interactions.

In the following years, we shifted our focus to the study of extracellular tDRs in human cells. By that time, several studies had either compared intracellular and extracellular small RNA profiles, revealing human EV-associated tDRs (Nolte'T Hoen et al., 2012), or compared the distribution of miRNAs between cells, EVs, and an EV-free extracellular fraction containing mostly ribonucleoproteins (RNPs) (Arroyo et al., 2011; Turchinovich, Weiz, Langheinz, & Burwinkel, 2011). However, whether extracellular tDRs were mostly present inside or outside EVs was unclear. We found that extracellular samples were enriched in tDRs (compared to miRNAs and other small RNA families), and that most of these extracellular tDRs were not in EVs (Tosar et al., 2015). In addition, nonvesicular extracellular tDRs were mostly 5′ tRNA halves derived from $tRNA^{Gly}_{GCC}$ and $tRNA^{Glu}_{CUC}$ (Tosar et al., 2015). Bias toward these specific tRNAs was also observed in human serum and plasma (Srinivasan et al., 2019).

To get a comprehensive picture of the exRNAs that are released by cells irrespectively of their stability, we designed RI-SEC-seq (Tosar et al., 2020; Tosar, Gámbaro, Castellano, & Cayota, 2021; Tosar, Witwer, & Cayota, 2021). This method is based on small RNA sequencing of chromatographic fractions obtained after separating nonvesicular extracellular RNAs, with or without prior addition of ribonuclease inhibitors (RI) into the media. Surprisingly, this method showed that, in the presence of RI, extracellular nonvesicular tRNA halves became larger (~ 34–35 nt vs ~ 30–31 nt). By northern blot, we confirmed a shift toward larger 5′ tRNA halves in the media, but we also observed a new peak corresponding to full-length tRNAs (Tosar et al., 2020). Another research group arrived independently to a similar conclusion (Nechooshtan, Yunusov, Chang, & Gingeras, 2020).

The model that arises from these studies is the following: cells not only release EVs into the extracellular space; they also release ribosomes and full-length tRNAs that are not associated with EVs and remain in 100,000 × g centrifugation supernatants. Whether nonvesicular exRNAs are actively released by living cells, or passively released by damaged or dead cells remains an open question. These extracellular tRNAs are then cleaved by extracellular RNases to produce nonvesicular tRNA halves. While dimerization could potentially explain the stability of some of these tRNA halves in the extracellular space (Tosar et al., 2018), later research from our lab showed that most extracellular nonvesicular tRNA halves are intrinsically stable nicked tRNAs, rather than *bona fide* tDRs (Costa et al., 2023).

Thus, the abundance of nonvesicular tRNA halves in extracellular samples is better explained by survivorship bias than by preferential release into the extracellular space (Tosar & Cayota, 2020; Tosar, Gambaro et al., 2021; Tosar, Witwer et al., 2021), due to the intrinsic stability of nicked tRNAs against further RNase A-mediated processing (Costa et al., 2023).

In summary, interpreting small RNA sequencing data generated on extracellular samples is complicated because:

a) Extracellular tDRs are found both inside and outside EVs (Tosar et al., 2015)

b) Full-length tRNAs are stable and abundant inside EVs (Shurtleff et al., 2017; Tosar et al., 2020), but they are also present, transiently, in nonvesicular fractions (Nechooshtan et al., 2020; Tosar et al., 2020). Furthermore, they are later converted into nicked tRNAs (Costa et al., 2023), which look exactly like tRNA halves and tDRs by standard sequencing techniques (Tosar, Castellano, Costa, & Cayota, 2024).

c) Vesicular and nonvesicular tRNA halves / tDRs can play a role in intercellular communication, as both can be internalized by recipient cells (Costa et al., 2023; Gámbaro et al., 2020). They might also serve as disease biomarkers for early-stage disease detection and treatment monitoring (Dhahbi, Spindler, Atamna, Boffelli, & Martin, 2014).

It is therefore important to obtain methods that: (i) achieve almost perfect separation between EVs and nonvesicular fractions, to study tRNAs/tDRs separately in both compartments, and (ii) have the capacity of distinguishing between full-length tRNAs, nicked tRNAs and tDRs, despite all having virtually identical sequences. The latter is presented in Chapter 11 of this volume. The former is usually performed by differential ultracentrifugation, as we described earlier (Tosar & Cayota, 2018), or by the use of EV precipitation reagents. However, these methods do not achieve acceptable levels of separation for exRNA profiling applications, with EVs usually being contaminated with nonvesicular nicked tRNAs/tRNA halves.

Reverse isopycnic centrifugation ("flotation gradients"), where concentrated extracellular samples are loaded in the bottom of an iodixanol (OptiPrep™) density gradient, was shown to achieve perfect separation between vesicular and nonvesicular extracellular fractions (Jeppesen et al., 2019). We adapted this method to profile EVs and the entire extracellular nonvesicular fraction (Tosar et al., 2020), as described in one of the protocols presented in this chapter. However, this method is time-consuming and requires expertise and the availability of an ultracentrifuge. In many cases, researchers already know if the RNA they are studying is vesicular or non-vesicular, and they simply want to obtain both extracellular fractions with a reasonable level of purity for downstream analysis. For these cases, we provide a second protocol based on commercial size exclusion columns designed for EV purification. When coupled with an automated fraction collector, this alternative protocol is rapid, convenient, and highly reproducible.

2. Purification of vesicular and nonvesicular tRNA/tDRs by isopycnic centrifugation (iodixanol flotation gradients)

EVs and nonvesicular RNAs (or other extracellular particles) have traditionally been purified by differential ultracentrifugation, relaying on their size and weight differences. However, this method does not achieve high purity. Consequently, EVs and nonvesicular fractions tend to be cross-contaminated (Jeppesen et al., 2019). There are many examples in the literature where functions attributed to EV are actually mediated by nonvesicular proteins that co-isolate with EVs during ultracentrifugation. An interesting alternative is to employ buoyant density centrifugation, also known as equilibrium density-gradient centrifugation or isopycnic centrifugation. This technique can separate EVs from other extracellular particles and macromolecules, thanks to differences in density between these components. Density-gradient centrifugation with iodixanol (sold as a sterile 60 % m/v solution called OptiPrep™) can efficiently separate EVs from other RNA-containing extracellular complexes and particles (Jeppesen et al., 2019; Tosar et al., 2020; Zhang, Jeppesen, Higginbotham, Franklin, & Coffey, 2023). Compared with sucrose, which is a commonly used density gradient-forming molecule, iodixaol has the advantage of having lower viscosity and osmolarity, as well as being highly soluble.

2.1 Materials

- Sterile plastics, media and supplements for mammalian cell culture
- RNase inhibitor, murine (New England Biolabs, #M0314S) – OPTIONAL
- Amicon® ULTRACEL®−10 regenerated cellulose filters, 10 kDa MWCO (Merck, #UFC9019)
- PBS or DPBS (Gibco), 1x, sterile

- 60 % w/v iodixanol (OptiPrep™ Density Gradient Medium, Sigma-Aldrich # D1556). Keep stock sterile.
- 14 mL ultracentrifugation polypropylene tubes (14 ×95 mm; Beckman Coulter #331374)
- TRIzol™ Reagent (Invitrogen, #15596026).
- Chloroform, isopropanol, absolute ethanol and acetone (for RNA purification)

2.2 Equipment

- Optima XPN ultracentrifuge (Beckman Coulter)
- SW 40 Ti swinging-bucket rotor (Beckman Coulter, # 331301)

2.3 Procedure

This protocol describes the purification and characterization of extracellular tRNAs and nicked tRNAs/tDRs from cell-conditioned media obtained from U2 O-S or MCF-7 cells, grown under standard culture conditions (DMEM + 10 % FBS). It can be readily applied to other cell types and culture conditions with minimal modifications. It can also be adjusted to the use of biofluid samples. However, when working with serum or plasma, the high concentration of albumin can cause problems during the concentration step, and when analyzing the denser gradient fractions.

2.3.1. In a T150 flask, grow U-2 OS or MCF-7 cells with 30–35 mL of DMEM, supplemented with 10 % FBS, until 60–70 % confluence is reached.

Note: cell confluence should be adjusted depending on the growth rate of the cells

2.3.2. Remove and discard the cell-conditioned medium (CCM), and wash cells with pre-warmed fresh medium or warm PBS. Discard the wash. Add fresh medium and grow cells for an additional 24 h.

Note: at this point, the medium can be substituted for a serum-free defined formulation where the effect of RI addition can be tested, if desired. With MCF-7 cells, we use MEGM (Lonza) without the addition of the antibiotics or the bovine pituitary extract included in the kit. The cell density after this 24 h period should be 90 % or less. When adding RI to defined, serum-free media, we repeat RI addition at the point of collection of the cell-conditioned medium, due to concerns on the activity of RI after the 24 h incubation (see Section 3). Addition of RI does not make much sense when growing cells in 10 % FBS, unless adding high volumes of RI to completely inhibit all serum-derived RNases.

2.3.3. OPTIONAL: If working with serum-free media, add 1–2 μL of RI per 10 mL of CCM to avoid further RNA degradation during centrifugation.
2.3.4. Collect CCM; put on ice for 5 min
2.3.5. Centrifuge the CCM at 500 x g for 10 min at 4°C to remove cells that could have detached. Transfer the supernatant to a new tube.
2.3.6. Repeat step 2.3.5.
2.3.7. Centrifuge the supernatant from step 6 at 2000 x g for 10 min at 4°C to remove apoptotic bodies / cell debris or other large particles.
2.3.8. Concentrate the supernatant up to ~500 μL by ultrafiltration using Amicon® ULTRACEL®−10 regenerated cellulose filters, 10 kDa MWCO

Note: rinse the membrane with water and then briefly spin PBS to hydrate and clean the membrane before adding the sample. Be aware that samples containing 10 % FBS might take time to concentrate. Every 5–10 min, pause the centrifuge and gently pipette up and down the concentrate to avoid the formation of a protein gradient in the upper chamber (easily seen with the naked eye). If the starting volume is > 25 mL, split the sample in two and use two separate ultrafiltration devices. Remember to balance the centrifuge with a separate ultrafiltration device.

2.3.9. Dilute the concentrate in ice-cold PBS to a final volume of 1.2 mL
2.3.10. Mix the sample from step 2.3.9 with 1.8 mL iodixanol (60 % w/v) to make 3 mL of a 36 % iodixanol solution containing the sample
2.3.11. Load 2.4 mL of the sample from step 2.3.10 in the bottom of a 14 mL ultracentrifugation polypropylene tube.
2.3.12. Prepare the gradient:
- mix 1.5 mL of iodixanol (60 % w/v) and 1.5 mL of ice-cold PBS to make 3 mL of a 30 % iodixanol solution
- mix 1.2 mL of iodixanol (60 % w/v) and 1.8 mL of ice-cold PBS to make 3 mL of a 24 % iodixanol solution
- mix 0.9 mL of iodixanol (60 % w/v) and 2.1 mL of ice-cold PBS to make 3 mL of a 18 % iodixanol solution
- mix 0.6 mL of iodixanol (60 % w/v) and 2.4 mL of ice-cold PBS to make 3 mL of a 12 % iodixanol solution

2.3.13. Carefully, add sequential layers of ice-cold, 30 %, 24 %, 18 % and 12 % iodixanol solutions (2.4 mL each), to form a discontinuous 12–36 % iodixanol gradient.

Note: this protocol is a variation of the protocol described in (Jeppesen et al., 2019). *The main difference is that, in* Jeppesen et al. (2019)*, the* *authors loaded a 120,000 x g pellet in the bottom of the tube. Their main objective was to discriminate true EV components from nonvesicular proteins that co-isolate with EVs by ultracentrifugation. Here, we are loading the entire concentrated cell-conditioned medium (*i.e.*, we skipped the 120,000 x g ultracentrifugation step). These samples contain both EV-RNA and most nonvesicular exRNA (and their associated proteins).*

2.3.14. Centrifuge overnight (for 15 h) at 120,000 × g (30,800 rpm) and 4°C, using a SW40 Ti rotor. With max acceleration (1) and a deceleration of 7.

Note: sample volumes and centrifugation speeds can be adjusted to other ultracentrifuges, tubes and rotors. Ultracentrifugation is a technique that requires expertise to manage potential risks. If running an odd number of gradients, equilibrate the rotor with identical gradients containing PBS instead of the sample.

2.3.15. The next day, slowly and gently collect twelve 1 mL fractions using a p1000 pipette, starting from the top of the gradient. Transfer each fraction to a nuclease-free 1.5 mL tube.

Note: the gradient is linear after the 15 h ultracentrifugation step. Keep the pipette's tip about 1 cm below the meniscus and move it down as the liquid's level moves down as well. Avoid the entrance of air or the generation of convection forces in the gradient that could mix the content of each collected fraction.

2.3.16. Split each sample into two 0.5 mL aliquots.

2.3.17. To one of the aliquots, add an equal volume (0.5 mL) of TRIzol for RNA purification, following manufacturer's instructions. Use the purified RNA for downstream applications (e.g., RT-qPCR, sequencing, northern blot)

Note: if the original sample was CCM obtained in the presence of 10 % FBS, fraction 12 contains a high concentration of albumin. This can interfere with RNA purification.

2.3.18. Precipitate proteins from the other aliquot by adding two volumes of pure acetone, previously chilled at −20°C. Spin down the sample. Wash the pellet with 60 % acetone (at −20°C) and spin down again. Suspend the pellet in 1x loading buffer and proceed for western blot analysis. The loading buffer should not contain reducing agents if the primary antibodies recognize epitopes containing disulfide bonds (common with some antibodies for EV surface markers).

Note: same as in 2.3.17, fraction 12 contains too much albumin if starting from FBS-containing cell-conditioned media (Fig. 1). We suggest not running this sample in the gel as it can induce artefacts during electrophoresis.

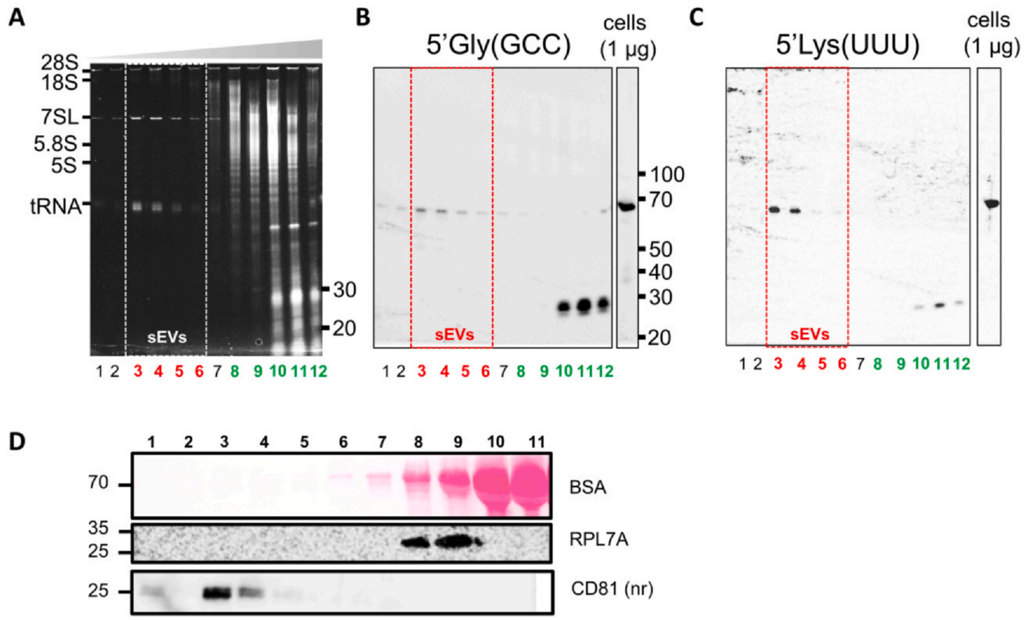

Fig. 1 Expected results. Cell-conditioned medium from U-2 OS cells grown in DMEM + 10 % FBS for 24 h was analyzed using iodixanol 12–36 % density gradients. RNA was extracted from each sample and run on a 10 % TBE-Urea gel, and stained with SYBR Gold (A). As can be seen, most extracellular RNA is present in the high-density fractions (8 – 12), and contains mostly fragmented RNA. The EV fractions (3 – 6) contain full-length 7SL RNA and full-length tRNA. This can be confirmed by northern blot using probes against the 5′ half of $tRNA^{Gly}_{GCC}$ (B) and $tRNA^{Lys}_{UUU}$ (C). On the contrary, nonvesicular fractions do not contain full-length tRNAs (in samples containing 10 % FBS). They do contain 5′ tDRs, at least some of them being nicked tRNAs. A control was performed running only RNA from fresh DMEM + 10 % FBS medium (not shown). This control confirmed that all the signal at this level of detection came from U-2 OS cells and not from FBS. An aliquot of each fraction was analyzed by western blot using antibodies against RPL7a (a ribosomal protein; not EV-associated) and CD81 (a typical EV marker). The gel was run under non-reducing conditions (D). Ponceau red staining of the membrane shows the distribution of albumin in the gradient. As can be seen, EV fractions are free from albumin and hence represent true vesicular contents. Data from: Tosar et al. (2020).

3. Purification of vesicular and nonvesicular tRNA/tDRs using commercial size-exclusion chromatography (SEC) columns

The flotation gradients (Section 2) are better suited for situations where it is crucial to distinguish between vesicular and nonvesicular RNA. However, it is not a practical separation method for everyday applications. For these cases, the method described below is, in our opinion, the best suited in terms of balance between purity and simplicity.

Unlike the protocol described in Section 2, which separates EVs from nonvesicular RNAs or RNPs based on density, this protocol separates based on size. Using SEC columns with a pore size of 70 nm, EVs elute in the exclusion volume, or in the first fractions. Fractions 5 + can be considered, in practical terms, EV-free. It is important to consider that large macromolecular particles, if present in the extracellular space, might also co-isolate with EVs.

We have used this protocol to show that the nonvesicular fraction of U-2 OS CCM contains nicked tRNAs (Costa et al., 2023). Nevertheless, the protocol can be adapted to other applications such as the purification and analysis of EV-associated tRNAs or tDRs, etc.

Maximum efficiency is obtained using an automatic fraction collector. However, samples can also be collected manually.

3.1 Materials

- Mammary Epithelial Cell Growth Medium (MEGM, Lonza, reference number: CC-2551; not complemented with the Bovine Pituitary Extract included in the MEGM kit)
- 1.5 mL RNase Free DNase Free Eppendorf test tubes (CNWTC, reference number: #TYA10)
- DPBS (Invitrogen, reference number: 14190144)
- RNase inhibitor, murine (New England Biolabs, #M0314S)
- Size exclusion chromatography 75 nm columns (Izon qEV Original, reference number SP1)
- Vivaspin 6 Ultrafilter MWCO 10 kDa (Sartorius, #VS0601)

3.2 Equipment

- Automatic Fraction Collector (Izon, model code: AFC-V1) with 1.5-2 mL carrousel

3.3 Procedure

3.3.1. Incubate 4 million U-2 OS cells in a 75 cm^2 cell culture flask with 7 mL MEGM at 37°C, 5 % CO_2, for 24 h. Add 1-2 μL (40–80 U) murine RNase inhibitor to the media, before adding it to the cell monolayer.

Note: in this example, we are using serum-free medium to isolate a mixture of full-length tRNAs and nicked tRNAs from the nonvesicular fraction of the extracellular space. If using culture medium containing FBS (as in Section 2), virtually all full-length tRNAs are going to be either degraded or nicked. Under these experimental conditions, full-length tRNAs are only expected in the fractions containing EVs.

3.3.2. Harvest the cell-conditioned medium (CCM). Add 1-2 μL murine RNase inhibitor and centrifuge at 300 × g at 4°C for 15 min. Discard the pellet.

3.3.3. Centrifuge the supernatant at 2000 × g at 4°C for 20 min. Discard the pellet.

3.3.4. Concentrate the supernatant using a Vivaspin 6 Ultrafilter, MWCO 10 kDa. Centrifuge at 3000 rpm at 4°C for as long as it takes to bring down the total volume to 500 μL

Note: this step usually takes around 30 min. However, every five minutes, stop the centrifuge and pipette up and down the concentrator filter with a 1000 μL micropipette to prevent clogging.

3.3.5. Once the total CCM has been concentrated down to 500 μL, open a new 75 nm Izon qEV Original SEC column and place it in the automatic fraction collector.

Note: the sample should be placed on ice until it is loaded onto the column. Columns can be reused up to five times if stored appropriately. It is crucial to check if reused columns do not induce on-column RNA degradation due to contamination with RNases.

3.3.6. Assemble the fraction collection plastic tube to the lower end of the column.

Note: if the collection tube is not new, it is important to clean it with 20 % ethanol and rinse it multiple times with PBS to rid it of particles and debris. To perform this action, use a 5 mL syringe tube.

3.3.7. Flush the column with 15 mL of ice-cold PBS.

3.3.8. Place 1.5 mL sterile, RNase-Free microcentrifuge tubes in the fraction collector. One for every fraction that will be collected. Label the tubes.

Note: after loading the carrousel with the tubes, set up the automatic fraction collector to collect 1 mL fractions consecutively just after a 2 mL void volume that should be discarded (or analyzed separately).

3.3.9. After the column has been flushed down, load the 500 μL sample onto the column's top filter

Note: it is important to avoid touching the white filter on top of the column with the tip. This could create fissures inside the column that could ruin the sample.

Note: the sample will run through the filter for a few seconds. During those few seconds, the system end will drip down PBS from inside the column. When the sample finishes going through the filter, PBS will stop dripping down.

3.3.10. Once the sample has gone through the filter and entered into the SEC resin, add 15 mL ice-cold PBS to the column's mobile phase container. Let 2 mL of PBS (void volume) go through to the waste container.

3.3.11. After the void volume has been discarded, start collecting the 1 mL fractions.

Note: after the first mL has dripped down into the test tube, immediately close the lid, label the tube as "fraction #1" and place it in ice.

IMPORTANT NOTE: *fractions 1-3 contain most EVs and fractions 5-12 correspond to the nonvesicular fractions. Fraction 4 might contain both types of extracellular RNA carriers. Proceed to downstream applications.*

3.3.12. After all samples have been collected and placed in ice, flush the column twice with 15 mL PBS. Load another sample or flush the coloumn with water and store it in ethanol following manufacturer's instructions.

Note: this is of great importance to clean the column of particles and debris.

4. Conclusion

In this chapter, we addressed the problem of separating extracellular vesicles from nonvesicular extracellular RNAs using two efficient protocols. Adequate separation between both extracellular RNA carrier types is essential because tRNAs/tDRS are found both inside and outside EVs. In our experience, EVs contain mostly full-length tRNAs, while nonvesicular fractions contain either full-length tRNAs and nicked tRNAs (in RI-treated samples lacking RNases or serum), or only nicked tRNAs (in samples containing active RNases or biofluids, Fig. 1) (Costa et al., 2023; Tosar et al., 2020).

The two protocols described herein achieve adequate levels of separation between both extracellular RNA carriers and are much better in terms of purity than other popular methods like differential ultracentrifugation. The first protocol has a better resolution but is more time consuming and requires experience with handling density gradients. The second protocol is fast but also efficient.

Acknowledgments

This work was supported in part by Universidad de la República, Uruguay (CSIC I+D_2020_433; CSIC Grupos 22620220100069UD), Agencia Nacional de Investigación e Innovación (ANII, Uruguay; FMV_1_2023_1_176438), and the NIH Office of the Director (UG3/UH3CA241694). JPT, MRG and AC are members of the National System of Researchers (SNI, Uruguay). They are also researchers from the Program for the Development of Basic Science (PEDECIBA, Uruguay).

Conflict of interest statement

JPT and AC have filed a patent on a characterization method for extracellular RNAs. JPT is a founder of B4-RNA diagnostics that uses such a method.

References

Arroyo, J. D., Chevillet, J. R., Kroh, E. M., Ruf, I. K., Pritchard, C. C., Gibson, D. F., ... Tewari, M. (2011). Argonaute2 complexes carry a population of circulating microRNAs independent of vesicles in human plasma. *Proceedings of the National Academy of Sciences of the United States of America, 108*(12), 5003–5008.

Costa, B., Li Calzi, M., Castellano, M., Blanco, V., Cuevasanta, E., Litvan, I., ... Tosar, J. P. (2023). Nicked tRNAs are stable reservoirs of tRNA halves in cells and biofluids. *Proceedings of the National Academy of Sciences of the United States of America, 120*(4), e2216330120.

Dhahbi, J. M., Spindler, S. R., Atamna, H., Boffelli, D., & Martin, D. I. K. (2014). *Deep sequencing of serum small RNAs identifies patterns of 5′ tRNA half and YRNA fragment expression associated with breast cancer. Biomarkers in Cancer, Vol. 6*, BICS20764.

Dhahbi, J. M., Spindler, S. R., Atamna, H., Yamakawa, A., Boffelli, D., Mote, P., & Martin, D. I. K. (2013). 5′ tRNA halves are present as abundant complexes in serum, concentrated in blood cells, and modulated by aging and calorie restriction. *BMC Genomics, 14*, 298.

Fernandez-Calero, T., Garcia-Silva, R., Pena, A., Robello, C., Persson, H., Rovira, C., ... Cayota, A. (2015). Profiling of small RNA cargo of extracellular vesicles shed by Trypanosoma cruzi reveals a specific extracellular signature. *Molecular and Biochemical Parasitology, 199*(1–2), 19–28.

Fu, H., Feng, J., Liu, Q., Sun, F., Tie, Y., Zhu, J., ... Zheng, X. (2009). Stress induces tRNA cleavage by angiogenin in mammalian cells. *FEBS Letters, 583*(2), 437–442.

Gámbaro, F., Li Calzi, M., Fagúndez, P., Costa, B., Greif, G., Mallick, E., ... Tosar, J. P. (2020). Stable tRNA halves can be sorted into extracellular vesicles and delivered to recipient cells in a concentration-dependent manner. *RNA Biology, 17*(8), 1168–1182.

Garcia-Silva, M. R., Cura Das Neves, R. F., Cabrera-Cabrera, F., Sanguinetti, J., Medeiros, L. C., Robello, C., ... Cayota, A. (2014). Extracellular vesicles shed by Trypanosoma cruzi are linked to small RNA pathways, life cycle regulation, and susceptibility to infection of mammalian cells. *Parasitology Research, 113*(1), 285–304.

Garcia-Silva, M. R., Frugier, M., Tosar, J. P., Correa-Dominguez, A., Ronalte-Alves, L., Parodi-Talice, A., ... Cayota, A. (2010). A population of tRNA-derived small RNAs is actively produced in Trypanosoma cruzi and recruited to specific cytoplasmic granules. *Molecular and Biochemical Parasitology, 171*(2), 64–73.

Garcia-Silva, M. R., Tosar, J. P., Frugier, M., Pantano, S., Bonilla, B., Esteban, L., ... Cayota, A. (2010). Cloning, characterization and subcellular localization of a Trypanosoma cruzi argonaute protein defining a new subfamily distinctive of trypanosomatids. *Gene, 466*(1–2), 26–35.

Godoy, P. M., Bhakta, N. R., Barczak, A. J., Cakmak, H., Fisher, S., MacKenzie, T. C., ... Erle, D. J. (2018). Large differences in small RNA composition between human biofluids. *Cell Reports, 25*(5), 1346–1358.

Haiser, H. J., Karginov, F. V., Hannon, G. J., & Elliot, M. A. (2008). Developmentally regulated cleavage of tRNAs in the bacterium Streptomyces coelicolor. *Nucleic Acids Research, 36*(3), 732–741.

Hulstaert, E., Morlion, A., Cobos, F. A., Verniers, K., Nuytens, J., Eynde, E., et al. (2020). Charting extracellular transcriptomes in The Human Biofluid RNA Atlas. *Cell Reports, 33*(13), 108552.

Jeppesen, D. K., Fenix, A. M., Franklin, J. L., Higginbotham, J. N., Zhang, Q., Zimmerman, L. J., ... Coffey, R. J. (2019). Reassessment of exosome composition. *Cell, 177*(2), 428–445.
Jöchl, C., Rederstorff, M., Hertel, J., Stadler, P. F., Hofacker, I. I., Schrettl, M., ... Hüttenhofer, A. (2008). Small ncRNA transcriptome analysis from Aspergillus fumigatus suggests a novel mechanism for regulation of protein synthesis. *Nucleic Acids Research, 36*(8), 2677–2689.
Lee, S. R., & Collins, K. (2005). Starvation-induced cleavage of the tRNA anticodon loop in Tetrahymena thermophila. *Journal of Biological Chemistry, 280*(52), 42744–42749.
Li, Y., Luo, J., Zhou, H., Liao, J. Y., Ma, L. M., Chen, Y. Q., & Qu, L. H. (2008). Stress-induced tRNA-derived RNAs: A novel class of small RNAs in the primitive eukaryote Giardia lamblia. *Nucleic Acids Research, 36*(19), 6048–6055.
Nechooshtan, G., Yunusov, D., Chang, K., & Gingeras, T. R. (2020). Processing by RNase 1 forms tRNA halves and distinct Y RNA fragments in the extracellular environment. *Nucleic Acids Research, 48*(14), 8035–8049.
Nolte'T Hoen, E. N. M., Buermans, H. P. J., Waasdorp, M., Stoorvogel, W., Wauben, M. H. M., & T Hoen, P. A. C. (2012). Deep sequencing of RNA from immune cell-derived vesicles uncovers the selective incorporation of small non-coding RNA biotypes with potential regulatory functions. *Nucleic Acids Research, 40*(18), 9272–9285.
Shurtleff, M. J., Yao, J., Qin, Y., Nottingham, R. M., Temoche-Diaz, M. M., Schekman, R., & Lambowitz, A. M. (2017). Broad role for YBX1 in defining the small noncoding RNA composition of exosomes. *Proceedings of the National Academy of Sciences of the United States of America, 114*(43), E8987–E8995.
Srinivasan, S., Yeri, A., Cheah, P. S., Chung, A., Danielson, K., De Hoff, P., ... Laurent, L. C. (2019). Small RNA sequencing across diverse biofluids identifies optimal methods for exRNA isolation. *Cell, 177*(2), 446–462.
Thompson, D. M., Lu, C., Green, P. J., & Parker, R. (2008). tRNA cleavage is a conserved response to oxidative stress in eukaryotes. *RNA (New York, N. Y.), 14*(10), 2095–2103.
Tosar, J. P., Castellano, M., Costa, B., & Cayota, A. (2024). Small RNA structural biochemistry in a post-sequencing era. *Nature Protocols, 19*(3), 595–602.
Tosar, J. P., & Cayota, A. (2018). Detection and analysis of non-vesicular extracellular RNA. *Methods in Molecular Biology, 1740*, 125–137.
Tosar, J. P., & Cayota, A. (2020). Extracellular tRNAs and tRNA-derived fragments. *RNA Biology, 17*(8), 1149–1167.
Tosar, J. P., Gambaro, F., Darre, L., Pantano, S., Westhof, E., & Cayota, A. (2018). Dimerization confers increased stability to nucleases in 5′ halves from glycine and glutamic acid tRNAs. *Nucleic Acids Research, 46*(17), 9081–9093.
Tosar, J. P., Gámbaro, F., Sanguinetti, J., Bonilla, B., Witwer, K. W., & Cayota, A. (2015). Assessment of small RNA sorting into different extracellular fractions revealed by high-throughput sequencing of breast cell lines. *Nucleic Acids Research, 43*(11), 5601–5616.
Tosar, J. P., Segovia, M., Castellano, M., Gámbaro, F., Akiyama, Y., Fagúndez, P., ... Cayota, A. (2020). Fragmentation of extracellular ribosomes and tRNAs shapes the extracellular RNAome. *Nucleic Acids Research, 48*(22), 12874–12888.
Tosar, J. P., Gámbaro, F., Castellano, M., & Cayota, A. (2021). Ri-sec-seq: Comprehensive profiling of nonvesicular extracellular rnas with different stabilities. *Bio-Protocol, 11*(4).
Tosar, J. P., Witwer, K., & Cayota, A. (2021). Revisiting extracellular RNA release, processing, and function. *Trends in Biochemical Sciences, 46*(6), 438–445.
Turchinovich, A., Weiz, L., Langheinz, A., & Burwinkel, B. (2011). Characterization of extracellular circulating microRNA. *Nucleic Acids Research, 39*(16), 7223–7233.
Wei, Z., Batagov, A. O., Schinelli, S., Wang, J., Wang, Y., El Fatimy, R., ... Krichevsky, A. M. (2017). Coding and noncoding landscape of extracellular RNA released by human glioma stem cells. *Nature Communications, 8*(1), 1145.

Wu, W., Shen, A., Lee, I., Miranda-Morales, E. G., Spratt, H., Pappolla, M. A., ... Bao, X. (2023). Changes of tRNA-derived fragments by Alzheimer's disease in cerebrospinal fluid and blood serum. *Journal of Alzheimer's Disease, 96*(3).

Yamasaki, S., Ivanov, P., Hu, G.-F., & Anderson, P. (2009). Angiogenin cleaves tRNA and promotes stress-induced translational repression. *The Journal of Cell Biology, 185*(1), 35–42.

Zhang, Q., Jeppesen, D. K., Higginbotham, J. N., Franklin, J. L., & Coffey, R. J. (2023). Comprehensive isolation of extracellular vesicles and nanoparticles. *Nature Protocols, 18*(5).

Zhang, Y., Zhang, Y., Shi, J., Zhang, H., Cao, Z., Gao, X., ... Duan, E. (2014). Identification and characterization of an ancient class of small RNAs enriched in serum associating with active infection. *Journal of Molecular Cell Biology, 6*(2), 172–174.

Discusión

La discusión específica de cada uno de los artículos que conforman esta tesis se encuentra en las secciones de "Discusión" correspondientes a los mismos. A continuación, se presenta una discusión global sobre los alcances, hallazgos y limitaciones de esta tesis, poniendo énfasis en aspectos poco discutidos en los artículos en cuestión.

Como fue mencionado previamente, la caracterización de los exRNAs en el espacio extracelular y el estudio de la comunicación intercelular mediada por estas moléculas ha sido casi exclusivamente estudiada en el contexto de EV. Sin embargo, la mayoría de los exRNAs en biofluidos y en el medio condicionado de células en cultivo, se encuentra por fuera de las EV. Es posible que la abundancia de RNasas en el espacio extracelular haya disuadido a la comunidad científica de hacer foco en esta fracción de exRNAs, al extenderse la idea de que el nV-exRNA sería degradado casi de inmediato luego de ser liberado. Esto ha resultado en un conocimiento limitado sobre la biogénesis y composición de biotipos de nV-exRNA; la relevancia que los nV-exRNA, en particular los exRNAs desnudos, podrían tener en la comunicación célula-célula; y el papel que podrían desempeñar las RNasas extracelulares en la regulación de ambos procesos. Mediante estrategias de inhibición de las RNasas extracelulares, esta tesis buscó echar luz sobre ambas problemáticas que son centrales al campo del exRNA.

En el artículo 1 observamos que modular y/o inhibir la actividad de las RNasas en el medio condicionado de células en cultivo junto a la aplicación de técnicas bioquímicas clásicas y de estrategias de *small RNA sequencing* nos permitió evidenciar que lo que normalmente vemos en el medio extracelular no guarda relación alguna con el conjunto de moléculas de RNA liberadas por las células. Lo que induce a conclusiones erróneas. Por ejemplo, nuestro grupo de investigación observó, en 2015, que ciertas mitades de tRNA están altamente enriquecidas en la fracción nV-exRNA, concluyendo que las mismas podrían ser liberadas selectivamente por las células.[70] Sin embargo, en el artículo 1 comprendimos que las células en realidad liberan tRNAs completos, y que estas mitades de tRNA se enriquecen debido a su estabilidad diferencial. Lo que se complementan con otro de los artículos en los que he participado como coautor en el período (no incluido como artículo *de* la tesis), en el que evidenciamos que los “nicked tRNAs” son extremadamente resistentes a la degradación.[49]

Ahondando un poco más en los resultados, al inhibir a las RNasas extracelulares se logró secuenciar diversos biotipos de RNAs: miRNAs, tRNAs enteros, fragmentos de tRNA y rRNA, yRNAs, snoRNAs e incluso reads que mapeaban a mRNAs. A su vez, fue posible detectar ribosomas extracelulares y, mediante otras técnicas (incluyendo secuenciación directa de RNA por Oxford Nanopore), mRNAs enteros asociados a estos ribosomas extracelulares. En contraposición, al no inhibir a las RNasas, la fracción no vesicular consistió mayormente de fragmentos de tRNA, principalmente derivados de tRNA de glicina. Estos hallazgos tienen profundas relevancias para el campo e implican que: 1) las células son capaces de liberar a la fracción extracelular no vesicular gran parte de su transcriptoma intracelular. 2) Las RNasas rápidamente degradan aquellos nV-exRNA menos estables moldeando la composición final de esta fracción. Debido a esto, los nV-exRNAs que perduran, y son detectados aún en ausencia de RI, serían aquellos más resistentes frente a la acción de las RNasas extracelulares.

La liberación de casi la totalidad del transcriptoma celular al espacio no vesicular plantea la interrogante sobre los mecanismos subyacentes que podrían estar explicando este fenómeno. Una posibilidad es que algunos nV-exRNAs escapen por transportadores/canales de RNA localizados en la membrana plasmática, aunque este mecanismo no sería viable para complejos macromoleculares de gran tamaño como ribosomas extracelulares, sí podría explicar la presencia de pequeños nV-exRNA. Aunque existirían transportadores de RNA de esta naturaleza como las proteínas SIDT1 y SIDT2, estos parecen localizarse mayormente en la membrana de endosomas y lisozomas y permitir la translocación de RNA desde el lumen de estos organelos hacia el citosol.[185–187] Otra posibilidad, tal vez un poco descabellada, es que algunos nV-exRNAs sean secretados por mecanismos similares a los que utilizan las proteínas secretorias. Esta posibilidad se basa en el reciente descubrimiento de una nueva población de RNAs glicosilados post transcripcionalmente que se detectan desnudos en el espacio extracelular en asociación a las membranas plasmáticas de las células.[74] Al igual que para las proteínas, la glicosilación de estos RNAs ocurriría en el retículo endoplasmático/golgi, lo que implica que estos RNAs deben ingresar y transitar por compartimientos del sistema secretor antes de ser liberados.[74] Otro mecanismo plausible podría estar ligado a la llamada “autofagia secretora”. Por ejemplo, se ha visto que los amfisomas, un organelo degradatorio formados por la fusión de autofagosomas y lisosomas, pueden fusionarse a la membrana plasmática[188] y liberar su contenido al exterior celular. Por último, es posible que distintos procesos de muerte celular no apoptótica tales como la necrosis, piroptosis, y netosis puedan dar origen a al menos parte de los exRNAs detectados en la fracción no vesicular. En este sentido, la necrosis se caracteriza por la ruptura de la membrana plasmática y liberación de gran parte del contenido citoplasmático al exterior.[76] Durante la activación del inflamasoma y la posterior muerte por piroptosis, se generan poros en la membrana celular a través de los cuales se secretan, de forma no canónica, IL-1β e IL-18.[77,78] Pensamos que por estos poros también podrían escapar ciertos nV-exRNAs. En la Netosis se liberan trampas extracelulares que además de contener exDNA, tienen exRNA.[79] Aunque la apoptosis es generalmente considerada un proceso de muerte celular silencioso, y el exRNA liberado estaría en principio confinado dentro de vesículas membranosas, se ha visto que las vesículas apoptóticas son permeables y liberan parte de su contenido al exterior, lo que se exacerba si las mismas no son rápidamente removidas de las muestras con las que se trabaja.[189]

La rápida liberación de nV-exRNA observada durante los lavados celulares, el hecho de que sucesivos lavados no atenuaran la liberación de nV-exRNAs y la gran diversidad de biotipos y tamaños de exRNAs detectados lleva a especular que esta estrategia experimental posiblemente haya desestabilizado membranas ya débiles de células apoptóticas o cursando algún tipo de muerte celular en el cultivo, lo cual pudo haber provocado la liberación de su contenido al exterior. La muerte celular es un proceso fisiológico clave, de hecho, miles de millones de células mueren a diario en el organismo, con algunos estimativos llegando a sugerir que hasta 1millon por segundo.[190] Además, en patologías como el cáncer y ciertas enfermedades autoinmunes, la muerte celular se encuentra exacerbada.[191,192] Por lo tanto, aunque la muerte celular pueda parecer menos atractiva como mecanismo de liberación de nV-exRNA que otros procesos activos y más selectivos del tipo de RNA a liberar, es posible que constituya la principal vía de liberación al espacio extracelular de estas moléculas. Tanto en homeostasis como en condiciones patológicas.

Como se mencionó en la introducción, nuestro grupo y otros autores han observado que la fracción no vesicular del medio condicionado de células en cultivo y de biofluidos está enriquecida en ciertos biotipos particulares de RNA como fragmentos de tRNA, yRNAs, rRNA y algunos miRNAs. Naturalmente esto lleva a proponer mecanismos de secreción selectiva de estas moléculas.[65] Sin embargo, la observación de que las células liberan gran parte de su transcriptoma al medio extracelular, y que las RNasas moldean de forma dramática el RNAoma extracelular no vesicular, sugiere una explicación alternativa a la secreción selectiva: las células liberan de forma no selectiva nV-exRNAs y, producto de la acción de las RNasas extracelulares, sobreviven únicamente los nV-exRNAs más estables.[15] En otras palabras: la estabilidad extracelular diferencial de distintos RNAs puede confundirse con la liberación selectiva de los mismos, y postulamos que la inhibición de RNasas es la forma más efectiva de distinguir ambos fenómenos.

La alta estabilidad extracelular de ciertos nV-exRNAs podría explicarse por la asociación de los exRNAs con proteínas. Por ejemplo, algunos snRNAs como RNU2 se asocian al complejo proteico U2 del espliceosoma[123], mientras que los miRNAs se encuentran protegidos por su unión a la proteína Ago2.[48] Otra explicación es la existencia de secuencias de exRNAs desnudas intrínsicamente estables. Tal es el caso de los tRNA en el espacio extracelular no vesicular.[41] Nuestro grupo ha observado que algunos fragmentos de tRNA puede formar dímeros de dsRNA cuya naturaleza doble cadena los vuelve intrínsicamente resistentes a las RNasas.[71] Más recientemente observamos que gran parte de los "fragmentos de tRNA" extracelulares son de hecho "tRNAs enteros mellados" con un corte a nivel del anticodón en donde las mitades permanecen unidas y probablemente conserven la estructura secundaria y terciara del tRNA entero. La estructura de los tRNAs se caracteriza por presentar extensas regiones de RNA doble cadena y plegamientos sobre si misma que hemos visto le confieren una elevada resistencia a las RNasas extracelulares. Además, los tRNAs son extensamente modificados postranscripcionalmente.[193] Y esto es esperable que impacte también en su estabilidad. Por ejemplo, se ha observado recientemente que ciertas modificaciones como la pseudouridina, abundante en los tRNAs, confieren una mayor resistencia a la degradación por RNasas en comparación con la uridina.[194] No sería sorprendente que en el futuro cercano se constatara que otras bases modificadas aún más voluminosas también puedan conferir mayor estabilidad a los tRNAs extracelulares. En tal sentido, hemos visto que el tRNA de lisina UUU posee una estabilidad extracelular muy mayor a la de otros tRNAs, lo cual atribuimos a la base mcm5s2U en la primera posición del anticodón.[49]

Si la muerte celular es principal fuente de liberación de nV-exRNAs ¿qué relevancia biológica podría esto tener? Esta pregunta llevó a cambiar nuestro foco desde la célula liberadora de los nV-exRNAs, hacia la célula receptora de los mismos. Una célula que se muere podrá no tener ninguna "intención" de liberar cierto tipo de molécula de RNA (si se me permite este antropomorfismo por fines didácticos), pero el sistema inmune sí que podría beneficiarse en leer estas moléculas e interpretarlas como DAMPs, o PAMPs cuando las moléculas liberadas ocurren como consecuencia de una infección, y se corresponden con RNAs virales o bacterianos. En suma: pensar en la muerte celular como fuente de nV-exRNAs llevó a uno de mis tutores a interesarse (un poco más) por la inmunología, establecer una incipiente colaboración con mi otra tutora, y de allí podríamos decir que nació esta tesis.

Volviendo a los resultados del artículo 1, en este trabajo se observó que la fracción no vesicular rica en ribosomas extracelulares puede inducir la maduración de células dendríticas y que el tratamiento con RNasa impide estos efectos. Esto sugiere que algunos nV-exRNAs, posiblemente ribosomas, podrían actuar como señales de peligro. En esta línea se ha observado que el rRNA ribosomal purificado o el rRNA 18S generado por transcripción *in vitro* induce la producción de citoquinas proinflamatorias en macrófagos y astrocitos cuando se lo incuba junto a agonistas de TLR2.[195–197] En modelos *in vivo* de isquemia y reperfusión, la liberación de ribosomas o de rRNA -posiblemente a la fracción no vesicular- parecería ser responsable de parte del daño cardíaco.[138] Además, se ha identifica que el eje TLR3-TRIFF participaría en este proceso.[198] Esto podría ser indicativo de que tal vez parte de la respuesta inflamatoria desencadenada por la fracción "P0" (utilizando la nomenclatura del artículo 1) se deba al reconocimiento de estos nV-exRNAs por parte de los TLRs que sensan RNA.

Los resultados previos nos llevaron a preguntarnos sobre la posibilidad de que los nV-exRNAs, en particular los exRNAs desnudos, pudieran participar en la comunicación intercelular, y ser reconocidos por células del sistema inmune. La noción ampliamente aceptada de que los exRNAs son inestables, a menos que se encuentren encapsulados en nanopartículas lipídicas, junto con la idea de que las membranas plasmáticas son impermeables a exRNAs desnudos, ha sustentado la creencia de que las células no pueden captarlos ni responder a ellos.

En el artículo 2 se propuso desafiar estos conceptos y explorar si la comunicación mediada por exRNAs desnudos, lejos de ser una excepción, podría constituir un fenómeno más común de lo que se ha considerado hasta el momento, al menos bajo determinadas condiciones. Utilizando diversos modelos celulares murinos (cultivo primario de BMDCs, línea de macrófagos Raw264.7) y humanos (monocitos y macrófagos THP-1, líneas epiteliales U-2 OS y MCF-7) demostramos que al inhibir las RNAsas extracelulares las células internalizan, reconocen y responden a diversos tipos de exRNAs desnudos como: RNA total bacteriano, RNA ribosomal bacteriano, pequeños oligonucleótidos sintéticos, poly(I:C) e incluso mRNA. En BMDCs y la línea de macrófagos Raw264.7, el RNA desnudo de *E. coli* desencadenó una fuerte respuesta inflamatoria únicamente cuando se inhibieron las RNasas extracelulares con el agregado de RI. Mediante aproximaciones genéticas y farmacológicas demostramos que esta respuesta es dependiente del ingreso del RNA a la vía endocítica y del reconocimiento de estos exRNAs desnudos por sensores endosomales de la inmunidad innata, en particular TLR13. En macrófagos humanos observamos que el RNA, una vez internalizado, es capaz de escapar de los endosomas y ser reconocidos por los RLRs citosólicos, también en forma dependiente de la actividad de las RNasas extracelulares. Asimismo, observamos que tanto las BMDCs como las líneas celulares epiteliales U-2 OS y MCF-7 pueden internalizar y traducir mRNAs extracelulares desnudos en presencia de RI. Esta traducción no se detecta si las células son tratadas con Dynasore, lo que indica que la internalización de los mRNAs depende de una vía endocítica activa. Dado que la traducción solo ocurre en el citosol, estos resultados sugieren que los exRNAs desnudos, una vez internalizados, escapan del compartimento endosomal y acceden al citosol, donde pueden ejercer sus funciones biológicas.

En conjunto, los resultados *in vitro* obtenidos en este trabajo aportan evidencia de que: 1) Las membranas plasmáticas no son completamente impermeables al exRNA desnudo. 2) tanto exRNAs desnudos de cadena simple como doble, y de distintos tamaños, pueden ser internalizados si su estabilidad extracelular es lo suficientemente alta. 3) El exRNA desnudo puede ingresar a las células por vía endocítica, escapar del compartimento endosomal y alcanzar el citosol. 4) el exRNA desnudo tiene el potencial de modular la expresión génica en las células aceptoras, ya sea mediante la activación de receptores de reconocimiento de patrones como TLRs y RLRs, o a través de la interacción con su blanco fisiológico, como los ribosomas en el caso de los mRNAs. 5) La funcionalidad de los exRNAs desnudos está estrictamente supeditada a la actividad de las RNasas extracelulares.

Aunque no podemos descartar completamente que algunos exRNA desnudos atraviesen la membrana plasmática e ingresen directamente al citosol, este no parecería ser un mecanismo de ingreso relevante para estas moléculas dada su carga, tamaño e inexistencia de transportadores de RNA en las membranas plasmáticas de mamíferos.[55] Al igual que otros autores, hemos observado que la internalización y respuesta al exRNA desnudo requiere de su endocitosis, ya que Dynasore, un inhibidor de dinaminas, inhibió la respuesta inflamatoria previamente observada. Las dinaminas son requeridas para dos tipos de endocitosis gatilladas por interacción receptor-ligando: endocitosis media por clatrinas y endocitosis mediada por endofilina A2.[199] Esto sugieren la existencia de uno o más receptores de superficie que reconocen y gatillan el ingreso del exRNA desnudo a los endosomas. En este sentido, el receptor RAGE (*del inglés, Receptor for advance glycation end-products*) ha sido involucrado en la internalización de RNA extracelular[200], pero aún se desconoce qué otros receptores podrían estar involucrados en la internalización de exRNAs desnudos. Llegado este punto, es importante mencionar que dynasore podría tener efectos *off-target* sobre otras vías endocíticas, en particular vías dependientes de filamentos de actina como la macropinocitosis y la fagocitosis[199,201], por lo cual no podemos desestimar la posibilidad de que estos mecanismos jueguen un papel en la internalización de los exRNAs desnudos. De hecho, otros trabajos han mostrado que mRNAs desnudos administrados por vía intradérmica o intranodal son captados por células dendríticas residentes mediante macropinocitosis, lo que fue confirmado utilizando inhibidores de la polimerización de actina como la rottlerina y la citocalasina D.[202,203] Esto sugiere que los exRNAs desnudos podrían también ingresar a la vía endocítica sin la necesidad de unirse a receptores específicos en las membranas celulares, al menos para las células dendríticas. Sin lugar a duda, futuros estudios son necesarios para elucidar completamente los mecanismos moleculares que median el ingreso del exRNA desnudo y las múltiples variables que podrían afectar este proceso como: tipo celular, presencia-ausencia de receptores RNA célula-específicos, etc.

En este trabajo observamos que mRNAs largos (de aproximadamente 1000 pares de bases) y RNAs doble cadena largos pueden escapar de endosomas, alcanzar el citosol, y desencadenar cambios en la expresión génica. Los pocos trabajos publicados que han estudiado el escape endosomal de RNAs desnudos se han focalizado en pequeños siRNAs y ASOs terapéutico.[204] Esto trabajos sugieren que más del 99% del RNA que ingresa a estos compartimentos es incapaz de alcanzar el citoplasma celular debido a: reciclaje y exocitosis de los endosomas; imposibilidad de atravesar la bicapa lipídica endosomal; fusión con lisosomas y posterior degradación del RNA. De hecho, se estima que solamente entre un 0.3-1% de los siRNAs y ASOs terapéuticos logran escapar de endosomas y alcanzar el citosol.[205] El escape endosomal es uno de los grandes cuellos de botella para el *delivery* de RNAs terapéuticos, tanto para pequeños oligonucleótidos desnudos como

RNAs encapsulados en EVs o nanopartículas lipídicas.[206] Los mecanismos por los cuales ocurre el escape endosomal de RNAs desnudos no se comprenden completamente y existe un gran esfuerzo por poder modular este fenómeno y así aumentar la eficacia de las terapias basadas en RNA. Se cree que las membranas endosomales podrían experimentar perturbaciones transitorias en la bicapa lipídica, generando poros temporales a través de los cuales el RNA desnudo podría escapar.[207] Asimismo, durante la maduración endosomal, los endosomas se fusionan entre sí formando endosomas tardíos / cuerpos multivesiculares, los cuales se convierten luego en endolisosomas degradatorios por fusión con los lisosomas; se cree estos eventos de fusión podrían inducir pequeñas fugas que liberen moléculas de RNA desnudo al citosol.[207] Desconocemos si estos procesos también pueden estar implicados en el escape de RNA desnudos largos como los mRNAs que observamos en esta tesis. Por otra parte, tampoco puede descartarse la posibilidad de que algunos RNAs desnudos escapen al citosol a través de transportadores endo-lisosomales de RNA. En este sentido, se ha propuesto que las proteínas de membrana SIDT1 y SIDT2 podrían cumplir este rol, al menos para RNAs doble cadena.[185,187] Trabajos de la tesis de doctorado del Dr. Marco Li Calzi sugieren que el proceso de acidificación de los endosomas sería clave para que ocurra el escape de RNAs desnudos ya que la inhibición farmacológica de este fenómeno retiene el RNA desnudo dentro de los endosomas. Sin embargo, como dicho trabajo también muestra, la inhibición de la acidificación endosomal provoca un detenimiento de la maduración endosomal e inhibe las fusiones entre vesículas endocíticas, por lo que resulta difícil establecer exactamente la razón por la que el escape endosomal del RNA se ve inhibida.

Un aspecto a comentar es que la activación de TLR7, TLR8 y TLR13 requiere que el RNA endocitado sea parcialmente clivado por RNasas endosomales.[94–97,208,209] A priori, podría pensarse que el RI añadido al medio de cultivo también ingresa a los endosomas, donde podría inhibir la actividad de algunas de estas enzimas y, en consecuencia, dificultar el reconocimiento del RNA desnudo. Se desconoce si RI logra ingresar a los endosomas y/o si permanece funcional en su interior. Sin embargo, una de las principales nucleasas implicadas en la generación de ligandos para estos sensores es la RNasa T2. Esta enzima no pertenece a la familia A y, por lo tanto, no sería inhibida por RI. De todas formas, en el caso del TLR8 humano, se ha reportado que ciertas RNasas de la familia A, como la RNasa 2 y la RNasa 6, sí son necesarias para generar los sustratos que activan este receptor.[95,97] En este contexto, cabe preguntarse si la estabilización con RI de exRNAs desnudos potencialmente agonistas de TLR8 y tal vez de TLR7 podría impedir la activación de estos sensores.

Las células del sistema inmune emplean diversas estrategias para discriminar lo propio de lo ajeno.[81] En este sentido, observamos una respuesta dramáticamente diferente de las BMDCs al RNA desnudo de origen murino en comparación con el RNA desnudo bacteriano, cuando ambos fueron incubados en presencia de RI. Considerando que en ausencia de RI el RNA bacteriano desnudo no genera respuesta, podemos afirmar que el efecto de RI fue tan o más importante que la capacidad de los sensores de RNA, en particular TLR13, de discriminar el RNA propio del foráneo. Esto sugiere que el control de los niveles de exRNA desnudo por parte de las RNasas posiblemente constituye un mecanismo central de regulación de la activación de los sensores innatos de RNA, que opera río arriba de otros mecanismos como: la compartimentalización de estos sensores, su especificidad por ciertos motivos de secuencia o su capacidad para reconocer modificaciones en las bases del RNA que difieran entre RNAs propios y RNAsde patógenos. Como se mencionó en la introducción, cada vez se acumula más evidencia de que la activación aberrante y sostenida en el tiempo de los sensores de RNA juega un rol en el desarrollo de patologías autoinflamatorias y autoinmunes. Nuestros resultados sugieren que las RNasas extracelulares probablemente sean un brazo del sistema inmune innato que regula los niveles de exRNAs endógenos no vesiculares evitando que se desencadenen estas respuestas patológicas. Apoyando esto, se ha observado que la administración exógena de RNasa reduce la inflamación en modelos de isquemia/reperfusión[138,210] y traumatismo encéfalocraniano[211] mientras que la sobreexpresión de RNasa mejora la sobrevida en un modelo de LES que sobre expresa TLR7.[139] En humanos, la inflamación estéril y liberación de complejos ribonucleoprotéicos al espacio extracelular está implicada en la desarrollo y patogenia del LES.[212,213] En este sentido, ensayos clínicos con RNasas ingenierzadas han mostrado eficacia en esta y otras enfermedades autoinmunes, posiblemente al remover algunos nV-exRNAs que estén ocasionando inflamación.[214,215]

En los experimentos *in vivo* en ratón, observamos que la inyección de exRNAs desnudos por vía intravenosa indujo la activación de células inmunes innatas y adaptativas del bazo y, en el caso de los linfocitos B y T, estos efectos se ven fuertemente potenciados por la inhibición de las RNasas extracelulares que circulan en la sangre. Sin embargo, en el peritoneo los efectos inflamatorios de exRNA desnudos fueros independientes de la inhibición de las RNasas extracelulares. En acuerdo con esto, determinamos que la actividad RNasa del fluido peritoneal es significativamente menor a la del suero. Estos resultados sugieren que en el organismo existen compartimentos, tejido y órganos con diferente actividad RNasa extracelular, y que esto podría correlacionar con la conveniencia o no del uso de los RNAs extracelulares para la vigilancia inmunológica en dichos compartimientos. En aquellos con baja actividad RNasa es posible concebir que la comunicación intercelular mediada por nV-exRNAs liberados por el propio organismo o por patógenos sea clave. En este sentido, los ganglios linfáticos, la dermis y ciertos músculos -sitios clave de vigilancia inmunológica e inicio de respuestas frente a patógenos- parecen presentar una baja actividad de RNasas, ya que se ha detectado traducción tras la inyección de mRNAs desnudos.[203,216,217]

En conjunto, y en contraste con lo que se consideraba previamente, los resultados de esta tesis de doctorado demuestran que el exRNA desnudo es bioactivo por sí mismo y no requiere encapsulación en vesículas lipídicas, sintéticas o biológicas, para su captación y funcionalidad celular. Estos hallazgos respaldan fuertemente la hipótesis de una forma de comunicación intercelular mediada por exRNAs desnudos que está supeditada a la presencia/ausencia de RNasas. Además, nuestros estudios aportan evidencia de que las múltiples RNasas presentes en el espacio extracelular podrían haber evolucionado como un mecanismo para controlar y regular los niveles de exRNAs desnudos circulantes, ya sea de origen endógeno o patógeno, y así evitar respuestas inflamatorias sistémicas que podrían contribuir a desencadenar o exacerbar patologías autoinflamatorias o autoinmunes.

El artículo 3 de esta tesis es un protocolo extraído en parte del artículo 1, que resulta conveniente para la separación de exRNAs vesiculares y no vesiculares, y, por lo tanto, facilita el estudio de nV-exRNAs. Aunque de utilidad para los investigadores que trabajan en este campo de estudio, no amerita mayores comentarios en esta discusión. El artículo 4 (Anexo 1) es una revisión relevante sobre los sesgos que existen en los distintos métodos de *small RNA sequencing*, sobre todo cuando a partir de sus resultados se intentan explicar observables como la abundancia de distintos RNAs en el medio extracelular que, como dijimos, no pueden entenderse sin un análisis exhaustivo de cuestiones bioquímicas que los métodos de secuenciación no suelen ser capaces de inferir. Dicho artículo se construye sobre experiencia acumulada a lo largo de los años en nuestro laboratorio, mucha de la cual proviene del artículo 1 y del artículo 5 (Anexo 1; PNAS 2023, que ya fue comentado). Además, posee un apartado específico sobre la problemática del estudio de transferencia vertical de RNAs no reguladores, desde los espermatozoides a la progenie, lo cual se ve afectado por estos factores, tomando como modelo de estudio el artículo 6 (Anexo 2), al que contribuí desde el análisis bioinformático de los datos. Como puede verse, los artículos incluidos en el Anexo 1 conforman por tanto una unidad temática coherente con los artículos 1 a 3, dándole forma y unidad a esta tesis doctoral.

Conclusión

Esta tesis abordó el estudio del nV-exRNA y el impacto crucial de las RNasas extracelulares en las transformaciones que sufren los RNAs al ser liberados al medio extracelular. La primera fase de la tesis (artículos 1, 3, 4, 5) abordó esta problemática en cultivos celulares, intentando entender estas transformaciones. La segunda parte de la tesis (artículos 2 y 6) intentaron llevar este conocimiento bioquímico a un contexto biológico, relacionado con la comunicación intercelular en un modelo de herencia epigenética (artículo 6) y, sobre todo, en el contexto de las respuestas inmunológicas mediadas por RNAs extracelulares desnudos (artículo 2). La tesis demostró que nuestras células son capaces de internalizar y sensar RNAs extracelulares no vesiculares, demostrando además que los mismos pueden ser sensados tanto a nivel endosomal como a nivel citosólico, lo que implicaría la existencia de mecanismos de escape endosomal que deben aún esclarecerse. Además, nuestros resultados explican por qué biofluidos como la sangre tendrían tan alta actividad RNasas, ya que estas enzimas parecerían evitar respuestas inflamatorias sistémicas inducidas por RNAs liberados al medio extracelular. El sensado de estas moléculas, sin embargo, posiblemente sea relevante en otros compartimientos del organismo. Algo que, junto con las potenciales aplicaciones biotecnológicas derivadas de estos hallazgos, pretendemos seguir explorando en el futuro inmediato.

Perspectivas

Este trabajo genera nuevas preguntas sobre el papel de la RNasas extracelulares en la comunicación intercelular mediada por nV-exRNAs en situaciones de homeostasis y su papel en el desarrollo de algunas patologías. Además, abre la puerta a posibles nuevas estrategias de terapia basadas en RNA que podrían sortear algunos de los principales problemas que afectan a este campo.

El cáncer es una enfermedad de enorme complejidad, tanto en su origen como en su abordaje terapéutico. Dos características clave de los tumores son su capacidad para estimular la formación de nuevos vasos sanguíneos, con el fin de satisfacer las elevadas demandas metabólicas asociadas al rápido crecimiento celular[218], y la activación de mecanismos de inmunoevasión que dificultan su eliminación por parte del sistema inmune, especialmente por linfocitos T citotóxicos.[219] Las RNasas han sido implicadas en el proceso tumoral, ya que alteraciones en la expresión de estas enzimas se asocian con variaciones en la sobrevida en distintos tipos de cáncer.[146,220] A futuro, resultaría interesante explorar el uso de RI como potencial estrategia terapéutica, dado que podría ejercer un efecto antitumoral dual en modelos murinos de tumores sólidos. Especulo que este efecto antitumoral podría derivarse de dos mecanismos: por un lado, el secuestro de RNasa 5 (Angiogenina) reduciría la neovascularización; por otro, la administración de RI podría estabilizar nV-exRNAs liberados al microambiente tumoral como consecuencia de la muerte celular asociada al crecimiento tumoral. Estos nV-exRNAs podrían ser internalizados tanto por células tumorales como por células inmunes infiltrantes, desencadenando respuestas inflamatorias que favorezcan generar nuevas respuestas adaptativas contra neoantígenos tumorales o la reversión de señales inhibitorias presentes en el microambiente tumoral. Además, el RI podría tener efectos sinérgicos ya que al inhibir la vascularización generaría más muerte celular basal y más liberación de nV-exRNAs. Esta acción dual del RI y la altísima afinidad entre el RI y la RNasa 5 podría resultar en respuestas aún mejores que terapias antitumorales ya aprobadas que solamente inhiben la neovascularización tumoral mediante anticuerpos monoclonales contra VEGF-A (del inglés, *vascular endothelial growth factor A*) o contra su receptor, VEGFR-2 (del inglés, *vascular endothelial growth factor receptor 2*). Considerando estas posibilidades, hemos dado algunos pasos iniciales como la generación de líneas tumorales capaces de secretar RI en el microambiente tumoral, en el caso de tumores murinos generados por inyección de estas células. Nos gustaría investigar si estas líneas, que podrían inducir la secreción condicionada de RI, desarrollan tumores inmunológicamente más calientes y, por consiguiente, de menor tamaño o más susceptibles de ser eliminados en comparación con sus respectivas líneas salvajes.

Otra perspectiva interesante consiste en esclarecer el rol de las RNasas y los nV-exRNA en el desarrollo de patologías autoinmunes y autoinflamatorias. De este trabajo de doctorado y de otros estudios se desprende que una de las funciones principales de las RNasas de la familia A en mamíferos sería degradar exRNAs circulantes y prevenir respuestas inflamatorias patológicas que podrían desencadenar o agravar este tipo de enfermedades. Aunque se han identificado mutaciones en RNasa 5 asociadas con el Parkinson y la esclerosis lateral amiotrófica[221] -dos enfermedades neurológicas con componente inflamatorio en las que los exRNAs podrían desempeñar un papel- no se han hallado, hasta el momento, mutaciones en RNasas de la familia A vinculadas a patologías autoinmunes como el LES. De hecho, ratones *knockout* para RNasa1, si bien presentan niveles reducidos de exRNA circulante, son viables y no desarrollan autoinmunidad. Esto sugiere que las distintas RNasas de la familia A podrían tener funciones complementarias o sinérgicas, lo que explicaría por qué la ausencia de solo una de ellas no es suficiente para generar efectos evidentes. En este sentido, sería interesante desarrollar modelos murinos KO para múltiples RNasas de esta familia o, alternativamente, un ratón transgénico condicionado espacial y temporalmente cuyas células endoteliales expresen y secreten RI a la circulación. En estos ratones sería muy interesante estudiar si desarrollan autoinmunidad y poder cuantificar, identificar y caracterizar nV-exRNAs circulantes clave que puedan estar involucrados en estos procesos.

Esta tesis de doctorado también abre la posibilidad de desarrollar nuevas estrategias terapéuticas basadas en la inhibición de las RNasas y en la administración de mRNAs desnudos con fines terapéuticos, como alternativa a algunas de las plataformas actualmente disponibles. Las terapias basadas en RNA están revolucionado la medicina, como lo evidenció el rotundo éxito de las vacunas de mRNA frente a la COVID-19.[222] Estas vacunas podrían emplearse no solo contra enfermedades infecciosas, sino también en el tratamiento del cáncer mediante vacunas personalizadas.[223] Además, la tecnología de mRNA tendría otras aplicaciones como expresar proteínas faltantes, expresar citoquinas o ser una plataforma para la edición génica mediante

CRISPR/Cas9.[223] No es sorprendente, por tanto, que exista una gran cantidad de ensayos clínicos en curso explorando estas posibilidades.[224] En la actualidad, la mayoría de las terapias con mRNA emplean nanopartículas lipídicas (LNPs) como sistema de *delivery* al interior celular.[225] Sin embargo, los complejos LNP-mRNA son intrínsecamente inflamatorios, debido al reconocimiento del mRNA por sensores de la inmunidad innata, así como debido a la ruptura endosomal que gatillan las LNPs, lo que constituye un paso fundamental que permite la liberación del mRNA al citoplasma. Esta propiedad constituye un arma de doble filo: es beneficiosa en aplicaciones que sí requieren iniciar una respuesta inflamatoria, como en vacunas contra patógenos o tumores, pero representa una limitación en terapias donde es crucial evitar la activación del sistema inmune, como en la edición génica o en la expresión de proteínas terapéuticas.[224] Una posible alternativa es evitar el uso de LNPs y emplear mRNA desnudo. No obstante, los ensayos clínicos realizados hasta el momento con mRNA desnudo han arrojado resultados poco alentadores. En este contexto, sería interesante explorar la viabilidad de coadministrar mRNA desnudo junto con inhibidores de RNasas y compuestos que modulen el escape endosomal sin inducir respuestas inflamatorias exacerbadas. Recientemente, se ha aprobado un proyecto de articulación financiado por ANII que apunta precisamente en esta dirección.

Bibliografía

1. Avery, O. T., Macleod, C. M. & McCarty, M. STUDIES ON THE CHEMICAL NATURE OF THE SUBSTANCE INDUCING TRANSFORMATION OF PNEUMOCOCCAL TYPES : INDUCTION OF TRANSFORMATION BY A DESOXYRIBONUCLEIC ACID FRACTION ISOLATED FROM PNEUMOCOCCUS TYPE III. *J. Exp. Med.* **79**, 137–58 (1944).

2. WATSON, J. D. & CRICK, F. H. C. Molecular Structure of Nucleic Acids: A Structure for Deoxyribose Nucleic Acid. *Nature* **171**, 737–738 (1953).

3. Barbieri, I. & Kouzarides, T. Role of RNA modifications in cancer. *Nat Rev Cancer* 1–20 (2020) doi:10.1038/s41568-020-0253-2.

4. Taoka, M. *et al.* Landscape of the complete RNA chemical modifications in the human 80S ribosome. *Nucleic Acids Res* **46**, gky811- (2018).

5. Cech, T. R. & Steitz, J. A. The Noncoding RNA Revolution—Trashing Old Rules to Forge New Ones. *Cell* **157**, 77–94 (2014).

6. Jia, X. *et al.* Protein translation: biological processes and therapeutic strategies for human diseases. *Signal Transduct. Target. Ther.* **9**, 44 (2024).

7. Villa, T., Pleiss, J. A. & Guthrie, C. Spliceosomal snRNAs. *Cell* **109**, 149–152 (2002).

8. Huang, Z., Du, Y., Wen, J., Lu, B. & Zhao, Y. snoRNAs: functions and mechanisms in biological processes, and roles in tumor pathophysiology. *Cell Death Discov.* **8**, 259 (2022).

9. Guerrier-Takada, C., Gardiner, K., Marsh, T., Pace, N. & Altman, S. The RNA moiety of ribonuclease P is the catalytic subunit of the enzyme. *Cell* **35**, 849–857 (1983).

10. Mattick, J. S. *et al.* Long non-coding RNAs: definitions, functions, challenges and recommendations. *Nat. Rev. Mol. Cell Biol.* **24**, 430–447 (2023).

11. Ivanov, P., Emara, M. M., Villen, J., Gygi, S. P. & Anderson, P. Angiogenin-Induced tRNA Fragments Inhibit Translation Initiation. *Mol. Cell* **43**, 613–623 (2011).

12. Xie, Y. *et al.* Action mechanisms and research methods of tRNA-derived small RNAs. *Signal Transduct Target Ther* **5**, 109 (2020).

13. Anderson, P. & Ivanov, P. tRNA fragments in human health and disease. *FEBS Lett.* **588**, 4297–4304 (2014).

14. Cao, X., Zhang, Y., Ding, Y. & Wan, Y. Identification of RNA structures and their roles in RNA functions. *Nat. Rev. Mol. Cell Biol.* **25**, 784–801 (2024).

15. Tosar, J. P., Witwer, K. & Cayota, A. Revisiting Extracellular RNA Release, Processing, and Function. *Trends Biochem Sci* (2021) doi:10.1016/j.tibs.2020.12.008.

16. Valadi, H. *et al.* Exosome-mediated transfer of mRNAs and microRNAs is a novel mechanism of genetic exchange between cells. *Nat Cell Biol* **9**, 654–659 (2007).

17. Garcia-Silva, M. R. *et al.* Extracellular vesicles shed by Trypanosoma cruzi are linked to small RNA pathways, life cycle regulation, and susceptibility to infection of mammalian cells. *Parasitol. Res.* **113**, 285–304 (2014).

18. Tosar, J. P., García-Silva, M. R. & Cayota, A. Circulating SNORD57 rather than piR-54265 is a promising biomarker for colorectal cancer: common pitfalls in the study of somatic piRNAs in cancer. *Rna* **27**, 403–410 (2020).

19. Skog, J. *et al.* Glioblastoma microvesicles transport RNA and proteins that promote tumour growth and provide diagnostic biomarkers. *Nat. Cell Biol.* **10**, 1470–1476 (2008).

20. Zhang, Q. *et al.* Supermeres are functional extracellular nanoparticles replete with disease biomarkers and therapeutic targets. *Nat Cell Biol* 1–15 (2021) doi:10.1038/s41556-021-00805-8.

21. Cheung, K.-H. *et al.* Extending gene ontology in the context of extracellular RNA and vesicle communication. *J. Biomed. Semant.* **7**, 19 (2016).

22. Murillo, O. D. *et al.* exRNA Atlas Analysis Reveals Distinct Extracellular RNA Cargo Types and Their Carriers Present across Human Biofluids. *Cell* **177**, 463-477.e15 (2019).

23. P., M. & P., M. Les acides nucléiques du plasma sanguin chez l'Homme. *C. R. Seances Soc. Biol. Ses Fil* (1948).

24. Kolodny, G. M., Culp, L. A. & Rosenthal, L. J. Secretion of RNA by normal and transformed cells. *Exp. Cell Res.* **73**, 65–72 (1972).

25. Stroun, M. *et al.* Presence of RNA in the nucleoprotein complex spontaneously released by human lymphocytes and frog auricles in culture. *Cancer Res.* **38**, 3546–54 (1978).

26. Kolodny, G. M. Evidence for transfer of macromolecular RNA between mammalian cells in culture. *Exp. Cell Res.* **65**, 313–324 (1971).

27. Kolodny, G. M. Cell to cell transfer of RNA into transformed cells. *J. Cell. Physiol.* **79**, 147–150 (1972).

28. Niu, M. C., Cordova, C. C., Niu, L. C. & Radbill, C. L. RNA-INDUCED BIOSYNTHESIS OF SPECIFIC ENZYMES*. *Proc. Natl. Acad. Sci.* **48**, 1964–1969 (1962).

29. Zhang, L. *et al.* Microenvironment-induced PTEN loss by exosomal microRNA primes brain metastasis outgrowth. *Nature* **527**, 100–104 (2015).

30. Das, S. *et al.* The Extracellular RNA Communication Consortium: Establishing Foundational Knowledge and Technologies for Extracellular RNA Research. *Cell* **177**, 231–242 (2019).

31. Mateescu, B. *et al.* Phase 2 of extracellular RNA communication consortium charts next-generation approaches for extracellular RNA research. *iScience* **25**, 104653 (2022).

32. Godoy, P. M. *et al.* Large Differences in Small RNA Composition Between Human Biofluids. *Cell Rep.* **25**, 1346–1358 (2018).

33. Akat, K. M. *et al.* Detection of circulating extracellular mRNAs by modified small-RNA-sequencing analysis. *Jci Insight* **4**, e127317 (2019).

34. Freedman, J. E. *et al.* Diverse human extracellular RNAs are widely detected in human plasma. *Nat. Commun.* **7**, 11106 (2016).

35. Srinivasan, S. *et al.* Small RNA Sequencing across Diverse Biofluids Identifies Optimal Methods for exRNA Isolation. *Cell* **177**, 446-462.e16 (2019).

36. Giraldez, M. D. *et al.* Comprehensive multi-center assessment of small RNA-seq methods for quantitative miRNA profiling. *Nat. Biotechnol.* **36**, 746–757 (2018).

37. Mitchell, P. S. *et al.* Circulating microRNAs as stable blood-based markers for cancer detection. *Proc. Natl. Acad. Sci.* **105**, 10513–10518 (2008).

38. Zhou, W. *et al.* Cancer-Secreted miR-105 Destroys Vascular Endothelial Barriers to Promote Metastasis. *Cancer Cell* **25**, 501–515 (2014).

39. Khurana, R. *et al.* Identification of urinary exosomal noncoding RNAs as novel biomarkers in chronic kidney disease. *Rna New York N Y* **23**, 142–152 (2016).

40. Akat, K. M. *et al.* Comparative RNA-sequencing analysis of myocardial and circulating small RNAs in human heart failure and their utility as biomarkers. *Proc. Natl. Acad. Sci.* **111**, 11151–11156 (2014).

41. Zhang, Y. *et al.* Identification and characterization of an ancient class of small RNAs enriched in serum associating with active infection. *J Mol Cell Biol* **6**, 172–174 (2014).

42. Chen, F. *et al.* Circulating exosomal microRNAs as biomarkers of lupus nephritis. *Front. Immunol.* **14**, 1326836 (2023).

43. Heitzer, E., Haque, I. S., Roberts, C. E. S. & Speicher, M. R. Current and future perspectives of liquid biopsies in genomics-driven oncology. *Nat. Rev. Genet.* **20**, 71–88 (2019).

44. Reggiardo, R. E. *et al.* Profiling of repetitive RNA sequences in the blood plasma of patients with cancer. *Nat. Biomed. Eng.* **7**, 1627–1635 (2023).

45. Chai, P., Lebedenko, C. G. & Flynn, R. A. RNA Crossing Membranes: Systems and Mechanisms Contextualizing Extracellular RNA and Cell Surface GlycoRNAs. *Annu. Rev. Genom. Hum. Genet.* **24**, 85–107 (2023).

46. Tosar, J. P. & Cayota, A. Extracellular RNA, Methods and Protocols. *Methods Mol Biology Clifton N J* **1740**, 125–137 (2018).

47. Vickers, K. C., Palmisano, B. T., Shoucri, B. M., Shamburek, R. D. & Remaley, A. T. MicroRNAs are transported in plasma and delivered to recipient cells by high-density lipoproteins. *Nat Cell Biol* **13**, 423–433 (2011).

48. Arroyo, J. D. *et al.* Argonaute2 complexes carry a population of circulating microRNAs independent of vesicles in human plasma. *Proc National Acad Sci* **108**, 5003–5008 (2011).

49. Costa, B. *et al.* Nicked tRNAs are stable reservoirs of tRNA halves in cells and biofluids. *Proc National Acad Sci* **120**, e2216330120 (2023).

50. Mathieu, M., Martin-Jaular, L., Lavieu, G. & Théry, C. Specificities of secretion and uptake of exosomes and other extracellular vesicles for cell-to-cell communication. *Nat Cell Biol* **21**, 9–17 (2019).

51. Colombo, M., Raposo, G. & Théry, C. Biogenesis, Secretion, and Intercellular Interactions of Exosomes and Other Extracellular Vesicles. *Annu Rev Cell Dev Bi* **30**, 1–35 (2014).

52. Kalluri, R. & LeBleu, V. S. The biology, function, and biomedical applications of exosomes. *Science* **367**, eaau6977 (2020).

53. Thomou, T. *et al.* Adipose-derived circulating miRNAs regulate gene expression in other tissues. *Nature* **542**, 450–455 (2017).

54. O'Brien, K., Breyne, K., Ughetto, S., Laurent, L. C. & Breakefield, X. O. RNA delivery by extracellular vesicles in mammalian cells and its applications. *Nat Rev Mol Cell Bio* **21**, 585–606 (2020).

55. Gruner, H. N. & McManus, M. T. Examining the evidence for extracellular RNA function in mammals. *Nat Rev Genet* **22**, 448–458 (2021).

56. Gámbaro, F. *et al.* Stable tRNA halves can be sorted into extracellular vesicles and delivered to recipient cells in a concentration-dependent manner. *Rna Biol* 1–15 (2019) doi:10.1080/15476286.2019.1708548.

57. Mateescu, B. *et al.* Obstacles and opportunities in the functional analysis of extracellular vesicle RNA – an ISEV position paper. *J Extracell Vesicles* **6**, 1286095 (2017).

58. Tkach, M. & Théry, C. Communication by Extracellular Vesicles: Where We Are and Where We Need to Go. *Cell* **164**, 1226–1232 (2016).

59. Williams, Z. *et al.* Comprehensive profiling of circulating microRNA via small RNA sequencing of cDNA libraries reveals biomarker potential and limitations. *Proc. Natl. Acad. Sci.* **110**, 4255–4260 (2013).

60. Chevillet, J. R. *et al.* Quantitative and stoichiometric analysis of the microRNA content of exosomes. *Proc. Natl. Acad. Sci.* **111**, 14888–14893 (2014).

61. Chiou, N.-T., Kageyama, R. & Ansel, K. M. Selective Export into Extracellular Vesicles and Function of tRNA Fragments during T Cell Activation. *Cell Reports* **25**, 3356-3370.e4 (2018).

62. Hoen, E. N. M. N.-'t *et al.* Deep sequencing of RNA from immune cell-derived vesicles uncovers the selective incorporation of small non-coding RNA biotypes with potential regulatory functions. *Nucleic Acids Res.* **40**, 9272–9285 (2012).

63. Temoche-Diaz, M. M. *et al.* Distinct mechanisms of microRNA sorting into cancer cell-derived extracellular vesicle subtypes. *eLife* **8**, e47544 (2019).

64. Villarroya-Beltri, C. *et al.* Sumoylated hnRNPA2B1 controls the sorting of miRNAs into exosomes through binding to specific motifs. *Nat Commun* **4**, 2980 (2013).

65. Garcia-Martin, R. *et al.* MicroRNA sequence codes for small extracellular vesicle release and cellular retention. *Nature* **601**, 446–451 (2021).

66. Théry, C. *et al.* Minimal information for studies of extracellular vesicles 2018 (MISEV2018): a position statement of the International Society for Extracellular Vesicles and update of the MISEV2014 guidelines. *J Extracell Vesicles* **8**, 1535750 (2018).

67. Hoshino, A. *et al.* Tumour exosome integrins determine organotropic metastasis. *Nature* **527**, 329–335 (2015).

68. Turchinovich, A., Weiz, L., Langheinz, A. & Burwinkel, B. Characterization of extracellular circulating microRNA. *Nucleic Acids Res.* **39**, 7223–7233 (2011).

69. Geekiyanage, H., Rayatpisheh, S., Wohlschlegel, J. A., Brown, R. & Ambros, V. Extracellular microRNAs in human circulation are associated with miRISC complexes that are accessible to anti-AGO2 antibody and can bind target mimic oligonucleotides. *Proc National Acad Sci* **117**, 24213–24223 (2020).

70. Tosar, J. P. *et al.* Assessment of small RNA sorting into different extracellular fractions revealed by high-throughput sequencing of breast cell lines. *Nucleic Acids Res.* **43**, 5601–5616 (2015).

71. Tosar, J. P. *et al.* Dimerization confers increased stability to nucleases in 5′ halves from glycine and glutamic acid tRNAs. *Nucleic Acids Res* **46**, gky495- (2018).

72. Shih, J. D. & Hunter, C. P. SID-1 is a dsRNA-selective dsRNA-gated channel. *RNA* **17**, 1057–1065 (2011).

73. Winston, W. M., Sutherlin, M., Wright, A. J., Feinberg, E. H. & Hunter, C. P. Caenorhabditis elegans SID-2 is required for environmental RNA interference. *Proc. Natl. Acad. Sci.* **104**, 10565–10570 (2007).

74. Flynn, R. A. *et al.* Small RNAs are modified with N-glycans and displayed on the surface of living cells. *Cell* (2021) doi:10.1016/j.cell.2021.04.023.

75. Graziano, V. R. *et al.* RNA N-glycosylation enables immune evasion and homeostatic efferocytosis. *Nature* 1–9 (2025) doi:10.1038/s41586-025-09310-6.

76. Park, W. *et al.* Diversity and complexity of cell death: a historical review. *Exp. Mol. Med.* **55**, 1573–1594 (2023).

77. Broz, P. Pyroptosis: molecular mechanisms and roles in disease. *Cell Res.* **35**, 334–344 (2025).

78. Broz, P. & Dixit, V. M. Inflammasomes: mechanism of assembly, regulation and signalling. *Nat Rev Immunol* **16**, 407–420 (2016).

79. Herster, F. *et al.* Neutrophil extracellular trap-associated RNA and LL37 enable self-amplifying inflammation in psoriasis. *Nat Commun* **11**, 105 (2020).

80. Zhang, N. *et al.* Cell surface RNAs control neutrophil recruitment. *Cell* **187**, 846-860.e17 (2024).

81. Murphy, K. & Weaver, C. *Janeway's Immunobiology, 9th Edition*. (Garland Science, 2016).

82. Yin, X., Chen, S. & Eisenbarth, S. C. Dendritic Cell Regulation of T Helper Cells. *Annu. Rev. Immunol.* **39**, 1–32 (2021).

83. Castellano, M. *Estudio de Dos Componentes de Las Defensas Innatas Del Esturión Cultivado En Un Establecimiento de Piscicultura En Uruguay.* 1–69 (2015).

84. Medzhitov, R. & Janeway, C. A. Innate immunity: the virtues of a nonclonal system of recognition. *Cell* **91**, 295–298 (1997).

85. Takeuchi, O. & Akira, S. Pattern Recognition Receptors and Inflammation. *Cell* **140**, 805–820 (2010).

86. Cabeza-Cabrerizo, M., Cardoso, A., Minutti, C. M., Costa, M. P. da & Sousa, C. R. e. Dendritic Cells Revisited. *Annu Rev Immunol* **39**, (2021).

87. An, J., Marwaha, A. & Laxer, R. M. Autoinflammatory Diseases – A Review. *J. Rheumatol.* **51**, jrheum.2023-1209 (2024).

88. Pisetsky, D. S. Pathogenesis of autoimmune disease. *Nat. Rev. Nephrol.* **19**, 1–16 (2023).

89. Moulton, V. R. *et al.* Pathogenesis of Human Systemic Lupus Erythematosus: A Cellular Perspective. *Trends Mol Med* **23**, 615–635 (2017).

90. Gürtler, C. & Bowie, A. G. Innate immune detection of microbial nucleic acids. *Trends Microbiol* **21**, 413–420 (2013).

91. Lind, N. A., Rael, V. E., Pestal, K., Liu, B. & Barton, G. M. Regulation of the nucleic acid-sensing Toll-like receptors. *Nat Rev Immunol* **22**, 224–235 (2022).

92. Liu, L. *et al.* Structural Basis of Toll-Like Receptor 3 Signaling with Double-Stranded RNA. *Science* **320**, 379–381 (2008).

93. Choe, J., Kelker, M. S. & Wilson, I. A. Crystal Structure of Human Toll-Like Receptor 3 (TLR3) Ectodomain. *Science* **309**, 581–585 (2005).

94. Bérouti, M. *et al.* Lysosomal endonuclease RNase T2 and PLD exonucleases cooperatively generate RNA ligands for TLR7 activation. *Immunity* **57**, 1482-1496.e8 (2024).

95. Ostendorf, T. *et al.* Immune Sensing of Synthetic, Bacterial, and Protozoan RNA by Toll-like Receptor 8 Requires Coordinated Processing by RNase T2 and RNase 2. *Immunity* **52**, 591-605.e6 (2020).

96. Greulich, W. *et al.* TLR8 Is a Sensor of RNase T2 Degradation Products. *Cell* **179**, 1264-1275.e13 (2019).

97. Nunes, I. V. *et al.* Bacterial RNA sensing by TLR8 requires RNase 6 processing and is inhibited by RNA 2’O-methylation. *EMBO Rep.* **25**, 4674–4692 (2024).

98. Zhang, Z. *et al.* Structural Analysis Reveals that Toll-like Receptor 7 Is a Dual Receptor for Guanosine and Single-Stranded RNA. *Immunity* **45**, 737–748 (2016).

99. Tanji, H. *et al.* Toll-like receptor 8 senses degradation products of single-stranded RNA. *Nat Struct Mol Biol* **22**, 109–115 (2015).

100. Oldenburg, M. *et al.* TLR13 Recognizes Bacterial 23S rRNA Devoid of Erythromycin Resistance–Forming Modification. *Science* **337**, 1111–1115 (2012).

101. Song, W. *et al.* Structural basis for specific recognition of single-stranded RNA by Toll-like receptor 13. *Nat. Struct. Mol. Biol.* **22**, 782–787 (2015).

102. Rehwinkel, J. & Gack, M. U. RIG-I-like receptors: their regulation and roles in RNA sensing. *Nat Rev Immunol* 1–15 (2020) doi:10.1038/s41577-020-0288-3.

103. Duan, T., Du, Y., Xing, C., Wang, H. Y. & Wang, R.-F. Toll-Like Receptor Signaling and Its Role in Cell-Mediated Immunity. *Front. Immunol.* **13**, 812774 (2022).

104. Joosten, L. A. B., Abdollahi-Roodsaz, S., Dinarello, C. A., O'Neill, L. & Netea, M. G. Toll-like receptors and chronic inflammation in rheumatic diseases: new developments. *Nat. Rev. Rheumatol.* **12**, 344–357 (2016).

105. McNab, F., Mayer-Barber, K., Sher, A., Wack, A. & O'Garra, A. Type I interferons in infectious disease. *Nat. Rev. Immunol.* **15**, 87–103 (2015).

106. Veen, A. G. van der *et al.* The RIG-I-like receptor LGP2 inhibits Dicer-dependent processing of long double-stranded RNA and blocks RNA interference in mammalian cells. *EMBO J.* **37**, EMBJ201797479 (2018).

107. Junior, A. G. D., Sampaio, N. G. & Rehwinkel, J. A Balancing Act: MDA5 in Antiviral Immunity and Autoinflammation. *Trends Microbiol.* **27**, 75–85 (2019).

108. Fitzgerald, K. A. & Kagan, J. C. Toll-like Receptors and the Control of Immunity. *Cell* **180**, 1044–1066 (2020).

109. Mishra, H. *et al.* Disrupted degradative sorting of TLR7 is associated with human lupus. *Sci. Immunol.* **9**, eadi9575 (2024).

110. Brown, G. J. *et al.* TLR7 gain-of-function genetic variation causes human lupus. *Nature* 1–8 (2022) doi:10.1038/s41586-022-04642-z.

111. Souyris, M. *et al.* TLR7 escapes X chromosome inactivation in immune cells. *Sci. Immunol.* **3**, (2018).

112. Giltiay, N. V. *et al.* Overexpression of TLR7 promotes cell-intrinsic expansion and autoantibody production by transitional T1 B cells. *J Exp Med* **210**, 2773–2789 (2013).

113. Hwang, S.-H. *et al.* B Cell TLR7 Expression Drives Anti-RNA Autoantibody Production and Exacerbates Disease in Systemic Lupus Erythematosus–Prone Mice. *J Immunol* **189**, 5786–5796 (2012).

114. Majer, O., Liu, B., Kreuk, L. S., Krogan, N. & Barton, G. M. Unc93b1 recruits Syntenin-1 to dampen TLR7 signaling and prevent autoimmunity. *Nature* **575**, 366–370 (2019).

115. Feng, Y. *et al.* Cardiac RNA Induces Inflammatory Responses in Cardiomyocytes and Immune Cells via Toll-like Receptor 7 Signaling. *J Biol Chem* **290**, 26688–26698 (2015).

116. Cavassani, K. A. *et al.* TLR3 is an endogenous sensor of tissue necrosis during acute inflammatory events. *J Exp Medicine* **205**, 2609–2621 (2008).

117. Cabrera-Fuentes, H. *et al.* Regulation of monocyte/macrophage polarisation by extracellular RNA. *Thromb Haemostasis* **113**, 473–481 (2015).

118. Takahashi, T. *et al.* Cathelicidin promotes inflammation by enabling binding of self-RNA to cell surface scavenger receptors. *Sci Rep-uk* **8**, 4032 (2018).

119. Ganguly, D. *et al.* Self-RNA–antimicrobial peptide complexes activate human dendritic cells through TLR7 and TLR8. *J Exp Medicine* **206**, 1983–1994 (2009).

120. Savarese, E. *et al.* U1 small nuclear ribonucleoprotein immune complexes induce type I interferon in plasmacytoid dendritic cells through TLR7. *Blood* **107**, 3229–3234 (2006).

121. Lau, C. M. *et al.* RNA-associated autoantigens activate B cells by combined B cell antigen receptor/Toll-like receptor 7 engagement. *J Exp Medicine* **202**, 1171–1177 (2005).

122. Sistigu, A. *et al.* Cancer cell–autonomous contribution of type I interferon signaling to the efficacy of chemotherapy. *Nat Med* **20**, 1301–1309 (2014).

123. Tosar, J. P., Cayota, A. & Witwer, K. Exomeres and supermeres: Monolithic or diverse? *J Extracell Biology* **1**, (2022).

124. Roers, A., Hiller, B. & Hornung, V. Recognition of Endogenous Nucleic Acids by the Innate Immune System. *Immunity* **44**, 739–754 (2016).

125. Ontiveros, R. J., Stoute, J. & Liu, K. F. The chemical diversity of RNA modifications. *Biochem J* **476**, 1227–1245 (2019).

126. Li, X., Xiong, X. & Yi, C. Epitranscriptome sequencing technologies: decoding RNA modifications. *Nat Methods* **14**, 23–31 (2016).

127. Karikó, K., Buckstein, M., Ni, H. & Weissman, D. Suppression of RNA Recognition by Toll-like Receptors: The Impact of Nucleoside Modification and the Evolutionary Origin of RNA. *Immunity* **23**, 165–175 (2005).

128. Karikó, K. *et al.* Incorporation of Pseudouridine Into mRNA Yields Superior Nonimmunogenic Vector With Increased Translational Capacity and Biological Stability. *Mol Ther* **16**, 1833–1840 (2008).

129. Pardi, N. *et al.* Nucleoside-modified mRNA vaccines induce potent T follicular helper and germinal center B cell responses. *J Exp Med* **215**, 1571–1588 (2018).

130. Polack, F. P. *et al.* Safety and Efficacy of the BNT162b2 mRNA Covid-19 Vaccine. *N. Engl. J. Med.* **383**, NEJMoa2034577 (2020).

131. Baden, L. R. *et al.* Efficacy and Safety of the mRNA-1273 SARS-CoV-2 Vaccine. *N. Engl. J. Med.* **384**, 403–416 (2020).

132. Liddicoat, B. J. *et al.* RNA editing by ADAR1 prevents MDA5 sensing of endogenous dsRNA as nonself. *Science* **349**, 1115–1120 (2015).

133. George, C. X., Ramaswami, G., Li, J. B. & Samuel, C. E. Editing of Cellular Self-RNAs by Adenosine Deaminase ADAR1 Suppresses Innate Immune Stress Responses. *J Biol Chem* **291**, 6158–6168 (2016).

134. Tang, Q. *et al.* Adenosine-to-inosine editing of endogenous Z-form RNA by the deaminase ADAR1 prevents spontaneous MAVS-dependent type I interferon responses. *Immunity* **54**, 1961-1975.e5 (2021).

135. Roberts, A. W. *et al.* Tissue-Resident Macrophages Are Locally Programmed for Silent Clearance of Apoptotic Cells. *Immunity* **47**, 913-927.e6 (2017).

136. Benner, S. A. & Allemann, R. K. The return of pancreatic ribonucleases. *Trends Biochem. Sci.* **14**, 396–397 (1989).

137. Benner, S. A. Extracellular 'communicator RNA.' *FEBS Lett.* **233**, 225–228 (1988).

138. Cabrera-Fuentes, H. *et al.* RNase1 prevents the damaging interplay between extracellular RNA and tumour necrosis factor-α in cardiac ischaemia/reperfusion injury. *Thromb Haemostasis* **112**, 1110–1119 (2014).

139. Sun, X. *et al.* Increased Ribonuclease Expression Reduces Inflammation and Prolongs Survival in TLR7 Transgenic Mice. *J Immunol* **190**, 2536–2543 (2013).

140. Garnett, E. R. *et al.* Phenotype of ribonuclease 1 deficiency in mice. *Rna* **25**, 921–934 (2019).

141. Jones, W. THE ACTION OF BOILED PANCREAS EXTRACT ON YEAST NUCLEIC ACID. *Am. J. Physiol.-Leg. Content* **52**, 203–207 (1920).

142. Hirs, C. H. W., Moore, S. & Stein, W. H. The Sequence of the Amino Acid Residues in Performic Acid-oxidized Ribonuclease. *J. Biol. Chem.* **235**, 633–647 (1960).

143. Raines, R. T. Ribonuclease A. *Chem. Rev.* **98**, 1045–1066 (1998).

144. FINDLY, D., HERRIES, D. G., MATHIAS, A. P., RABIN, B. R. & ROSS, C. A. The Active Site and Mechanism of Action of Bovine Pancreatic Ribonuclease. *Nature* **190**, 781–784 (1961).

145. KARTHA, G. Tertiary Structure of Ribonuclease. *Nature* **214**, 234–234 (1967).

146. Sun, D., Han, C. & Sheng, J. The role of human ribonuclease A family in health and diseases: A systematic review. *iScience* **25**, 105284 (2022).

147. Cho, S., Beintema, J. J. & Zhang, J. The ribonuclease A superfamily of mammals and birds: identifying new members and tracing evolutionary histories. *Genomics* **85**, 208–220 (2005).

148. Sorrentino, S. The eight human "canonical" ribonucleases: Molecular diversity, catalytic properties, and special biological actions of the enzyme proteins. *Febs Lett* **584**, 2194–2200 (2010).

149. Lomax, J. E., Eller, C. H. & Raines, R. T. Comparative functional analysis of ribonuclease 1 homologs: molecular insights into evolving vertebrate physiology. *Biochem. J.* **474**, 2219–2233 (2017).

150. Cuchillo, C. M. *et al.* The role of 2', 3'-cyclic phosphodiesters in the bovine pancreatic ribonuclease A catalysed cleavage of RNA: intermediates or products? *FEBS Lett.* **333**, 207–210 (1993).

151. Rushizky, G. W., Knight, C. A. & Sober, H. A. Studies on the Preferential Specificity of Pancreatic Ribonuclease as Deduced from Partial Digests. *J. Biol. Chem.* **236**, 2732–2737 (1961).

152. delCardayre, S. B. & Raines, R. T. Structural Determinants of Enzymic Processivity. *Biochemistry* **33**, 6031–6037 (1994).

153. Sorrentino, S. & Libonati, M. Human Pancreatic-Type and Nonpancreatic-Type Ribonucleases: A Direct Side-by-Side Comparison of Their Catalytic Properties. *Arch. Biochem. Biophys.* **312**, 340–348 (1994).

154. Sorrentino, S. Human extracellular ribonucleases: multiplicity, molecular diversity and catalytic properties of the major RNase types. *Cell Mol Life Sci Cmls* **54**, 785–794 (1998).

155. Loveland, A. B., Koh, C. S., Ganesan, R., Jacobson, A. & Korostelev, A. A. Structural mechanism of angiogenin activation by the ribosome. *Nature* **630**, 769–776 (2024).

156. FUTAMI, J. *et al.* Tissue-Specific Expression of Pancreatic-Type RNases and RNase Inhibitor in Humans. *DNA Cell Biol.* **16**, 413–419 (1997).

157. Uhlén, M. *et al.* Tissue-based map of the human proteome. *Science* **347**, 1260419 (2015).

158. Landré, J. B. P. *et al.* Human endothelial cells selectively express large amounts of pancreatic-type ribonuclease (RNase 1). *J. Cell. Biochem.* **86**, 540–552 (2002).

159. Fischer, S. *et al.* Expression and localisation of vascular ribonucleases in endothelial cells. *Thromb. Haemost.* **105**, 345–355 (2011).

160. Lu, L., Li, J., Moussaoui, M. & Boix, E. Immune Modulation by Human Secreted RNases at the Extracellular Space. *Front Immunol* **9**, 1012 (2018).

161. Becknell, B. *et al.* Ribonucleases 6 and 7 have antimicrobial function in the human and murine urinary tract. *Kidney Int* **87**, 151–161 (2015).

162. Becknell, B., Ching, C. & Spencer, J. D. The Responses of the Ribonuclease A Superfamily to Urinary Tract Infection. *Front. Immunol.* **10**, 2786 (2019).

163. Cortado, H. *et al.* Murine Ribonuclease 6 Limits Bacterial Dissemination during Experimental Urinary Tract Infection. *J. Innate Immun.* **16**, 283–294 (2024).

164. Yang, D. *et al.* Eosinophil-derived neurotoxin acts as an alarmin to activate the TLR2–MyD88 signal pathway in dendritic cells and enhances Th2 immune responses. *J Exp Medicine* **205**, 79–90 (2008).

165. Botos, I., Segal, D. M. & Davies, D. R. The Structural Biology of Toll-like Receptors. *Structure* **19**, 447–459 (2011).

166. Garnett, E. R. & Raines, R. T. Emerging biological functions of ribonuclease 1 and angiogenin. *Crit Rev Biochem Mol* **57**, 244–260 (2021).

167. Chao, T.-Y. & Raines, R. T. Mechanism of Ribonuclease A Endocytosis: Analogies to Cell-Penetrating Peptides. *Biochemistry* **50**, 8374–8382 (2011).

168. Tsuji, T. *et al.* Angiogenin Is Translocated to the Nucleus of HeLa Cells and Is Involved in Ribosomal RNA Transcription and Cell Proliferation. *Cancer Res.* **65**, 1352–1360 (2005).

169. Fu, H. *et al.* Stress induces tRNA cleavage by angiogenin in mammalian cells. *FEBS Lett.* **583**, 437–442 (2009).

170. Yamasaki, S., Ivanov, P., Hu, G. & Anderson, P. Angiogenin cleaves tRNA and promotes stress-induced translational repression. *J. Cell Biol.* **185**, 35–42 (2009).

171. Kobe, B. & Deisenhofer, J. Crystal structure of porcine ribonuclease inhibitor, a protein with leucine-rich repeats. *Nature* **366**, 751–756 (1993).

172. Dickson, K. A., Haigis, M. C. & Raines, R. T. Ribonuclease Inhibitor: Structure and Function. *Prog. Nucleic Acid Res. Mol. Biol.* **80**, 349–374 (2005).

173. Rutkoski, T. & Raines, R. Evasion of Ribonuclease Inhibitor as a Determinant of Ribonuclease Cytotoxicity. *Curr. Pharm. Biotechnol.* **9**, 185–199 (2008).

174. Leland, P. A., Schultz, L. W., Kim, B.-M. & Raines, R. T. Ribonuclease A variants with potent cytotoxic activity. *Proc. Natl. Acad. Sci.* **95**, 10407–10412 (1998).

175. Thomas, S. P., Hoang, T. T., Ressler, V. T. & Raines, R. T. Human angiogenin is a potent cytotoxin in the absence of ribonuclease inhibitor. *Rna* **24**, 1018–1027 (2018).

176. Thomas, S. P., Kim, E., Kim, J.-S. & Raines, R. T. Knockout of the Ribonuclease Inhibitor Gene Leaves Human Cells Vulnerable to Secretory Ribonucleases. *Biochemistry-us* **55**, 6359–6362 (2016).

177. Kim, B., Schultz, L. W. & Raines, R. T. Variants of ribonuclease inhibitor that resist oxidation. *Protein Sci.* **8**, 430–434 (1999).

178. Hoang, T. T. & Raines, R. T. Molecular basis for the autonomous promotion of cell proliferation by angiogenin. *Nucleic Acids Res.* **45**, 818–831 (2017).

179. Suen, A. O. *et al.* Extracellular RNA Sensing Mediates Inflammation and Organ Injury in a Murine Model of Polytrauma. *J. Immunol.* **210**, 1990–2000 (2023).

180. Hardin, J. A. *et al.* Antibodies from patients with connective tissue diseases bind specific subsets of cellular RNA-protein particles. *J Clin Invest* **70**, 141–147 (1982).

181. Lerner, M. R. & Steitz, J. A. Antibodies to small nuclear RNAs complexed with proteins are produced by patients with systemic lupus erythematosus. *Proc National Acad Sci* **76**, 5495–5499 (1979).

182. Rinke, J. & Steitz, J. A. Association of the lupus antigen La with a subset of U6 snRNA molecules. *Nucleic Acids Res* **13**, 2617–2629 (1985).

183. Dowdy, S. F. Overcoming cellular barriers for RNA therapeutics. *Nat. Biotechnol.* **35**, 222–229 (2017).

184. Sha, W. *et al.* Human NLRP3 inflammasome senses multiple types of bacterial RNAs. *Proc National Acad Sci* **111**, 16059–16064 (2014).

185. Nguyen, T. A. *et al.* SIDT2 Transports Extracellular dsRNA into the Cytoplasm for Innate Immune Recognition. *Immunity* **47**, 498-509.e6 (2017).

186. Aizawa, S. *et al.* Lysosomal putative RNA transporter SIDT2 mediates direct uptake of RNA by lysosomes. *Autophagy* **12**, 565–578 (2016).

187. Nguyen, T. A. *et al.* SIDT1 Localizes to Endolysosomes and Mediates Double-Stranded RNA Transport into the Cytoplasm. *J Immunol* **202**, 3483–3492 (2019).

188. Ganesan, D. & Cai, Q. Understanding amphisomes. *Biochem. J.* **478**, 1959–1976 (2021).

189. Wickman, G. R. *et al.* Blebs produced by actin–myosin contraction during apoptosis release damage-associated molecular pattern proteins before secondary necrosis occurs. *Cell Death Differ.* **20**, 1293–1305 (2013).

190. Green, D. R. A Matter of Life and Death. *Cold Spring Harb. Perspect. Biol.* **14**, (2022).

191. Wang, W., Li, T. & Wu, K. Cell death in tumor microenvironment: an insight for exploiting novel therapeutic approaches. *Cell Death Discov.* **11**, 93 (2025).

192. Mistry, P. & Kaplan, M. J. Cell death in the pathogenesis of systemic lupus erythematosus and lupus nephritis. *Clin. Immunol.* **185**, 59–73 (2017).

193. Suzuki, T. The expanding world of tRNA modifications and their disease relevance. *Nat Rev Mol Cell Bio* **22**, 375–392 (2021).

194. Gutierrez, C. S. *et al.* Pseudouridine Residues as Substrates for Serum Ribonucleases. *bioRxiv* 2025.06.18.660232 (2025) doi:10.1101/2025.06.18.660232.

195. Grote, K. *et al.* Extracellular Ribosomal RNA Acts Synergistically with Toll-like Receptor 2 Agonists to Promote Inflammation. *Cells* **11**, 1440 (2022).

196. Fischer, S. *et al.* Self-extracellular RNA promotes pro-inflammatory response of astrocytes to exogenous and endogenous danger signals. *J Neuroinflamm* **18**, 252 (2021).

197. Noll, F. *et al.* Self-extracellular RNA acts in synergy with exogenous danger signals to promote inflammation. *Plos One* **12**, e0190002 (2017).

198. Chen, C. *et al.* Role of Extracellular RNA and TLR3-Trif Signaling in Myocardial Ischemia–Reperfusion Injury. *J Am Heart Assoc* **3**, e000683 (2014).

199. Rennick, J. J., Johnston, A. P. R. & Parton, R. G. Key principles and methods for studying the endocytosis of biological and nanoparticle therapeutics. *Nat Nanotechnol* **16**, 266–276 (2021).

200. Bertheloot, D. *et al.* RAGE Enhances TLR Responses through Binding and Internalization of RNA. *J. Immunol.* **197**, 4118–4126 (2016).

201. Park, R. J. *et al.* Dynamin triple knockout cells reveal off target effects of commonly used dynamin inhibitors. *J. Cell Sci.* **126**, 5305–5312 (2013).

202. Diken, M. *et al.* Selective uptake of naked vaccine RNA by dendritic cells is driven by macropinocytosis and abrogated upon DC maturation. *Gene Ther* **18**, 702–708 (2011).

203. Selmi, A. *et al.* Uptake of synthetic naked RNA by skin-resident dendritic cells via macropinocytosis allows antigen expression and induction of T-cell responses in mice. *Cancer Immunol Immunother* **65**, 1075–1083 (2016).

204. Juliano, R. L. Intracellular Trafficking and Endosomal Release of Oligonucleotides: What We Know and What We Don't. *nucleic acid Ther.* **28**, 166–177 (2018).

205. Dowdy, S. F. Endosomal escape of RNA therapeutics: How do we solve this rate-limiting problem? *RNA* **29**, rna.079507.122 (2023).

206. Chatterjee, S., Kon, E., Sharma, P. & Peer, D. Endosomal escape: A bottleneck for LNP-mediated therapeutics. *Proc. Natl. Acad. Sci.* **121**, e2307800120 (2024).

207. Dowdy, S. F., Setten, R. L., Cui, X.-S. & Jadhav, S. G. Delivery of RNA Therapeutics: The Great Endosomal Escape! *nucleic acid Ther.* **32**, 361–368 (2022).

208. Gomez-Diaz, C. *et al.* RNase T2 restricts TLR13-mediated autoinflammation in vivo. *J. Exp. Med.* **222**, e20241424 (2025).

209. Liu, K. *et al.* Skewed endosomal RNA responses from TLR7 to TLR3 in RNase T2-deficient macrophages. *Int. Immunol.* **33**, 479–490 (2021).

210. Ma, G. *et al.* Ribonuclease attenuates hepatic ischemia reperfusion induced cognitive impairment through the inhibition of inflammatory cytokines in aged mice. *Biomed Pharmacother* **90**, 62–68 (2017).

211. Krämer, T. J. *et al.* Ribonuclease-1 treatment after traumatic brain injury preserves blood–brain barrier integrity and delays secondary brain damage in mice. *Sci. Rep.* **12**, 5731 (2022).

212. Doedens, J. R. *et al.* Blood-Borne RNA Correlates with Disease Activity and IFN-Stimulated Gene Expression in Systemic Lupus Erythematosus. *J. Immunol.* **197**, 2854–2863 (2016).

213. Dou, D. R. *et al.* Xist ribonucleoproteins promote female sex-biased autoimmunity. *Cell* **187**, 733-749.e16 (2024).

214. Burge, D. J., Werth, V. P., Boackle, S. A. & Posada, J. Evaluation of RNase therapy in systemic lupus erythematosus: a randomised phase 2a clinical trial of RSLV-132. *Lupus Sci. Med.* **11**, e001113 (2024).

215. Posada, J. *et al.* Improvement of Severe Fatigue Following Nuclease Therapy in Patients With Primary Sjögren's Syndrome: A Randomized Clinical Trial. *Arthritis Rheumatol.* **73**, 143–150 (2021).

216. Kreiter, S. *et al.* Intranodal Vaccination with Naked Antigen-Encoding RNA Elicits Potent Prophylactic and Therapeutic Antitumoral Immunity. *Cancer Res* **70**, 9031–9040 (2010).

217. Wolff, J. A. *et al.* Direct Gene Transfer into Mouse Muscle in Vivo. *Science* **247**, 1465–1468 (1990).

218. Hanahan, D. & Weinberg, R. A. Hallmarks of Cancer: The Next Generation. *Cell* **144**, 646–674 (2011).

219. Hanahan, D. Hallmarks of Cancer: New Dimensions. *Cancer Discov.* **12**, 31–46 (2022).

220. Győrffy, B. Integrated analysis of public datasets for the discovery and validation of survival-associated genes in solid tumors. *Innov.* **5**, 100625 (2024).

221. Es, M. A. van *et al.* Angiogenin variants in Parkinson disease and amyotrophic lateral sclerosis. *Ann. Neurol.* **70**, 964–973 (2011).

222. Parhiz, H., Atochina-Vasserman, E. N. & Weissman, D. mRNA-based therapeutics: looking beyond COVID-19 vaccines. *Lancet* **403**, 1192–1204 (2024).

223. Qin, S. *et al.* mRNA-based therapeutics: powerful and versatile tools to combat diseases. *Signal Transduct. Target. Ther.* **7**, 166 (2022).

224. Shi, Y., Shi, M., Wang, Y. & You, J. Progress and prospects of mRNA-based drugs in pre-clinical and clinical applications. *Signal Transduct. Target. Ther.* **9**, 322 (2024).

225. Hou, X., Zaks, T., Langer, R. & Dong, Y. Lipid nanoparticles for mRNA delivery. *Nat Rev Mater* **6**, 1–17 (2021).

Anexo 1: Artículos relacionados a la temática del doctorado que no forman parte de la tesis por compendio de artículos

Artículo 4: Small RNA structural biochemistry in a post-sequencing era.

nature protocols

Perspective

https://doi.org/10.1038/s41596-023-00936-2

Small RNA structural biochemistry in a post-sequencing era

Received: 23 February 2023

Accepted: 25 August 2023

Published online: 6 December 2023

Check for updates

Juan Pablo Tosar [1,2] ✉, Mauricio Castellano [1,3], Bruno Costa [1,2] & Alfonso Cayota [1,4]

High-throughput sequencing has had an enormous impact on small RNA research during the past decade. However, sequencing only offers a one-dimensional view of the transcriptome and is often highly biased. Additionally, the 'sequence, map and annotate' approach, used widely in small RNA research, can lead to flawed interpretations of the data, lacking biological plausibility, due in part to database issues. Even in the absence of technical biases, the loss of three-dimensional information is a major limitation to understanding RNA stability, turnover and function. For example, noncoding RNA-derived fragments seem to exist mainly as dimers, tetramers or as nicked forms of their parental RNAs, contrary to widespread assumptions. In this perspective, we will discuss main sources of bias during small RNA-sequencing, present several useful bias-reducing strategies and provide guidance on the interpretation of small RNA-sequencing results, with emphasis on RNA fragmentomics. As sequencing offers a one-dimensional projection of a four-dimensional reality, prior structure-level knowledge is often needed to make sense of the data. Consequently, while less-biased sequencing methods are welcomed, integration of orthologous experimental techniques is also strongly recommended.

Small RNAs are more than just short sequences composed of A, C, G and U. They are integral constituents of complex gene regulatory pathways shaped by evolution. Although exceptions do exist, such as the noncanonical biogenesis of miR-451 (ref. 1), a rule of thumb is to always consider small RNAs in their biological context.

For the three main small RNA classes (small interfering RNAs, microRNAs (miRNAs) and PIWI-interacting RNAs (piRNAs)), biogenesis and effector pathways are reasonably well understood and several updated reviews are available[1,2]. In addition, high-throughput sequencing (HTS) has shown the ubiquity of a new small RNA class composed of noncoding RNA fragments[3]. Among the members of this newly defined (but evolutionary ancestral) small RNA class, tRNA-derived fragments (tDRs) are undoubtedly the best studied. These fragments have been shown to participate in a variety of cellular processes, from translation regulation to epigenetic inheritance.[4]

Recent reports have shown that many tDRs might correspond to in vitro-dissociated nicked tRNAs[5,6], which are stable intermediates of tRNA fragmentation[5–8]. This example illustrates an important caveat of conventional small RNA-sequencing (RNA-seq): it is constrained to one-dimensional (1D) information and often fails to provide the structural insights that would be needed to interpret sequencing data correctly. To address this issue, several structure probing methods have been developed to identify solvent-accessible regions by HTS[9]. However, these methods have several limitations, especially when it comes to handling transient and long-range RNA interactions[9]. Better and less-biased sequencing methods can provide a more comprehensive

[1]Functional Genomics Laboratory, Institut Pasteur de Montevideo, Montevideo, Uruguay. [2]Analytical Biochemistry Unit, Center for Nuclear Research, School of Science, Universidad de la República, Montevideo, Uruguay. [3]Biochemistry Department, School of Science, Universidad de la República, Montevideo, Uruguay. [4]Hospital de Clínicas, Universidad de la República, Montevideo, Uruguay. ✉e-mail: jptosar@pasteur.edu.uy

153

view of the small RNA transcriptome[3]. Nevertheless, prior knowledge and understanding of the underlying biochemistry is essential to make sense of the data.

In the following sections, we briefly discuss the main sources of bias in small RNA-seq. We then highlight other potential issues, such as contamination and erroneous sequence annotations. Finally, we show the importance of obtaining structure-level information for the correct interpretation of sequence-level HTS results.

Sources of bias in small RNA-seq library preparation

Inferring RNA abundance from RNA-seq data has two major problems.[3] The first is that sequencing is not an absolute quantification technique. Irrespective of the normalization method, read counts of any given RNA will be affected by variations in the levels of other abundant species. The second problem is that all RNA-seq methods are biased and fail to provide an accurate representation of the small RNA content of any given sample. As such, within-sample relative abundances are unreliable. In other words, 'A' can be more abundant than 'B', despite 'B' producing a higher number of reads. Fortunately, between-sample comparisons tend to be highly reproducible[10]. As most studies focus on differential expression (comparing treated versus control samples), this is reassuring. Although no single method is bias-free, several improvements (Table 1) have allowed small RNA-seq methods to become more quantitatively reliable, as reviewed in the following sections.

Biases introduced during adapter ligation

During library preparation, sequencing adapters need to be attached to the RNA's 5′ and 3′ ends. The 3′ adapter provides a binding site to initiate reverse transcription, while both adapters provide sites for PCR amplification and the addition of platform-specific sequences. Adapters can be efficiently attached to RNA molecules by using a combination of phage RNA ligases (Fig. 1a,b). This ligation-based approach is used in several popular small RNA-seq library preparation kits (Fig. 1m). We refer to these methods as 'miRNA-seq', due to their capacity to capture miRNAs efficiently, at the expense of other small RNAs.

Adapter ligation presents two important problems. First, it requires specific end chemistries in the input RNA. Second, ligation efficiencies are strongly sequence dependent, introducing a strong bias in the process[11]. As such, overestimation or underestimation of RNA abundance can be as high as 10,000 fold (ref. 10). At least in part, this can be addressed by the use of adapters containing terminal randomized bases[10] (Fig. 1i), such as those used in Absolute Quantification sequencing[12] (AQRNA-seq; Fig. 1n) or in commercial kits such as PerkinElmer's NEXTFLEX Small RNA-seq v3 (Fig. 1m). It should be noted that the new version of this kit (v4) no longer employs degenerated adapters. Another way to minimize ligase-dependent biases is to maximize ligation efficiency using molecular crowding agents (e.g., polyethylene glycol) while optimizing adapter concentration and incubation times[13,14] (Table 1).

Ligase-free methods also avoid this source of bias. RNA can be enzymatically polyadenylated to attach an oligo(dT)-containing 3′ adapter during reverse transcription[15] (Fig. 1d). Subsequently, 5′ adapters can be attached to the 3′ end of the cDNA in a ligase-free manner using the SMART method[16] (Fig. 1c). This method requires the terminal transferase (TT) activity shown by several reverse transcriptases (RTs), which can add a few nontemplated nucleotides to the cDNA's 3′ end. Subsequently, a template-switching oligonucleotide containing the desired 5′ adapter sequence plus three terminal RNA guanine moieties pairs with the cDNAs containing nontemplated Cs added by the TT activity of the RT. Then, the RT extends the cDNA, using the template-switching oligonucleotide as the new template. This process is often called 'template-switching', although we will refer to it as template jumping (for reasons explained in ref. 17). It should be noted that the addition of nontemplated nucleotides is influenced by the sequence composition and the 5′ end chemistry of the RNA[18], which could constitute a potential source of bias. The polyadenylation step can also affect the performance of these methods[19].

An alternative to Poly(A) tailing is to attach the 3′ adaptor using the template-jumping activity of retroelement-derived RTs such as the Thermostable Group II Intron RT (TGIRT)[20–22] or the *Bombyx mori* BoMoC[17] (Fig. 1f). Template jumping is defined as the ability of an RT to extend a cDNA using a new RNA molecule as the template, when only a few base pairs exist between the cDNA and the 3′ end of the new RNA template (a configuration that would only be stable within the enzyme active site)[17]. A variation of the TT activity-based SMART method[16] can be combined with the aforementioned 3′ adapter attachment strategy to add both 5′ and 3′ adapters in a protocol comprising two sequential template-jumping steps[17] (OTTR-seq; Fig. 1n).

DNA ligases can be used to ligate 5′ adapters to the 3′ end of the cDNAs (Fig. 1e,h). This strategy is used, for example, in some versions of TGIRT-seq[22,23] and in AQRNA-seq[12] (Fig. 1n). Alternatively, circularization of the cDNA bypasses the need to attach a 5′ adapter[20,21,24,25] (Fig. 1g). However, in both cases, the 5′ end of a read no longer corresponds to the 5′ end of the sequenced small RNA, due to the possibility of having shortened cDNAs caused by premature RT stops[21].

Although ligase-free methods are considered 'low bias', they are not entirely bias free. For example, there are reported sequence biases associated with the template-jumping reaction[20,23]. Additionally, nontemplated nucleotides added by the TT activity of retroviral RTs are also affected by the RNA's 5′ sequence content[18]. Of note, AQRNA-seq is ligationbased but still showed excellent quantitative responses when benchmarked against several commercial methods[12], probably due to the addition of several other bias-reducing steps, such as degenerated adapters and RNA demethylation (Fig. 1n). However, it has not yet been benchmarked against other low-bias methods such as TGIRT-seq[20,23] or OTTR-seq[17]. It is therefore still not possible to say that one specific adapter attachment strategy is superior to the others, as the overall performance of each method depends on multiple factors.

Effect of modified bases

Noncoding RNAs are heavily posttranscriptionally modified. Several of these modifications can abort reverse transcription. As a consequence, transcripts containing 'hard-stop' modifications can either disappear from the sequencing output[26] or appear as shorter transcripts in circularization-based protocols that avoid 5′ adapter ligation[21]. Compared with retroviral RTs, TGIRT has the ability to read through these modified bases (Fig. 1j), enabling base modifications to be identified by misincorporation analysis[24]. Alternatively, treating the RNA with the demethylase AlkB can remove several of the roadblocks that impair efficient reverse transcription (Fig. 1l). This strategy has been successfully implemented both with TGIRT[21,27] and retroviral RTs[12,26,28]. However, the impact of AlkB treatment in the overall performance of several other tRNA-seq methods was not dramatic[24,29]. Additionally, RNA fragmentation can occur during incubation with AlkB and complicate data interpretation[3,12,28].

Effects of RNA structure

Highly structured RNAs (e.g., tRNAs) are not efficiently reverse transcribed unless the RT reaction is done at high temperatures (≥50 °C). This requires engineered RT enzymes with increased thermostability such as TGIRT[21,24], PrimeScript[12] and Superscript III[30] or IV[5]. For example, tRNA halves have been reported as major constituents of extracellular vesicles in several studies using conventional small RNA-seq[31–33]. However, TGIRT-seq later showed that full-length tRNAs (rather than tDRs) are the most abundant transcripts in extracellular vesicles[34], consistent with data obtained by northern blot[35]. This example illustrates how some sequencing library preparation methods can provide radically different pictures of the RNA content of a sample by failing to capture certain RNA types.

154

Table 1 | Problems and biases in standard small RNA-seq (miRNA-seq) and potential solutions to minimize bias

Process	Problem	Solutions
Ligation of the 3′ adapter	RNA ligases have strong sequence biases[11]	Use adapters with randomized terminal bases to mitigate T4 RNA ligase-induced biases[10,12]
		Optimize adapter ligation conditions[13,14]
		Use ligase-free approaches, such as: (i) Poly(A) tailing and an oligo(dT)-modified 3′ adapter to prime reverse transcription[15] or (ii) template jumping by retroelement-derived RTs[17,20–22]
	Requires a 3′-OH termini in the RNA	T4 PNK treatment converts 3′-P and 3′-cP into 3′-OH, enabling detection of RNA fragments (e.g., tDRs)[27,28,38,40]
		Lowering salt concentration enhances 3′ adapter attachment based on the template jumping activity of TGIRT in 2′-O-methylated transcripts (e.g., piRNAs) or transcripts ending in 3′-P (or 3′-cP) (e.g., tDRs)[58]
Ligation of the 5′ adapter	RNA ligases have strong sequence biases[11]	Use adapters with randomized terminal bases to mitigate T4 RNA ligase-induced biases[10,12]
		Optimize adapter ligation conditions[13,14]
		Use ligase-free approaches, such as: (i) variations of the SMART method[16], exploiting the TT activity exhibited by several RTs[15–17], (ii) ligate a 5′ DNA adapter to the 3′ end of the cDNA using T4 DNA ligase[12] and (iii) circularize the cDNA to bypass the need for a 5′ adapter[20,21,24,25]
	Requires a 5′-P termini in the RNA	T4 PNK treatment, in the presence of ATP, converts 5′-OH into 5′-P, enabling detection of RNA fragments (e.g., tDRs)[27,28,38,40]
		Pyrophosphatases (e.g., RppH) can convert 5′-PPP into 5′-P (ref. 59)
Reverse transcription	Base modifications can induce RT stops	Use RTs that can read through modified bases (e.g., TGIRT)[20,23,24]
		Enzymatically remove problematic modifications (e.g., AlkB treatment)[12,21,26–28]
	Structured RNAs might not be efficiently reverse transcribed	Use thermostable RTs (e.g., TGIRT, Superscript III, Superscript IV)[5,21,24,30,34]
		Hydrolyze RNA and sequence the fragments[36]
Analysis	Contamination can lead to erroneous conclusions	Beware low-input samples, which are contamination prone[60]
		Check potential sources of contamination, including media, plastics and reagents[42]. If possible, sequence blank samples with spike-ins
	Transcriptomic databases contain erroneous entries[44,47]	Use curated databases (e.g., MirGeneDB for miRNAs)[44]
		Consider biological plausibility: are sequencing results consistent with what is known about the biogenesis of this specific small RNA family?
		Always do a Basic Local Alignment Search Tool (BLAST) search to identify potential alternative annotations, and explore the genomic loci that could have produced the sequence under study: what else is encoded in that genomic region?[48]
Small RNA-seq (all steps)	RNAs with short half-lives are not sequenced	Use RNase inhibitors to understand what is lost due to RNases[35,54]
		Think about survivorship bias when the existence of undetectable RNAs could change conclusions (e.g., extracellular RNAs)[61]
	Intermolecular RNA interactions are lost	Use RNA extraction methods that preserve RNA:RNA interactions[5]
		Use T4 PNK + T4 Rnl1 (or RtcB) to repair nicked RNAs[5]
		Use separation methods to preserve RNA:RNA interactions (e.g., chromatography) to isolate macromolecular complexes before performing sRNA-seq[5,35,54]
		Think about sRNA-seq as a projection of a four-dimensional reality into 1D space, to avoid overinterpretation of sequencing results

Hydro-tRNA-seq bypasses issues related to base modifications and tRNA secondary and tertiary structure by hydrolyzing tRNAs and sequencing their fragments[36]. A size-selection step at the start of the protocol avoids interference of tDRs. However, bioinformatic reconstitution of tRNAs from sequenced fragments is not straightforward due to sequence similarities among tRNAs.

RNA end chemistry

Small RNAs (<200 nt) can be present in the cell as primary transcripts or as processed RNAs. Unprocessed small RNAs are mainly RNA Pol III transcripts bearing a 5′ triphosphate (5′-PPP RNAs) such as the 5S rRNA, YRNAs, intergenic small nucleolar RNAs (snoRNAs), etc. Others, such as small nuclear RNAs (snRNAs), are transcribed by RNA Pol II and bear a (modified) 5′ cap. The 5′-PPP RNAs, either capped or not, are incompatible with protocols requiring the ligation of adapters to both ends of the RNA. In fact, these protocols were designed for capturing 5′ monophosphate-containing miRNAs. However, cellular phosphatases can convert 5′-PPP-RNAs into 5′-P-RNAs, making a fraction of primary transcripts amenable to standard small RNA-seq[37]. This might explain why some 5′ YRNA-derived fragments are efficiently sequenced when using conventional miRNA-seq protocols[31,32].

Most small RNAs must be processed by ribonucleases to acquire their mature, functional form. Depending on the nucleases involved, processed RNAs will have different end chemistries. For example, miRNAs are sequentially processed by Drosha and Dicer, two RNase III enzymes that leave a 5′ monophosphate and a 3′ OH; a characteristic that is exploited by miRNA-seq. Pre-tRNAs contain a 5′ leader and a 3′ trailer sequence that are cleaved by RNase P and tRNase Z, respectively, also leaving a 5′-P and a 3′-OH in the mature tRNA. Then, a CCA sequence is posttranscriptionally added to the 3′ end. While the CCA addition still leaves a 3′-OH that is amenable to adapter ligation, this is impaired by tRNA aminoacylation.

Unlike full-length tRNAs, tDRs are endonucleolytically processed by RNase A family members. These ubiquitous enzymes leave a 3′ cyclic phosphate (3′-cP), which is later converted into a 3′ monophosphate (3′-P), and a 5′-OH. In theory, 5′ tRNA fragments should not appear in the output of miRNA-seq, because they would bear a 5′-P and a 3′-cP; in practice, they do[31,32], perhaps due to exonucleolytic trimming. Nevertheless, tDR diversity increases after treating the RNA with T4 polynucleotide kinase (T4 PNK)[38], an enzyme that converts 3′-cP into 3′-OH and, in the presence of ATP, 5′-OH into 5′-P.

Treatment with T4 PNK therefore makes both 5′ and 3′ coding[39] and noncoding[38,39] RNA fragments amenable to standard adapter ligation protocols (Fig. 1k). This is a key step in methods claiming to provide an unbiased picture of the small RNA transcriptome, such as cP-RNA-seq[38], phospho-RNA-seq[40], Cap-Clip acid pyrophosphatase, T4 PNK and AlkB-facilitated small RNA sequencing (CPA-seq)[27] and panoramic

https://doi.org/10.1038/s41596-023-00936-2

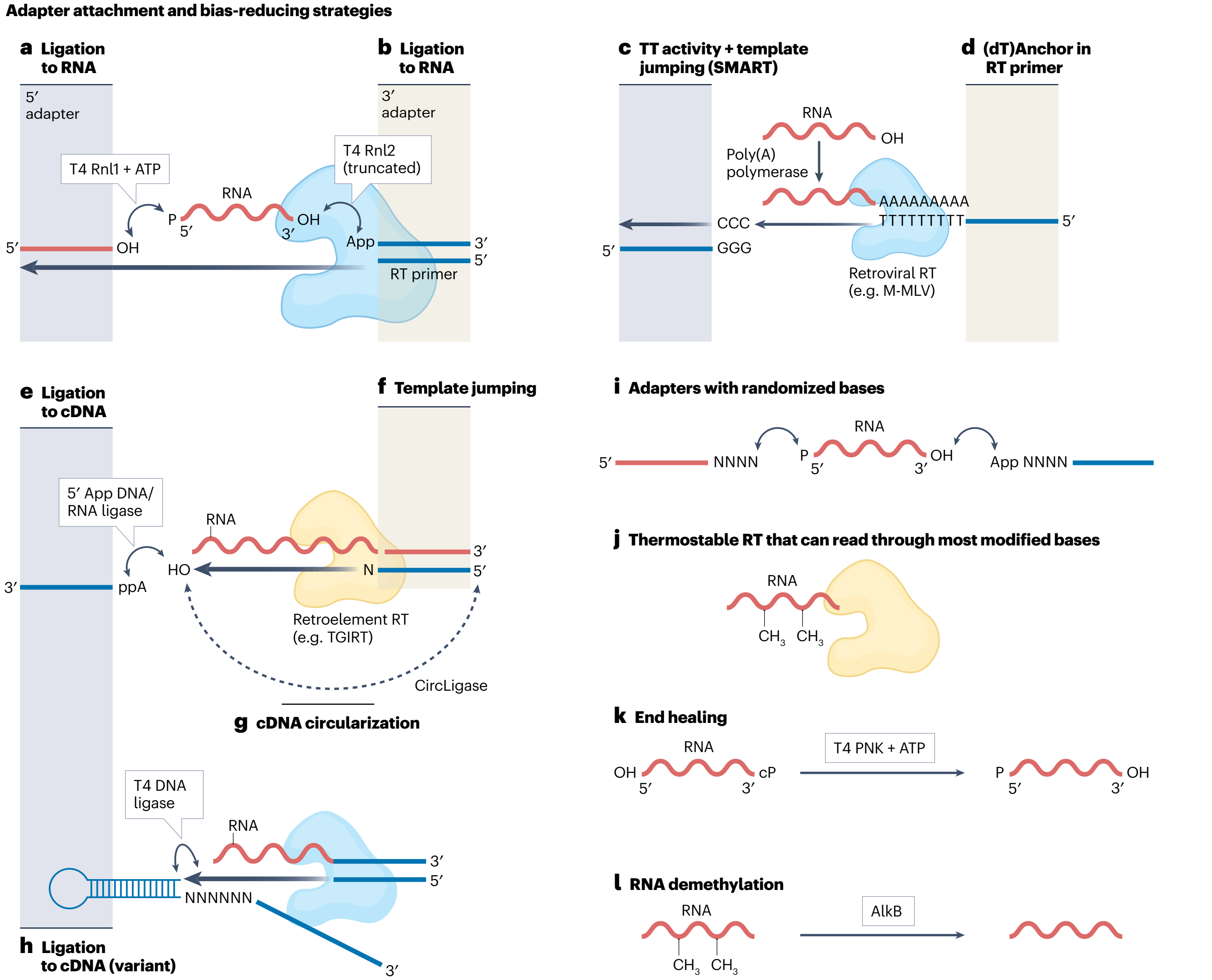

m Strategies used in some popular commercial kits

	3′ adapter	5′ adapter	↓Bias strat.
• Illumina TruSeq • *NEB* NEBNext • Lexogen • *QIAGEN* QIAseq miRNA • TriLink Clean Tag	b	a	
• PerkinElmer NEXTFLEX (v3)	b	a	i
• TakaraBio SMARTer • Diagenode D-Plex	d	c	

n Strategies used in some published low-bias small RNA-seq methods

	3′ adapter	5′ adapter	↓Bias strat.
TGIRT-seq (circ.)[20]	f	g	j
TGIRT-seq[22,23]	f	e	j
AQRNA-seq[12]	b	h	i, l
CPA-seq[27]	b	a	i, j, k, l
PANDORA-seq[28]	b	a	k, l
OTTR-seq[17]	f	c	k, l

Fig. 1 | Overview of small RNA-seq library preparation methods. a–l, Strategies for 3′ adapter attachment (**b**, ligation; **d**, anchored oligo(dT) adapter; **f**, template jumping), 5′ adapter attachment (**a**, ligation; **c**, template switching/jumping; **e**,**h**, ligation to the cDNA) or methodological innovations to reduce sequencing bias (**i**, randomized bases; **j**, thermostable RTs with tolerance to modified bases; **k**, end healing; **l**, removal of RNA modifications). Nucleic acids with RNA backbone (input RNAs and RNA adapters) are depicted in red. Nucleic acids with DNA backbone are depicted in blue. 5′ phosphate and 3′ OH groups are shown only when required for efficient adapter attachment. **m**, Examples of commercial library preparation kits and their adapter attachment or bias-reducing strategies (↓ bias strat.). **n**, Examples of published library preparation methods and their adapter attachment or bias-reducing strategies. Codes in **m** and **n** correspond to strategies depicted in **a**–**l**. App, 5′ pre-adenylated adapter; circ., circularization-based protocol; M-MLV, Moloney murine leukemia virus RT.

RNA display by overcoming RNA modification aborted sequencing (PANDORA-seq)[28] (Fig. 1n). These methods strongly enhance the representation of tDRs and rRNA-derived fragments, including internal tDRs (5′-OH and 3′-cP)[28] that are obscured by traditional methods, at the expense of miRNA-derived reads.

It is not just adaptor ligation-based protocols that are affected by RNA end chemistries. For instance, the terminal (3′) 2′-O-methylation that is characteristic of mammalian piRNAs inhibits TGIRT template jumping[20,22]. The same effect happens with 3′-cP or 3′-P groups, which are characteristic of ncRNA fragments[20,41]. Template jumping at

156

lower salt concentrations reduces these biases, but produces more concatamers due to multiple template switches[41].

Other frequent pitfalls in small RNA-seq

Contamination

Due to the high sensitivity of next-generation sequencing, contamination is a pervasive and often underestimated problem. Low levels of background contaminants can be irrelevant in concentrated samples, but samples containing minute amounts of RNA are particularly vulnerable. Documented sources of contaminating nucleic acids include spin columns, laboratory reagents such as glycogen, FBS and cross-contamination between samples processed in parallel.[42] Even serum-free media formulations can be a source of contaminating miRNAs, due to the use of protein growth factors containing RNA impurities[43].

Erroneous entries in transcriptomic databases

Mapping a read to a transcriptomic database (e.g., miRbase for miRNAs and piRBase for piRNAs) does not mean that such a read was produced from a bona fide miRNA or piRNA, respectively. This is not simply a semantic problem; labeling a sequence as a miRNA, for example, allows several assumptions to be made about its biogenesis and function that often go untested. Additionally, misclassified sequences erode conceptual frameworks built across the years. Paradigm-shifting research is exciting but should not be based on erroneously annotated sequences.

Built as a community resource with an inclusive policy, miRbase contains entries that are known not to be miRNAs. Curated databases such as MirGeneDB[44] do not list several miRbase entries that, in sequencing studies, lack the processing pattern that is expected based on miRNA biogenesis. Among these, miR-1246 has been widely described as an extracellularly enriched miRNA. However, extracellular enrichment could be a consequence of contamination, since it is the second-most abundant small RNA sequence in FBS[45]. Additionally, miR-1246 is a short fragment derived from the U2 small nuclear RNA that, in the extracellular space, is protected as part of a ribonucleoprotein complex involving core spliceosome proteins[46].

The situation is no better in the piRNA field. Mammalian piRNA databases contain a small percentage of entries mislabeled as piRNAs that actually belong to other small RNA classes[47]. Although these ambiguous entries account for only ~1% of most databases, they account for virtually all human piRNAs recently described in cancer cells and in biofluids[47,48]. Claims based on somatic piRNA expression in mammals are, therefore, built on top of a misclassification problem.

RNA fragments

It has been shown that tDRs can form dimers[49] or tetramers[50], with increased resistance to degradation[49,50]. Intermolecular RNA structures can also define binding partners and, hence, small RNA function[51]. Additionally, we have recently shown that many (if not most) cellular and extracellular tDRs are derived from nicked tRNAs[5]. The endonucleolytic cleavage of a tRNA molecule at the anticodon loop produces a nicked tRNA and these species were originally thought to rapidly dissociate into tRNA halves. However, later studies have shown that nicked tRNA dissociation is a laboratory artifact, at least in some cases.[5,6]

Nicked tRNAs are stable against RNases[5], and the cell might need the action of helicases to unwind them[7], paying an energetic cost. We used phage enzymes to repair and regenerate nicked tRNAs in vitro[5], but nicked tRNA healing could also occur naturally inside human[8] or bacterial[6] cells, as part of a stress or DNA-damage response, respectively. Importantly, heat or denaturing agents induce nicked tRNA dissociation in vitro[5,6]. Therefore, it is possible that many tDRs observed when using small RNA-seq or northern blot are produced by laboratory techniques inducing nicked tRNA dissociation.

How to distinguish between a bona fide 5′ tRNA half, dimers or tetramers of 5′ tRNA halves, or a nicked tRNA? They all look the same by denaturing northern blot, by miRNA-seq or even by the less-biased TGIRT-seq (Fig. 2). To solve this, we have designed an enzymatic RNA repair protocol[5] that, when combined with thermostable RTs with tolerance to base modifications or RT roadblock removal steps (i.e., 'REJOIN-seq'), can differentiate between monomeric or oligomeric tRNA halves and nicked tRNAs (Fig. 2). However, it is not a one-size-fits-all method. For example, aminoacylated tRNAs could be missed when using REJOIN-seq unless a tRNA deacylation step is included.

As sequencing is limited to 1D information, we only see projections of what is happening at a higher, structural level, which should be considered when we interpret data and design validation experiments. For example, it is not clear from sequencing data which sperm small RNAs mediate epigenetic inheritance (Box 1). Structure probing (e.g., selective 2′-hydroxy acylation and primer extension sequencing (SHAPE-seq)[52] and dimethyl sulfate mutational profiling with sequencing (DMS-MaPseq[53]) and structure-aware methods (e.g., REJOIN-seq) can be helpful, but a combination of biochemical and sequencing techniques[54] will probably be needed to push the small RNA field forward.

Conclusions

RNA biology occurs in four dimensions. RNA structure determines protein partners and interactions with other nucleic acids. Structure and modifications also determine RNA stability, which in turn dictates RNA abundance and function. Structural plasticity is a major challenge in RNA research. For example, ATP-dependent helicases can induce RNA folding and unfolding, depending on cell metabolic states[55]. Riboswitches also illustrate how RNA structures can be altered in the presence of ligands. Altogether, understanding RNA biology from a structural perspective is no easy task. Nevertheless, most researchers working on RNA acknowledge this need and are aware of the limitations of 1D sequencing data.

Small RNA biology research has lagged behind other areas of research in this respect. MiRNA biology can be explained by relatively simple miRNA/mRNA pairing rules that operate at the sequence level. For example, biochemical and structural data show that mature miRNAs act as extended single-stranded molecules when bound to Argonaute proteins. This validates the design of target prediction algorithms based on sequence queries. However, extrapolating this approach to the study of other small RNA families, where we still lack generalizable biochemical models, can produce meaningless predictions. For nicked tRNAs,[5,6] analyzing small RNA sequencing data could lead to conclusions on the function of an RNA fragment that is actually not present in fragment form. The consequences of ignoring alternative possibilities that are consistent with the data (Fig. 2) are more obvious when thinking about validation experiments: should they be performed with synthetic single-stranded RNAs?[56]

There is no bias-free sequencing method that will give an accurate snapshot of reality. What we have are a variety of methods with different types of biases. These methods might be useful to answer specific questions. When doing long-read RNA-seq, mRNAs are enriched by polyA capture or ribosomal RNA depletion. We do not refer to these enrichment protocols as 'biased methods', even if they are indeed biased. When bias is explicitly acknowledged, we use the term 'enrichment' instead of the term 'bias'. Our goal is to understand the benefits and limitations of different small RNA-seq methods, and embrace sequencing bias to enrich specific small RNA populations. If the purpose of a study is to comprehensively explore the small RNA content of a sample, then a combination of different methods is probably needed to compensate for the intrinsic biases of each method.

Undoubtedly, the quest to obtain less biased small RNA sequencing protocols should be encouraged. However, we need progress in other directions too. Imagine the current state of protein science if efforts had only been made to obtain more powerful mass spectrometers. To move forward, we need interdisciplinary research, where biochemists, molecular biologists and computer scientists work together

https://doi.org/10.1038/s41596-023-00936-2

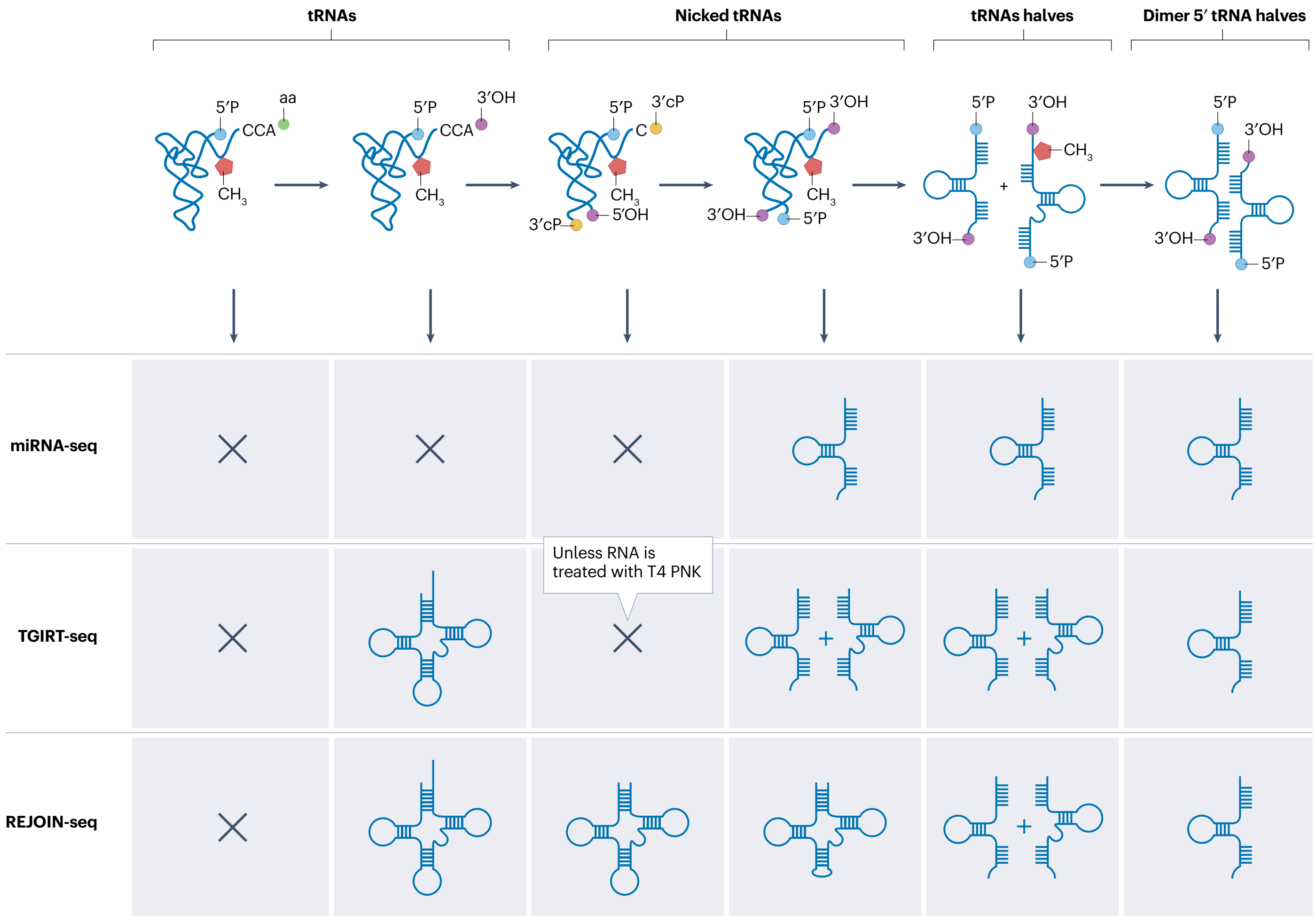

Fig. 2 | Small RNA-seq does not provide an accurate representation of structured small RNAs. Sequential steps in tRNA fragmentation are depicted[5] and the predicted outputs of miRNA-seq, TGIRT-seq and REJOIN-seq are shown below. Note that 3′ tRNA halves cannot be sequenced by miRNA-seq due to the presence of a hypothetical 'hard-stop' posttranscriptional modification (CH_3). In contrast, TGIRT-seq can handle these modifications and can also capture full-length tRNAs. The template-jumping reaction is inhibited by 3′ phosphates, but this can be remediated by treating the RNA with T4 PNK[22]. Nicked tRNAs are dissociated and sequenced as a collection of separate fragments. In contrast, REJOIN-seq converts nicked tRNAs back into (almost) full-length tRNAs.

BOX 1

Sperm small RNAs and epigenetic inheritance

Two landmark papers published in 2016 showed that sperm tRNA halves could carry epigenetic information, be delivered to mature oocytes and influence development[33,62]. Later studies in mice[63,64] and fish[65] confirmed the role of sperm-derived RNAs in the transmission of acquired heritable traits transmitted by the paternal lineage. While sperm tDRs have been proposed as the mediators of the observed transgenerational phenotypes[66], microinjection experiments in zygotes did not always recapitulate these traits when synthetic tDRs were used instead of sperm-derived RNAs[62]. One possibility is that endogenous tDRs harbor a set of methylated bases that is absent in synthetic RNAs, consistent with an involvement of the RNA methyltransferase DNMT2 (refs. 63,65). A second possibility is that other sperm RNAs (not tDRs) are the actual mediators of epigenetic inheritance. In this regard, PANDORA-seq showed that rRNA-derived fragments are the most abundant small RNAs in sperm[28]. The third possibility is that microinjection experiments with synthetic tDRs failed[62] because sperm actually contains nicked tRNAs, as recently suggested[56]. This possibility is consistent with sperm small RNA profiling by OTTR-seq[67]. Acquired paternal traits could shape sperm tDR profiles indirectly, by modifying tRNA methylation levels[63,65] and consequently affecting nicked tRNA formation.

to solve complex biological problems involving multiple experimental approaches. This means more than just collaboration. Several research projects are constructed on 'moving assembly lines', where one laboratory extracts RNA, then sends the RNA to a sequencing facility, then sends the data to a colleague with experience in bioinformatics. However, without adequate biological context, applying out-of-the-box computational algorithms can be problematic. Additionally, validation of sequencing data should involve new orthogonal experiments[57] to validate sequencing-derived hypothesis, rather than simply performing RT–qPCR or increasing the number of replicates.

158

References

1. Bartel, D. P. Metazoan microRNAs. *Cell* **173**, 20–51 (2018).
2. Wang, X., Ramat, A., Simonelig, M. & Liu, M. F. Emerging roles and functional mechanisms of PIWI-interacting RNAs. *Nat. Rev. Mol. Cell Biol.* **24**, 123–141 (2023).
3. Shi, J., Zhou, T. & Chen, Q. Exploring the expanding universe of small RNAs. *Nat. Cell Biol.* **24**, 415–423 (2022).
4. Chen, Q., Zhang, X., Shi, J., Yan, M. & Zhou, T. Origins and evolving functionalities of tRNA-derived small RNAs. *Trends Biochem. Sci.* **46**, 790–804 (2021).
5. Costa, B. et al. Nicked tRNAs are stable reservoirs of tRNA halves in cells and biofluids. *Proc. Natl Acad. Sci. USA* **120**, e2216330120 (2023).
6. Chen, X. & Wolin, S. L. Transfer RNA halves are found as nicked tRNAs in cells: evidence that nicked tRNAs regulate expression of an RNA repair operon. *RNA* https://doi.org/10.1261/rna.079575.122 (2023).
7. Drino, A. et al. Identification of RNA helicases with unwinding activity on angiogenin-processed tRNAs. *Nucleic Acids Res.* **51**, 1326–1352 (2023).
8. Akiyama, Y. et al. RTCB complex regulates stress-induced tRNA cleavage. *Int. J. Mol. Sci.* **23**, 13100 (2022).
9. Spitale, R. C. & Incarnato, D. Probing the dynamic RNA structurome and its functions. *Nat. Rev. Genet.* **24**, 178–196 (2023).
10. Giraldez, M. D. et al. Comprehensive multi-center assessment of small RNA-seq methods for quantitative miRNA profiling. *Nat. Biotechnol.* **36**, 746–757 (2018).
11. Hafner, M. et al. RNA-ligase-dependent biases in miRNA representation in deep-sequenced small RNA cDNA libraries. *RNA* **17**, 1697–1712 (2011).
12. Hu, J. F. et al. Quantitative mapping of the cellular small RNA landscape with AQRNA-seq. *Nat. Biotechnol.* **39**, 978–988 (2021).
13. Song, Y., Liu, K. J. & Wang, T. H. Elimination of ligation dependent artifacts in T4 RNA ligase to achieve high efficiency and low bias microRNA capture. *PLoS ONE* **9**, e94619 (2014).
14. Zhang, Z., Lee, J. E., Riemondy, K., Anderson, E. M. & Yi, R. High-efficiency RNA cloning enables accurate quantification of miRNA expression by deep sequencing. *Genome Biol.* **14**, R109 (2013).
15. Turchinovich, A. et al. Capture and amplification by tailing and switching (CATS): an ultrasensitive ligation-independent method for generation of DNA libraries for deep sequencing from picogram amounts of DNA and RNA. *RNA Biol.* **11**, 817–828 (2014).
16. Zhu, Y. Y., Machleder, E. M., Chenchik, A., Li, R. & Siebert, P. D. Reverse transcriptase template switching: a SMART approach for full-length cDNA library construction. *Biotechniques* **30**, 892–897 (2001).
17. Upton, H. E. et al. Low-bias ncRNA libraries using ordered two-template relay: serial template jumping by a modified retroelement reverse transcriptase. *Proc. Natl Acad. Sci. USA* **118**, e2107900118 (2021).
18. Wulf, M. G. et al. Non-templated addition and template switching by Moloney murine leukemia virus (MMLV)-based reverse transcriptases co-occur and compete with each other. *J. Biol. Chem.* **294**, 18220–18231 (2019).
19. Dard-Dascot, C. et al. Systematic comparison of small RNA library preparation protocols for next-generation sequencing. *BMC Genomics* **19**, 118 (2018).
20. Mohr, S. et al. Thermostable group II intron reverse transcriptase fusion proteins and their use in cDNA synthesis and next-generation RNA sequencing. *RNA* **19**, 958–970 (2013).
21. Zheng, G. et al. Efficient and quantitative high-throughput tRNA sequencing. *Nat. Methods* **12**, 835–837 (2015).
22. Nottingham, R. M. et al. RNA-seq of human reference RNA samples using a thermostable group II intron reverse transcriptase. *RNA* **22**, 597–613 (2016).
23. Xu, H., Yao, J., Wu, D. C. & Lambowitz, A. M. Improved TGIRT-seq methods for comprehensive transcriptome profiling with decreased adapter dimer formation and bias correction. *Sci. Rep.* **9**, 7953 (2019).
24. Behrens, A., Rodschinka, G. & Nedialkova, D. D. High-resolution quantitative profiling of tRNA abundance and modification status in eukaryotes by mim-tRNAseq. *Mol. Cell* **81**, 1802–1815.e7 (2021).
25. Heyer, E. E., Ozadam, H., Ricci, E. P., Cenik, C. & Moore, M. J. An optimized kit-free method for making strand-specific deep sequencing libraries from RNA fragments. *Nucleic Acids Res.* **43**, (2015).
26. Cozen, A. E. et al. ARM-seq: AlkB-facilitated RNA methylation sequencing reveals a complex landscape of modified tRNA fragments. *Nat. Methods* **12**, 879–884 (2015).
27. Wang, H. et al. CPA-seq reveals small ncRNAs with methylated nucleosides and diverse termini. *Cell Discov.* **7**, 25 (2021).
28. Shi, J. et al. PANDORA-seq expands the repertoire of regulatory small RNAs by overcoming RNA modifications. *Nat. Cell Biol.* **23**, 424–436 (2021).
29. Pinkard, O., McFarland, S., Sweet, T. & Coller, J. Quantitative tRNA-sequencing uncovers metazoan tissue-specific tRNA regulation. *Nat. Commun.* **11**, 4104 (2020).
30. Shigematsu, M. et al. YAMAT-seq: an efficient method for high-throughput sequencing of mature transfer RNAs. *Nucleic Acids Res.* **45**, e70 (2017).
31. Nolte'T Hoen, E. N. M. et al. Deep sequencing of RNA from immune cell-derived vesicles uncovers the selective incorporation of small non-coding RNA biotypes with potential regulatory functions. *Nucleic Acids Res.* **40**, 9272–9285 (2012).
32. Tosar, J. P. et al. Assessment of small RNA sorting into different extracellular fractions revealed by high-throughput sequencing of breast cell lines. *Nucleic Acids Res.* **43**, 5601–5616 (2015).
33. Sharma, U. et al. Biogenesis and function of tRNA fragments during sperm maturation and fertilization in mammals. *Science* **351**, 391–396 (2016).
34. Shurtleff, M. J. et al. Broad role for YBX1 in defining the small noncoding RNA composition of exosomes. *Proc. Natl Acad. Sci. USA* **114**, E8987–E8995 (2017).
35. Tosar, J. P. et al. Fragmentation of extracellular ribosomes and tRNAs shapes the extracellular RNAome. *Nucleic Acids Res.* **48**, 12874–12888 (2020).
36. Gogakos, T. et al. Characterizing expression and processing of precursor and mature human tRNAs by hydro-tRNAseq and PAR-CLIP. *Cell Rep.* **20**, 1463–1475 (2017).
37. Choi, J. H. & Sullivan, C. S. DUSP11 and triphosphate RNA balance during virus infection. *PLoS Pathog.* **17**, (2021).
38. Honda, S. et al. Sex hormone-dependent tRNA halves enhance cell proliferation in breast and prostate cancers. *Proc. Natl Acad. Sci. USA* **112**, E3816–E3825 (2015).
39. Akat, K. M. et al. Detection of circulating extracellular mRNAs by modified small-RNA-sequencing analysis. *JCI Insight* **4**, 127317 (2019).
40. Giraldez, M. D. et al. Phospho-RNA-seq: a modified small RNA-seq method that reveals circulating mRNA and lncRNA fragments as potential biomarkers in human plasma. *EMBO J.* **38**, (2019).
41. Lentzsch, A. M., Yao, J., Russell, R. & Lambowitz, A. M. Template-switching mechanism of a group II intron-encoded reverse transcriptase and its implications for biological function and RNA-seq. *J. Biol. Chem.* **294**, 19764–19784 (2019).
42. Tosar, J. P., Cayota, A., Eitan, E., Halushka, M. K. & Witwer, K. W. Ribonucleic artefacts: are some extracellular RNA discoveries driven by cell culture medium components? *J. Extracell. Vesicles* **6**, 1272832 (2017).

43. Auber, M., Fröhlich, D., Drechsel, O., Karaulanov, E. & Krämer-Albers, E.-M. Serum-free media supplements carry miRNAs that co-purify with extracellular vesicles. *J. Extracell. Vesicles* **8**, 1656042 (2019).
44. Fromm, B. et al. A uniform system for the annotation of vertebrate microRNA genes and the evolution of the human microRNAome. *Annu. Rev. Genet.* **49**, 213–242 (2015).
45. Wei, Z., Batagov, A. O., Carter, D. R. F. & Krichevsky, A. M. Fetal bovine serum RNA interferes with the cell culture derived extracellular RNA. *Sci. Rep.* **6**, 31175 (2016).
46. Tosar, J. P., Cayota, A. & Witwer, K. Exomeres and supermeres: monolithic or diverse? *J. Extracell. Biol.* **1**, e45 (2022).
47. Tosar, J. P., Rovira, C. & Cayota, A. Non-coding RNA fragments account for the majority of annotated piRNAs expressed in somatic non-gonadal tissues. *Commun. Biol.* **1**, 2 (2018).
48. Tosar, J. P., García-Silva, M. R. & Cayota, A. Circulating SNORD57 rather than piR-54265 is a promising biomarker for colorectal cancer: Common pitfalls in the study of somatic piRNAs in cancer. *RNA* **27**, 403–410 (2021).
49. Tosar, J. P. et al. Dimerization confers increased stability to nucleases in 5′ halves from glycine and glutamic acid tRNAs. *Nucleic Acids Res.* **46**, 9081–9093 (2018).
50. Lyons, S. M., Gudanis, D., Coyne, S. M., Gdaniec, Z. & Ivanov, P. Identification of functional tetramolecular RNA G-quadruplexes derived from transfer RNAs. *Nat. Commun.* **8**, 1127 (2017).
51. Lyons, S. M. et al. eIF4G has intrinsic G-quadruplex binding activity that is required for tiRNA function. *Nucleic Acids Res.* **48**, 6223–6233 (2021).
52. Loughrey, D., Watters, K. E., Settle, A. H. & Lucks, J. B. SHAPE-Seq 2.0: systematic optimization and extension of high-throughput chemical probing of RNA secondary structure with next generation sequencing. *Nucleic Acids Res.* **42**, (2014).
53. Zubradt, M. et al. DMS-MaPseq for genome-wide or targeted RNA structure probing in vivo. *Nat. Methods* **14**, 75–82 (2017).
54. Tosar, J. P., Gámbaro, F., Castellano, M. & Cayota, A. RI-SEC-seq: comprehensive profiling of nonvesicular extracellular RNAs with different stabilities. *Bio Protoc.* **11**, e3918 (2021).
55. Kharel, P. et al. Stress promotes RNA G-quadruplex folding in human cells. *Nat. Commun.* **14**, 205 (2023).
56. Kaymak, E. & Rando, O. J. Staying together after the breakup: tRNA halves in extracellular fluids. *Proc. Natl Acad. Sci. USA* **120**, e2300300120 (2023).
57. Munafò, M. R. & Smith, Davey G. Robust research needs many lines of evidence. *Nature* **553**, 399–401 (2018).
58. Lentzsch, A. M., Yao, J., Russell, R. & Lambowitz, A. M. Template-switching mechanism of a group II intron-encoded reverse transcriptase and its implications for biological function and RNA-Seq. *J. Biol. Chem.* **294**, (2019).
59. Almeida, M. V., de Jesus Domingues, A. M., Lukas, H., Mendez-Lago, M. & Ketting, R. F. RppH can faithfully replace TAP to allow cloning of 5′-triphosphate carrying small RNAs. *MethodsX* **6**, (2019).
60. Tosar, J. P., Rovira, C., Naya, H. & Cayota, A. Mining of public sequencing databases supports a non-dietary origin for putative foreign miRNAs: Underestimated effects of contamination in NGS. *RNA* **20**, 754–757 (2014).
61. Tosar, J. P., Witwer, K. & Cayota, A. Revisiting extracellular RNA release, processing, and function. *Trends Biochem. Sci.* **46**, 438–445 (2021).
62. Chen, Q. et al. Sperm tsRNAs contribute to intergenerational inheritance of an acquired metabolic disorder. *Science* **351**, 397–400 (2016).
63. Zhang, Y. et al. Dnmt2 mediates intergenerational transmission of paternally acquired metabolic disorders through sperm small non-coding RNAs. *Nat. Cell Biol.* **20**, (2018).
64. Sarker, G. et al. Maternal overnutrition programs hedonic and metabolic phenotypes across generations through sperm tsRNAs. *Proc. Natl Acad. Sci. USA* **116**, (2019).
65. Jimenez, N. A. et al. Paternal methotrexate exposure affects sperm small RNA content and causes craniofacial defects in the offspring. *Nat. Commun.* **14**, 1617 (2023).
66. Boskovic, A., Bing, X. Y., Kaymak, E. & Rando, O. J. Control of noncoding RNA production and histone levels by a 5′ tRNA fragment. *Genes Dev.* **34**, 118–131 (2020).
67. Gustafsson, H. T. et al. Deep sequencing of yeast and mouse tRNAs and tRNA fragments using OTTR. Preprint at *bioRxiv* https://doi.org/10.1101/2022.02.04.479139(2022).

Acknowledgements

This work was partially funded by the National Institutes of Health Office of the Director (UG3/UH3CA241694) and Universidad de la República, Uruguay (CSIC I+D_2020_433).

Competing interests

J.P.T., B.C. and A.C. have filed a patent in the United States on a method for RNA repair and sequencing.

Additional information

Correspondence should be addressed to Juan Pablo Tosar.

Peer review information *Nature Protocols* thanks Brian Gregory and the other, anonymous, reviewer(s) for their contribution to the peer review of this work.

Artículo 5: Nicked tRNAs are stable reservoirs of tRNA halves in cells and biofluids

PNAS | RESEARCH ARTICLE | BIOCHEMISTRY

Nicked tRNAs are stable reservoirs of tRNA halves in cells and biofluids

Bruno Costa[a,b,1], Marco Li Calzi[a,1], Mauricio Castellano[a,c], Valentina Blanco[a,c], Ernesto Cuevasanta[b,d,e], Irene Litvan[f], Pavel Ivanov[g], Kenneth Witwer[h], Alfonso Cayota[a,i], and Juan Pablo Tosar[a,b,2]

Edited by Adrian Krainer, Cold Spring Harbor Laboratory, Cold Spring Harbor, NY; received September 24, 2022; accepted December 14, 2022

Nonvesicular extracellular RNAs (nv-exRNAs) constitute the majority of the extracellular RNAome, but little is known about their stability, function, and potential use as disease biomarkers. Herein, we measured the stability of several naked RNAs when incubated in human serum, urine, and cerebrospinal fluid (CSF). We identified extracellularly produced tRNA-derived small RNAs (tDRs) with half-lives of several hours in CSF. Contrary to widespread assumptions, these intrinsically stable small RNAs are full-length tRNAs containing broken phosphodiester bonds (i.e., nicked tRNAs). Standard molecular biology protocols, including phenol-based RNA extraction and heat, induce the artifactual denaturation of nicked tRNAs and the consequent in vitro production of tDRs. Broken bonds are roadblocks for reverse transcriptases, preventing amplification and/or sequencing of nicked tRNAs in their native state. To solve this, we performed enzymatic repair of nicked tRNAs purified under native conditions, harnessing the intrinsic activity of phage and bacterial tRNA repair systems. Enzymatic repair regenerated an RNase R-resistant tRNA-sized band in northern blot and enabled RT-PCR amplification of full-length tRNAs. We also separated nicked tRNAs from tDRs by chromatographic methods under native conditions, identifying nicked tRNAs inside stressed cells and in vesicle-depleted human biofluids. Dissociation of nicked tRNAs produces single-stranded tDRs that can be spontaneously taken up by human epithelial cells, positioning stable nv-exRNAs as potentially relevant players in intercellular communication pathways.

extracellular RNA | liquid biopsies | tRNA halves | RNA stability | tRF

Extracellular RNAs (exRNAs) circulating in human bodily fluids can enable disease diagnosis before the onset of clinical symptoms (1). Beyond applications as disease biomarkers in liquid biopsies (2), exRNAs are also involved in intercellular communication pathways between cells in different tissues (3) and in host–pathogen interactions (4–6).

One key aspect governing both exRNA functionality and utility as biomarkers is their stability against ubiquitous extracellular RNases (7). This can be achieved by RNA encapsulation inside extracellular vesicles (EVs) such as exosomes and microvesicles (8, 9). However, despite the functional relevance (10) and biotechnological applications (11) of EV-encapsulated RNA, the majority of exRNAs in cell culture (12–15) and in human plasma (15–18) are not transported as part of EV cargo.

Transfer RNA-derived RNAs (tDRs) are among the most abundant nonvesicular small RNAs (nv-exRNAs) in cell culture (12, 13). Inside cells, tRNA cleavage and the consequent generation of specific tDRs is a conserved response to stress in all kingdoms of life (19–21). In humans, RNase A superfamily members, such as RNase 5 (Angiogenin), are responsible for stress-induced tRNA cleavage at the anticodon, generating stress-induced tRNA halves (tiRNAs) (22, 23). tiRNAs can regulate gene expression at various levels, including global inhibition of translation initiation (24, 25). Other, shorter tDRs can bind to mRNAs and regulate their translation (26) or silence genes by a miRNA-like mechanism (27).

Extracellular tDRs were first reported in EVs from murine immune cells (28) but were later shown to be present mainly outside vesicles in mouse serum (29, 30). In human breast cancer cell lines, tDRs can be detected in vesicular fractions but are overwhelmingly more abundant in EV-depleted ultracentrifugation supernatants (12). While a heterogeneous population of tDRs is detectable inside cells, extracellular nonvesicular tDRs are mainly 5′ tRNA halves of 30 or 31 nucleotides, derived from $tRNA^{Gly}$ and $tRNA^{Glu}$. These specific fragments are also ubiquitous in human biofluids (31). A possible explanation for the extracellular enrichment of these fragments is their enhanced stability against degradation, because 5′ $tRNA^{Gly}_{GCC}$ halves of 30 to 31 nt can form RNase-resistant homodimers in vitro (32).

To study exRNA processing in more detail, we added RNase inhibitors (RI) to cell-conditioned media and uncovered a population composed of nonvesicular ribosomes and full-length tRNAs (33). Knock-out of RNase 1 in K562 cells also shaped exRNA profiles from

Significance

tRNA-derived small RNAs (tDRs) regulate gene expression at multiple levels. Some tDRs are abundant in human biofluids, where they are mostly present outside extracellular vesicles. This poses the intriguing question about how extracellular tDRs resist degradation by extracellular RNases. In this work, we solved this mystery by finding out that some of the most frequently detected extracellular tDRs are nicked forms of full-length tRNAs and are therefore dsRNA molecules. Nicked tRNAs cannot be studied by standard molecular biology and/or sequencing techniques because they are discontinuous. However, we developed several methods for the analysis of nicked tRNAs under native conditions and showed their presence in cells and biofluids. We also uncovered a potential intercellular communication pathway mediated by stable nonvesicular RNAs.

Author contributions: J.P.T. designed research; B.C., M.L.C., M.C., V.B., and J.P.T. performed research; I.L., P.I., K.W., A.C., and J.P.T. contributed new reagents/analytic tools; B.C., E.C., and J.P.T. analyzed data; B.C., M.L.C., M.C., V.B., E.C., I.L., P.I., K.W., and A.C. edited the manuscript; and J.P.T. wrote the paper.

Competing interest statement: The authors have patent filings to disclose, J.P.T., B.C., A.C. and K.W. have filled a provisional patent in the US related to this work.

This article is a PNAS Direct Submission.

[1]B.C. and M.L.C. contributed equally to this work.

[2]To whom correspondence may be addressed. Email: jptosar@pasteur.edu.uy.

This article contains supporting information online at https://www.pnas.org/lookup/suppl/doi:10.1073/pnas.2216330120/-/DCSupplemental.

Published January 18, 2023.

162

tRNA halves into full-length tRNAs (34). Thus, most nonvesicular tRNA halves are generated directly in the extracellular space by endonucleolytic cleavage of extracellular full-length tRNAs (33–35).

We have found that extracellular ribosomes can induce dendritic cell activation in vitro in an exRNA-dependent manner (33). However, the involvement of nonvesicular exRNAs (nv-exRNAs) in intercellular communication pathways faces an important conceptual challenge. As a consequence of the strong ribonuclease activity that characterizes the extracellular space (36), nv-exRNAs are expected to be rapidly degraded unless protected by RNA-binding proteins. How, then, do these RNAs resist degradation, diffuse to recipient cells, and trigger downstream effects, or even remain measurable and thus serve as potential disease biomarkers?

In this study, we incubated protein-free RNA or purified ribonucleoprotein complexes in human biofluids and measured their decay kinetics by northern blot. As expected, the protective effect of RNA-binding proteins was confirmed. Interestingly, though, we also found that certain specific naked tRNAs are intrinsically stable. Furthermore, the stability of 5′ tRNA halves generated from the endonucleolytic cleavage of unstable tRNAs was extremely high, with half-lives of hours in certain human biofluids. Also surprisingly, these ultra-stable RNAs are not single stranded. Developing and employing different strategies of enzymatic repair and electrophoretic or chromatographic separations under native conditions, we show that these RNAs natively exist as full-length tRNAs containing broken phosphodiester bonds. Commonly used RNA purification methods, sequencing, and denaturing northern blotting do not detect these forms, forcing them to melt into single-stranded tRNA halves. Nevertheless, at low rates, nicked tRNAs also seem to disassemble spontaneously into tRNA halves in the extracellular space. These extracellular nonvesicular tDRs are unstable, but they can be efficiently internalized by recipient cells.

Results

Identification of Naked RNAs that Are Stable in the Presence of Serum. To search for intrinsically stable RNAs in extracellular samples, we first screened the most abundant cellular transcripts to see if, in the absence of their protein counterparts, they can resist degradation in serum-containing media (Fig. 1*A*). Unsurprisingly, naked rRNAs were degraded in less than one minute as judged by lack of northern blot signals in the absence of added RI. In contrast, and consistent with our previous observations (33), full-length $tRNA^{Lys}{}_{UUU}$ was present at input levels after 1.5 h, suggesting that this tRNA is not efficiently targeted by serum RNases. This was not observed for other tRNAs like $tRNA^{Gly}{}_{GCC}$, which, like rRNAs, were undetectable after one minute (Fig. 1*A*).

Ribosomal Proteins Stabilize rRNAs and Protect rRNA-Derived Fragments. To assess the effect of RNA-binding proteins on the stability of nv-exRNAs, we purified whole ribosomes from cells (*SI Appendix*, Fig. S1) and studied rRNA decay kinetics in 10% FBS (Fig. 1*B*). In ribosomes, full-length rRNAs and rRNA-derived fragments were detectable for at least 10 and 60 min at 37 °C, respectively, even in the absence of RI. Thus, ribosomes are more stable than naked rRNAs and ribosomal proteins greatly stabilize extracellular rRNA-derived fragments.

Based on these results, we searched for nonvesicular rRNA-derived fragments in a cell-conditioned medium (CCM) obtained in the presence of 10% FBS. We separated EVs from RNP complexes by

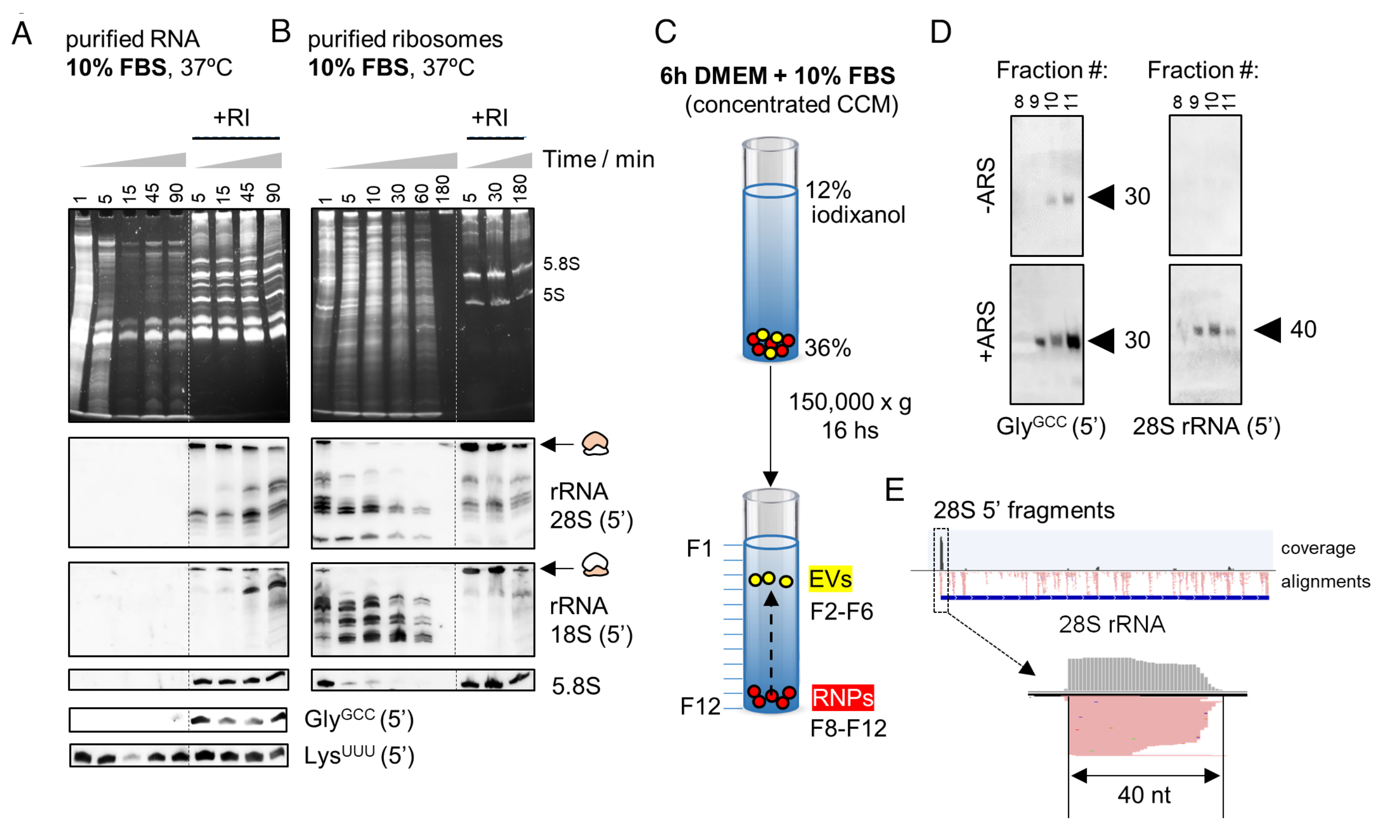

Fig. 1. Identification of stable nonvesicular RNAs. (*A* and *B*) Northern blot of different rRNAs and tRNAs after incubating purified RNA (*A*) or ribosomes (*B*) from human cells in 10% FBS. (*C* and *D*) Northern blot of 5′ $tRNA^{Gly}{}_{GCC}$ (*D*, *Left*) or 5′ 28S rRNA-derived fragments (*D*, *Right*) in extracellular nonvesicular fractions purified by density gradients (*C*). U2-OS cells were treated or not with $NaAsO_2$ (ARS) before collecting the CCM. (*E*) Read coverage in small RNA-seq data of extracellular ribosomes [from Tosar et al. (33)], revealing enrichment of 40-nt 5′-derived small RNAs among all other 28S rRNA-derived fragments.

163

flotation on iodixanol density gradients (Fig. 1*C*). Extensive characterization of this methodology has shown that the densest fractions (F8-F12) are devoid of EVs (33, 37). We reproduced our previous findings (33) showing the presence of 5′ $tRNA^{Gly}_{GCC}$ halves of 30 to 31 nt and the absence of full-length tRNAs in these nonvesicular fractions (Fig. 1*D*). Interestingly, northern blot detection of these fragments was enhanced when cells were treated with the cytotoxic agent sodium arsenite (Fig. 1*D*, +ARS). Additionally, using a probe complementary to the first 20 nucleotides of the 28S rRNA resulted in a single band of 40 nt in the conditioned medium of arsenite-treated cells. Purified extracellular ribosomes analyzed by small RNA-seq (33) also showed enrichment of these 40-nt 5′ fragments (Fig. 1*E*). Detection of these fragments in the presence of serum suggests that at least some stable RNA-containing RNPs are produced after the release and subsequent fragmentation of extracellular ribosomes, in agreement with recent findings (38).

Naked Full-Length $tRNA^{Lys}_{UUU}$ Is Intrinsically Stable in Biofluids. To precisely measure tRNA half-lives, we repeated the previous assay with better temporal resolution (Fig. 2*A*), confirming complete degradation of rRNAs and the 7SL RNA within seconds, while $tRNA^{Lys}_{UUU}$ was still detectable after 1 h at 37 °C. The full-length $tRNA^{Gly}_{GCC}$ was also rapidly degraded, generating fragments that lasted as much as the full-length $tRNA^{Lys}_{UUU}$. In fact, $tRNA^{Lys}_{UUU}$ and $tRNA^{Gly}_{GCC}$ constitute two extreme cases in a wide range of extracellular stabilities shown by different tRNAs (*SI Appendix*, Fig. S2*A*). In vitro incubation of RNA with recombinant human RNase 1 (r-RNase1), representing the most common RNase in human blood, resulted in virtually identical results (Fig. 2*A*). This observation argues against the possibility of $tRNA^{Lys}_{UUU}$ being stabilized by the interaction with FBS-derived proteins or metabolites. Therefore, we conclude that naked $tRNA^{Lys}_{UUU}$ is intrinsically resistant to the action of RNase A family members.

We then repeated these assays in human biofluids including urine, diluted and undiluted serum, and cerebrospinal fluid (CSF) (Fig. 2*B* and *SI Appendix*, Figs. S2*B* and S3*A*). Strikingly, the stability of full-length $tRNA^{Lys}_{UUU}$ was always higher than the stability of any other tested RNA, irrespective of the sample type. RNA decay kinetics were highly consistent among independent replicates (*SI Appendix*, Fig. S2*B*).

Glycine tRNA Halves Produced in Biofluids Are Extremely Stable. Full-length $tRNA^{Gly}_{GCC}$ was almost completely degraded in less than one minute in 10% FBS (Fig. 2*A*) and in human biofluids (Fig. 2*B*). However, its cleavage resulted in the formation of 5′

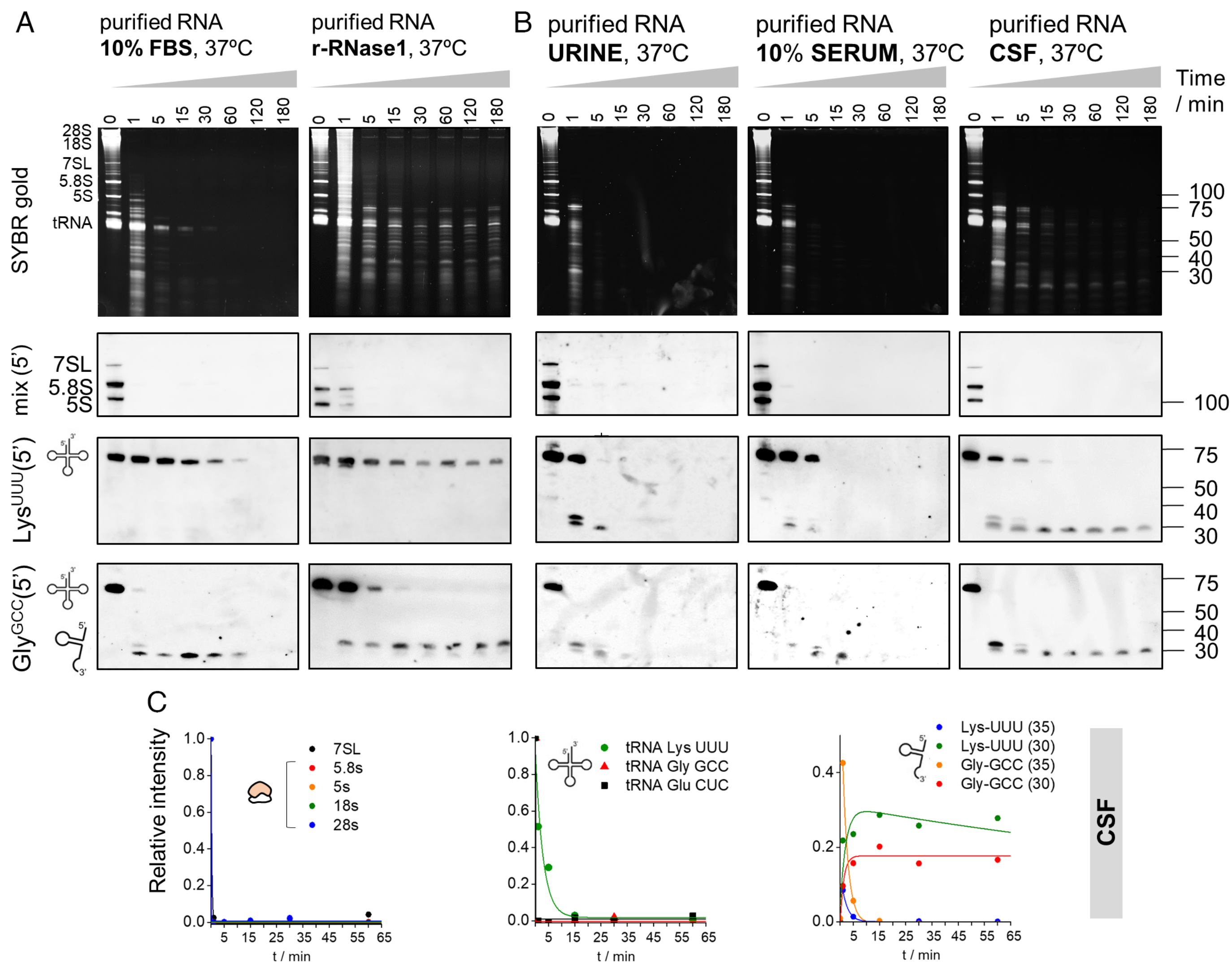

Fig. 2. Naked tRNA halves are extremely stable in human biofluids. (*A*) Northern blot of several RNAs after incubating purified total RNA from human cells in 10% FBS or with recombinant human RNase 1 for different periods. (*B*) Samples were also incubated in human urine, 10% serum, and CSF. (*C*) Data were fitted to a kinetic decay model, as explained in *SI Appendix*, *Supplementary Methods*. Half-lives in each biofluid, calculated after inclusion of experimental replicates, are presented in *SI Appendix*, Fig. S3 *B* and *C*. r-RNase1: recombinant human RNase 1.

halves that showed remarkable long half-lives, even in undiluted human sera (Fig. 2 *A* and *B* and *SI Appendix*, Fig. S3*A*). For instance, the half-life ($t_{1/2}$) of 5′ $tRNA^{Gly}{}_{GCC}$ halves of 30 nt in CSF was >2 h (Fig. 2*C*; 2 ± 1 h when replicates were combined, *SI Appendix*, Fig. S3 *B* and *C*), meaning that these RNAs are highly stable once they are generated and will therefore persist in biofluids.

A closer inspection of the data shows strong differences in the stability of fragments derived from the same parental tRNAs but with slightly different lengths. Consistent with our previous report (33), $tRNA^{Gly}{}_{GCC}$ is first cleaved at the anticodon loop, generating 34 to 35-nt 5′ halves that rapidly disappear. These fragments are subsequently replaced by highly stable shorter fragments of approximately 30 to 31 nt ($t_{1/2}$ = 6 ± 1, 8 ± 2, and 126 ± 65 min in urine, diluted serum and CSF, respectively, Fig. 2*B*), with a cleavage site at the start of the anticodon loop. An additional cleavage site in the TΨC loop (position 54) could be identified and exposed by using lower r-RNase1 concentrations (*SI Appendix*, Fig. S4*A*).

The sequential production of first longer (34 to 35 nt) and then shorter (30–31) 5′ halves from $tRNA^{Gly}{}_{GCC}$ was also observed with recombinant human RNase 5 or Angiogenin (r-Ang; *SI Appendix*, Fig. S5). Thus, cleavage sites and tRNA processing dynamics seem to be conserved among different RNase A family members.

Overall, tRNAs are more resistant to degradation than other longer noncoding RNAs, but differences in stability among tRNAs (e.g., $tRNA^{Lys}{}_{UUU}$ vs. $tRNA^{Gly}{}_{GCC}$) are also substantial (>30-fold in CSF). Consistent with our previous reports (32, 33), naked 5′ $tRNA^{Gly}{}_{GCC}$ halves of 30 to 31 nt are accumulated at higher RNase concentrations or after longer incubations in biofluids and are extremely stable.

Nicked tRNAs Are a Source of 5′ and 3′ tRNA Halves. Next, we compared the relative stabilities of 5′ and 3′ $tRNA^{Gly}{}_{GCC}$-derived fragments (*SI Appendix*, Fig. S6). Surprisingly, 30 to 35-nt 3′ fragments were observed, and their rate of decay was comparable to their 5′ counterparts. In certain biofluids, such as FBS (*SI Appendix*, Fig. S6*A*) and urine (*SI Appendix*, Fig. S6*B*), 3′ tRNA-derived fragments <20 nt were observed after short incubations (1 min; black asterisks). However, these fragments were rapidly degraded, in sharp contrast with the 5′ and 3′ halves.

We considered the possibility that 5′ and 3′ $tRNA^{Gly}{}_{GCC}$ halves could remain physically associated with each other after RNase cleavage, representing a full-length tRNA bearing a cleaved phosphodiester bond at the anticodon loop (i.e., in the form of "nicked tRNAs"). This would explain the similar decay kinetics of each half among different biofluids. The introduction of any irreversible denaturation steps in analytical determinations, such as those used in standard molecular biology approaches, would induce dissociation of nicked tRNAs into single-stranded tRNA halves. Therefore, testing this hypothesis required the generation of new assays capable of interrogating oligomeric RNA complexes under native conditions.

Nicked tRNAs are the natural substrates of T4 polynucleotide kinase (PNK) and T4 RNA ligase 1 (Rnl1) (39). When *Escherichia coli* is infected by the T4 Phage, a bacterial anticodon nuclease is activated and cleaves the host's $tRNA^{Lys}$ in an attempt to prevent the translation of viral proteins (40). This results in a nicked tRNA bearing a 3′ cyclic phosphate (3′ cP) and a 5′-OH adjacent to the cleavage site. However, the phage evolved two enzymes capable of performing end-healing (PNK) and tRNA repair (Rnl1). We harnessed the intrinsic activity of these enzymes and used them to investigate the native structure of human tRNA halves in extracellular samples.

To optimize the system, we purified total RNA from cells and incubated the RNA with r-RNase1 for 0, 15, or 60 min (Fig. 3*A*). As expected, by 60 min, full-length $tRNA^{Gly}{}_{GCC}$ was completely degraded and converted to a collection of tDRs (Fig. 3*A*). RNase 1 degradation products were purified by phenol-free silica-based solid phase extraction (SPE) columns and treated with either PNK alone, PNK followed by Rnl1, or PNK followed by Rnl2 (a dsRNA-specific ligase). Surprisingly, treatment with PNK and Rnl1 regenerated a single band of approximately the size of the cognate full-length tRNA (Fig. 3 *A* and *B*). Ligation with Rnl2 was less efficient.

To demonstrate that the tRNA-sized religated products are indeed repaired tRNAs, we designed a third probe (termed ACL, for anticodon loop) bridging both sides of the anticodon of $tRNA^{Gly}{}_{GCC}$ (Fig. 3*C*). This probe was designed so that the T_m of its pairing with either the 5′ or the 3′ half was below the hybridization temperature of the assay (42 °C). Thus, the ACL probe would fail to detect 5′ or 3′ tDRs but should be able to hybridize with full-length or repaired $tRNA^{Gly}{}_{GCC}$. Due to sequence similarities among tRNAs, ACL also recognizes the anticodon loop of $tRNA^{Asp}{}_{GUC}$, but fortunately, these tRNAs migrate slightly differently in denaturing urea gels, making this assay multiplex. Strikingly, treatment of RNase 1-treated RNA with PNK and Rnl1 regenerated tRNA-sized products observable with the 5′, the 3′ or the ACL probes (Fig. 3*D*). Furthermore, heating (Δ) and then cooling the RNase-treated RNA before the addition of the enzymatic cocktail (Δ + PNK + Rnl1) prevented the generation of a tRNA-sized band, demonstrating that ligation occurs in cis under the assay conditions. Rnl1 alone or following incubation with a mutant version of T4 PNK lacking its 3′ phosphatase activity [(-)PNK] also failed to reconstitute a full-length tRNA.

Next, we studied whether tRNA halves generated in human biofluids (Fig. 2*B*) are in fact nicked tRNAs. Indeed, a short incubation in CSF (1 min) produced 5′ $tRNA^{Asp}{}_{GUC}$ halves that could be enzymatically repaired back into a full-length tRNA (*SI Appendix*, Fig. S7*A*). Enzymatic repair of $tRNA^{Gly}{}_{GCC}$ produced after longer (1 h) incubations in CSF was also highly efficient (*SI Appendix*, Fig. S7*B*). However, the main religated product was approximately 11 nt shorter than the parental full-length tRNA, consistent with an irreversible loss of the entire anticodon loop (7 nt) plus the single-stranded NCCA 3′ overhang.

In summary, nicked tRNAs are produced in vitro and in biofluids using different tRNAs as substrates. These nicked tRNAs can be repaired enzymatically to regenerate an almost full-length tRNA, presumably lacking the 3′ NCCA overhang in in vitro settings (34, 41). Additional bases can be trimmed after prolonged exposure to extracellular RNases, but these shorter forms are still reparable using our assay.

Nicked tRNAs Are Irreversibly Melted by Popular RNA Extraction Methods. Whereas heating RNase-treated RNA before tandem incubation with PNK and Rnl1 prevented the formation of a tRNA-sized band, this also affected the detection of monomeric 5′ and 3′ tRNA halves (Fig. 3*D*; Δ + PNK + Rnl1 lane). However, when we repeated SPE purification under conditions optimized for small RNA recovery (*SI Appendix*, Fig. S7*C*), monomeric tRNA halves were now detectable in the control (i.e., heat) reaction (Fig. 4*A*; red arrows).

Given that heat irreversibly affects nicked tRNAs, we studied the effects of phenol-based RNA extraction methods, because this chemical agent, like heat, can disrupt base-pairing interactions. A recent study of different RNA purification methods for liquid biopsies found that the miRNeasy kit (Qiagen) recovered a broad spectrum of exRNAs associated with different carrier subclasses (31). However, when we purified RNase1-treated RNA with this kit following the manufacturer's instructions, tRNA halves were no longer amenable to enzymatic repair (*SI Appendix*, Fig. S7*D*).

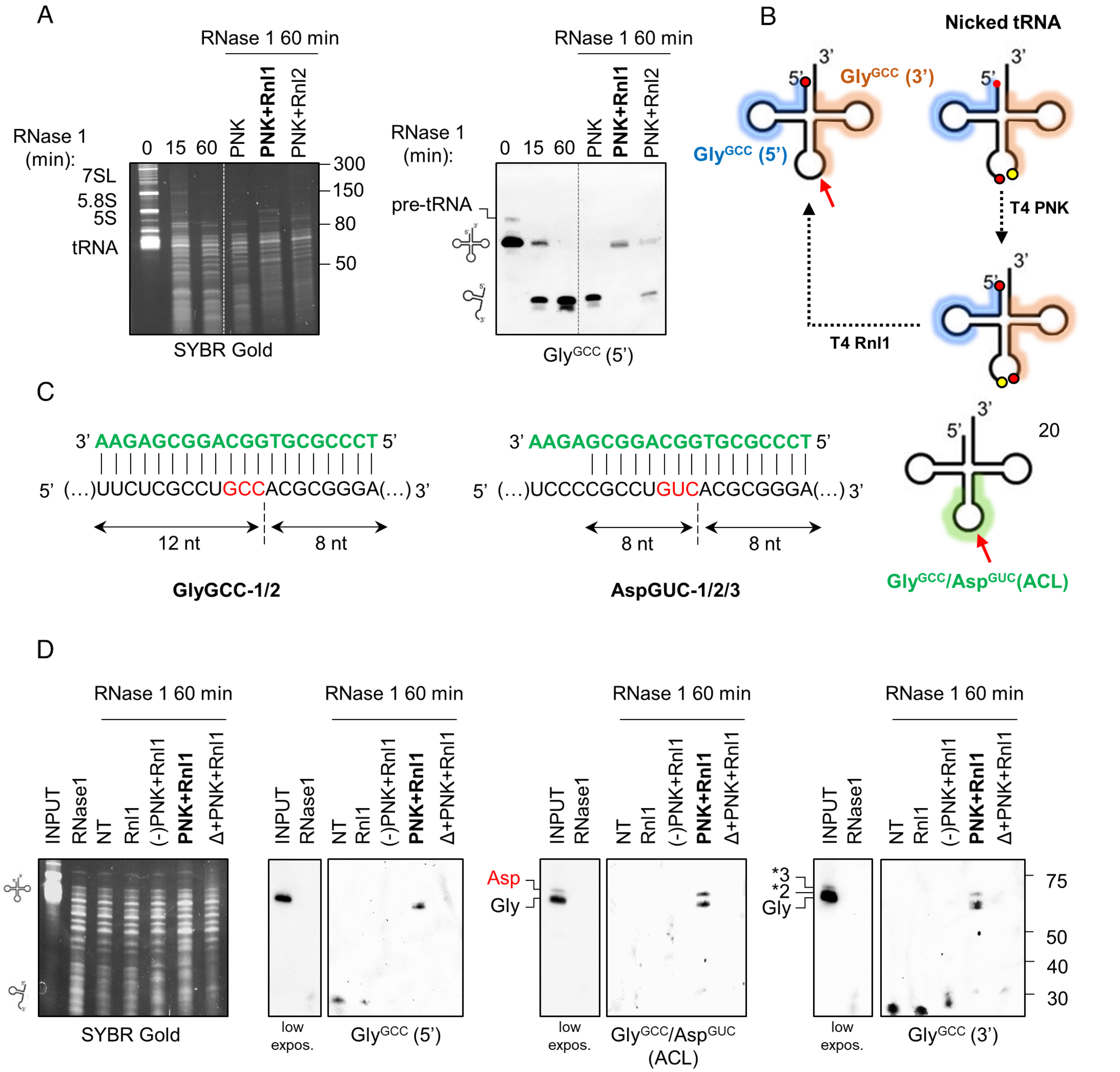

Fig. 3. Glycine tRNA halves identified by northern blot are nicked tRNAs. (*A*) RNase 1-treated RNA (60 min) was incubated with the indicated enzymatic combinations. Repair of $tRNA^{Gly}_{GCC}$ was analyzed by northern blot using a 5′-targeting probe. (*B*) schematic representation of the nicked tRNA repair strategy and 5′ (blue) and 3′ (orange) probe binding sites in $tRNA^{Gly}_{GCC}$. (*C*) Design of a third probe targeting the anticodon loop (ACL) of $tRNA^{Gly}_{GCC}$ and $tRNA^{Asp}_{GUC}$. (*D*) enzymatic repair of $tRNA^{Gly}_{GCC}$ evidenced with either the 5′, ACL or 3′ probes. NT: fragmented RNA purified by SPE but without treatment with the enzymatic repair cocktail. (-)PNK: mutant PNK lacking phosphatase activity. Δ: heat.

Similar results were obtained when comparing phenol-free SPE-based purification vs. TRIzol (Fig. 4*B*). Interestingly, adding a second SPE-based purification round recovered reparable tRNA halves with a yield close to 100%. Thus, guanidine salts included in the SPE binding buffer do not affect nicked tRNAs, while heat and phenol induce their irreversible separation. As previously observed, the length of the repaired tRNA was slightly shorter (4 to 5 nt) than that of the parental full-length tRNA (*SI Appendix*, Fig. S7*E*).

To confirm the effects of phenol and heat by an orthogonal method, we studied RNase-1-treated RNAs by native northern blot (run on TB + Mg^{2+} gels) (Fig. 4*C*). Under native conditions, the electrophoretic migration of RNase1-treated $tRNA^{Gly}_{GCC}$ was almost identical to that of untreated full-length tRNAs. Only <10% of the total signal in the treated lane corresponded to bona-fide tDRs. This confirms that the rapid disappearance of the full-length tRNA band observed in Fig. 2*A* is in fact an artifact caused by denaturing conditions, with >90% of tRNAs remaining as nicked tRNAs after 1 h of enzymatic digestion. Interestingly, the migration of nicked tRNAs in native gels was slightly faster than that of full-length tRNAs, consistent with the irreversible loss of the NCCA 3′ overhang inferred from previous assays (*SI Appendix*, Fig. S7*E*). Additionally, heat or standard RNA purification methods such as TRIzol or miRNeasy, unlike phenol-free RNA cleanup columns (SPE), induced the irreversible dissociation of nicked tRNAs (Fig. 4*C*).

166

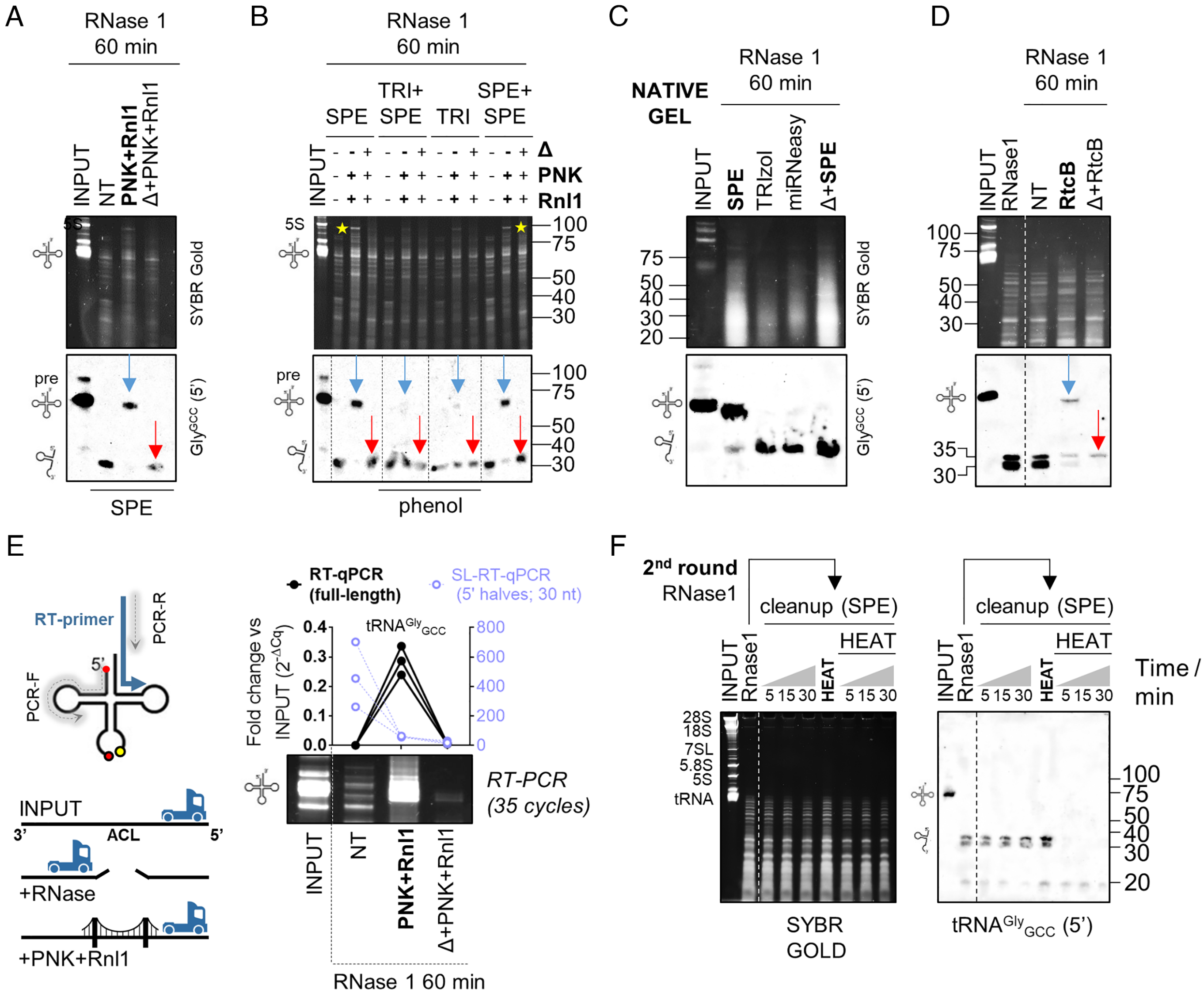

Fig. 4. Nicked tRNAs are stable, dissociated by phenol, can be repaired by PNK+Rnl1 or by RtcB, and cannot be reverse-transcribed otherwise. (*A*) Enzymatic nicked tRNA repair under optimized SPE conditions. Blue arrow: repaired product (ligation in cis). Red arrow: single-stranded tRNA halves generated by heat before enzymatic treatment. (*B*) RNA purification by TRIzol (TRI) impairs enzymatic nicked tRNA repair. Yellow stars: other RNAs are also repaired (ligated in cis) by our protocol. (*C*) Northern blot of RNAse1-treated RNA purified by SPE, TRIzol, miRNeasy or heated before SPE purification, after separation in native gels. (*D*) Nicked tRNA repair with RtCB from *E. coli*. (*E*) RNase treatment generates a roadblock for thermostable reverse transcriptases (RT) at the anticodon loop (ACL), inhibiting RT-PCR amplification of nicked tRNAs. Treated samples were analyzed by end-point RT-PCR (SYBR gold-stained gel) or RT-qPCR for the full-length $tRNA^{Gly}_{GCC}$ (black, *Left* axis) or by SL-RT-qPCR for 5′ $tRNA^{Gly}_{GCC}$ halves of 30 nt (purple, *Right* axis). (*F*) Purification of RNase1-treated RNA by SPE and reexposure to RNase 1, with or without previous heat denaturation. Δ: heat.

The 3′–5′ RNA Ligase RtcB Can also Ligate Nicked tRNAs. RtcB is a ligase involved in tRNA splicing and RNA repair in all domains of life (42–44). Unlike the 5′–3′ T4 Rnl1, RtcB seals broken RNAs with 2′,3′ cyclic phosphate (2,3-cP) and 5′-OH ends (45). Thus, RtcB should be sufficient to repair RNase1-treated RNAs without prior end-healing by T4 PNK. Indeed, RtcB regenerated a tRNA-sized band when incubated with RNase1-treated RNAs, and generation of this ligation product was inhibited by heat (Fig. 4*D*). Once again, the repaired tRNA-sized band was 4 to 5 nt shorter than the parental full-length tRNA (*SI Appendix*, Fig. S7*F*).

Nicked tRNAs Are Reverse-Transcribed Inefficiently unless Repaired. Broken phosphodiester bonds could act as roadblocks inhibiting reverse transcription (RT) of nicked tRNAs in their native state, preventing the analysis of nicked tRNAs by RT-PCR or sequencing. To evaluate this possibility, we used a thermostable retroviral reverse transcriptase primed by a gene-specific RT primer aligning to the 3′ end of $tRNA^{Gly}_{GCC}$ (Fig. 4*E*). Forward and reverse PCR primers were placed closed to the 5′ and 3′ ends of $tRNA^{Gly}_{GCC}$, respectively. Surprisingly, RNase-1-treated RNA was not amplified unless enzymatic repair (T4 PNK + T4 Rnl1) was performed before RT. Consistent with northern blot results (Figs. 3*D* and 4 *A*–*D*), heating the samples before enzymatic repair also inhibited RT-PCR amplification (Fig. 4*E*). Conversely, 5′ $tRNA^{Gly}_{GCC}$ halves of 30 nt increased 200 to 700-fold in RNase1-treated samples vs. input, illustrating the limitations of small RNA expression analysis in samples containing nicked forms of their parental RNAs.

Nicked tRNAs Are Resistant to RNase 1 Cleavage In Vitro. Having observed that nicked tRNAs can be purified efficiently by SPE, we generated and purified nicked tRNAs and treated them with r-RNase 1 (Fig. 4*F*). Nicked tRNAs were not degraded by this treatment (up to 30 min at 37 °C). However, heating and then cooling the nicked tRNAs before exposure to r-RNase1 induced complete degradation of the tRNA halves, now in their single-stranded form. This effect was not induced by heat itself. In conclusion, nicked tRNAs are stable reservoirs of 5′ tRNA halves, which are degradation prone once dissociated from their 3′ counterparts.

Nicked tRNAs as a Source of Intracellular Stress-Induced tRNA Halves. Our enzymatic repair assays were not useful to interrogate the existence of nicked tRNAs inside cells due to the large excess of full-length tRNAs in intracellular samples. We thus resorted to a different strategy based on intracellular RNA fractionation under nondenaturing conditions by size-exclusion chromatography (SEC) (Fig. 5 *A*–*D*).

To stimulate the formation of stress-induced tRNA halves inside cells (tiRNAs), U2-OS cells were treated with sodium arsenite (23). Upregulation of tRNA halves in stressed cells was confirmed by northern blot (Fig. 5*B*). We then lysed tiRNA-containing stressed cells by phenol-free methods, purified intracellular RNA by SPE to avoid potential nicked RNA denaturation, and size-fractionated the purified RNA by SEC in RNase-free PBS as running buffer. Two peaks with ABS 260 nm > ABS 280 nm were observed, corresponding to the elution of rRNAs and tRNAs (Fig. 5*C*, *Left*). The elution of full-length tRNAs at elution volume (Ve) = 9.80 mL was confirmed by northern blot (Fig. 5*C*, *Center*; fractions 2 to 4). Surprisingly, intracellular 5′ tRNA halves (of 35 and 30 nt) coeluted with full-length tRNAs, suggesting that tiRNAs are not single-stranded molecules inside cells. We considered the possibility that the sensitivity of our DIG-based northern blot assay was not sufficient to detect monomeric tiRNAs, which would be expected at Ve ≥ 11 mL (fraction ≥ #6) based on the injection of synthetic single-stranded RNAs of 30 nt (32). To study this, a highly sensitive stem-loop RT-qPCR (SL-RT-qPCR) assay was used (Fig. 5*C*, *Right*). This assay is specific for mature miRNAs or tRNA halves and does not amplify their precursors (pre-miRNAs or full-length tRNAs, respectively) (32, 46). miR-21-5p eluted at V_e = 11.4 mL (fraction #7), 5′ $tRNA^{Gly}{}_{GCC}$ halves of 30 nt (Fig. 5*C*) or 35 nt (*SI Appendix*, Fig. S8*A*) were again undetectable, except in fraction #3, containing most full-length tRNAs. Heating the RNA before injection (Fig. 5*D*) shifted the amplification of 5′ $tRNA^{Gly}{}_{GCC}$ halves toward fraction #6 (Ve = 11 mL), consistent with the expected denaturation of nicked tRNAs and the release of single-stranded tRNA halves, which now coeluted with miR-21-5p.

Overall, while we do not discard that bona fide single-stranded intracellular tiRNAs could be degraded upon cell lysis, our results strongly suggest that at least some (if not most) intracellular tiRNAs are predominantly present in the form of nicked tRNAs.

Detection of Nonvesicular Nicked tRNAs in Cell-Conditioned Media. To explore the presence of nicked tRNAs in extracellular samples, we collected cell-conditioned media (CCM, t = 24 h) from U2-OS cells grown under-serum-free conditions and separated EVs from nonvesicular proteins and RNAs by SEC, using commercial qEV columns (Fig. 5*E*). To preserve both nicked tRNAs and single-stranded tDRs, we added RI to the media. As expected in RI-treated serum-free CCM (33), we observed full-length tRNAs in nonvesicular fractions by northern blot (Fig. 5*E*; NT lane), albeit most of the signal corresponded to ~30-nt fragments. In this case, sequential treatment with PNK and Rnl1 generated at least three bands with sizes close to, but slightly shorter than, the size of the parental full-length tRNA. Once again, heating and cooling the samples before ligation abrogated generation of these products, arguing against nonspecific ligation in trans. The lowest and most intense band had a size of 61 nt, consistent with the main ligation product observed when incubating RNAs in CSF for long periods of time (*SI Appendix*, Fig. S7*B*). As previously discussed, this suggests the presence of trimmed forms of nicked tRNAs, lacking both the 3′ NCCA tail and the entire anticodon loop. Once formed, these ligation products could be heated and remained resistant to the processive 3′ to 5′ exonuclease RNase R (*SI Appendix*, Fig. S8*B*), suggesting the ligated products are highly structured. In contrast, the remaining 30 to 35-nt band after enzymatic repair was completely degraded by RNase R.

Interestingly, a band of approximately 24 nt was generated by the combined action of PNK and Rnl1 in both heated and nonheated samples (Fig. 5*E*; red stars). Because this band was resistant to RNase R (*SI Appendix*, Fig. S8*B*), we speculate that it corresponds to a circularized RNA generated by head-to-tail ligation of 5′ tRNA halves. Formation of this product in nonheated samples implies that at least some extracellular tRNA halves are present in fragment form in RI-treated CCM. This suggests that nicked tRNAs are spontaneously separating and releasing single-stranded tRNA halves into the extracellular space. Their detection is facilitated by the low RNase activity in the conditions of this assay.

Nonvesicular Nicked tRNAs Circulate in Human Biofluids. Having validated a method capable of separating nicked tRNAs from single-stranded tRNA halves (Fig. 5 *C* and *D*), we implemented this methodology to address the question of whether nicked tRNAs circulate in human biofluids. To do so, small volumes of serum or CSF were diluted in PBS, and EVs were pelleted by ultracentrifugation. RNA was then isolated from Proteinase K-treated supernatants and fractionated by SEC. Surprisingly, 30-nt 5′ $tRNA^{Gly}{}_{GCC}$ halves could be amplified by SL-RT-qPCR (Fig. 5 *F* and *G*), mostly in the size range corresponding to full-length tRNAs, which are expected to be absent in these samples (Fig. 2*B*).

Spontaneous Uptake of Nonvesicular tRNA Halves by Human Epithelial Cells. Unless stabilized by dimerization or RNP complex formation, we would expect single-stranded tRNA halves to be degraded in a matter of seconds in extracellular samples with high RNase activity (Fig. 4*F*). However, if stable nicked tRNAs diffuse from the sites in which they are generated and they can reach farther cellular populations, their spontaneous dissociation could release single-stranded tRNA halves close to the surface of potentially recipient cells. Could cells then internalize these single-stranded tDRs?

We incubated synthetic and biotinylated 5′ $tRNA^{Gly}{}_{GCC}$ halves of 30 and 35 nt, or scrambled (SCR) versions of these oligonucleotides, with MCF-7 cells grown in serum-free media (Fig. 6*A*). No lipids or transfection reagents were used. After 30 min, cells were thoroughly washed, fixed, stained with APC-coupled streptavidin and observed under a confocal microscope. Surprisingly, the red signal of the fluorophore's emission was observed within cellular boundaries in all conditions where labeled RNAs were included (Fig. 6 *B* and *C*). As an orthogonal approach, we incubated cells with nonbiotinylated SCR oligonucleotides (which do not exist in recipient cells), washed cells thoroughly, and observed a drop of almost 15 PCR cycles when comparing with nontreated cells, based on a SCR-specific SL-RT-qPCR assay (Fig. 6*D*). Taken together, these results show that human epithelial cells can spontaneously incorporate single-stranded small RNAs present in the media. Although this uptake route seems to be sequence- independent, most naked exRNAs will degrade before having the opportunity to interact with recipient cells. However, tRNA halves are

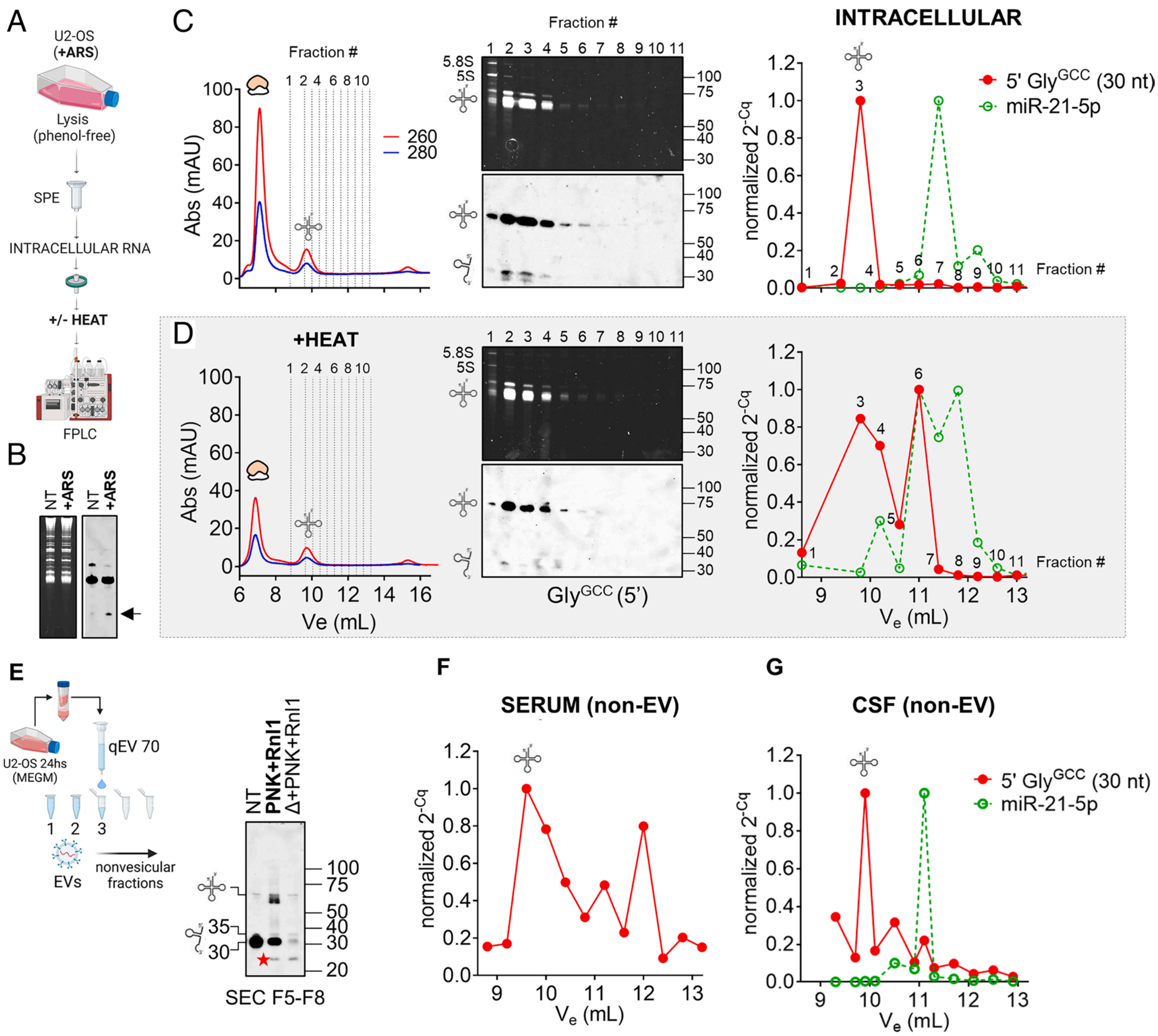

Fig. 5. Detection and analysis of nicked tRNAs in intracellular (*A–D*) and extracellular (*E–G*) samples. (*A*) Schematic representation of SEC-based (native) intracellular RNA fractionation as performed in (*C*) and (*D*). (*B*) Northern blot of intracellular RNAs showing the presence of 5′ tRNA halves in arsenite (ARS)-treated samples (i.e., tiRNAs). (*C*) Purified RNA from ARS-treated U2-OS cells was separated on a Superdex 75 column using an FPLC system. Selected fractions were analyzed by northern blot (*Center*) or by stem-loop RT-qPCR (*Right*). C_q values were normalized to the fraction containing the highest signal. (*D*) Same as in (*C*), but the RNA was heat-denatured before injection. (*E*) Cell-conditioned, RI-treated, serum-free medium from U2-OS cells was fractionated with an Izon 70-nm qEVoriginal column to prepare EV-depleted fractions. Northern blot analysis of tRNAs & tDRs in pooled nonvesicular extracellular fractions (F5 to F8) before and after enzymatic repair with T4 PNK and T4 Rnl1. Red star: a ~24-nt band that was only observed in the presence of Rnl1. (*F* and *G*) Separation by SEC (as done in *C*) of purified RNA from Proteinase K-treated ultracentrifugation supernatants of human serum (*E*) or CSF (*F*). Selected eluted fractions were analyzed by SL-RT-qPCR using primers specific for 5′ $tRNA^{Gly}_{GCC}$ halves of 30 nt (red) and miR-21-5p (green). A tRNA icon in this figure indicates fractions where full-length tRNAs are expected to elute (if present).

extremely stable in extracellular samples (Fig. 2), presumably due to their transport in the form of nicked tRNAs. For this reason, and because their extracellular concentration is increased in the presence of cell stress (Fig. 1*D*), we foresee the involvement of extracellular tRNA halves in intercellular communication pathways mediated by naked, nonvesicular RNAs (Fig. 6*E*).

Discussion

This work challenges the widespread belief that all RNAs are intrinsically unstable and cannot circulate in extracellular samples unless in the context of RNPs, lipoproteins and/or EVs. Although this holds true for rRNA-derived fragments (Fig. 1), full-length or nicked tRNAs showed surprisingly long half-lives in human biofluids, even when incubated in their naked forms. While these RNAs might also be present in RNP complexes in the extracellular space, our results demonstrate that protein complexation is not a prerequisite for their remarkable extracellular stability.

An aspect of this study that certainly deserves more attention is the differences in extracellular stabilities observed among tRNAs. We are tempted to speculate that posttranscriptionally modified bases at the anticodon are at least partially responsible for these different behaviors. However, the difference in stability between tRNAs is less pronounced when considering that nicked tRNAs, and not tDRs, are the stable degradation intermediates dictating the abundance of nonvesicular glycine tRNA halves.

Is the full-length $tRNA^{Gly}_{GCC}$ unstable in human biofluids? It is efficiently cleaved at several positions by extracellular RNases. So the immediate answer would be "yes". However, the result of these cleavage events is a molecule that probably still resembles a tRNA, although it bears some broken phosphodiester bonds.

169

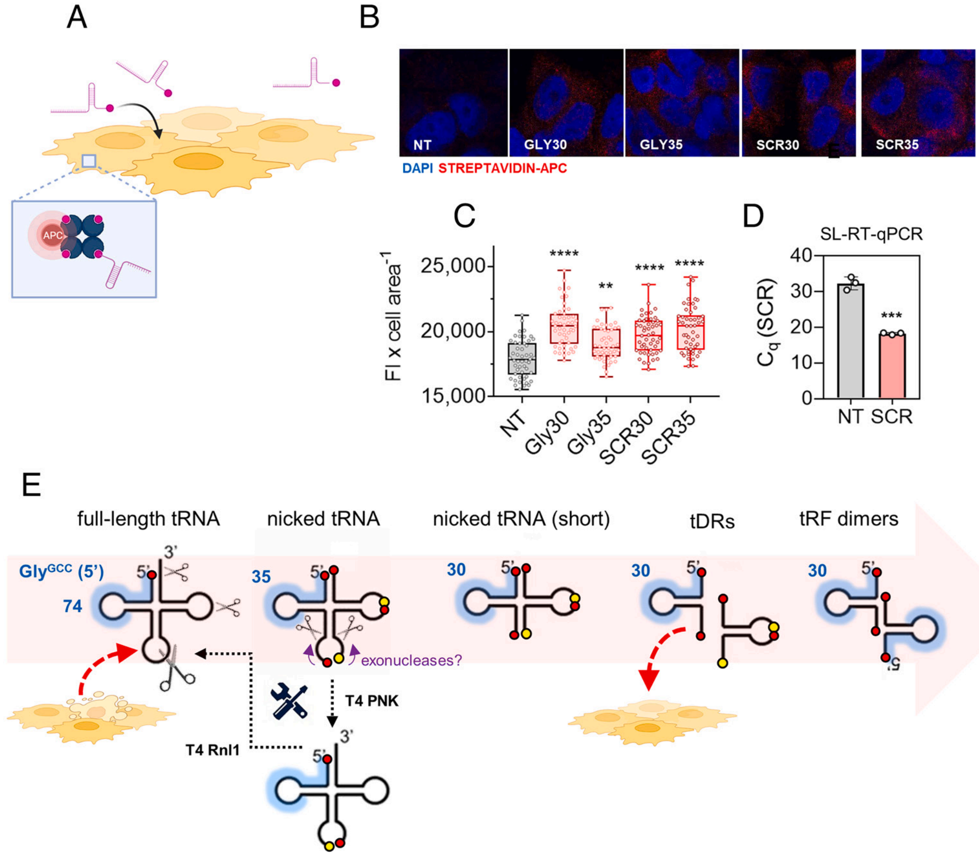

Fig. 6. Nicked tRNAs are a source of nonvesicular single-stranded tRNA halves that can be taken up by recipient cells. (*A*) Synthetic 5′ biotinylated RNAs were added to the media of MCF-7 cells, and oligonucleotide uptake was confirmed by confocal microscopy using APC-coupled streptavidin (*B* and *C*) or by SL-RT-qPCR (*D*). (*E*) Proposed model.Red circles: phosphate groups. Yellow circles: OH groups.

Thus, although $tRNA^{Lys}_{UUU}$ and $tRNA^{Gly}_{GCC}$ show completely different behaviors when analyzed by northern blot after being exposed to RNases, this difference is exaggerated because standard northern blotting forces nicked tRNAs to denature. This is also the case when purifying RNA using phenol and when RNA is heated at any stage in a protocol (e.g., as done during small RNA-seq library preparation). The important conclusion is that we do not always apprehend the true, native form of RNA because most available analytical techniques contain denaturation steps at some point. Additionally, nicked tRNAs cannot be reverse-transcribed and amplified unless repaired or denatured into fragments.

The case of $tRNA^{Lys}_{UUU}$ is also interesting. Although it is highly resistant to degradation, once cleaved by r-RNase 1 or by FBS-derived RNase A, it typically does not survive as a nicked tRNA (Fig. 2*A*). This implicates extracellular RNases in the degradation of tDRs (47). In contrast, $tRNA^{Gly}_{GCC}$ is sensitive to initial cleavage events, but nicked tRNAs produced therefrom are intrinsically stable. Differential stabilities among distinct tRNA sequences could be considered a new example of noncanonical "moonlighting" functions of tRNAs, what has been related to the diversity of the tRNA isodecoder pool (48).

In bacteria, phage infection (40) or DNA-damage (49) induces regulated tRNA cleavage at the anticodon loop. This process can be reversed by host-encoded tRNA ligases such as RtcB (44) or by phage antitoxins like T4 PNK and T4 Rnl1. Thus, the existence of nicked tRNAs that can be enzymatically repaired back into full-length tRNAs is well established in prokaryotes.

In plants, the phloem sap (PS) has been shown to contain 70 to 80-nt RNAs, which resemble tRNAs, that are capable of inhibiting translation. Importantly, this activity was lost when purifying PS RNA by TRIzol (50). Thus, plants also seem to generate nicked tRNAs in their vasculature. Nonvesicular tRNA halves were also recently identified in the extracellular apoplastic fluid (51). The theoretical capacity of nicked tRNAs to act as regulators of the translation machinery was recognized early (52). However, nicked tRNAs were not considered as stable degradation intermediates in the subsequent literature (53).

Stress-induced tRNA cleavage at the anticodon loop is thought to be an irreversible process. Nevertheless, it should be considered that most of the enzymatic activities used in this work to repair anticodon-cleaved nicked tRNAs are present in human cells (54, 55). Reversibility of stress-induced nicked tRNA formation in cellulo arises as an exciting possibility (56).

In the clinical setting, double-stranded RNAs usually require encapsulation in lipid nanoparticles or GalNAc conjugation for efficient uptake, but single-stranded oligonucleotides are spontaneously endocytosed (57). Thus, our proposed model where nonvesicular nicked tRNAs are carriers of tRNA halves that can transfer information to recipient cells is at least feasible (Fig. 6*E*).

On the applied side, we took advantage of phage and bacterial enzymes involved in damaged tRNA repair to develop an analytical technique that can be used to detect and measure stable nonvesicular RNAs circulating in biofluids. Although we focused mostly on tRNAs, close inspection of gels shows additional bands that could be restored by combined treatment with PNK and Rnl1 and that were lost in heated samples (Fig. 4*B*, yellow stars). This strongly suggests that the nonvesicular RNAome is much more complex than previously thought, in accordance with recent findings (33). Many stable nonvesicular RNAs are single-stranded

170

molecules tightly bound and protected by exRNA-binding proteins (15, 16, 38). However, intrinsically stable RNAs could also circulate freely in biofluids (58). These molecules are predicted to be both highly structured and nicked. There are sequencing methods that can efficiently handle highly structured RNAs (59, 60). However, nicked RNAs are more challenging because they contain roadblocks for reverse transcriptases (i.e., the broken phosphodiester bonds) and because nicked RNAs are dissociated by phenol or heat. Our enzymatic repair protocol therefore increases the number and types of RNA molecules that can be analyzed and used as disease biomarkers.

Materials and Methods

Detailed versions of these protocols and additional methods are included in *SI Appendix, Supplementary Materials and Methods*.

Biofluids and Cell Culture. Biofluids samples were obtained at UC San Diego (CSF) or at the Pasteur Institute of Montevideo (serum, urine), and deidentified prior to use. Samples were spun down at 2,000 × g before storage at ≤ −20 °C. Fetal bovine serum (FBS) was from Gibco. Cell-conditioned media (CCM) were obtained from either U2-OS cells grown under serum-free (MEGM, Lonza) or serum-containing conditions (10% FBS), with or without addition of murine RI (NEB). Intracellular tRNA-derived fragments were generated by exposing cells to 500 μM sodium arsenite (Sigma) for 2 h.

RNA Purification by SPE. RNA was purified by silica-based SPE using Monarch RNA Cleanup Kits (for in vitro assays) or the Total RNA Miniprep Kit for intracellular samples (NEB).

RNA Decay Assays. For determination of RNA half-lives in biofluids, 1 μg heated and refolded U2-OS total RNA was incubated at 37 °C for variable periods with 50 μL undiluted or PBS-diluted biofluid samples. Digested RNAs were purified by SPE and analyzed by northern blot.

In Vitro RNA Digestion. For in vitro generation of nicked tRNAs and/or tDRs, 1 μg heated and refolded U2-OS total RNA was incubated with recombinant human RNase 1 (Bon Opus Bio; 0.0625 μg/mL) for 15, 30, or 60 min at 37 °C, and purified by SPE.

RNA Ligation Assays. In vitro-digested or CCM-derived nonvesicular RNA was incubated for 1 h at 37 °C in a 10 μL reaction containing 20 U RI, 1 mM ATP, 1X T4 PNK reaction buffer, 10 U T4 RNA ligase 1 (Rnl1, NEB), and/or 10 U of T4 PNK (wild type or 3′ phosphatase minus, NEB). For RtcB ligation, reaction mixtures contained 5 μL in vitro-digested digested RNA, 20 U RI, 1X RtcB ligase buffer, 1 mM GTP, 1 mM Mn^{2+}, and 1 μM RtcB ligase from *E. coli* (NEB).

Preparation of Nonvesicular RNAs from Cell-Conditioned Media. Nonvesicular RNAs from U2-OS cell-conditioned media were separated from EVs by either iodixanol 12 to 36% density gradients (33, 37) or by size-exclusion chromatography using 70-nm qEVoriginal columns (IZON).

Chromatographic Fractionation of Nonvesicular RNAs from Biofluids. EVs were depleted from human serum or CSF samples by ultracentrifugation (256,000 × g and 4 °C for 1 h). The supernatants were concentrated by ultrafiltration (10 kDa MWCO), treated with phenol-free RNA Binding Buffer (included in RNA Cleanup Kits from NEB) and Proteinase K, and the RNA was purified by SPE. Purified RNAs were then injected in a Superdex 75 10/300 column (GE), using an Äkta Pure FPLC system. Fractions of 0.2 mL were collected and analyzed by stem-loop RT-qPCR.

Northern Blot, RT-qPCR for Full-Length tRNAs and SL-RT-qPCR for tDRs. DIG-based northern blot and stem-loop RT-qPCR were done as described in ref. 33 and 32, respectively. RT-PCR for full-length tRNAs was done using Superscript IV at 50 °C. Probes, primers, and assay conditions are provided in *SI Appendix, Supplementary Materials and Methods*.

Data, Materials, and Software Availability. All study data are included in the article and/or *SI Appendix*.

ACKNOWLEDGMENTS. We thank Sergio Bianchi and other members of the Functional Genomics Laboratory (IPMon) and the Analytical Biochemistry Unit (UdelaR). This work was supported in part by the NIH (R01GM126150, R01GM146997), the National Cancer Institute (NCI) and NIH Office of the Director (UG3/UH3CA241694), and Universidad de la República, Uruguay (CSIC I+D_2020_433). B.C. received a fellowship from the National Agency of Research and Innovation (ANII, Uruguay; POS_NAC_M_2020_1_163868). J.P.T., E.C., and A.C. are members of the National System of Researchers (ANII, Uruguay) and the Program for the Development of Basic Science (PEDECIBA, Uruguay).

Author affiliations: [a]Functional Genomics Laboratory, Institut Pasteur de Montevideo, Montevideo 11400, Uruguay; [b]Analytical Biochemistry Unit, Center for Nuclear Research, School of Science, Universidad de la República, Montevideo 11400, Uruguay; [c]Biochemistry Department, School of Science, Universidad de la República, Montevideo 11400, Uruguay; [d]Laboratory of Enzymology, School of Science, Universidad de la República, Montevideo 11400, Uruguay; [e]Centro de Investigaciones Biomédicas, Universidad de la República, Montevideo 11800, Uruguay; [f]Department of Neurosciences, University of California San Diego, La Jolla, CA 92093; [g]Brigham and Women's Hospital and Harvard Medical School, Boston, MA 02115; [h]Molecular and Comparative Pathobiology, Neurology, and The Richman Family Precision Medicine Center of Excellence in Alzheimer's Disease, Johns Hopkins University School of Medicine, Baltimore, MD 21205; and [i]Hospital de Clínicas, Universidad de la República, Montevideo 11600, Uruguay

1. M. N. Moufarrej *et al.*, Early prediction of preeclampsia in pregnancy with cell-free RNA. *Nature* **602**, 689–694 (2022).
2. E. Heitzer, I. S. Haque, C. E. S. Roberts, M. R. Speicher, Current and future perspectives of liquid biopsies in genomics-driven oncology. *Nat. Rev. Genet.* **20**, 71–88 (2019).
3. T. Thomou *et al.*, Adipose-derived circulating miRNAs regulate gene expression in other tissues. *Nature* **542**, 450–455 (2017).
4. M. R. Garcia-Silva *et al.*, Extracellular vesicles shed by Trypanosoma cruzi are linked to small RNA pathways, life cycle regulation, and susceptibility to infection of mammalian cells. *Parasitol. Res.* **113**, 285–304 (2014).
5. Q. Cai *et al.*, Plants send small RNAs in extracellular vesicles to fungal pathogen to silence virulence genes. *Science* **360**, 1126–1129 (2018).
6. A. H. Buck *et al.*, Exosomes secreted by nematode parasites transfer small RNAs to mammalian cells and modulate innate immunity. *Nat. Commun.* **5**, 5488 (2014).
7. J. P. Tosar, K. Witwer, A. Cayota, Revisiting extracellular RNA release, processing, and function. *Trends Biochem. Sci.* **46**, 438–445 (2021).
8. J. Skog *et al.*, Glioblastoma microvesicles transport RNA and proteins that promote tumour growth and provide diagnostic biomarkers. *Nat. Cell Biol.* **10**, 1470–1476 (2008).
9. H. Valadi *et al.*, Exosome-mediated transfer of mRNAs and microRNAs is a novel mechanism of genetic exchange between cells. *Nat. Cell Biol.* **9**, 654–659 (2007).
10. B. Mateescu *et al.*, Obstacles and opportunities in the functional analysis of extracellular vesicle RNA - An ISEV position paper. *J. Extracell. Vesicles* **6**, 1286095 (2017).
11. K. O'Brien, K. Breyne, S. Ughetto, L. C. Laurent, X. O. Breakefield, RNA delivery by extracellular vesicles in mammalian cells and its applications. *Nat. Rev. Mol. Cell Biol.* **21**, 585–606 (2020).
12. J. P. Tosar *et al.*, Assessment of small RNA sorting into different extracellular fractions revealed by high-throughput sequencing of breast cell lines. *Nucleic Acids Res.* **43**, 5601–5616 (2015).
13. Z. Wei *et al.*, Coding and noncoding landscape of extracellular RNA released by human glioma stem cells. *Nat. Commun.* **8**, 1145 (2017).
14. Q. Zhang *et al.*, Supermeres are functional extracellular nanoparticles replete with disease biomarkers and therapeutic targets. *Nat. Cell Biol.* **23**, 1240–1254 (2021).
15. A. Turchinovich, L. Weiz, A. Langheinz, B. Burwinkel, Characterization of extracellular circulating microRNA. *Nucleic Acids Res.* **39**, 7223–7233 (2011).
16. J. D. Arroyo *et al.*, Argonaute2 complexes carry a population of circulating microRNAs independent of vesicles in human plasma. *Proc. Natl. Acad. Sci. U.S.A.* **108**, 5003–5008 (2011).
17. H. Geekiyanage, S. Rayatpisheh, J. A. Wohlschlegel, R. Brown, V. Ambros, Extracellular microRNAs in human circulation are associated with miRISC complexes that are accessible to anti-AGO2 antibody and can bind target mimic oligonucleotides. *Proc. Natl. Acad. Sci. U.S.A.* **117**, 24213–24223 (2020).
18. K. C. Vickers, B. T. Palmisano, B. M. Shoucri, R. D. Shamburek, A. T. Remaley, MicroRNAs are transported in plasma and delivered to recipient cells by high-density lipoproteins. *Nat. Cell Biol.* **13**, 423–435 (2011).
19. D. M. Thompson, C. Lu, P. J. Green, R. Parker, tRNA cleavage is a conserved response to oxidative stress in eukaryotes. *RNA* **14**, 2095–2103 (2008).
20. Y. Li *et al.*, Stress-induced tRNA-derived RNAs: A novel class of small RNAs in the primitive eukaryote Giardia lamblia. *Nucleic Acids Res.* **36**, 6048–6055 (2008).
21. M. David, G. D. Borasio, G. Kaufmann, Bacteriophage T4-induced anticodon-loop nuclease detected in a host strain restrictive to RNA ligase mutants. *Proc. Natl. Acad. Sci. U.S.A.* **79**, 7097–7101 (1982).
22. H. Fu *et al.*, Stress induces tRNA cleavage by angiogenin in mammalian cells. *FEBS Lett.* **583**, 437–442 (2009).
23. S. Yamasaki, P. Ivanov, G.-F. Hu, P. Anderson, Angiogenin cleaves tRNA and promotes stress-induced translational repression. *J. Cell Biol.* **185**, 35–42 (2009).
24. P. Ivanov, M. M. Emara, J. Villen, S. P. Gygi, P. Anderson, Angiogenin-induced tRNA fragments inhibit translation initiation. *Mol. Cell* **43**, 613–623 (2011).
25. S. M. Lyons *et al.*, eIF4G has intrinsic G-quadruplex binding activity that is required for tiRNA function. *Nucleic Acids Res.* **48**, 6223–6233 (2021).

171

26. H. K. Kim *et al.*, A transfer-RNA-derived small RNA regulates ribosome biogenesis. *Nature* **552**, 57–62 (2017).
27. C. Kuscu *et al.*, tRNA fragments (tRFs) guide Ago to regulate gene expression post-transcriptionally in a Dicer-independent manner. *RNA* **24**, 1093–1105 (2018).
28. E. N. M. Nolte'T Hoen *et al.*, Deep sequencing of RNA from immune cell-derived vesicles uncovers the selective incorporation of small non-coding RNA biotypes with potential regulatory functions. *Nucleic Acids Res.* **40**, 9272–9285 (2012).
29. J. M. Dhahbi *et al.*, 5′ tRNA halves are present as abundant complexes in serum, concentrated in blood cells, and modulated by aging and calorie restriction. *BMC Genomics* **14**, 298 (2013).
30. Y. Zhang *et al.*, Identification and characterization of an ancient class of small RNAs enriched in serum associating with active infection. *J. Mol. Cell Biol.* **6**, 172–174 (2014).
31. S. Srinivasan *et al.*, Small RNA sequencing across diverse biofluids identifies optimal methods for exRNA isolation. *Cell* **177**, 446–462 (2019).
32. J. P. Tosar *et al.*, Dimerization confers increased stability to nucleases in 5′ halves from glycine and glutamic acid tRNAs. *Nucleic Acids Res.* **46**, 9081–9093 (2018).
33. J. P. Tosar *et al.*, Fragmentation of extracellular ribosomes and tRNAs shapes the extracellular RNAome. *Nucleic Acids Res.* **48**, 12874–12888 (2020).
34. G. Nechooshtan, D. Yunusov, K. Chang, T. R. Gingeras, Processing by RNase 1 forms tRNA halves and distinct Y RNA fragments in the extracellular environment. *Nucleic Acids Res.* **48**, 8035–8049 (2020).
35. N. Sanadgol, L. König, A. Drino, M. Jovic, M. R. Schaefer, Experimental paradigms revisited: oxidative stress-induced tRNA fragmentation does not correlate with stress granule formation but is associated with delayed cell death. *Nucleic Acids Res.* **50**, 6919–6937 (2022).
36. S. Sorrentino, The eight human "canonical" ribonucleases: Molecular diversity, catalytic properties, and special biological actions of the enzyme proteins. *FEBS Lett.* **584**, 2194–2200 (2010).
37. D. K. Jeppesen *et al.*, Reassessment of exosome composition. *Cell* **177**, 428–445 (2019).
38. J. P. Tosar, A. Cayota, K. Witwer, Exomeres and supermeres: Monolithic or diverse? *J. Extracell. Biol.* **1**, e45 (2022).
39. B. Schwer, R. Sawaya, C. K. Ho, S. Shuman, Portability and fidelity of RNA-repair systems. *Proc. Natl. Acad. Sci. U.S.A.* **101**, 2788–2793 (2004).
40. G. Kaufmann, Anticodon nucleases. *Trends Biochem. Sci.* **25**, 70–74 (2000).
41. Y. Akiyama *et al.*, Selective cleavage at CCA ends and anticodon loops of tRNAs by stress-induced RNases. *Front. Mol. Biosci.* **9**, 791094 (2022).
42. M. Englert, K. Sheppard, A. Aslanian, J. R. Yates, D. Söll, Archaeal 3′-phosphate RNA splicing ligase characterization identifies the missing component in tRNA maturation. *Proc. Natl. Acad. Sci. U.S.A.* **108**, 1290–1295 (2011).
43. J. Popow *et al.*, HSPC117 is the essential subunit of a human tRNA splicing ligase complex. *Science* **331**, 760–764 (2011).
44. N. Tanaka, S. Shuman, RtcB is the RNA ligase component of an Escherichia coli RNA repair operon. *J. Biol. Chem.* **286**, 7727–7731 (2011).
45. A. K. Chakravarty, R. Subbotin, B. T. Chait, S. Shuman, RNA ligase RtcB splices 3′-phosphate and 5′-OH ends via covalent RtcB-(histidinyl)-GMP and polynucleotide-(3′)pp(5′)G intermediates. *Proc. Natl. Acad. Sci. U.S.A.* **109**, 6072–6077 (2012).
46. C. Chen *et al.*, Real-time quantification of microRNAs by stem-loop RT-PCR. *Nucleic Acids Res.* **33**, e179 (2005).
47. G. Li *et al.*, Distinct stress-dependent signatures of cellular and extracellular tRNA-derived small RNAs. *Adv. Sci.* **9**, e2200829 (2022).
48. I. Avcilar-Kucukgoze, A. Kashina, Hijacking tRNAs from translation: Regulatory functions of tRNAs in mammalian cell physiology. *Front. Mol. Biosci.* **7**, 610617 (2020).
49. K. J. Hughes, X. Chen, A. M. Burroughs, L. Aravind, S. L. Wolin, An RNA repair operon regulated by damaged tRNAs. *Cell Rep.* **33**, 108527 (2020).
50. S. Zhang, L. Sun, F. Kragler, The phloem-delivered RNA pool contains small noncoding RNAs and interferes with translation. *Plant Physiol.* **150**, 378–387 (2009).
51. H. Zand Karimi *et al.*, Arabidopsis apoplastic fluid contains sRNA- and circular RNA-protein complexes that are located outside extracellular vesicles. *Plant Cell* **34**, 1863–1881 (2022).
52. D. M. Thompson, R. Parker, Stressing out over tRNA cleavage. *Cell* **138**, 215–219 (2009).
53. Q. Chen, X. Zhang, J. Shi, M. Yan, T. Zhou, Origins and evolving functionalities of tRNA-derived small RNAs. *Trends Biochem. Sci.* **46**, 790–804 (2021).
54. A. Kroupova *et al.*, Molecular architecture of the human tRNA ligase complex. *Elife* **10**, e71656 (2021).
55. P. H. Pinto *et al.*, ANGEL2 is a member of the CCR4 family of deadenylases with 2′,3′-cyclic phosphatase activity. *Science* **369**, 524–530 (2020).
56. Y. Akiyama *et al.*, RTCB complex regulates stress-induced tRNA cleavage. *Int. J. Mol. Sci.* **23**, 13100 (2022).
57. A. A. Levin, Treating disease at the RNA Level with oligonucleotides. *N. Engl. J. Med.* **380**, 57–70 (2019).
58. J. P. Tosar, Die hard: Resilient RNAs in the blood. *Nat. Rev. Mol. Cell Biol.* **22**, 373–373 (2021).
59. Y. Qin *et al.*, High-throughput sequencing of human plasma RNA by using thermostable group II intron reverse transcriptases. *RNA* **22**, 111–128 (2016).
60. A. Behrens, G. Rodschinka, D. D. Nedialkova, High-resolution quantitative profiling of tRNA abundance and modification status in eukaryotes by mim-tRNAseq. *Mol. Cell* **81**, 1802–1815.e7 (2021).

Anexo 2: Otros artículos publicados durante el doctorado que no forman parte de la tesis por compendio de artículos

Artículo 6: Paternal methotrexate exposure affects sperm small RNA content and causes craniofacial defects in the offspring

nature communications

Article

https://doi.org/10.1038/s41467-023-37427-7

Paternal methotrexate exposure affects sperm small RNA content and causes craniofacial defects in the offspring

Received: 9 July 2022

Accepted: 14 March 2023

Published online: 23 March 2023

Check for updates

Nagif Alata Jimenez[1,2], Mauricio Castellano[3,4], Emilio M. Santillan[5], Konstantinos Boulias[6,7], Agustín Boan[1,2], Luisa F. Arias Padilla[1,2], Juan I. Fernandino[1,2], Eric L. Greer[6,7], Juan P. Tosar[3,4], Luisa Cochella[5] & Pablo H. Strobl-Mazzulla[1,2]

Folate is an essential vitamin for vertebrate embryo development. Methotrexate (MTX) is a folate antagonist that is widely prescribed for autoimmune diseases, blood and solid organ malignancies, and dermatologic diseases. Although it is highly contraindicated for pregnant women, because it is associated with an increased risk of multiple birth defects, the effect of paternal MTX exposure on their offspring has been largely unexplored. Here, we found MTX treatment of adult medaka male fish (*Oryzias latipes*) causes cranial cartilage defects in their offspring. Small non-coding RNA (sncRNAs) sequencing in the sperm of MTX treated males identify differential expression of a subset of tRNAs, with higher abundance for specific 5′ tRNA halves. Sperm RNA methylation analysis on MTX treated males shows that m5C is the most abundant and differential modification found in RNAs ranging in size from 50 to 90 nucleotides, predominantly tRNAs, and that it correlates with greater testicular *Dnmt2* methyltransferase expression. Injection of sperm small RNA fractions from MTX-treated males into normal fertilized eggs generated cranial cartilage defects in the offspring. Overall, our data suggest that paternal MTX exposure alters sperm sncRNAs expression and modifications that may contribute to developmental defects in their offspring.

Folate is a water-soluble vitamin obtained from the diet that is essential for vertebrates. It is incorporated as an essential cofactor for the synthesis of nucleotides and the generation of S-adenosylmethionine (SAM) which serves as a universal donor of methyl groups for DNA, RNA and proteins implicated in gene regulation during early development[1–4]. Maternal folate deficiency leads to severe neural tube defects and craniofacial anomalies of descendants[5–7]. Importantly, the prevalence of these defects is highly reduced by folic acid supplementation prior and during pregnancy[8,9]. Despite global efforts to supplement the maternal diets with folate, there is still a worldwide prevalence of these congenital defects[10–12]. Methotrexate (MTX) is a recognized teratogenic folic acid antagonist that has been linked to an elevated incidence of congenital anomalies in children born from exposed women. Intrauterine MTX exposure has been linked to craniofacial and limb defects, as well as developmental delays[13,14]. In addition to oral clefts, folic acid antagonists may raise the risk of

[1]Laboratory of Developmental Biology, Instituto de Investigaciones Biotecnológicas- Instituto Tecnológico de Chascomús (CONICET-UNSAM), Chascomús, Argentina. [2]Escuela de Bio y Nanotecnologías (UNSAM), Chascomús, Argentina. [3]Functional Genomics Unit, Instituto Pasteur de Montevideo, Montevideo, Uruguay. [4]School of Science, Universidad de la República, Montevideo, Uruguay. [5]Department of Molecular Biology and Genetics, Johns Hopkins University School of Medicine, Baltimore, MA, USA. [6]Department of Pediatrics, HMS Initiative for RNA Medicine, Harvard Medical School, Boston, MA, USA. [7]Division of Newborn Medicine, Boston Children's Hospital, Boston, MA, USA. e-mail: strobl@intech.gov.ar

cardiovascular, neural tube, and urinary tract abnormalities[15]. As a result, current recommendations urge that mothers stop using MTX at least three months before conception[16]. Prior research has also identified a variety of issues concerning MTX use and a probable genotoxic effect on sperm, which might result in chronic disease or congenital anomalies[17]. However, medical care recommendations for males taking MTX while trying to conceive are less clear.

For decades, the sperm genome has been considered transcriptionally quiescent and solely contributing to the restoration of the ploidy of the zygote. However, more recently, a set of functional RNAs have been characterized in mature spermatozoa that are delivered to the oocyte upon fertilization, contributing to early embryo development and thus, influencing the phenotypic outcome of the offspring[18–24]. Intriguingly, paternal folate concentrations can affect the sperm epigenome[25,26]. Whereas the direct impact of these changes is expected to be minimal given the protamine exchange and resetting of DNA methylation during spermatogenesis and early development[27–29], we wondered whether paternal folate levels may also affect the RNA composition of mature sperm.

Small non-coding RNAs (sncRNAs) are a particularly attractive potential carrier of non-genetic information in the spermatozoa. In particular, tRNA-derived small RNAs (tsRNAs) and microRNAs (miRNAs) are the most abundant in mature spermatozoa[30,31]; and have been identified as molecular carriers of paternal experiences, including high fat diet[22,24,32], low protein diet[33], stress[21,34], and odoriferous sensitivity to chemicals[23]. Small RNA biogenesis, stability and functionality are highly dependent on their post-transcriptional modification status, primarily methylation[35–37]. Furthermore, transmission of paternally acquired metabolic disorders is dependent on the presence of post-transcriptional modifications in sperm sncRNAs[19,24].

Here, we explored the intriguing possibility that paternal folate deficiency impacts the offspring's development, and that it may do so through changes in sncRNA abundance and methylation levels. We injected medaka male fish with the folate inhibitor methotrexate (MTX) and characterized their offspring's developmental defects. Next, we analyzed and compared the abundance and modifications of sncRNAs present in the sperm of MTX-treated males to test the idea that they work as mediators of congenital developmental defects.

Results

Paternal folate deficiency induced cranial cartilage malformations in their offspring

To investigate the impact of paternal folate deficiency on the development of their progeny, we administered medaka male fish with an intraperitoneal injection of methotrexate (MTX), a well-known folate inhibitor[38–40], at 10 mg of MTX per Kg of body weight (10MTX) and 50 mg/Kg MTX (50MTX)(Fig. 1a). After 7 days, we fertilized wild type oocytes with sperm extracted from treated and untreated males. None of our treatments had a significant impact on sperm fecundity, hatching time, or overall embryo hatching (Fig. S1).

Several studies have shown that folate is an important vitamin for neural and neural crest development in several vertebrate species including humans[5,41,42]. Moreover, maternal folate deficiency during pregnancy leads to abnormal development of neural crest derivatives such as cranial cartilages[43–46]. Taking this into account, we first evaluated the effect of paternal folate deficiency on the development of the offspring's cranial cartilages by performing alcian blue staining at 3 days post hatching-stage (3dph). We measured the length of three dorsal cartilages (anterior orbital, epiphyseal bar and posterior orbital), four ventral cartilages (Meckel, ceratohyal, basibranchial and palatoquadrate), and the Meckel's area and ceratohyal angle (Fig. 1b–j). From the dorsal cartilages, we found a significant reduction in the length of the anterior orbital (also known as taenia marginalis anterior) in the 50MTX group (115.02 μm ± 9.03, one-way ANOVA followed by multiple comparison Tukey's test $p = 0.0164$) when compared to the 10MTX (130.02 μm ± 10.22) and control (125.98 μm ± 15.77). On the ventral side, the basibranchial and Meckel's cartilages were not affected. However, the ceratohyal was reduced to almost half the length, at both 10MTX (192.99 μm ± 7.55, $p < 0.0001$) and 50MTX (185.42 μm ± 8.71, $p < 0.0001$) compared with control (363.64 μm ± 18.96). Interestingly, when we looked at the morphology of those cranial cartilages, we found that two of them, the anterior orbital and basihyal, presented an abnormal shape (Fig. 2). In particular, the anterior orbital has an abnormal serpentine shape, compared with the normal curved shape (Fig. 2a, b). This phenotype was significantly prevalent ($p = 0.0059$) at the 50MTX group (Fig. 2c). However, one of the most drastically affected cartilages was the basihyal, whose phenotypes presented a curved trowel shape (mild) or hook shape (strong) (Fig. 2d). Quantitation of those phenotypes evidences a significant increase in the severity of them at both 10MTX ($p = 0.0329$) and 50MTX ($p = 0.0006$) compared with Control group (Fig. 2e). Overall, these findings support the notion that paternal MTX exposure affects the development of the offspring's cranial cartilage, indicating that sperm may convey some information involved in the observed phenotypic inheritance.

SncRNAs abundance is altered in the sperm of MTX-treated males

Epigenetic information, including histone modifications and DNA methylation, particularly from the paternal lineage, is largely reprogramed during germline and early embryo development. However, increasing evidence indicates that sncRNAs are a carrier of epigenetic information across generations and may act as mediators of paternally inherited traits[18–23,47]. To assess if paternal folate deficiency affects the small RNA content, we sequenced size selected (~18–30 nt long) RNAs from sperm of 10MTX and control males. Based on the analysis of three biological replicated for each group, we were able to identify different populations of sncRNAs including: ribosomal RNAs (rRNAs), small nuclear RNAs (snRNAs), small nucleolar RNAs (snoRNAs), micro RNAs (miRNAs), transfer RNA fragments (tRNAs), and other miscellaneous RNAs (miscRNA) (Fig. 3a). The comparative analysis showed that rRNAs and tRNA fragments were the most abundant on both control and 10MTX treatment. Some of the most abundant rRNAs mapped to 28S, 18S, and 5.8S rRNA. Reads mapping 5S rRNA and both 16S and 12S mitochondrial rRNA (mtrRNA) were also detected, albeit in a much lower proportion (Fig. 3b). Despite being the most abundant sncRNAs, we found no statistically significant difference in either cytoplasmic or mitochondrial rRNA expression between control and MTX-treated fish (Fig. 3c, d). On the other side, some of the most abundant tRNA fragments, aspartic acid (having the anticodon Asp^{GUC}), glutamic acid (Glu^{CUC} and Glu^{UUC}), lysine (Lys^{CUU}) and glycine (Gly^{GCC}) (Fig. 3b), became further significantly enriched upon MTX treatment (Fig. 3c, d). Together, these results demonstrate that paternal MTX exposure affects the relative abundance of specific sncRNAs in the sperm, with tRNA fragments being the most affected population.

5′ halves of particular tRNAs are preferentially affected by methotrexate treatment

tRNAs can be cleaved into 5′ and 3′ halves, known as tsRNAs, in response to stress or other external factors[19,24,35,48]. Of particular interest in the sperm RNA content is the large abundance of those tsRNA fragments and their potential regulatory roles in early embryo development[19,20,24,30,31]. Interestingly, we observed that 5′ tsRNA fragments, product of the cleavage of three of the most abundant tRNAs (5′ tsRNA of Asp^{GUC}, Lys^{CUU}, and Glu^{CUC}), were significantly increased in MTX sperm, without a concomitant increase in their respective 3′ tsRNA fragments (Fig. 4a, b, e). Quantification of the proportion of 5′ halves relative to their corresponding 3′ halves showed a significant increase in the percentage of 5′ halves for tRNA Asp^{GUC} and Gly^{GCC} in the MTX-treated samples (Fig. 4c, e). It is interesting to note that for some tRNAs (i.e., tRNA Glu^{CUC}, Glu^{UUC}, and Gly^{UCC}) we mostly retrieve reads

176

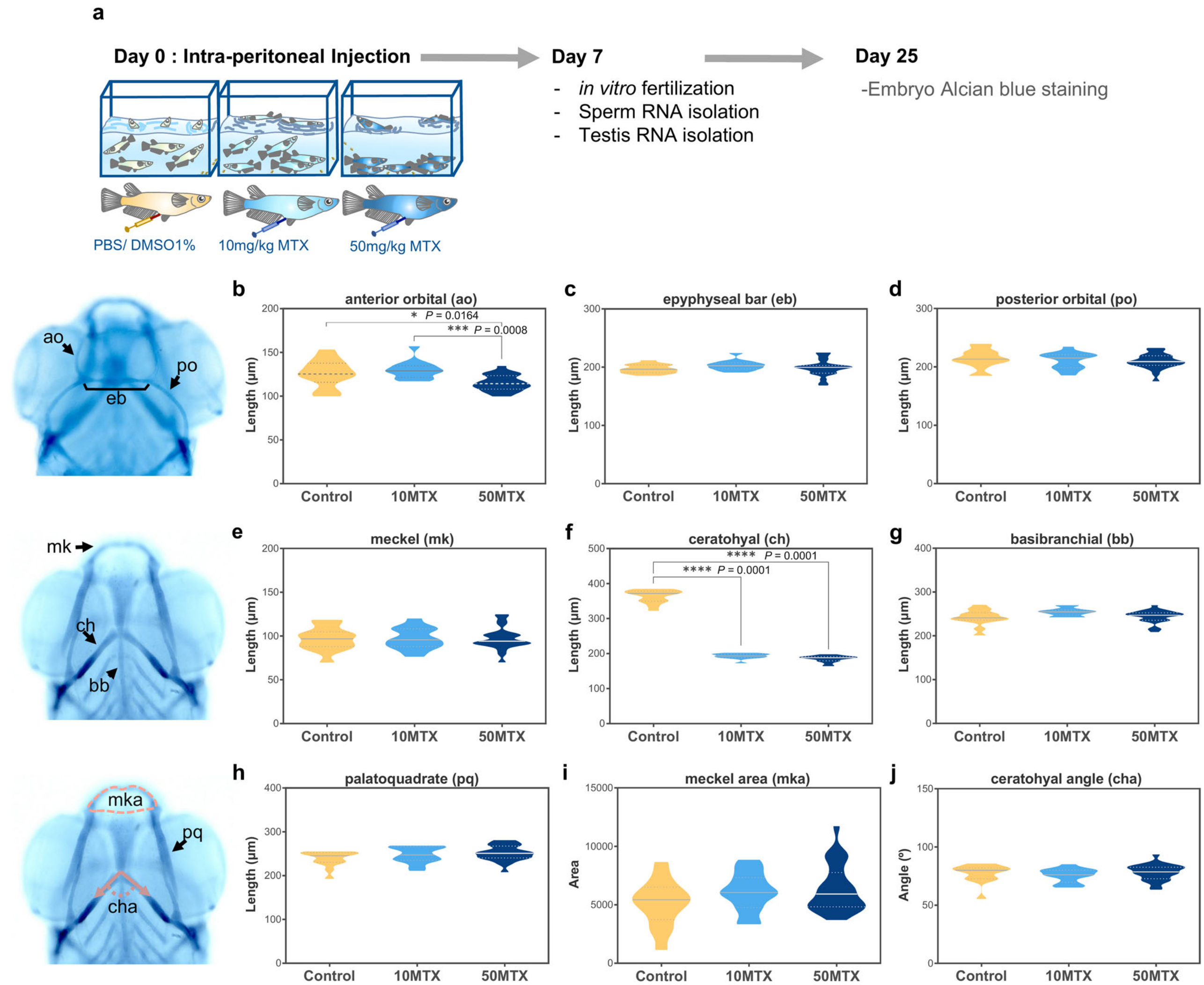

Fig. 1 | Paternal MTX injection affects offspring's cranial cartilages lengths. **a** scheme of experimental design. **b–j** Violin plots represent the measurement of different cranial cartilages lengths, angles and areas on control (Ctrl), 10MTX and 50MTX. Statistical analyses were performed using ANOVA one-way followed by multiple comparison Tukey's test. Numbers of analyzed embryos: Control ($n = 14$), 10MTX ($n = 14$), 50MTX ($n = 26$). *$P = 0.0164$, ***$P = 0.0008$, ****$P = 0.0001$.

for their 5′ halves, but their corresponding 3′ halves are almost undetected for both control and MTX. On the other hand, the 5′ halves of many (most) other tRNAs did not show differences compared with their 3′ halves (tRNA Pro^{UGG}, Arg^{UCU}), or a major proportion of their 3′ halves (tRNA Ser^{GCU}) (Fig. S2). These results suggest changes in processing or stability of specific tRNA fragments as a consequence of the MTX treatment.

Production of 5′ tsRNAs fragments in the 15–22 nt range occurs in multiple tissues and cell lines[49], whereas longer 5′ tsRNAs (31–40 nt long) are preferentially generated in response to different stresses[50,51]. We thus compared the length distribution of tRNAs-derived fragments in both conditions and observed a shift towards longer fragments in 10MTX relative to control samples (median length of 24 nt for control and 29 nt for MTX) (Fig. 4d). A similar situation is found for the tRNAs Glu^{CUC}, Asp^{GUC} and Lys^{CUU} where their 5′tsRNAs are significantly increased and their coverage lengths are greater in MTX-treated samples than in controls (Fig. 4f). There is a chance that bias size selection occurred when separating the small RNAs from the gel, resulting in these differences. However, we found that the read coverage and size distribution for the most abundant rRNA-derived fragments are slightly larger after MTX treatment (Fig. S3a), but this is not as dramatic as observed for tsRNAs (median length of 22 nt to 24 nt for rRNAs, vs. 24 nt to 29 nt for tsRNAs; Fig. S3b). These findings suggest that paternal MTX exposure alters the abundance and cleavage site of specific 5′tsRNAs in the sperm.

m5C modifications are increased by methotrexate

Post-transcriptional modifications of tRNAs, including methylation, are important for their specific cleavage, stability, and functionality, as well as for the transmission of paternal experiences to the offspring[35–37,52]. We thus evaluated the methylation status of two populations of RNAs isolated from polyacrylamide: a 20–50 nt population (mostly enriched for miRNAs and tsRNAs), and a 50–90 nt population (mostly enriched for mature tRNAs). Within the 20–50 nt RNA population we did not observe significant differences in the abundance of any of the analyzed methylation events between MTX and control groups (Fig. 5a). Conversely, within the 50–90 nt population, we found that MTX treatment led to a significant increase in the relative abundance of several modifications (Fig. 5b). From the two most abundant modifications analyzed (m1A and m5C) only m5C was significantly increased ($p = 0.0155$) in MTX treated samples. From the other less abundant modifications only m2G, m7G and m2′2G presented a significant increase in MTX samples (p value = 0.0027; 0.0063; and 0.0090, respectively). Interestingly, the most abundant modification observed to be differentially detected in MTX samples has been described to be located at the 3′ ends of tRNAs[53,54] (Fig. 5c).

177

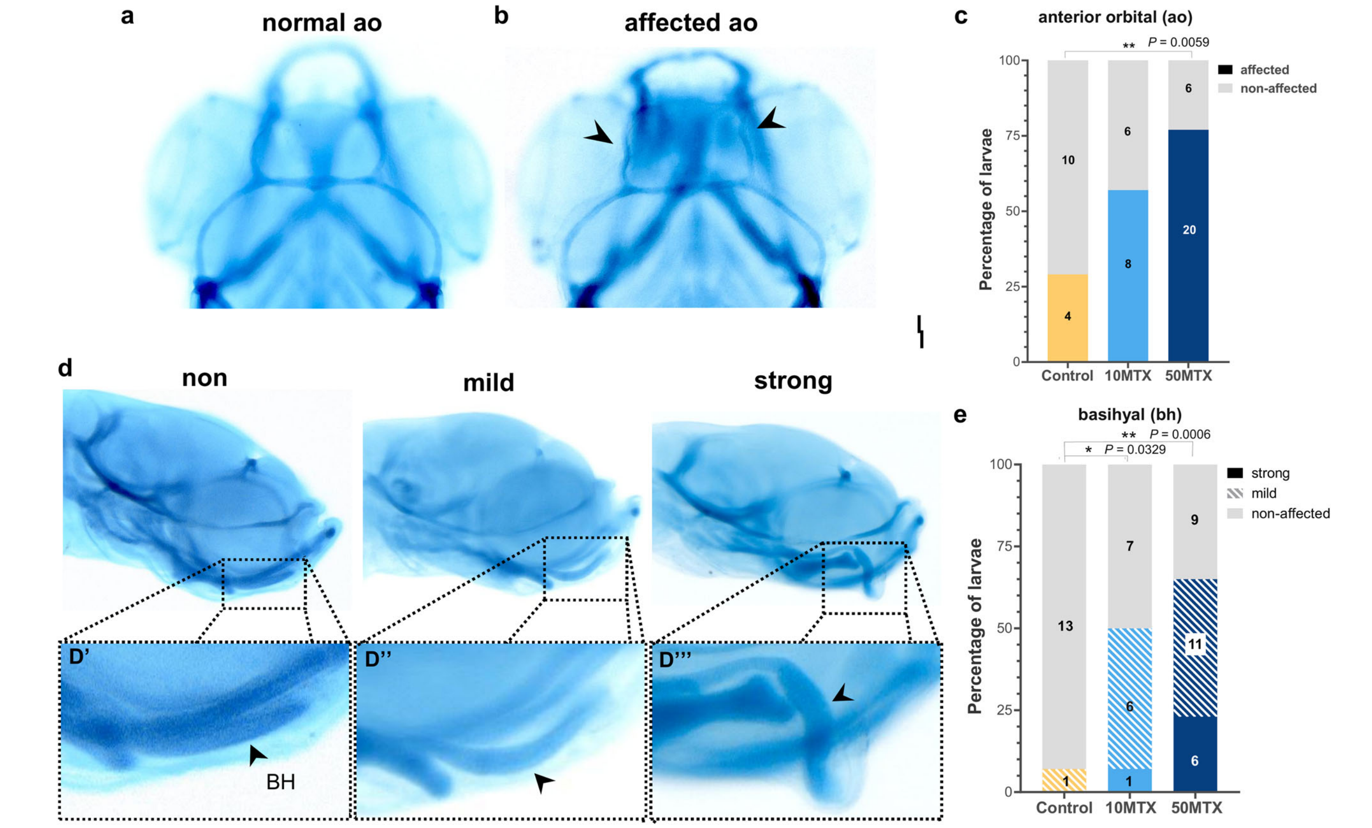

Fig. 2 | Paternal MTX injection produced offspring's cranial cartilages malformations. **a**, **b** Dorsal view of normal and affected anterior orbital (ao) showing a meandering shape mostly observed on the offspring from MTX treated males. **c** Quantification of the percentage of embryos presenting affected or normal anterior orbital cartilages. Numbers in the graph represent the analyzed embryos. **d** Lateral view of larvae presenting normal (trowel shape), mild (bended shape), and strong (hook shape) deformities of the basihyal cartilage. **e** Quantification of the percentage of embryos presenting normal (non-affected), mild, or strong basihyal cartilage abnormalities observed on the offspring from MTX-treated males. Numbers in the graph represent the analyzed embryos. Statistical analyses were performed using a contingency table followed by two-sided Fisher's exact test and each treatment were compared with the control independently. *$P = 0.0329$, **$P = 0.0059$, ***$P = 0.0006$.

Given the observed differences for certain RNA modifications, we examined the expression of specific RNA methyltransferases on the testis of control and 10MTX treated males (Fig. 5d). In agreement with our results, there was no significant change in the expression of *Trmt6* which catalyzes m1A methylation. Conversely, the expression of the enzymes that catalyzed m5C was only significantly upregulated for *Dnmt2* ($p = 0.01$), but not for *Nsun2* ($p = 0.46$). These results suggest that an increase of RNA methyltransferase expression leads to changes in the methylation status of sperm tRNAs upon MTX treatment.

Zygotic RNA injection derived from MTX-treated sperm partially recapitulates the craniofacial phenotype

To uncover the potential role of altered small RNAs on the sperm as the causes of offspring craniofacial defects, we isolated both 20–50nt and 50–90nt RNA fractions from MTX and control (DMSO) treated males and injected them independently or combined (20–90 nt) into fertilized wild-type eggs. Initially, we did not observe differences in the percentage of hatching and embryo survival between zygotic RNA injections derived from both control and MTX-treated sperm (Fig. S4).

We have focused our analysis on the ceratohyal and basihyal cartilages because they were most affected in our initial experiments. Importantly, we found that injection of 20–50 nt, 50–90 nt or the combination of both (20–90 nt) at the two doses of MTX-treated sperm showed a significant reduction ($p < 0.0001$) on the ceratohyal lengths compared to control (Fig. 6a). On the other side, when we analyze the basihyal phenotypes we were unable to evidence any hook shape malformation, but instead we evidenced embryos having curved trowel shape (affected) with the tip of the cartilage upward and downwards (Fig. 6b). Importantly, injection of 20–50 nt fraction from both 10MTX and 50MTX, but not the 50–90 nt, significantly increase the number of larvae having affected basyhial shape (Fig. 6b). Similarly, injection of 20–90 nt RNA fractions have a similar effect than the 20–50 nt. All these together suggest that RNAs from exposed males have the ability to alter the development of specific cranial cartilages on the offspring.

Discussion

MTX binds to and inhibits dihydrofolate reductase ~~activity~~, preventing folic acid from performing its biological tasks. For more than 30 years, this drug has been used to treat immunological illnesses (including rheumatoid arthritis), blood and solid organ cancers, dermatologic diseases, and for pregnancy termination[55,56]. Despite the drug's contraindication for pregnant women due to the risk of miscarriage and birth abnormalities, the paternal influence of MTX on their offspring was largely unknown. In addition to this, the vast majority of studies in fish models such as medaka and zebrafish has been performed during embryological stages[57–60], while few have evaluated the effect on adults[61] and the consequences on their offspring.

In agreement with other studies in mice[62,63], we found that paternal MTX treatments had no effect on the fertility or survival of their progeny during the early embryonic stages. Lifetime exposure to folic acid-deficient diets, on the other hand, lead to lower sperm counts, negative consequences in progeny, and epigenetic changes[62,63]. However, this may be due to folate deficiency during

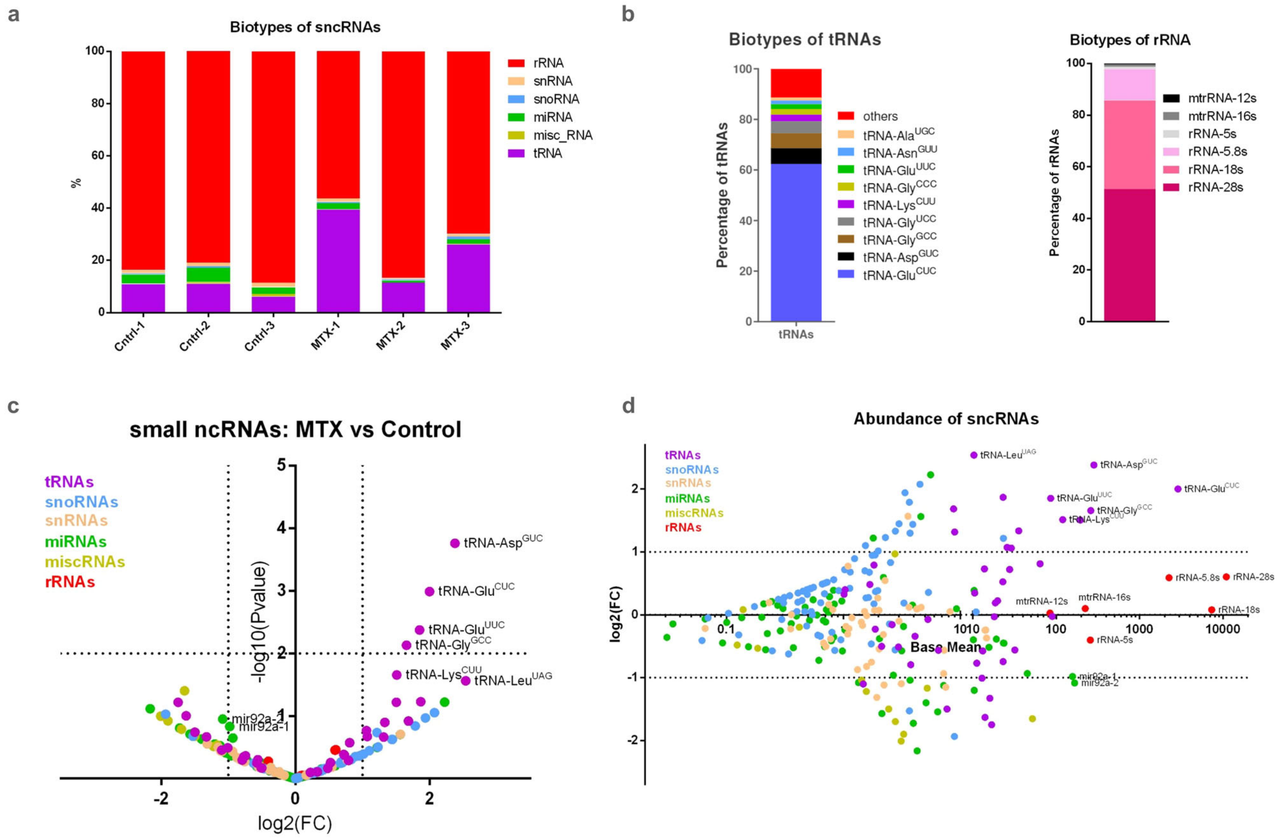

Fig. 3 | Paternal MTX injection alters sperm sncRNAs. a Histogram representing the comparison from sperm sncRNA on control (Ctrl1-3) and 10MTX (MTX-1-3) treated males. **b** Histogram displaying biotypes of tRNAs and rRNAs from sperm of MTX treated males. See also Supplementary Data 1 for **a** and **b**. **c** Volcano plot of depicting the fold changes in sperm sncRNAs identified as being differentially expressed within control versus MTX-treated males. Analysis of differential expression was performed by using DESeq2 which use the two-tailed Wald test. **d** MA plot displaying normalized counts (base mean) for different sncRNAs. Dotted lines depict thresholds values for significantly up and down-regulated (±≥1 $\log_2$ fold change and -$\log_{10}$ *P* value ≥ 1.3). See also Supplementary Data 2 for **c** and **d**.

embryonic and post-embryonic development, which could compromise early germ cell formation and adult spermatogenesis. Moreover, major epigenetic reprogramming occurs at these periods, and multiple imprinting areas may be altered as a result of the prolonged folate shortage.

For many years, paternal contribution to offspring's health was thought to be restricted to the haploid genome of spermatozoa, whereas mother health and nutrition were linked to offspring's wellness. However, multiple recent studies have revealed that spermatozoa carry a variety of RNAs[18,64–66] capable to transmit paternal experiences[19,22–24,32]. In this regard, our work illustrated the critical significance of MTX therapy and its impact on sperm small non-coding RNA content as a possible mechanism underlying the observed craniofacial abnormalities or possibly other unexplored effects of this treatment. We discovered that tsRNAs and miRNAs are the most common small non-coding RNA in medaka sperm, which is consistent with past findings in mammals[19,30,31,66,67]. Furthermore, we revealed that tsRNAs halves changed significantly owing MTX treatment, which is in agreement with previous studies showing that tsRNAs are a dynamic population that responds to a variety of environmental stressors[19,24,68]. Particularly, we observed a higher abundance of certain 5′tsRNAs, where 5′tsRNA-Asp^{GUC} was the most abundant. This result is in concordance with several studies where external factors also modulated the abundance of 5′tsRNA-Asp^{GUC}[20,24,31], thus highlighting the idea that certain tRNAs may be preferentially cleaved and their 5′ halves have a longer half-life compared to their respective 3′ halves.

tsRNAs can be generated through multistep cleavages, through the formation of various intermediates. Moreover, there is growing evidence that regulatory factors, such as RNA modifications and specific RNases, have a role in their specific cleavage and stability[66]. Interestingly, we found that 5′tsRNAs from Asp^{GUC} and Gly^{GCC} are consistently longer (~35 nt) on the sperm of MTX-treated males. This is in agreement with the discovery that small 15–22 nucleotide long fragments are normally formed in multiple tissues and cell lines[49], whereas longer 31–40 nucleotide tRNA halves are preferentially cleaved in response to different stresses[50,51].

The tsRNA functions are very speculative, but have been associated to translation, ribosome biogenesis, retrotransposition, cell-cell communication, and epigenetic inheritance, as well as how tsRNA dysregulation are related to a variety of human disorders (summarized in recent reviews[69,70]). Importantly, both tsRNAs and their precursor tRNAs are heavily modified, which contributes to multiple aspects of their function, biogenesis, stability, amino acid charging, and translational accuracy[71,72]. Our initial hypothesis was that MTX treatment may reduce the tRNA methylation thus inducing their cleavage. This is based on previous studies where the addition of m5C, which is controlled by DNMT2 and NSUN2, increase tRNA stability in flies and mice, but its deletion makes them more likely to be cleaved into tsRNAs under stress conditions[19,36,37]. However, and contrarily to our predictions, we observed that tRNAs-enriched samples (~50–70 nt) derived from MTX-treated sperm showed significantly greater levels of methylation in m5C, m2G, m7G and m2′2G. Increased levels of m5C and m2G have been observed in the 30–40 nucleotide fraction of sperm RNAs (predominantly tsRNAs) in mice fed with high-fat diets compared with those from males fed with normal diets[24]. However, it is important to mention that in our MTX-treatment we fail to observe

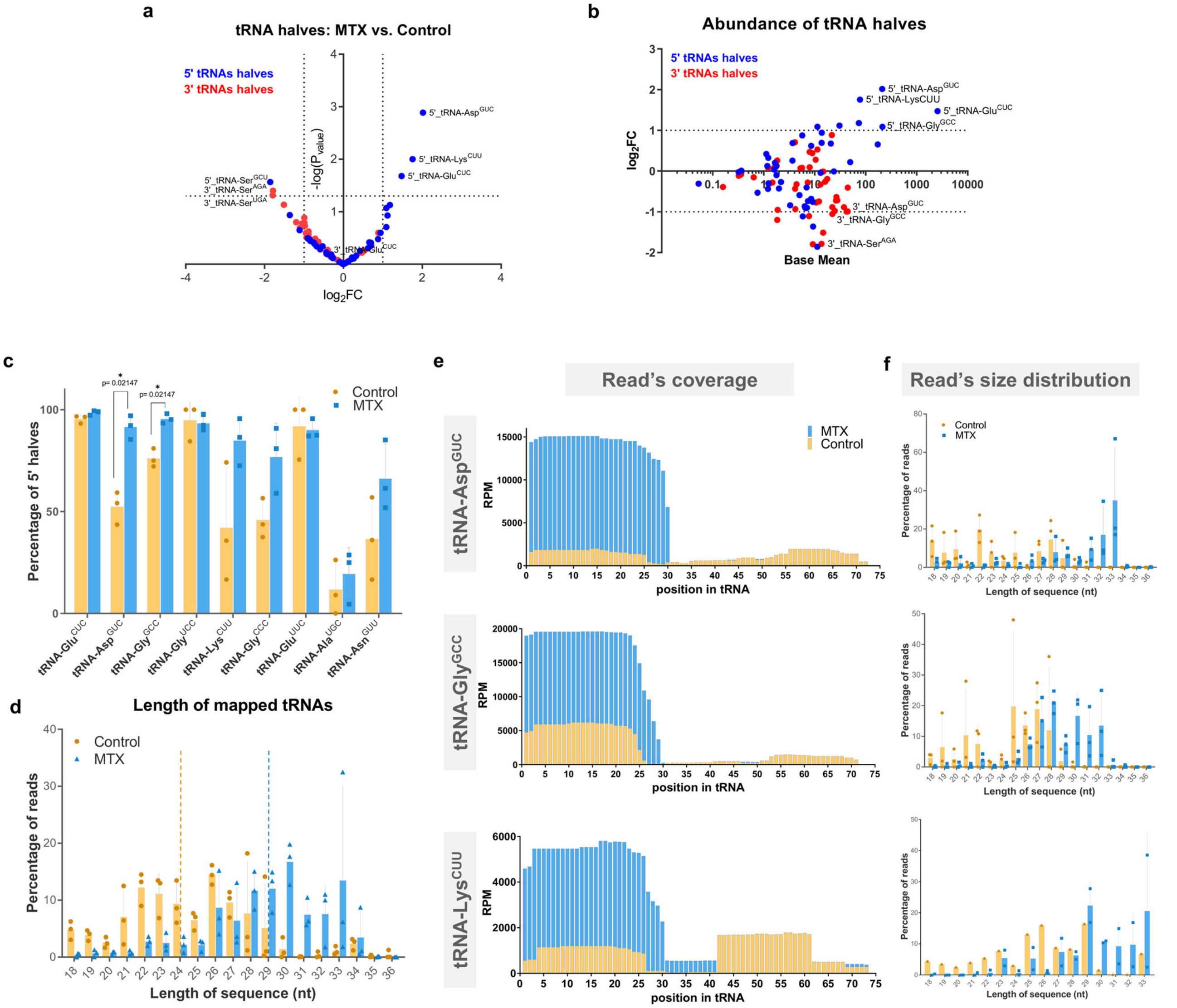

Fig. 4 | Paternal MTX injection induced the expression and cleavage of specific tRNAs. **a** Volcano plot of depicting the fold changes in sperm 5′ and 3′ tRNA halves as being differentially expressed within control versus MTX treated males. Analysis of differential expression was performed by using DESeq2 which use the two-tailed Wald test. **b** MA plot displaying normalized counts (base mean) for different 5′ and 3′tRNA halves. Dotted lines depict thresholds values for significantly up and down-regulated (±≥1 $\log_2$ fold change and $-\log_{10}$Pvalue ≥ 1.3). See also Supplementary Data 3 for **a** and **b**. **c** Histogram displaying percentage of 5′ halves relative to their corresponding 3′ halves from different tRNAs affected by MTX treatment. Asterisk indicated significant differences analyzed by multiple unpaired t-student' test followed by a correction for multiple comparison (Holm-Sidak method, with alpha = 0.05)). **d** Histogram showing the length variation of mapped tRNA reads on control and MTX-treated males. Dotted lines represent the median length. Histogram showing the read coverage (**e**) and size (**f**) distribution for the most abundant and having a significant increase in the 5′tsRNA (tRNA-Glu^{CUC}, tRNA-Asp^{GUC}, and tRNA-Gly^{GCC}) between control and MTX. Data on **c**, **d** and **f** represent three biologically independent replicates ($n = 3$) composed by a pool of 9 males' sperm. Values are means ± SD. See also Supplementary Data 4 for **c**–**f**.

differences in the methylation levels from the tsRNAs/miRNAs fraction (~20–50 nt). We speculate that because the most abundant tRNA modifications found in our study (5mC) are stated to be positioned at the 3′ end of tRNAs (positions 38C, 48C, 49C, 50C)[73], then the cleaved 3′tsRNAs halves, which accumulate the bulk of these methylations, may be preferentially degraded.

The high levels of 5mC in our 50–90nt fraction from MTX-treated males correlated with the higher expression of *Dnmt2* (also known as *Trdmt1*), but not *Nsun2*. *Dnmt2* is structurally close to other DNA methyltransferases but rather methylates only one tRNA, specifically at the cytosine 38 in the anticodon loop of aspartic acid (tRNA-Asp)[74]. The role of *Dnmt2* in paternal non-genetic inheritance have been demonstrated in mice[19,64], and recently associated with the Intergenerational effect of immune priming in insects, suggesting an evolutionary conservation of its functionality[75]. Interestingly, here we have found that 5′tsRNA-Asp^{GUC} was the second most abundant tRNA in MTX-treated males and presenting a significant increase respect to their 3′tsRNA-Asp^{GUC} half. In contradiction to our finding, Schaefe et al. [37]. demonstrated that m5C modification mediated by DNMT2 improves tRNA stability, where tRNA-Asp is protected from angiogenin cleavage during the heat shock response in Drosophila. In mammals, it is well known that angiogenin activity, RNase that cleaves tRNAs, is also inhibited by the presence of 5mC[19,36]. However, it is important to mention that since the endonuclease targeting the anti-codon loop of Drosophila tRNAs has not been identified yet, the authors analyzed the cleavage of tRNA-Asp induced by the addition of recombinant human angiogenin into Drosophila S2 cells[37], which may not reflect the truly physiological condition. Moreover, it has been shown that the presence of angiogenin is not mandatory for the generation of tsRNAs, and other RNases (Dicer, RNase T2, L) can also cleave tRNAs[69,76,77]. In that sense, fish does

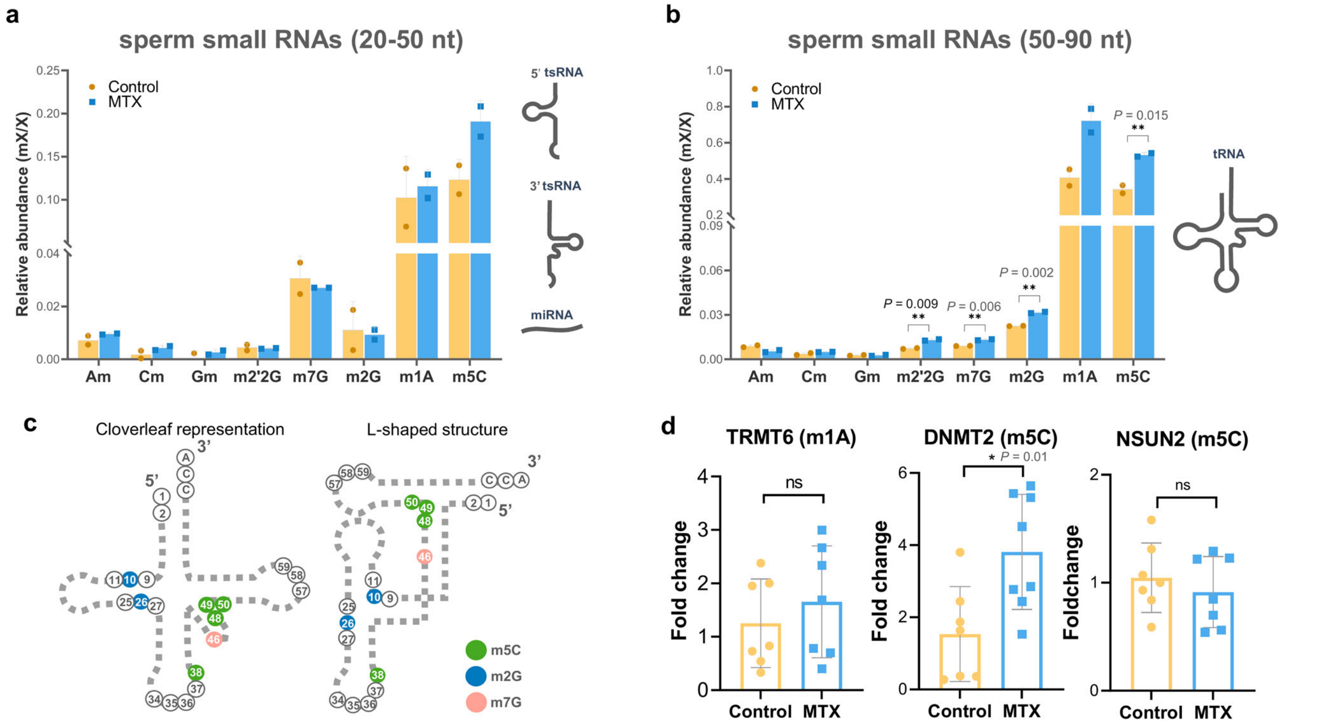

Fig. 5 | Paternal MTX injection alters smallRNA modifications in sperm tRNA fraction and the testicular expression of RNA-methyltransferases. Histogram comparing sperm RNA methylations on control and MTX analyzed by UHPLC-MS-MS in 50–90 nt (**a**) and 20–50 nt (**b**) fractions. Data represent two biologically independent replicates ($n = 2$) composed by RNA isolated from 9 males' sperm. Statistical analysis was performed by two-tailed unpaired t-student' test. Values are mean ± S.D. (**c**) Schematic representation of modified nucleotides in the tRNA at secondary and tertiary structure. **d** RT-qPCR for methyltransferases of m1A (TRMT6) and m5C (DNMT2 and NSUM2) on testis from control and MTX treated males, gene expression was normalized using Rpl7 and Ef1 as housekeeping genes. Statistical analysis was performed by using the two-tailed unpaired *t*-student' test. Each dot represents a biologically independent sample composed by RNA isolated from individual male testis. Valures are means ± SEM.

not have angiogenin, but instead orthologues genes with the capacity to cleave tRNAs have been found[78–80] suggesting that the generation of tRNA fragments is an evolutive response against environmental stressors. In addition, it is important to mention that the activity[78], structure[79–81], and targeted dinucleotides for cleavage are different in between fish and mammals RNases[81]. These facts suggest that the overall generation of tRNA fragments is an ancient response where RNases have maintained their main role and have evolved as the organisms did it. On the other hand, the presence of 5mC, and/or other modifications, might affect their activity in a different way as it was speculated by Barraud and Tisné[82]. These authors stated that tRNA modifications are critical features of the cellular stress responses, and described the existence of a streaky crosstalk among them regulating the tRNAs stability[82]. As a result, modifications may act as a "barcode" to regulate the specific tRNA cleavage and stability resulting in the accumulation of specific tsRNAs in the sperm, which could affect the phenotype of their offspring. Finally, we showed that the zygotic injection of small RNAs isolated from MTX-treated sperm can partially reproduce the basihyal malformation and ceratohyal´s length reduction, which were also the most affected cartilages observed in the offspring of MTX-treated males. It is important to mention that the ceratohyal and basihyal cartilages form the ventral region of the hyoid arch required for the stabilization of the jaw[83] which has evolved in mammals as a structure required for milk suckling[84]. Facial characteristics and growth deficiencies have been extensively linked to both folate deficiency and fetal alcohol syndrome. This phenotypic linkage is, in part, because chronic alcohol abuse affects the folate levels by reducing their initial hydrolysis and subsequent uptake into the cells[85]. Furthermore, fetal alcohol syndrome has also been connected with a weak sucking ability and other feeding difficulties in humans[86], which may presume a hyoid malformation.

In summary, our data suggests that paternal MTX-exposure influenced sperm tRNA methylation, as a result of alterations in the expression of certain RNA methyltransferases. These epitranscriptomic changes may cause the selective tRNA cleavage and the maintenance of certain 5′ tRNA halves. These changes in the sperm RNA content and modifications might affect transcriptional cascades in the fertilized oocyte, with possible implications in cranial cartilage formation (see hypothetical model in Fig. 6c). The understanding of how tRNA modifications and their derived fragments impact on the transcriptional cascades occurring during early embryo will provide valuable insights into several diseases and it is expected that this will be a main focus of research in this field in the near future.

Methods

Medaka Husbandry

All experiments were performed with medaka fish (*Oryzias latipes*) (strain hi-medaka, ID:MT835) supplied by the National BioResource Project (NBRP) Medaka (http://www.shingen.nig.ac.jp/medaka/). Fish were maintained and fed following standard protocols for medaka[87]. Fish were handled on the Care and Management of Laboratory Animals (http://www.ufaw.org.uk) and internal approved regulations (SICUAE-University of San Martín 33/2022). Adult fishes were divided and acclimatized in 4L fish tank during 3 weeks under a constant photoperiod (14L:10D) and controlled temperature (26 ± 0.5 °C), prior to experimental procedures.

Experimental design

Adults medaka fish were divided into 3 groups composed by 3 independent replicates having 9 males and 2 females per tank (all of them having a body weight of ~200 mg). After the acclimatizing period, each

181

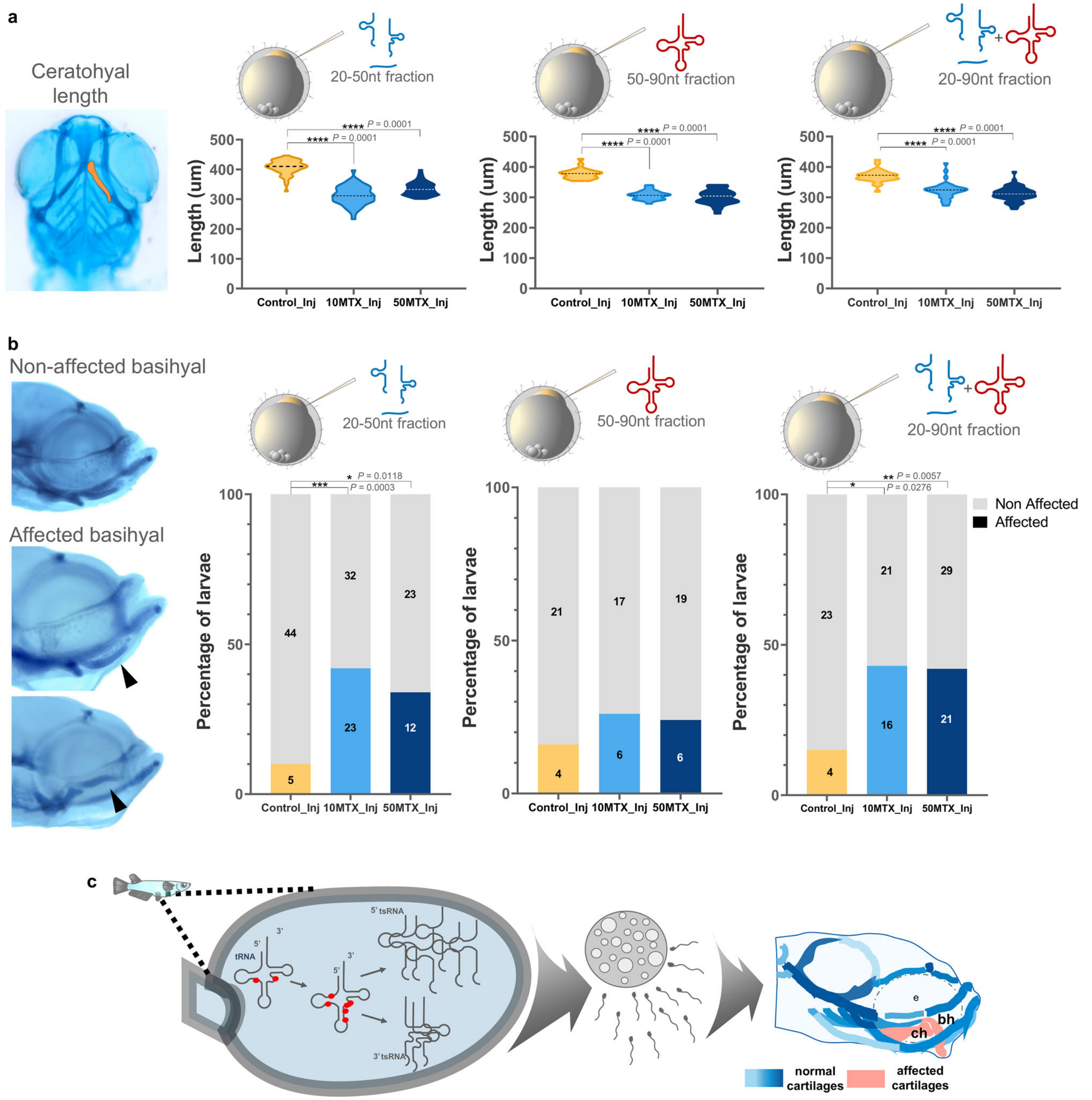

Fig. 6 | Zygotic RNA injection derived from MTX-treated sperm partially recapitulates the craniofacial phenotype. **a** Violin plots represent the measurement of ceratohyal lengths on wild-type fertilized eggs injected with sperm-RNA fractions (20–50nt, 50–90nt, or both together) obtained from control, 10MTX and 50MTX treated males. Statistical analyses were performed using ANOVA one-way followed by multiple comparison Tukey's test. **b** Lateral view of larvae presenting non-affected (trowel shape) or affected (bended upward or downward) basihyal cartilage shape. Quantification of the percentage of embryos presenting affected or non-affected basihyal cartilage abnormalities from zygotes injected with sperm-RNA fractions (20–50nt, 50–90nt, or both together) obtained from control, 10MTX and 50MTX treated males. Numbers in the graph represent the analyzed embryos. Statistical analyses were performed using a contingency table followed by two-sided Fisher's exact test. **c** Proposed model summarizing the results.

male was intraperitoneal injected with control solution (PBS/1% DMSO), 10 mg of MTX per kg of body weight (10 mg/kg MTX) or 50 mg/kg MTX (A6770-SigmaAldrich, diluted in PBS/1%DMSO). Briefly, males were anesthetized with 1% benzocaine solution (Parafarm), gently dried with a paper towel, and placed in a dampened sponge ventral side up, with their anal fin and cloaca exposed. Immediately, using a 10ul syringe (Hamilton), fish were injected using a binocular stereoscope (Nikon SMZ745) and then returned to their tanks for 7 days until sperm collection for in vitro fertilization and small RNA extraction.

In vitro fertilization

Sperm collection was carried by anesthetizing the fish and placed in a dampened sponge ventral side up following published protocols for medaka[87]. A micro-forceps was used to gently strip the fish and the released semen was collected by using a micropipette (~0.5 μl/fish) and pooled for the posterior in vitro fertilization and small RNA extraction. For the in vitro fertilization, 0.2 μl from obtained sperm were used to fertilize a pool of 24–28 eggs collected from mature untreated females. Fertilized eggs were immediately transferred and incubated in 60 mm petri dishes with embryo media (17 mM NaCl, 0.4 mM KCl, 0.27 mM

$CaCl_2.2H_2O$, and 0.66 mM $MgSO_4$; pH:7) until 3 days' post hatching (dph). Incubation was monitored and the percentage of fertilization and survival until hatching was evaluated.

Alcian blue staining

Cartilages from embryos were analyzed at 3 dph by using alcian blue staining. Larvae were fixed in 4% paraformaldehyde overnight at 4 °C and washed three times with PBSw (PBS-0.1% tween20). After that, embryos were incubated in a bleaching solution (0.5X SSC, 5% formamide, 10% hydrogen peroxide) and exposed to light during 2 h. Larvae were washed several times with PBSw and immediately incubated in alcian Blue solution (0.1%p/v alcian blue, 0.37%v/v HCl, 70%v/v EtOH) for 1 h on a nutator. Then, larvae were washed five times with 01%v/v HCl-70%v/v EtOH for 30 min on a nutator; the last wash was left overnight at room temperature. Next, larvae were washed six times with 50%v/v glycerol-0.5%v/v KOH for 30 min on a nutator and the last wash was left overnight. Finally, larvae were washed four times with the same solution and left in 90% glycerol-10% ETOH for imaging processing and phenotype analysis. Larvae were photographed at ventral, dorsal and lateral view by using a trinocular stereoscope (SteREO Discovery v20. Zeiss) and analyzed using the ImageJ software[88].

Small RNA extraction and library preparation

Small RNAs were isolated from sperm following manufacturer's instructions (illustra RNAspin Mini RNA isolation kit-GE Healthcare). The 3′ adapters (see Supplementary Table 2 for full list of adapter oligos utilized for library preparation) were ligated using SRBC barcode adapters for each sample, additionally 18-mer and 30-mer markers were ligated and used as control for the ligation process and markers for the product correct size. The 3′-ligated small RNAs were size selected using 15% denaturing urea polyacrylamide gels at a constant power of 40–50 W for ~30 min and stained by using SYBR Gold 0.05%V/V in TBE 0.5X and the 3′ ligated RNAs ranging from 18 −30 mer were cut out. RNAs were purified using Zymo PAGE elution kit (ZR™ small RNA PAGE recovery kit) according to manufacturer's instructions, the elute 3′-ligated small RNAs were elute in 5′ linker mix containing 5′ adaptor. The 3′-ligated RNAs + 5′ adapter were denaturated for 5 min at 70 °C, cooled on ice immediately, ligated with T4 RNA ligase (NEB) and incubated at 16 degrees overnight. Ligated small RNAs were purified by using MBS beads, briefly: MBS buffer, MBS bead slurry (beads + buffer), mixed by vortexing, added isopropanol and incubated at room temperature. Beads were separated on magnet and the supernatant was removed, after several washes with ethanol the RNA was eluted with ultrapure water and transferred into PCR strip. For reverse transcription, small-RNAseq RT primer to each sample were used and a negative control without reverse transcriptase was included, Superscript II reverse transcriptase was used to obtain the synthesis of the first strand. To amplify cDNA libraries, KAPA HiFi Real Time Library Amplification Kit (Roche) was used; PCR were performed using TruSeq Universal Adapter primer (Solexa_PCR_fwd) and TruSeq Index reverse primers (Solexa_IDX_rev), this latter includes barcodes assigned to each different sample. Briefly: master mix was added and TruSeq Index reverse primer were added to PCR strips containing cDNAs; then KAPA HiFi HS RM and Truseq Universal Adapter primer were added to the mix. The cycling program was: Denaturation at 98 °C for 45 s; 20 cycles of 98 °C for 15 s, 65 °C for 30 s, 72 °C for 30 s, 72 °C for 10 s; and a final extension at 72 °C for 1 min. The amplified cDNA was purified by using 3% Low-Range Ultra Agarose gel (Bio-Rad) according to the manufacturer's instructions at constant 80–100 V using GeneRuler 50 bp DNA Ladder (ThermoFischer Scientific) as molecular marker. Gel was visualized on a long wave UV transilluminator and DNA band between 150–200 bp were excised using a clean scalpel blade and put into a clean 15 ml Falcon tube; the DNA was purified using the Zymoclean Gel DNA recovery kit (Zymo Research) according to manufacturer's instructions.

Bioinformatics analysis

Adapters from reads were removed using CUTADAPT, the output were reads ≥15 bp, reads whose adapters were not identified were discarded. The output of 15 bp were used to analyze differential expression of sncRNAs (miRNAs, tRNAs, snRNAs, snoRNAs, and rRNAs) and differential expression of tRNAs, 5′ tRNA halves and 3′ tRNA halves by different strategies. First, differential expression of sncRNAs was analyzed on reads where the random nucleotides on 5′ (4 bp) and 3′ (6pb) were cut using FASTQ Trimmer. The obtained reads having <19 bp were discarded using Filter Fastq and the remaining reads were aligned against the medaka genome (Assembly ASM00223467v1) with RNA STAR (allowing multimapping reads, 1 mismatch, and not allowing introns). Expression of miRNAs, tRNAs, snRNAs, snoRNAs was analyzed using FeatureCounts (allowing multimapping reads to be counted, and assigning 1/n fractions to multimapping reads) with Ensembl annotation (Release v102). To analyze cytoplasmic and mitochondrial rRNA expression, reads were mapped to a custom fasta file containing 28s rRNA (RNA central: URS000215D18B_8090), 18s rRNA (refseq: XR_002874070.1), 5.8s rRNA (RNA central: URS0000671FD1_8090), 5s rRNA (refseq: XR_002875036.1), 16s mtRNA (RNA central: URS00003A7D46_8090) and 12s mtRNA (RNA central: URS000033338A_8090) sequences. Differential expression of all sncRNAs was calculated using DESEQ2. Second, to analyze differential expression of 5′ and 3′ tRNA halves, an additional 3 base pairs were removed with FASTQ Trimmer from the 3'end of all reads. Reads having less than 15 bp were discarded using Filter Fastq. The output was aligned to the reference genome and analyzed as mentioned before using custom GTF files with genomic coordinates for either 5′ or 3′ tRNA halves. To determine the sequence length of mapped tRNA and rRNA reads, BAM files were filtered (using GTFs files containing genomic coordinate for full length tRNAs o rRNAs), reads were extracted, converted to fasta and their length computed with in-house scripts. tRNA and rRNA read coverage was calculated with BamCoverage (bin size 1, no smoothing) with RPM values representing reads per million mapped to functional sncRNA categories (miRNAs, tRNAs, snRNAs, snoRNAs and rRNAs).

UHPLC-MS-MS

The analysis of modified ribonucleotides from spermatic RNAs were performed by UHPLC-MS-MS. For that purpose, ~1.5 μg of total RNAs were isolated from two independent pools of stripped sperm from ~9 control and 10MTX-treated males and run in denaturant polyacrylamide gel (15%, 7 M Urea). The gel was then stained with ethidium bromide and RNAs that have a ranged size from 20–50 nt and 50–90 nt were cut and recovered using the ZR small-RNA™ PAGE Recovery Kit (Zymo Research) by following the manufacturer's instruction. Approximately 100 ng of RNA was obtained on each fraction and utilized for UHPLC-MS-MS analysis. Then, 100 ng purified RNA samples were digested to nucleosides for 2 hr at 37 °C using the Nucleoside Digestion mix (NEB, M069S). Quantifications were performed as in[89], briefly: digested RNA samples were diluted to 100 µl with ddH20 and filtered through 0.22 µm Millex Syringe Filters. 5 µl of the filtered solution was injected for LC-MS/MS analysis using the Agilent 1290 UHPLC-MS/MS system with a Hypersil Gold C18 reversed-phase column (2.1 × 150 mm, 3 µm). Mobile phase A consisted of water with 0.1% (v/v) formic acid and mobile phase B consisted of acetonitrile with 0.1% (v/v) formic acid. Mass spectrometry detection was performed using an Agilent 6470 triple quadrupole mass spectrometer in positive electrospray ionization mode and data were quantified in dynamic multiple reaction monitoring (dMRM) mode, by monitoring the mass transitions 268→136 for Adenosine (A), 282→150 for N6-methyladenosine (m1A), 244→112 for Cytidine (C), 258→126 for C5-methylcytidine (m5C), 284→152 for Guanosine (G), 298→166 for N7'-methyladenosine (m7G) and N2-methylguanosine (m2G), 312→180 for N2,N2-dimethylguanosine (m2'2G), 282→136 for 2'-Omethyladenosine (Am), 258♋Ⅱ112 for 2′-O-methylcytidine (Cm) and 298♋Ⅱ152 for 2′-O-methylguanosine (Gm). To quantify the concentrations of the various methylation modifications we used pure nucleosides of A, C, G, m1A, m5C, m7G, m2G m2′2G, Am, Cm, and Gm to generate calibration standard curves through serial dilution.

RNA quantification by RT-PCR

Dissected testis from adult males (Control and 10MTX groups) were used for gene expression analysis. For this purpose, a complete testis from 8 males were individually grinded in 300 μl of TRIzol Reagent (Life Technologies) and total RNAs (~800 ng/testis) were isolated and retrotranscribed[90]. Expression of target genes were measured by qPCR using Fast Start Universal SYBR green Supermix (Roche Diagnostics, USA) on Thermal Cycler StepOne Plus (Applied Biosystem, USA), using ribosomal protein L7 (rpl7) and elongation factor 1 alpha (*ef1α*) as reference genes with the geometric mean calculation as described by Padilla et al. [90]. Real-time PCR primers are listed in Supplementary Table 1. Each sample was run in duplicate and a PCR reaction without the addition of template, was used as negative control. The amplification protocol consisted of an initial cycle of 1 min at 95 °C, followed by 40 cycles: 15 s at 95 °C and 30 s at 60 °C. After the amplification, a melt curve was performed by 1 cycle: 15 s at 95 °C, 60 s at 60 °C, and 15 s at 95 °C enabling confirmation of amplification of single products. Gene expression levels were calculated by the $2^{-\Delta\Delta Ct}$ comparative threshold cycle (Ct) method (where $\Delta\Delta Ct = \Delta Ct$ sample - ΔCt reference). The efficiency of amplification ranged 95–105% for all genes studied. The expression level in each group was normalized to the control and was presented as a fold of change[91].

Zygotic RNA injection

RNAs were isolated from pools from stripped sperm from ~9 control, 10MTX, and 50MTX-treated males and run in denaturant polyacrylamide gel (15%, 7 M Urea). RNAs that have a ranged size from 20–50 nt and 50–90 nt were cut and recovered using the ZR small-RNA™ PAGE Recovery Kit (Zymo Research) by following the manufacturer's instruction. Fertilized eggs at the stage of one cell were injected with 45.1 pg of purified RNAs from 20–50 nt, 50–90 nt or a combination of both (20–90 nt) by using the microinjector Nanoject II (Drummond Scientific Company). After this, the injected embryos were transferred into petri dish containing embryo media and let them grown up until 3 days post hatching. The embryos were monitored every day and alcian blue staining was performed for larvae as previously mentioned. Stained larvae were analyzed as previously mentioned.

Reporting summary

Further information on research design is available in the Nature Portfolio Reporting Summary linked to this article.

Data availability

Trimmed sequencing data that was generated in this study for the initial bioinformatics analysis have been submitted to the NCBI Sequence Read Archive under BioProject ID PRJNA857097. LC-MS/MS data have been uploaded to Metabolights [http://www.ebi.ac.uk/metabolights/MTBLS7368]. Source data are provided with this paper.

References

1. Sánchez-Vásquez, E., Alata Jimenez, N., Vázquez, N. A. & Strobl-Mazzulla, P. H. Emerging role of dynamic RNA modifications during animal development. *Mech. Dev.* **154**, 24–32 (2018).
2. Greenberg, M. V. C. & Bourc'his, D. The diverse roles of DNA methylation in mammalian development and disease. *Nat. Rev. Mol. Cell Biol.* **20**, 590–607 (2019).
3. Bernstein C., Bernstein H. Demethylation in early embryonic development and memory. In: *DNA Methylation Mechanism*. https://doi.org/10.5772/intechopen.90306 (2020).
4. O'Neill, C. The epigenetics of embryo development. *Anim. Front.* **5**, 42–49 (2015).
5. Li, J., Shi, Y., Sun, J., Zhang, Y. & Mao, B. Xenopus reduced folate carrier regulates neural crest development epigenetically. *PLoS One* **6**, e27198 (2011).
6. Shaw, G. M., Schaffer, D., Velie, E. M., Morland, K. & Harris, J. A. Periconceptional vitamin use, dietary folate, and the occurrence of neural tube defects. *Epidemiology* **6**, 219–226 (1995).
7. Tolarova, M. Periconceptional supplementation with vitamins and folic acid to prevent recurrence of cleft lip. *Lancet* **320**, 217 (1982).
8. McDonald, S. D., Ferguson, S., Tam, L., Lougheed, J. & Walker, M. C. The prevention of congenital anomalies with periconceptional folic acid supplementation. *J. Obstet. Gynaecol. Can.* **25**, 115–121 (2003).
9. Vergel, R. G., Sanchez, L. R., Heredero, B. L., Rodriguez, P. L. & Martinez, A. J. Primary prevention of neural tube defects with folic acid supplementation: Cuban experience. *Prenat. Diagn.* **10**, 149–152 (1990).
10. Blencowe, H., Kancherla, V., Moorthie, S., Darlison, M. W. & Modell, B. Estimates of global and regional prevalence of neural tube defects for 2015: a systematic analysis. *Ann. N. Y. Acad. Sci.* **1414**, 31–46 (2018).
11. Salari, N. et al. Global prevalence of cleft palate, cleft lip and cleft palate and lip: A comprehensive systematic review and meta-analysis. *J. Stomatol. Oral. Maxillofac. Surg.* **123**, 110–120 (2022).
12. Impellizzeri, A., Giannantoni, I., Polimeni, A., Barbato, E. & Galluccio, G. Epidemiological characteristic of Orofacial clefts and its associated congenital anomalies: Retrospective study. *BMC Oral. Health* **19**, 290 (2019).
13. Mahadevan, U., McConnell, R. A. & Chambers, C. D. Drug safety and risk of adverse outcomes for pregnant patients with inflammatory bowel disease. *Gastroenterology* **152**, 451–462.e2 (2017).
14. Hyoun, S. C., Običan, S. G. & Scialli, A. R. Teratogen update: Methotrexate. *Birth Defects Res A Clin. Mol. Teratol.* **94**, 187–207 (2012).
15. Hernández-Díaz, S., Werler, M. M., Walker, A. M. & Mitchell, A. A. Folic acid antagonists during pregnancy and the risk of birth defects. *N. Engl. J. Med.* **343**, 1608–1614 (2000).
16. Nguyen, G. C. et al. The Toronto consensus statements for the management of inflammatory bowel disease in pregnancy. *Gastroenterology* **150**, 734–757.e1 (2016).
17. Beghin, D., Cournot, M. P., Vauzelle, C. & Elefant, E. Paternal exposure to methotrexate and pregnancy outcomes. *J. Rheumatol.* **38**, 628–632 (2011).
18. Sharma, U. et al. Small RNAs are trafficked from the epididymis to developing mammalian sperm. *Dev. Cell* **46**, 481–494.e6 (2018).
19. Zhang, Y. et al. Dnmt2 mediates intergenerational transmission of paternally acquired metabolic disorders through sperm small non-coding RNAs. *Nat. Cell Biol.* **20**, 535–540 (2018).
20. Chen, X. et al. Early cleavage of preimplantation embryos is regulated by tRNAGln-TTG-derived small RNAs present in mature spermatozoa. *J. Biol. Chem.* **295**, 10885–10900 (2020).
21. Rodgers, A. B., Morgan, C. P., Leu, N. A. & Bale, T. L. Transgenerational epigenetic programming via sperm microRNA recapitulates effects of paternal stress. *Proc. Natl Acad. Sci. USA.* **112**, 13699–13704 (2015).
22. Fullston, T. et al. Paternal obesity initiates metabolic disturbances in two generations of mice with incomplete penetrance to the F2 generation and alters the transcriptional profile of testis and sperm microRNA content. *FASEB J.* **27**, 4226–4243 (2013).

23. Gapp, K. et al. Implication of sperm RNAs in transgenerational inheritance of the effects of early trauma in mice. *Nat. Neurosci.* **17**, 667–669 (2014).
24. Chen, Q. et al. Sperm tsRNAs contribute to intergenerational inheritance of an acquired metabolic disorder. *Science (1979)*. https://doi.org/10.1126/science.aad7977 (2016).
25. Aarabi, M. et al. High-dose folic acid supplementation alters the human sperm methylome and is influenced by the MTHFR C677T polymorphism. *Hum. Mol. Genet.* **24**, 6301–6313 (2015).
26. Boxmeer, J. C. et al. Low folate in seminal plasma is associated with increased sperm DNA damage. *Fertil. Steril.* **92**, 548–556 (2009).
27. Wang, Y. et al. Reprogramming of meiotic chromatin architecture during spermatogenesis. *Mol. Cell* **73**, 547–561.e6 (2019).
28. Santos, F., Hendrich, B., Reik, W. & Dean, W. Dynamic reprogramming of DNA methylation in the early mouse embryo. *Dev. Biol.* **241**, 172–182 (2002).
29. Feng, S., Jacobsen, S. E. & Reik, W. Epigenetic reprogramming in plant and animal development. *Science (1979)*. https://doi.org/10.1126/science.1190614 (2010).
30. Chen, Q., Yan, W. & Duan, E. Epigenetic inheritance of acquired traits through sperm RNAs and sperm RNA modifications. *Nat. Rev. Genet.* **17**, 733–743 (2016).
31. Sharma U., et al. Biogenesis and function of tRNA fragments during sperm maturation and fertilization in mammals. *Science (1979)*. 351 https://doi.org/10.1126/science.aad6780 (2016)
32. Grandjean, V. et al. RNA-mediated paternal heredity of diet-induced obesity and metabolic disorders. *Sci. Rep.* https://doi.org/10.1038/srep18193 (2015).
33. Carone, B. R. et al. Paternally induced transgenerational environmental reprogramming of metabolic gene expression in mammals. *Cell.* **143**, 1084–1096 (2010).
34. Wu, L. et al. Paternal psychological stress reprograms hepatic gluconeogenesis in offspring. *Cell Metab.* **23**, 735–743 (2016).
35. Blanco, S. et al. Aberrant methylation of t RNA s links cellular stress to neuro-developmental disorders. *EMBO J.* https://doi.org/10.15252/embj.201489282 (2014).
36. Tuorto, F. et al. RNA cytosine methylation by Dnmt2 and NSun2 promotes tRNA stability and protein synthesis. *Nat. Struct. Mol. Biol.* **19**, 900–905 (2012).
37. Schaefer, M. et al. RNA methylation by Dnmt2 protects transfer RNAs against stress-induced cleavage. *Genes Dev.* **24**, 1590–1595 (2010).
38. Kao, T. T. et al. Methotrexate-induced decrease in embryonic 5-Methyl-Tetrahydrofolate is irreversible with Leucovorin Supplementation. *Zebrafish* **10**, 326–337 (2013).
39. Cronstein, B. N. & Aune, T. M. Methotrexate and its mechanisms of action in inflammatory arthritis. *Nat. Rev. Rheumatol.* **16**, 145–154 (2020).
40. Dervieux, T., Greenstein, N. & Kremer, J. Pharmacogenomic and metabolic biomarkers in the folate pathway and their association with methotrexate effects during dosage escalation in rheumatoid arthritis. *Arthritis Rheum.* **54**, 3095–3103 (2006).
41. Alata Jimenez, N., Torres Pérez, S. A., Sánchez-Vásquez, E., Fernandino, J. I. & Strobl-Mazzulla, P. H. Folate deficiency prevents neural crest fate by disturbing the epigenetic Sox2 repression on the dorsal neural tube. *Dev. Biol.* **444**, S193–S201 (2018).
42. Antony, A. C. & Hansen, D. K. Hypothesis: Folate-responsive neural tube defects and neurocristopathies. *Teratology* **62**, 42–50 (2000).
43. van Rooij IALM, *et al*. Periconceptional folate intake by supplement and food reduces the risk of nonsyndromic cleft lip with or without cleft palate. *Prev. Med.* 39 https://doi.org/10.1016/j.ypmed.2004.02.036 (2004).
44. Wilcox, A. J. et al. Folic acid supplements and risk of facial clefts: National population-based case-control study. *Br. Med J.* **334**, 464 (2007).
45. Burgoon, J. M., Selhub, J., Nadeau, M. & Sadler, T. W. Investigation of the effects of folate deficiency on embryonic development through the establishment of a folate deficient mouse model. *Teratology* **65**, 219–227 (2002).
46. Prevention of neural tube defects: Results of the Medical Research Council Vitamin Study. *Lancet* **338**, 131–137 (1991).
47. Ord, J., Heath, P. R., Fazeli, A. & Watt, P. J. Paternal effects in a wild-type zebrafish implicate a role of sperm-derived small RNAs. *Mol. Ecol.* **29**, 2722–2735 (2020).
48. Rashad, S. et al. The stress-specific impact of ALKBH1 on tRNA cleavage and tiRNA generation. *RNA Biol.* **17**, 1092–1103 (2020).
49. Kumar, P., Anaya, J., Mudunuri, S. B. & Dutta, A. Meta-analysis of tRNA derived RNA fragments reveals that they are evolutionarily conserved and associate with AGO proteins to recognize specific RNA targets. *BMC Med.* **12**, 78 (2014).
50. Thompson, D. M., Lu, C., Green, P. J. & Parker, R. tRNA cleavage is a conserved response to oxidative stress in eukaryotes. *RNA* **14**, 2095–2103 (2008).
51. Yamasaki, S., Ivanov, P., Hu, G. F. & Anderson, P. Angiogenin cleaves tRNA and promotes stress-induced translational repression. *J. Cell Biol.* **185**, 35–42 (2009).
52. Mishima, E. et al. Conformational change in transfer RNA is an early indicator of acute cellular damage. *J. Am. Soc. Nephrol.* **25**, 2316–2326 (2014).
53. Huber, S. M., Leonardi, A., Dedon, P. C. & Begley, T. J. The versatile roles of the tRNA epitranscriptome during cellular responses to toxic exposures and environmental stress. *Toxics* **7**, 17 (2019).
54. Hori H. Methylated nucleosides in tRNA and tRNA methyltransferases. *Front Genet.* 5. https://doi.org/10.3389/fgene.2014.00144(2014).
55. Smith, S. W. & Nelson, L. S. Case files of the New York City Poison Control Center: antidotal strategies for the management of methotrexate toxicity. *J. Med. Toxicol.* **4**, 132–140 (2008).
56. LoVecchio, F., Katz, K., Watts, D. & Wood, I. Four-year experience with methotrexate exposures. *J. Med Toxicol.* **4**, 149–150 (2008).
57. Jacabacci, J., Guzzardi, M. & D'Aversa, T. G. Exogenous folic acid is not able to inhibit the effects of methotrexate on the folate pathway in zebrafish embryos. *Bios* **86**, 125–133 (2015).
58. Liu, S., Narumi, R., Ikeda, N., Morita, O. & Tasaki, J. Chemical-induced craniofacial anomalies caused by disruption of neural crest cell development in a zebrafish model. *Dev. Dyn.* **249**, 794–815 (2020).
59. Sun, S. et al. Effects of methotrexate on the developments of heart and vessel in zebrafish. *Acta Biochim Biophys. Sin.* **41**, 86–96 (2009).
60. Lee, M. S. et al. Disruption of the folate pathway in zebrafish causes developmental defects. *BMC Dev. Biol.* **12**, 12 (2012).
61. Hirako, A., Takeoka, Y., Furukawa, S. & Sugiyama, A. Effects of methotrexate exposure on medaka (Oryzias latipes) testes. *J. Toxicol. Pathol.* **30**, 283–289 (2017).
62. Lambrot, R. et al. Low paternal dietary folate alters the mouse sperm epigenome and is associated with negative pregnancy outcomes. *Nat. Commun.* **4**, 4 (2013).
63. Ly, L. et al. Intergenerational impact of paternal lifetime exposures to both folic acid deficiency and supplementation on reproductive outcomes and imprinted gene methylation. *Mol. Hum. Reprod.* **23**, 461–477 (2017).
64. Zhang, Y., Shi, J., Rassoulzadegan, M., Tuorto, F. & Chen, Q. Sperm RNA code programmes the metabolic health of offspring. *Nat. Rev. Endocrinol.* **15**, 489–498 (2019).
65. Johnson, G. D., Mackie, P., Jodar, M., Moskovtsev, S. & Krawetz, S. A. Chromatin and extracellular vesicle associated sperm RNAs. *Nucleic Acids Res.* **43**, 6847–6859 (2015).
66. Peng, H. et al. A novel class of tRNA-derived small RNAs extremely enriched in mature mouse sperm. *Cell Res.* **22**, 1609–1612 (2012).

67. Kawano, M., Kawaji, H., Grandjean, V., Kiani, J. & Rassoulzadegan, M. Novel small noncoding RNAs in Mouse Spermatozoa, Zygotes and Early Embryos. *PLoS One* **7**, e44542 (2012).
68. Fu, H. et al. Stress induces tRNA cleavage by angiogenin in mammalian cells. *FEBS Lett.* **583**, 437–442 (2009).
69. Su, Z., Wilson, B., Kumar, P. & Dutta, A. Noncanonical roles of tRNAs: TRNA fragments and beyond. *Annu. Rev. Genet.* **54**, 54–69 (2020).
70. Schimmel P. RNA Processing and Modifications: The emerging complexity of the tRNA world: Mammalian tRNAs beyond protein synthesis. *Nat. Rev. Mol. Cell Biol*. 19 https://doi.org/10.1038/nrm.2017.77 (2018).
71. Pan, T. Modifications and functional genomics of human transfer RNA. *Cell Res.* **28**, 395–404 (2018).
72. Suzuki, T. The expanding world of tRNA modifications and their disease relevance. *Nat. Rev. Mol. Cell Biol.* **22**, 375–392 (2021).
73. Pereira, M. et al. Impact of tRNA modifications and tRNA-modifying enzymes on proteostasis and human disease. *Int J. Mol. Sci.* **19**, 3738 (2018).
74. Goll M. G., et al. Methylation of tRNAAsp by the DNA methyltransferase homolog Dnmt2. *Science (1979)*. 311 https://doi.org/10.1126/science.1120976 (2006).
75. Schulz N. K. E., et al. Paternal knockdown of tRNA(cytosine-5-)-methyltransferase (Dnmt2) increases offspring susceptibility to infection in red flour beetles. *Insect Mol. Biol*. 31 (2022).
76. Chen, Q., Zhang, X., Shi, J., Yan, M. & Zhou, T. Origins and evolving functionalities of tRNA-derived small RNAs. *Trends Biochem Sci.* **46**, 790–804 (2021).
77. Akiyama Y., et al. Multiple ribonuclease A family members cleave transfer RNAs in response to stress. *bioRxiv*. (2019).
78. Cho, S. & Zhang, J. Zebrafish ribonucleases are bactericidal: Implications for the origin of the vertebrate RNase a superfamily. *Mol. Biol. Evol.* **24**, 1259–1268 (2007).
79. Pizzo, E. et al. Ribonucleases and angiogenins from fish. *J. Biol. Chem.* **281**, 27454–27460 (2006).
80. Kazakou, K., Holloway, D. E., Prior, S. H., Subramanian, V. & Acharya, K. R. Ribonuclease a homologues of the Zebrafish: Polymorphism, crystal structures of two representatives and their evolutionary implications. *J. Mol. Biol.* **380**, 206–222 (2008).
81. Prats-Ejarque, G., Lu, L., Salazar, V. A., Moussaoui, M. & Boix, E. Evolutionary trends in RNA base selectivity within the RNase A superfamily. *Front. Pharm.* **10**, 10 (2019).
82. Barraud, P. & Tisné, C. To be or not to be modified: Miscellaneous aspects influencing nucleotide modifications in tRNAs. *IUBMB Life* **71**, 1126–1140 (2019).
83. Fabik, J., Psutkova, V. & Machon, O. The mandibular and hyoid arches—from molecular patterning to shaping bone and cartilage. *Int J. Mol. Sci.* **22**, 7529 (2021).
84. Zhou C. F., Bhullar B. A. S., Neander A. I., Martin T., Luo Z. X. New Jurassic mammaliaform sheds light on early evolution of mammal-like hyoid bones. *Science (1979)*. **365** https://doi.org/10.1126/science.aau9345 (2019).
85. Halsted, C. H. et al. Folate deficiency disturbs hepatic methionine metabolism and promotes liver injury in the ethanol-fed micropig. *Proc. Natl Acad. Sci. USA* **99**, 10072–10077 (2002).
86. Streissguth A. P., Landesman-Dwyer S., Martin J. C., Smith D. W. Teratogenic effects of alcohol in humans and laboratory animals. *Science (1979)*. 209 https://doi.org/10.1126/science.6992275 (1980).
87. Kinoshita M., Murata K., Naruse K., Tanaka M. *Medaka: Biology, Management, and Experimental Protocols*. https://doi.org/10.1002/9780813818849 (2012).
88. Schneider, C. A., Rasband, W. S. & Eliceiri, K. W. NIH Image to ImageJ: 25 years of image analysis. *Nat. Methods* **9**, 671–675 (2012).
89. Liberman N., et al. Intergenerational hormesis is regulated by heritable 18S rRNA methylation. *bioRxiv*. (2021).
90. Padilla, L. F. A. et al. Cystic proliferation of germline stem cells is necessary to reproductive success and normal mating behavior in Medaka. *Elife* **10**, 10 (2021).
91. Schmittgen T. D., Livak K. J. Analysis of relative gene expression data using real-time quantitative PCR and the 2(-Delta Delta C(T)) Method. *Methods*. **25** (4–8) (2001).

Acknowledgements
We thank all the authors and members in LBD for their contribution and helpful discussions during the course of our study. This work was supported by the Agencia Nacional de Promoción Científica y Tecnológica (PICT 2018-1879 to P.H.S-M.). J.P.T. would like to acknowledge support from Universidad de la República, Uruguay (CSIC I+D_2020_433). Work in the Greer lab was supported by an NIH grant (DP2AG055947) to E.L.G.

Author contributions
N.A.J. and P.H.S-M. designed, performed the experiments, and wrote the manuscript; L.C. and E.M.S. contributed to making the sRNAs libraries and sequencing; J.P.T and M.C. contributed on the bioinformatics analysis of small RNAs; E.L.G. and K.B. contributed on the RNA methylation analysis; J.I.F., A.B., and L.A.P. contributed on the fish handling, sperm acquisition, eggs fertilization and RT-qPCRs. All the authors contributed on the final manuscript edition.

Competing interests
The authors declare no competing interests.

Additional information
Supplementary information The online version contains supplementary material available at https://doi.org/10.1038/s41467-023-37427-7.

Correspondence and requests for materials should be addressed to Pablo H. Strobl-Mazzulla.

Peer review information *Nature Communications* thanks the anonymous reviewer(s) for their contribution to the peer review of this work. Peer reviewer reports are available.

Supplementary Figures

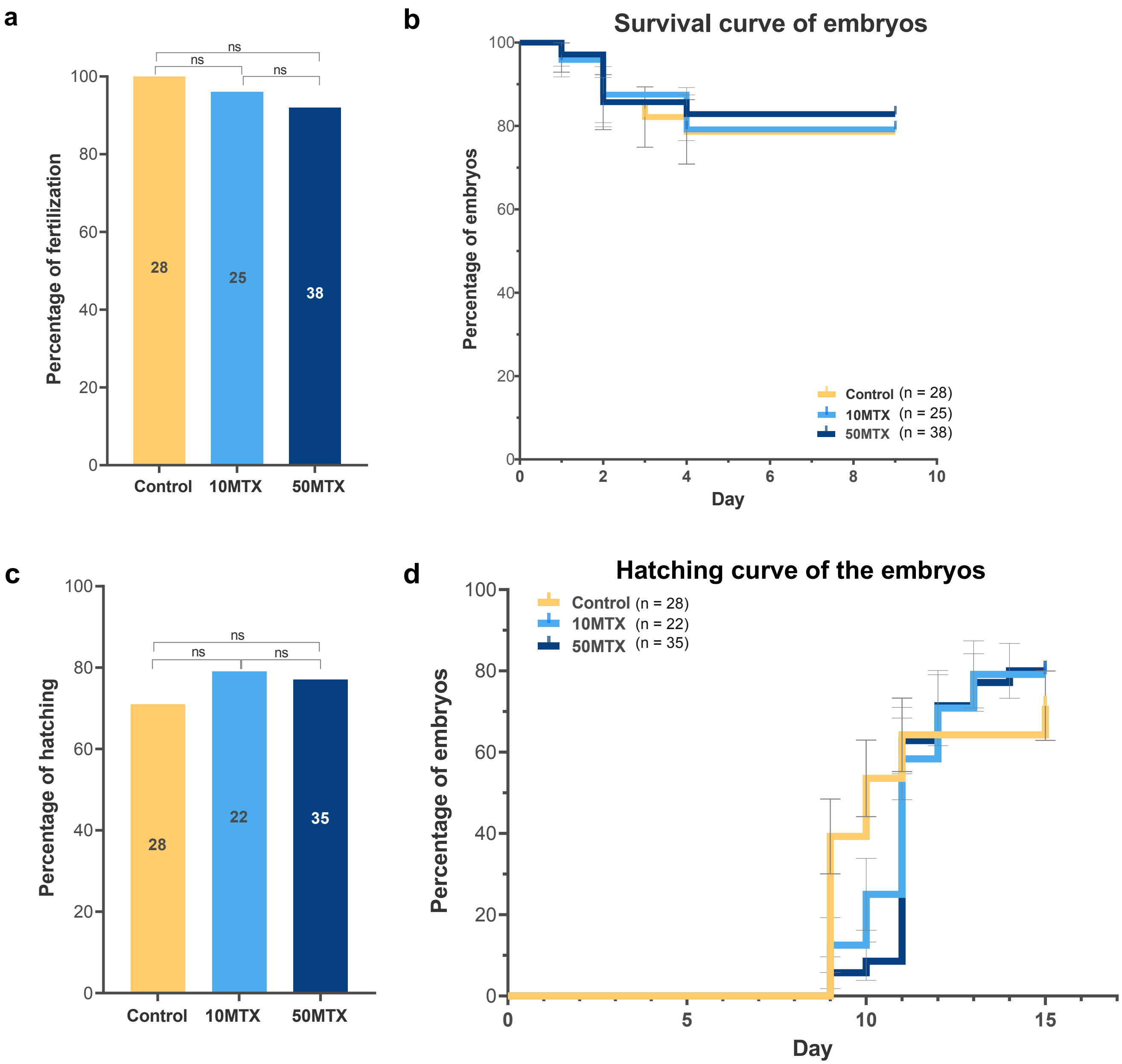

Figure S1: (a) Histogram showing the percentage of fertilization utilizing the sperm from control and MTX treated males. **(b)** Kaplan Meier plot displaying the survival of fertilized eggs until the beginning of hatch. Histogram showing the percentage of hatching embryos **(c)** and the day of hatching **(d)** on control and MTX group. Values are means ± SEM. Numbers in the graph represent the analyzed embryos. Statistics for A and C were generated by contingency table followed by Chi-square test. Statistics for B and D were generated by using the Long-rank (Matel-Cox) test, Gehan-Breslow-Wilcoxon test. ns: P > 0.05.

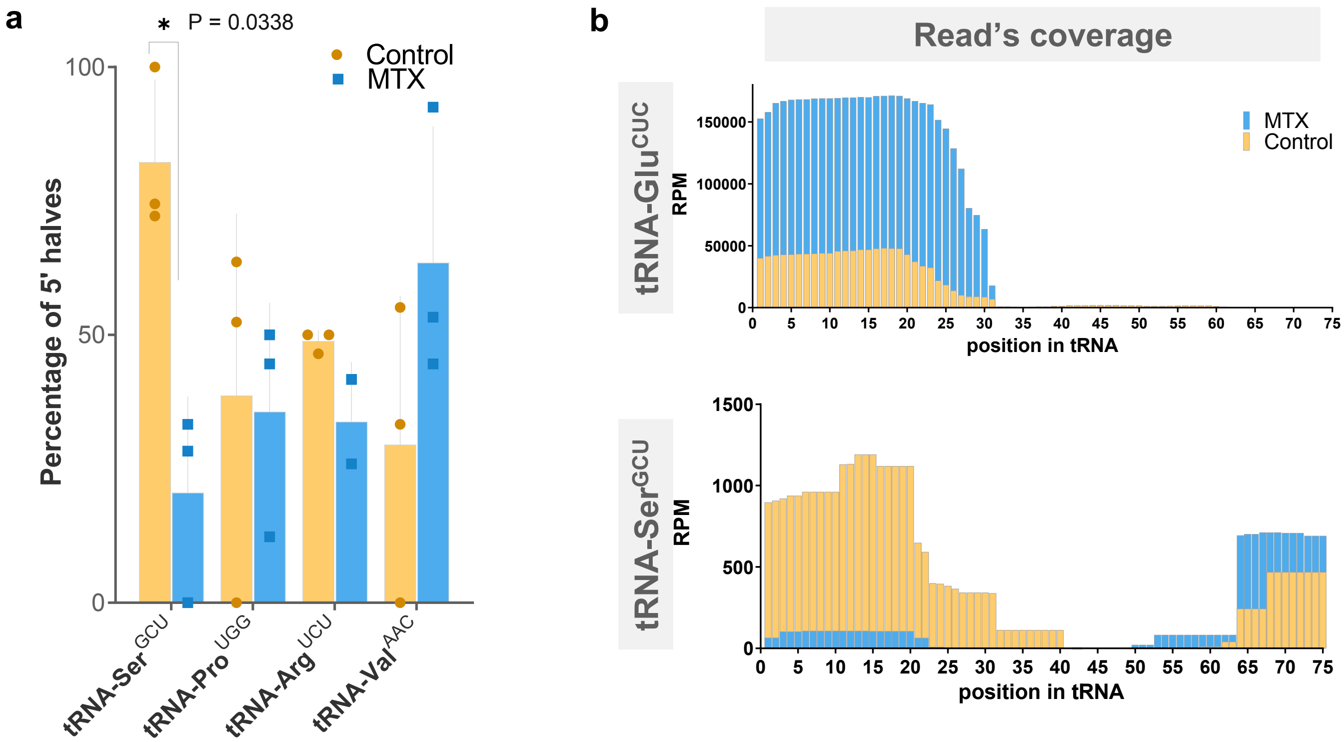

Figure S2: (a) Histogram displaying percentage of 5' halves relative to their corresponding 3' halves from tRNAs not affected (tRNA-Pro^{UGG}, -Arg^{UCU}, -Val^{AAC}) or having a reduction (tRNA-Ser^{GCU}) on MTX treatment. Data represent three biologically independent replicates (n = 3) composed by RNA isolated from 9 males' sperm. Asterisk indicated significant differences analyzed by multiple unpaired t-student' test followed by a correction for multiple comparison (Holm-Sidak method, with alpha = 0.05). Values are means ± SD. **(b)** Histogram showing the read coverage for tRNA-Glu^{CUC} and -Ser^{GCU}. See also **Supplementary Data 5**.

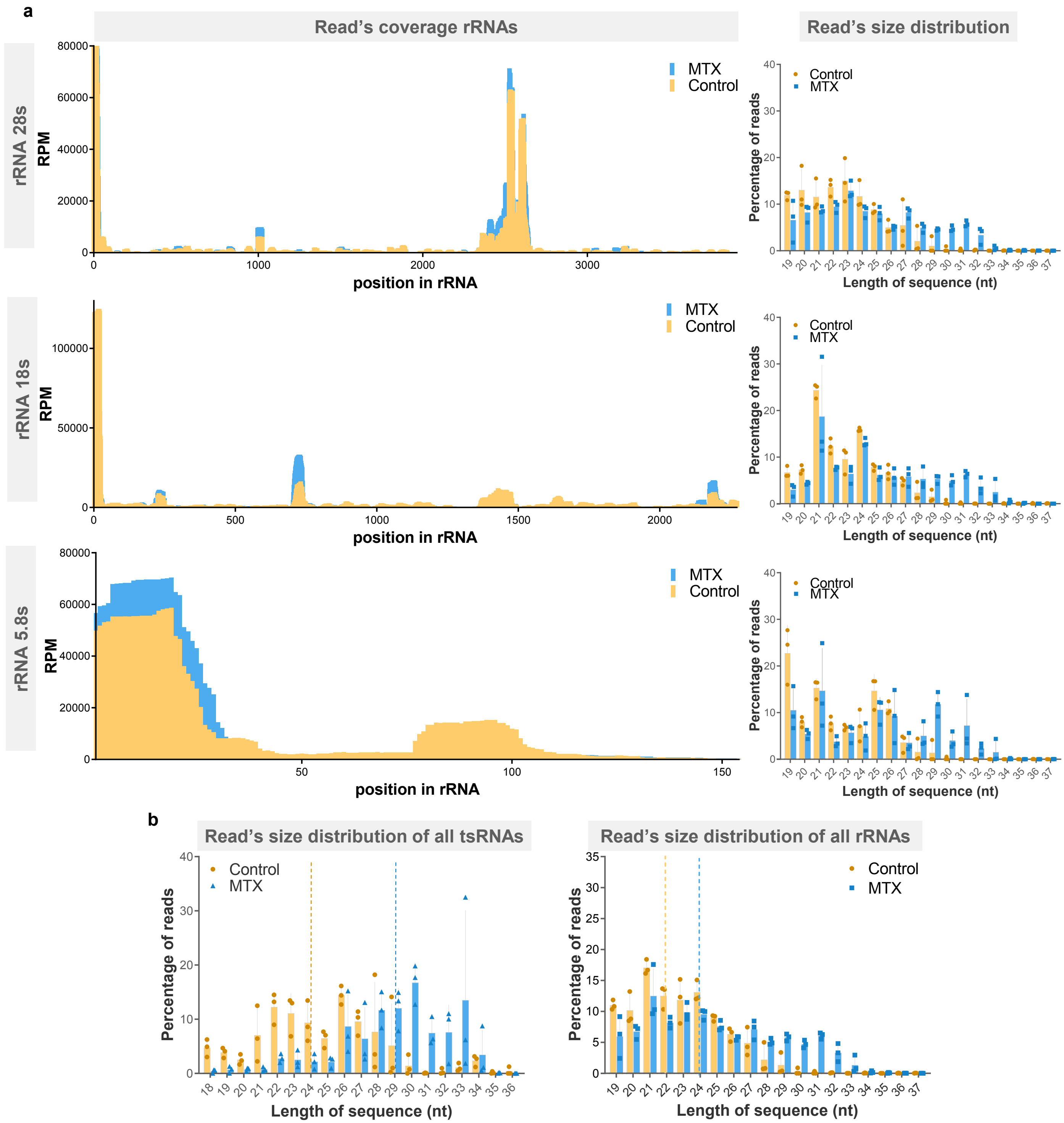

Figure S3: (a) Histogram showing the read coverage and size distribution for the most abundant rRNAs (28s, 18s and 5.8s) between control and MTX. **(b)** Histograms showing the size distribution for all mapped tsRNA and rRNA on control and MTX treated males. Dotted lines represent the median length. Values on read's size distribution are means ± SD. See also **Supplementary Data 5**.

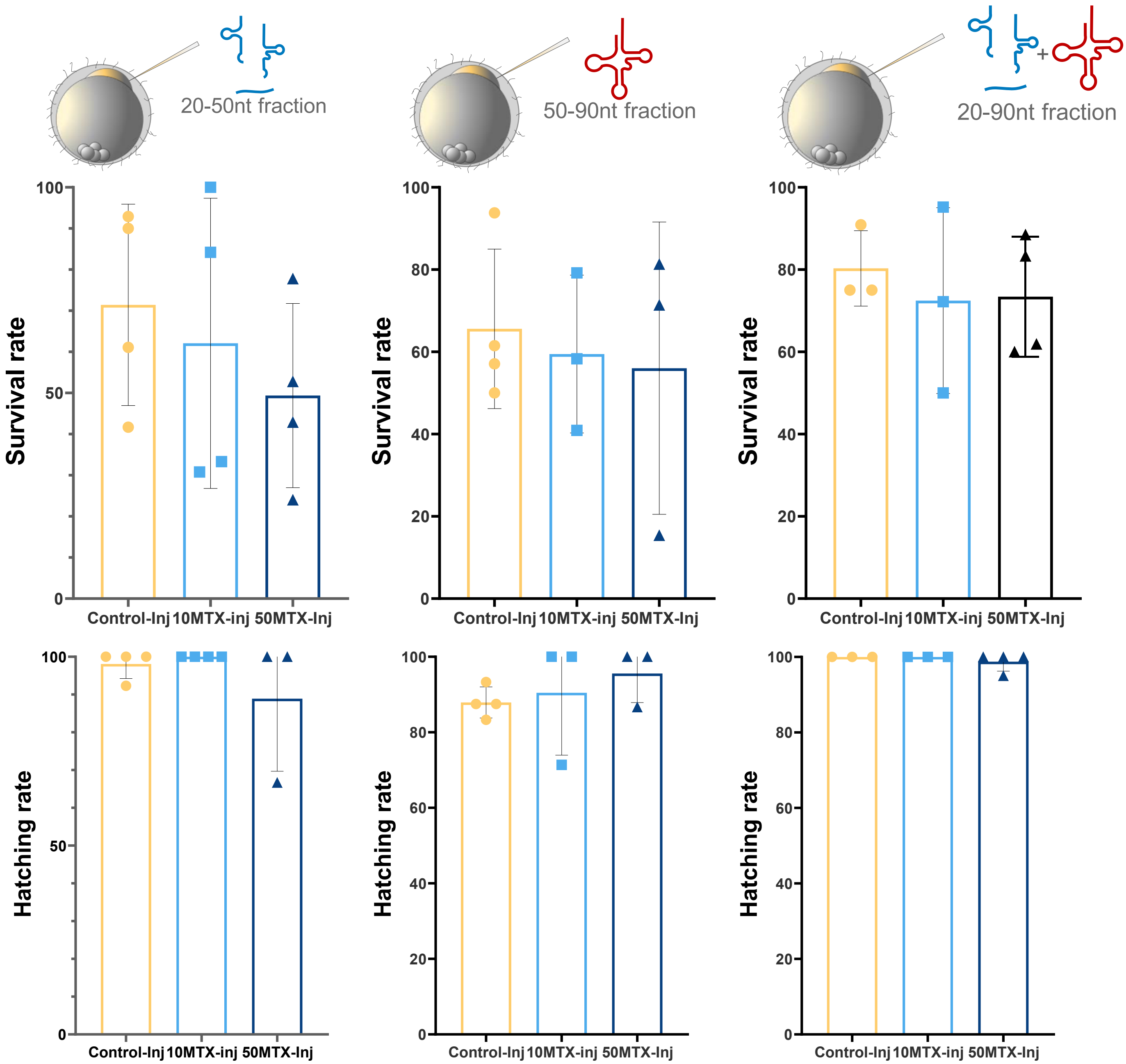

Figure S4: Histogram showing the percentage of survival and hatching of different batches of fertilized wild-type eggs injected with sperm RNA fractions obtained from control, 10MTX and 50MTX treated males.). Each dot represents a biological experimental replicate composed by a pool of embryos. Number of embryos utilized: 20-50nt RNA Control-Inj (n= 14, 24, 18, and 20); 10MTX-Inj (n= 26, 18, 20, and 38); and 50MTX-Inj (n= 9, 14, 25, and 36). 50-90nt RNA Control-Inj (n= 16, 13, 12, 14, and 12); 10MTX-inj (n= 24, 22, 12, and 22); and 50MTX-Inj (n= 16, 21, and 39). 20-90nt RNA Control-Inj (n= 11, 20, and 28); 10MTX-Inj (n= 21, 18, and 16); and 50MTX-Inj (n= 24, 26, 15, and 21).

Hatching rate; for 20-50nt RNA Injections: Control-Inj: n=13, 10, 11, 18; 10MTX-Inj: n= 8, 6, 20, 32: and 50MTX-Inj: n=7, 6, 6 viable embryos at the hatching start point. For 50-90 nt RNA Inj: Control-Inj: n= 15, 8, 6, 8, 11; 10MTX-Inj: n= 19, 9, 7, 18; 50MTX-Inj: n= 13, 15, 6 viable embryos at the hatching start point. For 20-90nt RNA injection: Control-Inj: n= 10, 15, 21; 10MTX-Inj: n= 20, 13, 8; 50MTX-Inj: n= 20, 23, 9, 13 viable embryos at the hatching start point. Statistics by one-way ANOVA followed by Turkey's multiple comparisons test. Non-significant differences were observed in all cases ($P > 0.05$). Values are means ± SE.

Supplementary Tables

Gene symbol	Accession Number	Primer sequence (5´- 3´)
Trmt6	ENSORLG00000009862.2	**Fw:** CGGGAACAGACAACAGGAATA **Rv:** GACCCTTCAGACCTTGATCTTT
Dnmt2 (Trdmt1)	ENSORLG00000019403.2	**Fw:** AGGCCACCTCGCTTTATTC **Rv:** CTTGTGGGAGAGGCCATAATC
Nsun2	ENSORLG00000014332.3	**Fw:**AGATGCTTCACGCTGACATG **Rv:** TTGTTGTCCACGTCATTGGC
RPL7	ENSORLG00000007967.2	**Fw:** CGCCAGATCTTCAACGGTGTAT **Rv:** AGGCTCAGCAATCCTCAGCAT
ef1α	ENSORLG00000007614	**Fw:** GGAGGCCAGCGACAAGATGAGC. **Rv:** ACACGGCCGACAGGGACAGTTC

Supplementary table 1: Primer sequences utilized for RT-qPCR

Sample	Species	3' Adapter used	3' Adapter barcode	3' barcoded adapter	5' Adapter	small-RNAseq RT primer	Solexa_PCR_fwd	Solexa_IDX_rev
Control-1	*O. latipes*	SRBC1	CAGTG	5'-/5rApp/NNNNNNCAGTGAGATCGGAAGAGCACACGTCT/3ddC/-3'	5'-ACACUCUUUCCCUACACGACGCUCUUCCGAUCUNNNN-3'	5'-AGACGTGTGCTCTTCCGATCT -3'	5'-AATGATACGGCGACCACCGAGATCTACACTCTTTCCCTACACGACGCTCTTCCGATCT -3'	5'-CAAGCAGAAGACGGCATACGAGATCAGTGGTGACTGGAGTTCAGACGTGTGCTCTTCCGATCT – 3'
Control-2	*O. latipes*	SRBC2	AGCAA	5'-/5rApp/NNNNNNAGCAAAGATCGGAAGAGCACACGTCT/3ddC/-3'	5'-ACACUCUUUCCCUACACGACGCUCUUCCGAUCUNNNN-3'	5'-AGACGTGTGCTCTTCCGATCT -3'	5'-AATGATACGGCGACCACCGAGATCTACACTCTTTCCCTACACGACGCTCTTCCGATCT -3'	5'-CAAGCAGAAGACGGCATACGAGATAGCAAGTGACTGGAGTTCAGACGTGTGCTCTTCCGATCT – 3'
Control-3	*O. latipes*	SRBC3	GGTAT	5'-/5rApp/NNNNNNGGTATAGATCGGAAGAGCACACGTCT/3ddC/-3'	5'-ACACUCUUUCCCUACACGACGCUCUUCCGAUCUNNNN-3'	5'-AGACGTGTGCTCTTCCGATCT -3'	5'-AATGATACGGCGACCACCGAGATCTACACTCTTTCCCTACACGACGCTCTTCCGATCT -3'	5'-CAAGCAGAAGACGGCATACGAGATGGTATGTGACTGGAGTTCAGACGTGTGCTCTTCCGATCT – 3'
10MTX-1	*O. latipes*	SRBC4	TACCA	5'-/5rApp/NNNNNNTACCAAGATCGGAAGAGCACACGTCT/3ddC/-3'	5'-ACACUCUUUCCCUACACGACGCUCUUCCGAUCUNNNN-3'	5'-AGACGTGTGCTCTTCCGATCT -3'	5'-AATGATACGGCGACCACCGAGATCTACACTCTTTCCCTACACGACGCTCTTCCGATCT -3'	5'-CAAGCAGAAGACGGCATACGAGATTACCAGTGACTGGAGTTCAGACGTGTGCTCTTCCGATCT – 3'
10MTX-2	*O. latipes*	SRBC5	GTCAG	5'-/5rApp/NNNNNNGTCAGAGATCGGAAGAGCACACGTCT/3ddC/-3'	5'-ACACUCUUUCCCUACACGACGCUCUUCCGAUCUNNNN-3'	5'-AGACGTGTGCTCTTCCGATCT -3'	5'-AATGATACGGCGACCACCGAGATCTACACTCTTTCCCTACACGACGCTCTTCCGATCT -3'	5'-CAAGCAGAAGACGGCATACGAGATGTCAGGTGACTGGAGTTCAGACGTGTGCTCTTCCGATCT – 3'
10MTX-3	*O. latipes*	SRBC6	TGACT	5'-/5rApp/NNNNNNTGACTAGATCGGAAGAGCACACGTCT/3ddC/-3'	5'-ACACUCUUUCCCUACACGACGCUCUUCCGAUCUNNNN-3'	5'-AGACGTGTGCTCTTCCGATCT -3'	5'-AATGATACGGCGACCACCGAGATCTACACTCTTTCCCTACACGACGCTCTTCCGATCT -3'	5'-CAAGCAGAAGACGGCATACGAGATTGACTGTGACTGGAGTTCAGACGTGTGCTCTTCCGATCT – 3'

Supplementary Table 2: Adapter oligos utilized for library preparation.